THE UNIVERSITY OF MICHIGAN

INDUSTRY PROGRAM OF THE COLLEGE OF ENGINEERING

INCIPIENT BOILING AND THE BUBBLE BOUNDARY LAYER FORMATION OVER A HEATED PLATE FOR FORCED CONVECTION FLOW IN A PRESSURIZED RECTANGULAR CHANNEL

Latif Menashi Jiji

A dissertation submitted in partial fulfillment
of the requirements for the degree of
Doctor of Philosophy in the
University of Michigan
Department of Mechanical Engineering
1962

IP-548

ACKNOWLEDGEMENT

The author wishes to express his gratitude to the Chairman of his Doctoral Committee, Professor John A. Clark, who guided this investigation throughout its course. His constant advice, assistance and encouragement are appreciated. The assistance of the Doctoral Committee members, Professors K. W. Hall, R. M. Tek, and H. Merte is also appreciated.

The many helpful suggestions given by Mr. Stanley J. Green and his staff of the Thermal and Hydraulics Engineering Reactor Development and Analysis Department, Atomic Power Division, Westinghouse Electric Corporation, are gratefully acknowledged.

The author wishes to convey his thanks to the Michigan Memorial-Phoenix Project and the Mechanical Engineering Department of the University of Michigan for sponsoring this investigation, and to Consumers Power Company, Erie, Michigan for providing two high pressure liquid level gages. He is also grateful to the Ford Foundation for awarding him an Engineering Faculty Development Fellowship.

Mr. Dale Hedding, a graduate student at the University of Michigan gave valuable assistance in taking and reducing data.

Finally, the prompt and efficient secretarial assistance of Mrs. Norlene H. Martin is gratefully acknowledged.

TABLE OF CONTENTS

Page

LIST OF TABLES

LIST OF FIGURES

NOMENCLATURE

A	Surface area, ft^2
b	Width of the heated surface, ft
C_p	Constant pressure specific heat, BTU/lbm-^oF
e	Base of Natural or Napierian logarithm
G	Mass velocity, lbm/hr-ft^2
H	Channel height, ft
h_x	Heat transfer coefficient, BTU/hr-ft^2-^oF
h_{fg}	Latent heat of evaporation, BTU/lbm
k	Thermal conductivity, BTU/hr-ft-^oF
M_n	Mean value
P	Pressure, psia
P_i	Inlet pressure, psia
q	Rate of heat transfer, BTU/hr.
q/A	Heat flux, BTU/hr-ft^2
$(q/A)_I$	Incipient heat flux, BTU/hr-ft^2
R	Result
T_b	Bulk temperature, ^oF
T_F	Film temperature defined by equation (7), ^oF
T_{MAX}	Maximum level of temperature fluctuations defined in Figure 56, ^oF
T_{MEAN}	Time average of temperature fluctuations, ^oF
T_{MIN}	Minimum level of temperature fluctuations defined in Figure 56, ^oF

T_{sat}	Saturation temperature, ^{o}F
T_w	Surface temperature, ^{o}F
V_i	Inlet velocity, ft/sec.
V_n	Independent variable
	Mass flow rate, lbm/hr.
W_n	Uncertainty interval of the variable V_n
W_R	Uncertainty interval of the result R
X	Distance from leading edge of the heated surface, ft (except in Equation (12) where it is in inches)
X_I	Distance from the leading edge of the heated surface to the point of initial nucleation, ft (except in Equation (12) where it is in inches)
y	Distance normal to the heated surface, in.
δ	Bubble boundary layer thickness, in.
μ	Viscosity, lbm/ft-hr.
ρ_L	Mass density of saturated liquid, lbm/ft^3
ρ_v	Mass density of saturated vapor, lbm/ft^3
σ	Surface tension, $lb_f/$ in.

CHAPTER I

INTRODUCTION

A. Background

Nucleate boiling is often utilized in removing large quantities of heat which are generated in systems having relatively small volumes such as the nuclear reactor and the rocket motor. Because of recent important applications of boiling heat transfer, a great deal of research has been done in this field (1, 2, 3). During the past 25 years considerable effort has been devoted to the study of boiling systems which has improved the scientific description and understanding of many aspects of two-phase phenomena. In spite of this intensified research activity, there is no theory which will adequately predict the various processes associated with forced convection boiling heat transfer such as incipient boiling, bubble formation and growth, pressure drop, density distribution, and burnout. The lack of such a theory is traced first to the complexity of boiling phenomenon and second, to the absence of a simplified model which adequately represents the actual processes and also lends itself to mathematical treatment. Much of the work which has been done has understandably dealt with measurements of gross effects rather than local effects. Any theory which will satisfactorily predict

boiling heat transfer and two-phase flow processes must rest on a complete description of the local hydrodynamic and thermodynamic mechanisms involved. An investigation which is directed at the study of the mechanics of vapor bubble formation processes in the boundary layer regions for forced convection flow over a heated plate is a favorable approach to this problem. Such flow conditions are encountered in the coolant channels of pressurized water nuclear reactors, in rocket motor coolant passages, cryogenic transfer lines, chemical reactors and other devices wherever surface boiling occurs. Under these circumstances the normal single-phase boundary layer processes are replaced by hydrodynamic and thermodynamic conditions imposed by the growth and mutual interaction of vapor bubbles. The mechanics of these processes are almost completely unknown, yet they control the thermodynamic behavior of the system.

B. Purpose

The object of this study is to investigate the inception of bubbles for forced convection flow of distilled, degassed water over a heated plate in a pressurized channel and their consequent mutual interaction in the formation of a type of two phase boundary layer which is called the "bubble boundary layer". The heated plate, which is 0.50" wide and 9.48" long is to be vertically oriented in

a 0.50" x 0.46" rectangular channel. The investigation is to be carried out at pressures of 200 to 1000 psia, velocities of 1 to 6 ft/sec and subcoolings of 50 to 300°F.

Specifically, the following three interrelated problems will be investigated:

1. The conditions necessary for the initial appearance of observable bubbles over a heated surface in subcooled forced convection boiling. The term "incipient boiling" shall refer to this phase of the investigation.

2. The growth of bubbles and the consequent development of a two-phase region along the heated surface. This region shall be called the "bubble boundary layer" as illustrated in Figure (1).

3. The temperature distribution and fluctuations within the single-phase liquid core and bubble boundary layer.

C. Literature Survey

A great deal of research has been done in the field of boiling heat transfer and two-phase flow. Most of the work was done on boiling outside heated wires and inside tubes (4, 5, 6, 7, 12, 13, 41). More recently work was done on boiling in rectangular channels (17, 18, 19, 22, 23, 24). Theoretical and experimental studies have been conducted on bubble formation (8, 9, 10, 11), pressure drop (7, 12, 13, 14, 15, 41, 50, 51, 52), burnout heat

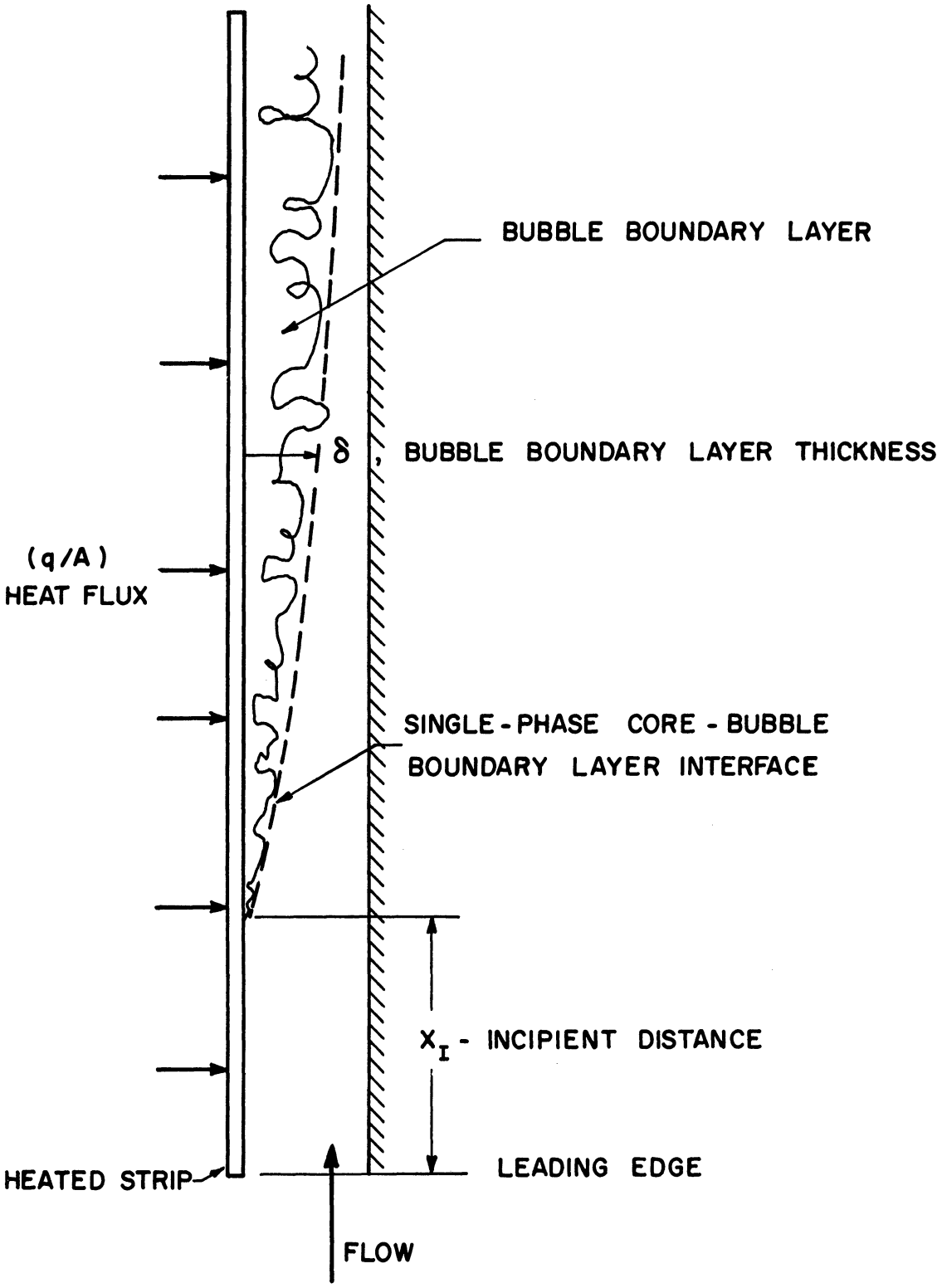

Figure 1. Incipient Boiling and the Bubble Boundary Layer

flux (4, 6, 16, 17, 18, 19, 41) and void fraction and density variation (20, 21, 22, 23, 37, 45, 47, 48, 49).

Incipient boiling for forced convection flow inside tubes was investigated by Buchberg, et al. (41). The point of initial nucleation was detected by means of surface temperature measurements. They observed that an abrupt change in the character of surface temperature fluctuations takes place at the point of initial nucleation of bubbles. In the region of the tube in which boiling is well established little or no fluctuations in the wall temperature were indicated, while fluctuations of at least 5°F were observed along the non-boiling portion of the tube.

Dyer (24) obtained photographs of the bubble boundary layer for the flow between two heated plates in a rectangular channel. The bubble boundary layer thickness was observed to increase in the downstream direction. He made gross measurements at the inlet and outlet of the test section for a limited range of heat flux, velocity, and subcooling at pressures up to 56 psia.

Other photographic investigations have been conducted on the boiling process. Gunther and Kreith (11) made photographic studies on the mechanism of surface boiling in a subcooled pool, using a metal strip as a heating element. To investigate the effect of forced convection on the mechanism of boiling heat transfer, Gunther (25) made a high speed photographic study of boiling in

rectangular channels. Similar studies have been carried out by various other investigators (26, 27, 28).

Because it is necessary to know the density of the coolant in a nuclear reactor, several investigations have been conducted to study the variation of density or void fraction along rectangular channels. The approach to predicting the density of steam-water mixtures has been almost completely empirical. An experimental program was conducted at the Battelle Memorial Institute by Egen, et al. (20) to investigate the formation and distribution of vapor in a rectangular channel under boiling conditions at 2000 psia. The effect of heat flux, flow rate and inlet temperature on the void distribution and formation was determined. Similar studies were conducted at the Argonne National Laboratory by Marchaterre (22). He investigated the effect of pressure on the density of a steam-water mixture in natural convection boiling in rectangular channels at pressures up to 600 psia. Void volume fraction was calculated from measurements of gamma ray attenuation. Neither the Battelle Memorial Institute nor the Argonne National Laboratory analysis and experiments treated the bubble boundary layer as a separate region from the single-phase liquid core.

Griffith, et al. (21), studied void volumes in a rectangular flow channel for subcooled boiling from a

single heated surface at pressures of 500, 1000, and 1500 psia. A semi-empirical method for predicting the void fraction along a heated surface in a rectangular channel was presented in this work.

Extensive studies on burnout in channels were conducted by the Westinghouse Atomic Power Division (18, 19, 29). Similar experiments were carried out at the Battelle Memorial Institute (17).

The effect of L/D ratio (L is the distance from inlet to point of initial burnout; D is the equivalent diameter) on burnout heat flux is an additional factor which needs careful study. It has been found that the burnout heat flux was more than halved by increasing the L/D ratio from 65 to about 300 (30).

Gunther (25) obtained an empirical expression for forced convection burnout heat flux for a heated metal strip suspended lengthwise along the center plane of a rectangular channel. The empirical equation fits the results of 38 burnout tests at low pressures (30 - 164 psia) and subcooling from 22°F to 282°F. Buchberg, et al. (41) studied burnout heat flux at 2000 psia. However, they indicated that prediction of burnout heat flux for pressures other than 2000 psia or tubes of different diameters cannot be made with confidence by using the same empirical equation.

Jens and Lottes (49) summarized experiments by Rohsenow and Clark (12) and Buchberg, et al.(41) on surface boiling of water flowing in vertical tubes. Data from these experiments on burnout heat flux and surface temperature were correlated.

In a recent study on the mechanism of subcooled nucleate boiling, Bankoff (43) proposed a three-step model for the transfer of heat. First the heat flows from the surface to the adjacent two-phase region. Secondly, heat flows through the two-phase region, and finally from the edge of this layer to the main core. Simplified expressions were deduced for the first and third steps which gave reasonable agreement with Gunther's (25) data. The author points out that these expressions are highly speculative in view of the many simplifying assumptions and that considerably more experimental data on the local parameters are needed. An approximate expression for estimating the temperature at the edge of the two-phase region was also deduced by Bankoff. Using Gunther's data this temperature was calculated and found to rise steeply towards the saturation temperature as burnout is approached.

CHAPTER II

THEORETICAL ANALYSIS OF INCIPIENT BOILING

It is desirable to make an analytical investigation of the conditions necessary for the inception of boiling for a fluid flowing over a heated surface. Specifically, the relation between heat flux and the position along the heated surface where initial nucleation takes place is desired as a function of inlet pressure, velocity and subcooling.

Referring to Figure 2, let X_I be the distance from the leading edge to the point of initial nucleation of bubbles. For a small element dX at $X = X_I$ one can write

$$dq_f = h_x (T_w - T_b) \, dA$$

or

$$\left(\frac{dq_f}{dA}\right)_I = h_x (T_w - T_b) \qquad (1)$$

Since for an electrically heated uniform plate in steady-state the energy dissipated per unit surface area is constant, equation (1) becomes

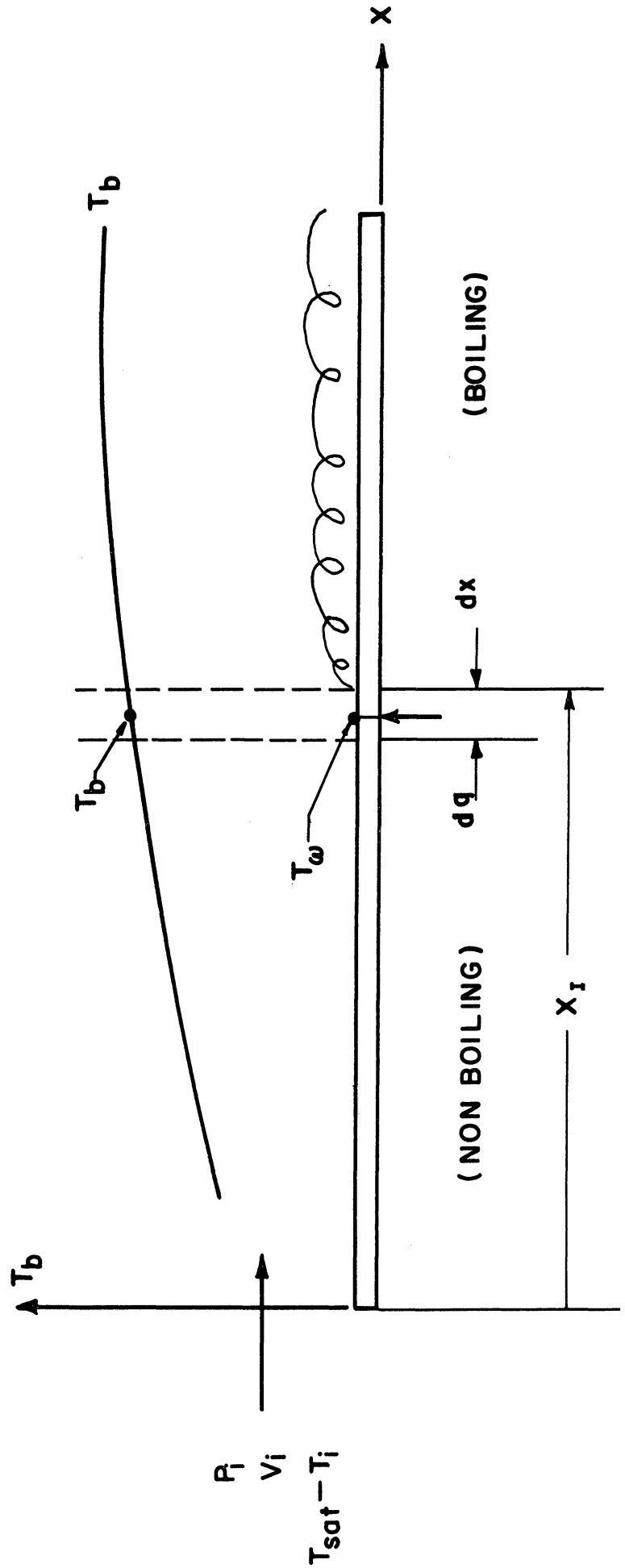

Figure 2. Anlaytical Model for Incipient Boiling

$$(q/A)_I = h_x (T_w - T_b) \tag{2}$$

where $(q/A)_I$ is the incipient heat flux, i.e. the flux necessary to initiate boiling at $X = X_I$ for a fixed inlet state.

The bulk temperature T_b may be determined from the first law of thermodynamics

$$q = \omega C_p (T_b - T_i)$$

or

$$T_b = T_i + \frac{(q/A)_I \, b \, X_I}{\omega C_p} \tag{3}$$

Boiling takes place when the surface temperature is equal to or greater than saturation temperature. As a first step towards the solution of this problem the assumption will be made that at $X = X_I$

$$T_w = T_{sat} \tag{4}$$

Substituting Equations (3) and (4) into Equation (2) one obtains

$$(q/A)_I = \frac{h_x (T_{sat} - T_i)}{1 + h_x \frac{b X_I}{C_p W}} \qquad (5)$$

The heat transfer coefficient h_x should be evaluated at $X = X_I$. Since by definition no boiling takes place in the region $0 < X < X_I$, it follows that the film coefficient h_x in the this region may be determined from existing correlation equations. For forced convection turbulent flow over a heated plate Knudsen and Katz (70) suggest the following equation

$$\frac{h_x X}{k} = 0.0292 \left(\frac{G X}{\mu}\right)^{0.8} \left(\frac{C_p \mu}{k}\right)^{1/3} \qquad (6)$$

Equation (6) applies to a flat plate at constant wall temperature. However, according to Seban and Shimazaki (72), for turbulent flow in tubes at Prandtl numbers close to unity, the ratio of heat transfer coefficient for constant wall temperature to the heat transfer coefficient for constant heat flux is equal to 0.97. Therefore, Equation (6) may be used, with good approximation, to describe the local heat transfer film coefficient for

turbulent flow over a flat plate at constant heat flux.

Fluid properties in Equation (6) are to be evaluated at the film temperature T_F defined as follows:

$$T_F = \frac{1}{2}(T_w + T_b) \tag{7}$$

Since T_w is assumed to be equal to saturation temperature, then

$$T_F = \frac{1}{2}(T_{sat} - T_i)$$

Thus, for a given inlet pressure, velocity, and subcooling the relation between incipient heat flux $(q/A)_I$ and the location of initial nucleation of bubbles X_I is given by Equation (5).

CHAPTER III

EXPERIMENTAL APPARATUS AND INSTRUMENTATION

A. Introduction

To meet the objectives of this investigation a system was designed such that boiling of distilled and degassified water flowing over a flat surface in a rectangular channel may be observed and photographed. Furthermore, the design incorporates a method for making temperature profile measurements of the fluid at various locations along the heated surface. Means for varying the heat flux, pressure, fluid velocity, and subcooling were also provided. The system was designed to operate within the flowing ranges:

Heat flux:	$0 - 1.7 \times 10^6$ BTU/hr-ft^2
Pressure:	30 - 1000 psia
Velocity:	1 - 6 ft/sec
Mass velocity:	$0.2 \times 10^6 - 1.2 \times 10^6$ lbm/hr-ft^2
Subcooling:	50 - 300 ^{o}F

The experimental apparatus is basically made up of a pressurizing system and three closed loops; the main loop, the ion-exchanger loop and the degassification loop. The main loop controls the flow to the test section while the ion-exchanger loop filters the fluid and maintains the electrical resistivity at a level above 1×10^6 ohm-cm.

The degassifier loop deaerates the distilled water prior to each test.

Since it was desired to observe boiling of distilled water, all the materials which come in contact with the fluid were carefully selected so that no corrosion takes place. All pipes, tubes, and fittings were made of stainless steel types 304 or 316. Type 304L, 316L, 321 or 347 stainless steel was used wherever welding was necessary. Compression fittings (Swagelok and Autoclave) were employed throughout the system so that each component can be removed from the system for possible repairs, inspection or cleaning.

Vents were provided at various points of the system where air pockets could form. Drain plugs were also provided so that the system can be drained when necessary.

A photograph of the experimental apparatus is shown in Figure 3.

B. Equipment and Apparatus

1. Main Loop

Figure 4 is a schematic diagram of the main loop which consists of the test section, heat exchanger, circulation pump, flow control valve, flowmeter and preheater. All these components are assembled in one plane with the

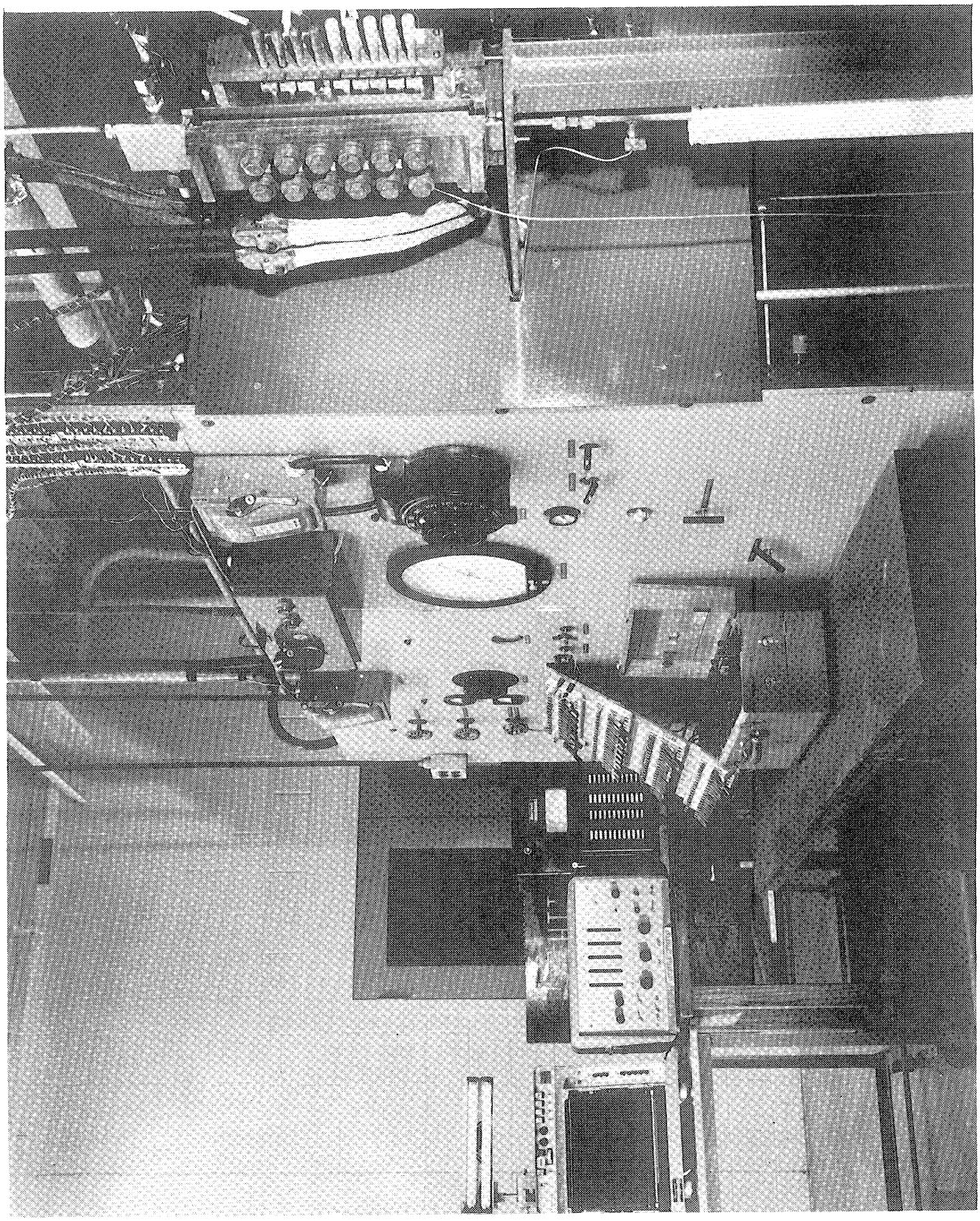

Figure 3. Photographic View of the Experimental Apparatus

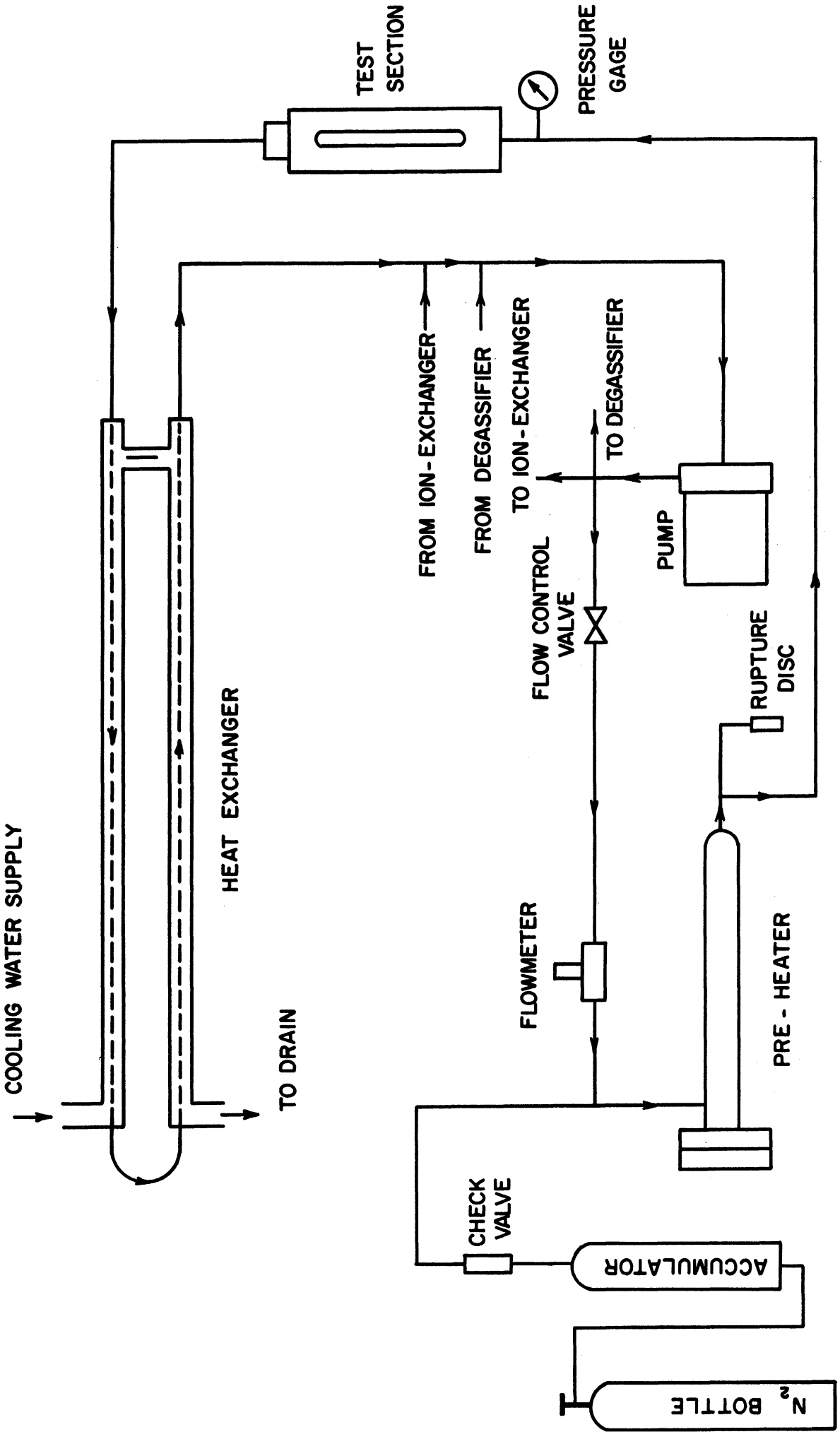

Figure 4. Schematic Diagram of the Main Loop

center of the test section window at 5 feet above floor level. Three different tube sizes were used throughout this loop: ½" gage 16, 3/4" gage 13, and 1" gage 11.

a. Test Section

1) General Considerations

The test section is the housing unit for the heated strip. It provides the means for observation of the boiling liquid and making fluid temperature profile measurements. It is oriented such that the flow over the strip is vertical and upward. Figure 5 is an assembly drawing of the test section and the strip. The test section is a modified design of a Yarway liquid level boiler gage. The modifications were necessary in order to provide a rectangular flow channel, the means for making temperature profile measurements, and also assembling and housing the strip. It has two viewing windows which are 10 inches long and 0.5 inches wide. Figure 6 is a cross section of the test section. All parts, except the test section body and the filler glass, are identical to that of Yarway gage No. 4191, 2500 psi series manufactured by Yarnell-Waring Co., Philadelphia, Pa. The test section body was redesigned to provide rectangular inlet and outlet flow channels and to meet the necessary instrumentation requirements. Figure 7 is a detailed drawing of the test section body. The filler glass was added so that the flow channel (of

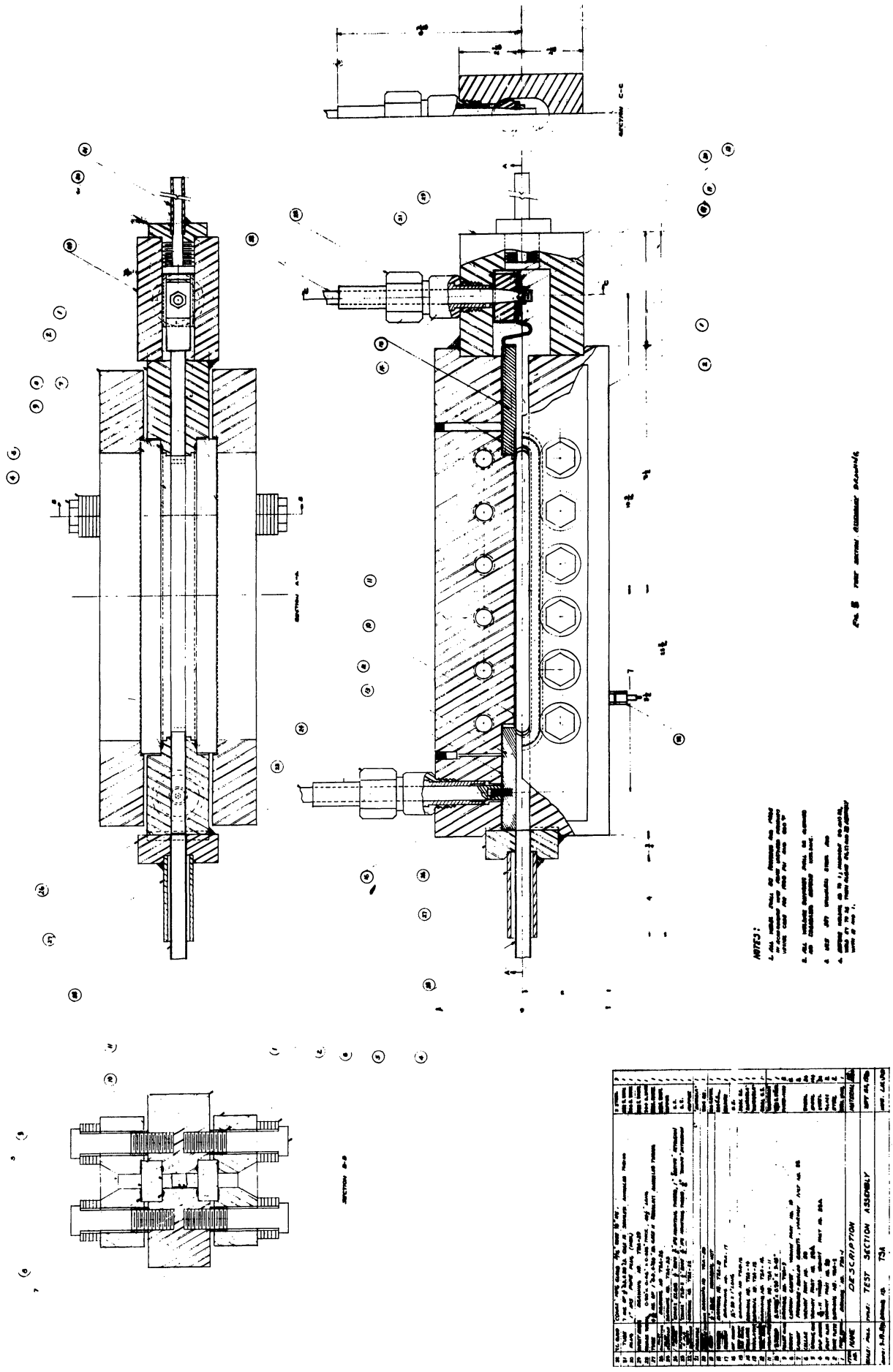

Figure 5. Test Section Assembly Drawing

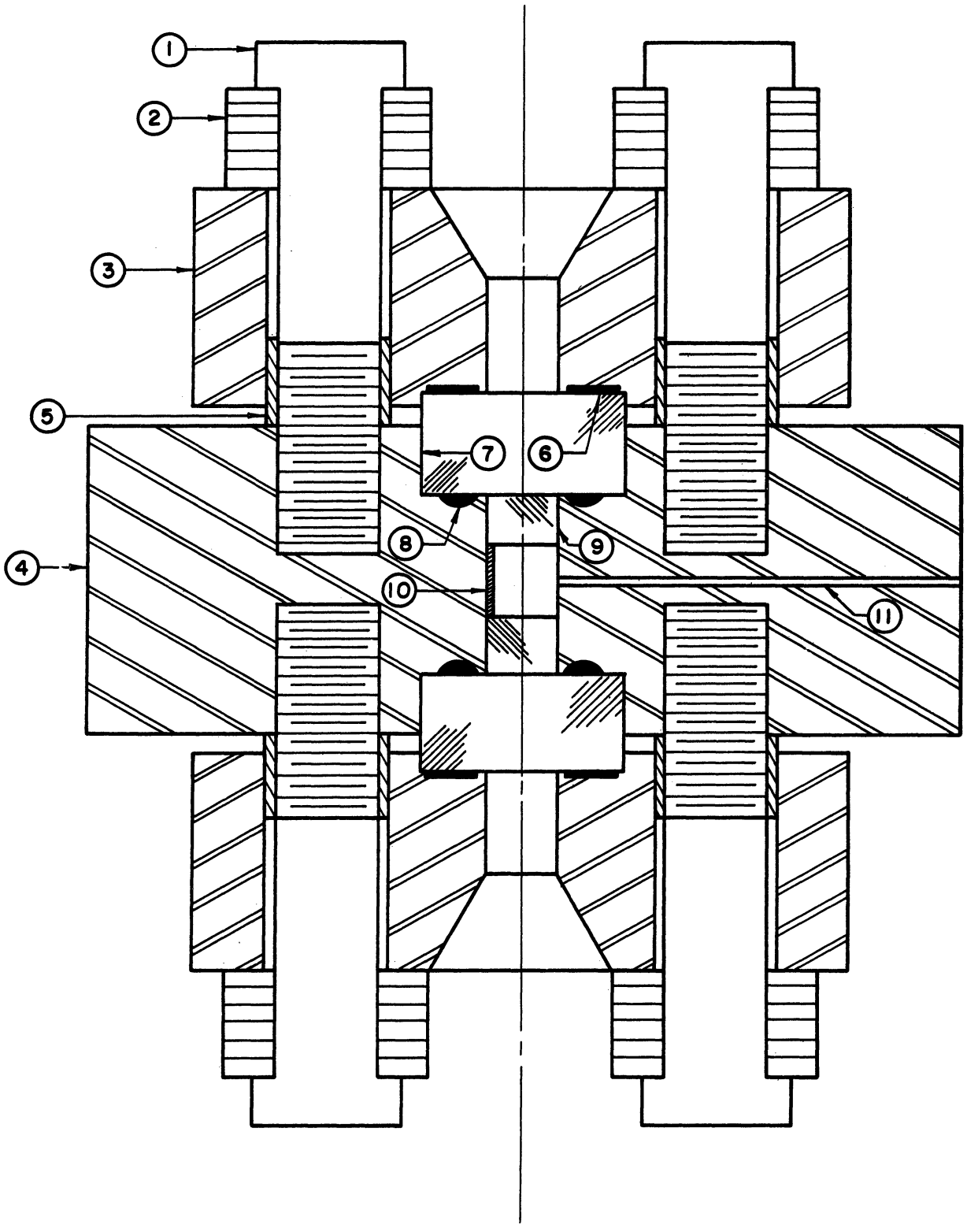

1- CAP SCREW
2- SPRING CONE
3- COVER
4- TEST SECTION BODY
5- COLLAR
6 - CUSHION GASKET
7 - FLAT GLASS
8 - PRESSURE-SEALED GASKET
9 - FILLER GLASS
10 - STRIP
11 - THERMOCOUPLE PROBE CHANNEL

Figure 6. Cross section View of the Test Section

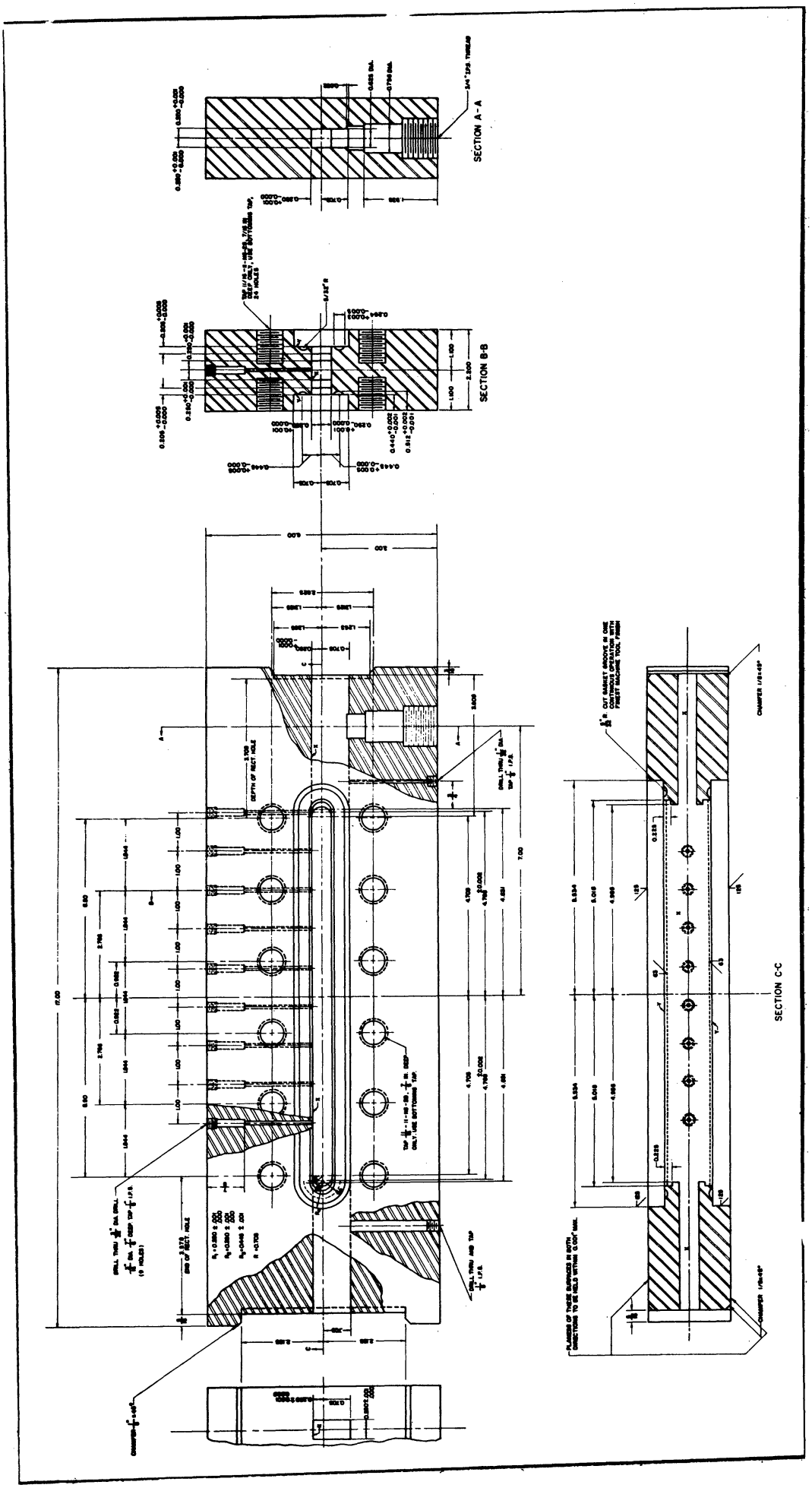

Figure 7. Detail Drawing of the Test Section Body

which the strip is one side) would have a cross section which is identical with that of the inlet section. This inlet section extends 3.5 inches up-stream from the leading edge of the strip. To insure that a fully developed flow is established at the leading edge of the strip, a 40.5 in. long rectangular tubing is connected to the inlet section. This arrangement provided a 44" long (approximately 90 diameters) approach channel with a cross section of 0.50" x 0.46", which is identical to that of the strip channel. The rectangular tubing is inserted inside a 1.0" O.D. gage 11 tube intended to withstand the liquid pressure.

Figure 8 is a photograph showing the test section assembly.

2) Strip Assembly

The strip is an electrically heated ribbon used as a boiling surface. It is designed to provide a heat flux of 1.7×10^6 BTU/hr-ft^2 at 800 amps and 21 volts. It is 0.500" wide, 0.0328" thick and 9.48" long. The strip material is commercially known as Chromel-A manufactured by the Hoskins Co., Detroit, Michigan. Chromel-A is an alloy with nominal composition of 80% Ni and 20% Cr. The resistance of the strip is 0.0323 $\pm$ 2% ohms/ft. The surface was polished and its roughness was measured in two directions with a profilometer. The profilometer registered approximately 3 rms when moved

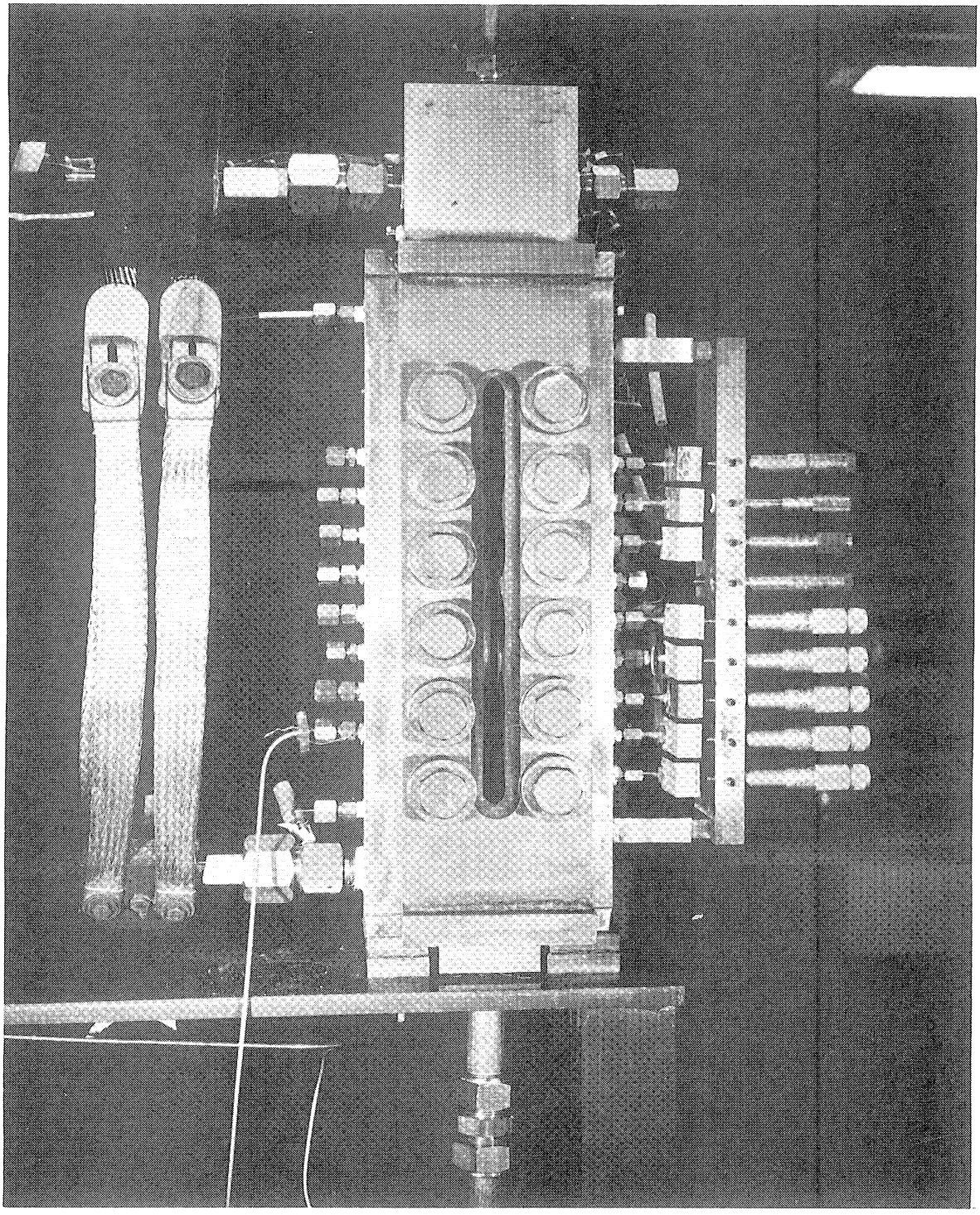

Figure 8. Photograph of the Test Section Assembly

in a lengthwise direction, and 10 rms when traversed the width of the strip.

Figure 9 shows the strip assembly which consists of the strip itself and two stainless steel end blocks. The strip was silver soldered to the blocks to provide good electric contact. To prevent any buckling of the strip at high temperatures, the exit end block is free to expand in the downstream direction. The electric circuit is closed at the exit block with four thin (gage 30) silver ribbons designed to buckle when the strip expands.

The strip was electrically insulated from the test section body with 0.015" thick insulation material commercially known as "Durabla". This material was used wherever electric insulation was necessary.

To prevent any bubbles which might form on the insulated side of the strip from finding their way to the flow channel, it was necessary to clamp the strip against the test section body. Gage 26 Chromel-A wires were discharge-welded along both edges of the strip at 3/8" intervals. These wires were then cut to 3/8" long. When the strip is assembled inside the test section the wires are wedged between the filler glass and the test section body as illustrated in Figure 10. This method prevented the strip from buckling and adequately sealed off any bubbles which may form underneath the strip.

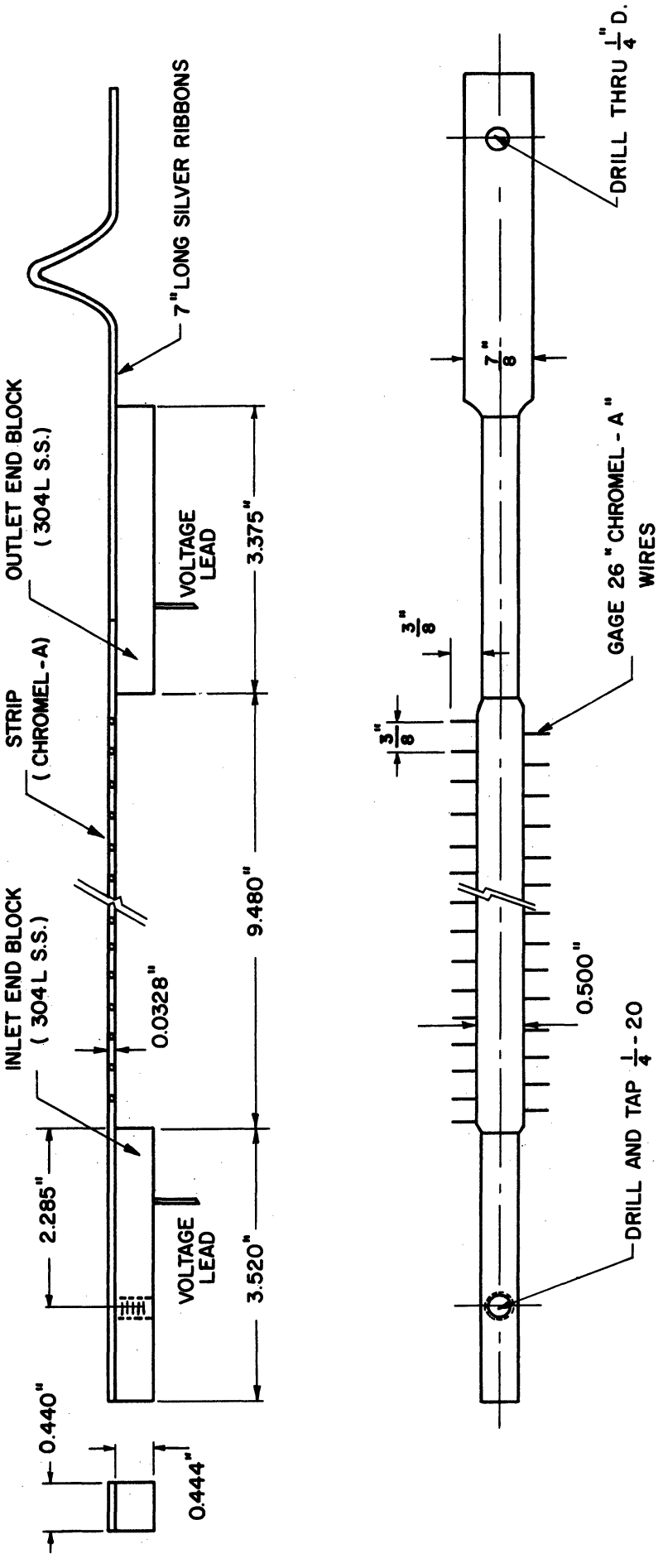

Figure 9. Strip Assembly Drawing

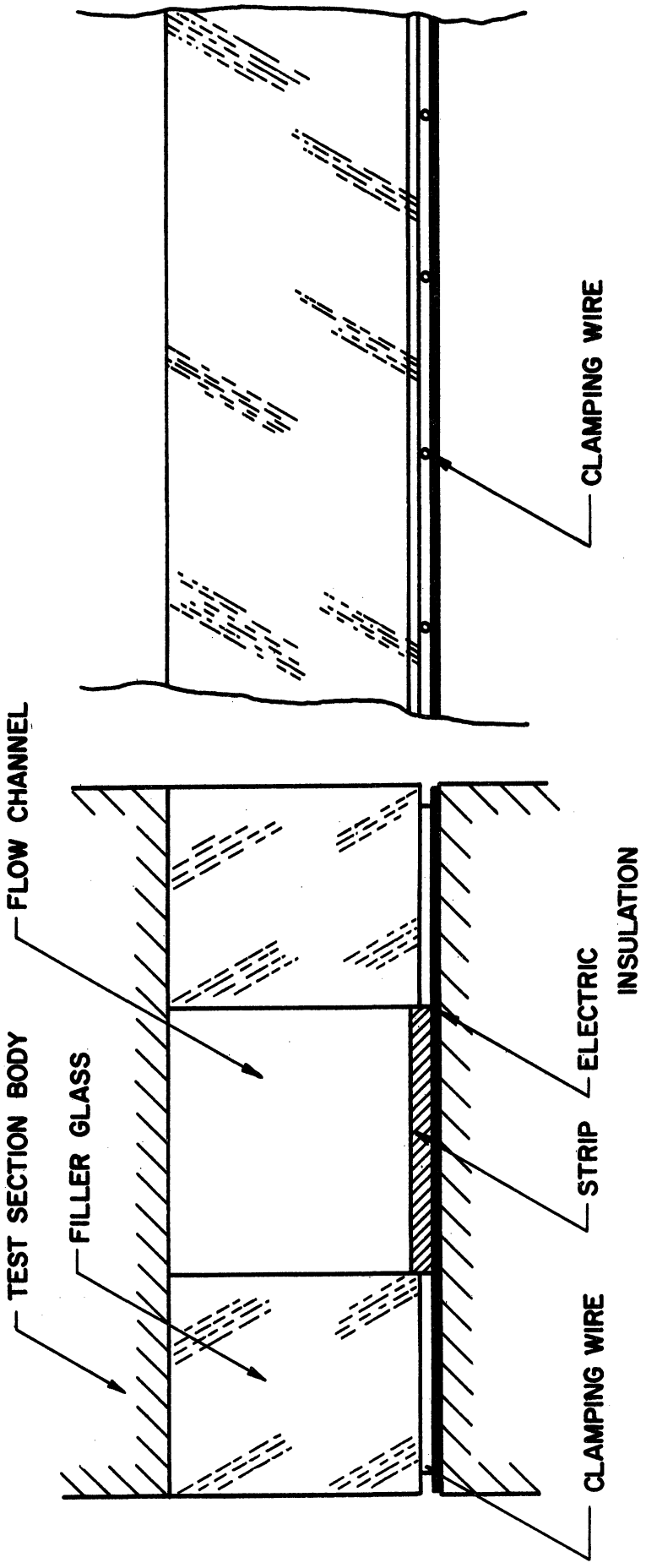

Figure 10. Method of Clamping the Strip to the Test Section Body (3 x size)

3) Electrodes

Two electrodes were used to connect the strip assembly to the bus bars. The two electrodes are essentially chrome plated copper rods. Because of assembly and disassembly problems it was not possible to weld the electrodes to the strip end blocks. At the inlet end of the strip the method of contact between the electrode and the end block is illustrated in Figure 11. A $\frac{1}{4}$-20 stainless steel set screw was used to establish contact between the electrode shoulder and the end block surface. To assure good contact a 1/16" silver washer was used. All contact surfaces were polished before assembly. This method was found to be adequate at currents up to 700 amps. Difficulties were experienced when a smaller screw (size 10-24) and a lead washer were used. The screw failed at high currents due to excessive heating. Figure 12 illustrates the method used to connect the outlet end of the strip assembly to the electrode. To seal and insulate the electrodes from the test section body, two Conax Electrode Glands (Type ELG-5) were used. These are special fittings designed for this purpose and manufactured by the Conax Corporation, Buffalo, New York. Figure 5 shows how the electrodes and the strip are assembled in the test section.

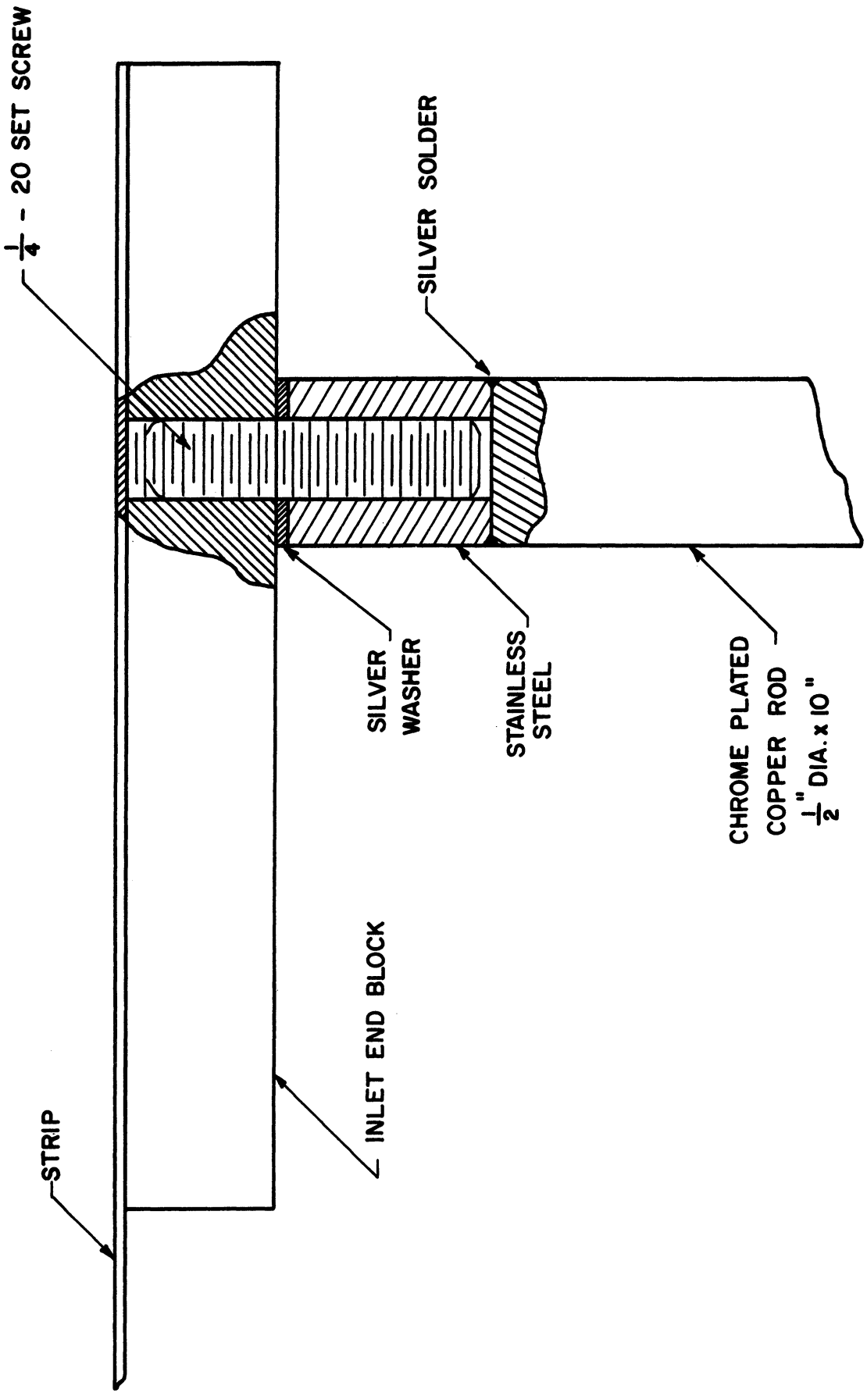

Figure 11. Inlet Electrode Assembly (2 x size)

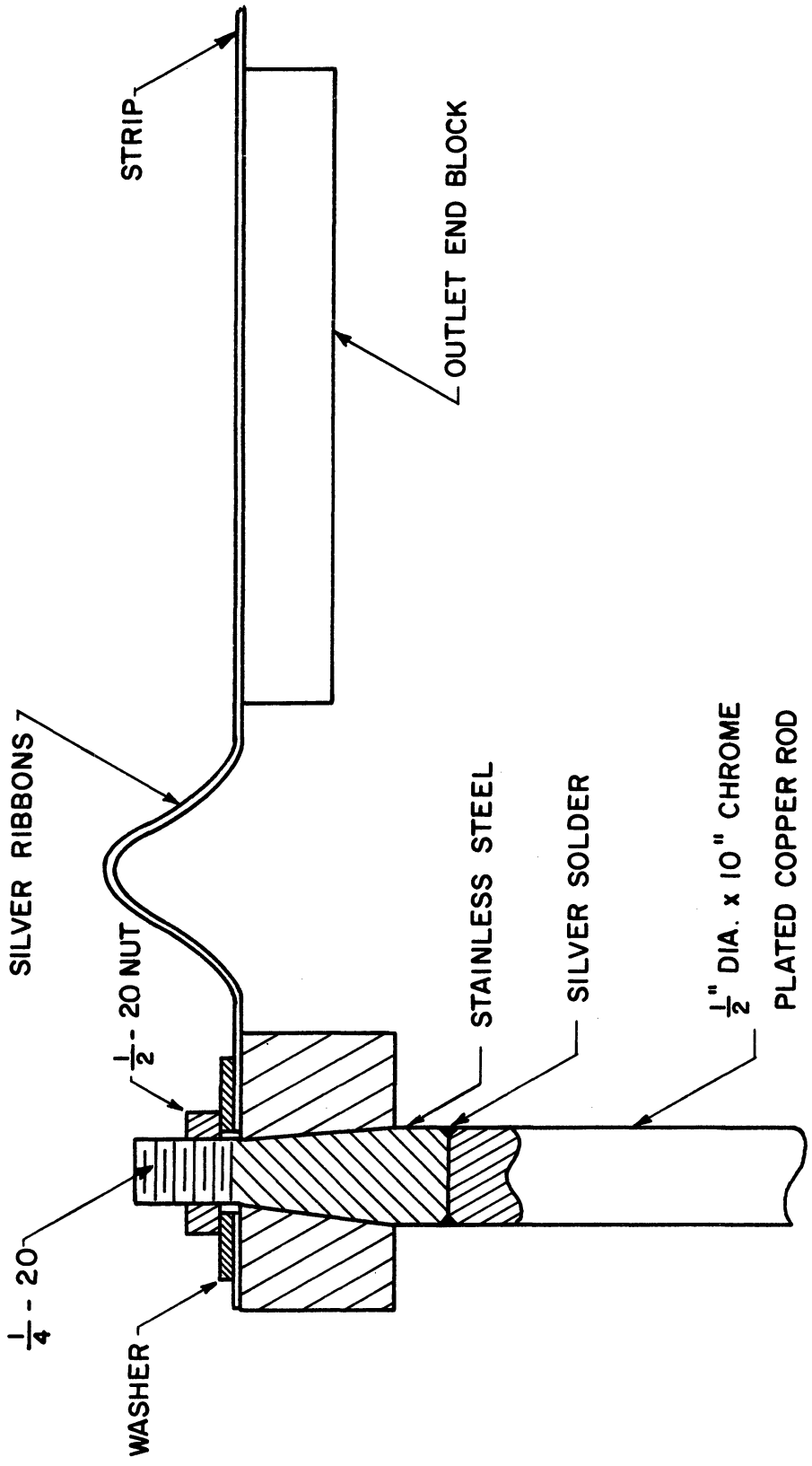

Figure 12. Outlet Electrode Assembly (Actual Size)

b. Preheater

To control the liquid temperature at the inlet to the strip a 9 kw electric heater was installed 10 ft upstream of the test section. It is an immersion type stainless steel electric heater designed for high pressure applications. The heating element (Chromalax type TMI 309B XX) is manufactured by the Edwin L. Wiegand Company, Pittsburgh, Pa. The heater is controlled by a three phase General Radio Variac type W20-G3. An assembly drawing of the preheater is shown in Figure 13.

c. Circulation Pump

A high pressure high temperature stainless steel pump was used to circulate the fluid through the three loops. It is Model CFH-$1\frac{1}{2}$ - 3/4 S Chempump manufactured by Chempump Division, Fostoria Corp., Huntingdon Valley, Pa. The pump and motor are built together into a single unit with a portion of the pumped fluid allowed to enter the motor section to cool it. The only moving part is the rotor-impeller assembly which turns in the pumped fluid, thereby eliminating the need for seals or stuffing boxes. Pumped fluid is isolated from the stator windings by a non-magnetic corrosion resistant "can" or liner welded into the air gap section of the motor. The pump was designed to operate at 1500 psi and deliver 15 gpm at 80 ft. head. A wrap around heat exchanger

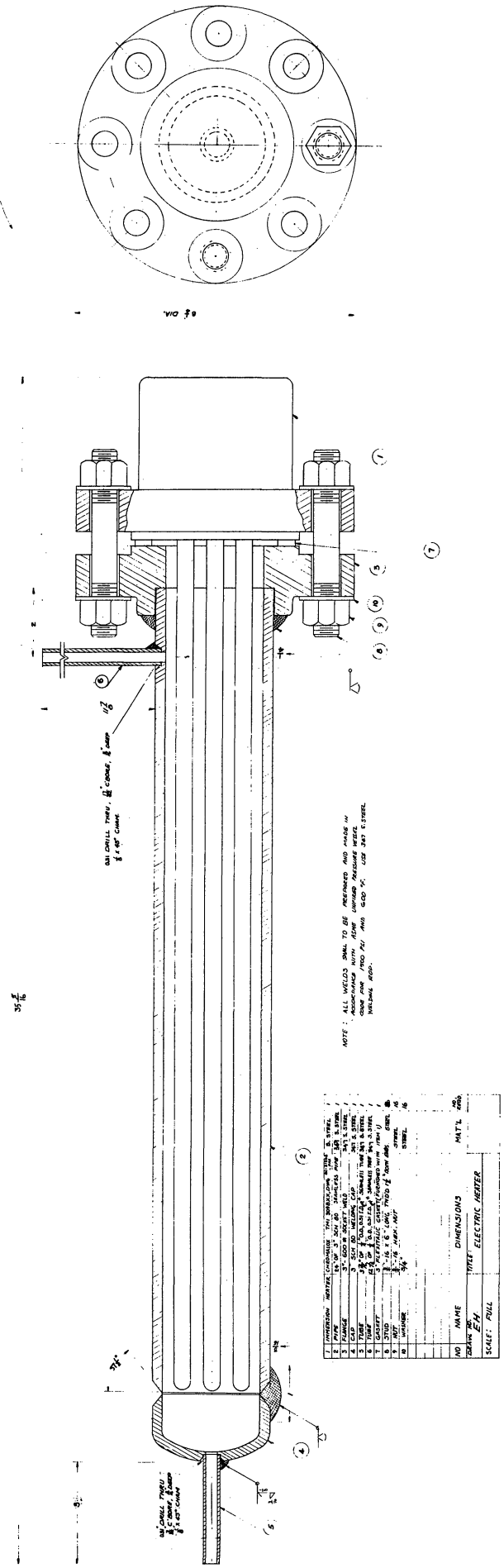

Figure 13. Preheater Assembly Drawing

permits the pump to operate at fluid temperatures up to 600°F. A drawing of the pump is shown in Figure 14.

d. Heat Exchanger

A tube and shell heat exchanger was used to remove some of the heat added to the fluid in the test section and the preheater. It consists of 16 ft. of 3/4" O.D. gage 13 stainless steel tube bent into a U-shape and two 1" pipe shells. Special fittings were used to allow for the expansion of the tube when operating at high temperatures. City water was used as the cooling liquid in the heat exchanger. A detailed drawing of the heat exchanger is shown in Figure 15.

e. Flow Control Valve

A needle valve is installed between the pump outlet and the preheater to control the flow through the test section. The valve (Autoclave Part No. TV-8001) is manufactured by the Autoclave Engineers Sales Corp., Erie, Pa.

2. Ion-Exchanger Loop

To filter the fluid and maintain its electrical resistivity at a high level (above 1 x 10^6 ohm-cm) an ion-exchanger equipment was incorporated with the system. It consists of an ion-exchanger, regenerative type heat exchanger, and cooler. These components were designed to withstand fluid working pressure up to 1500 psi.

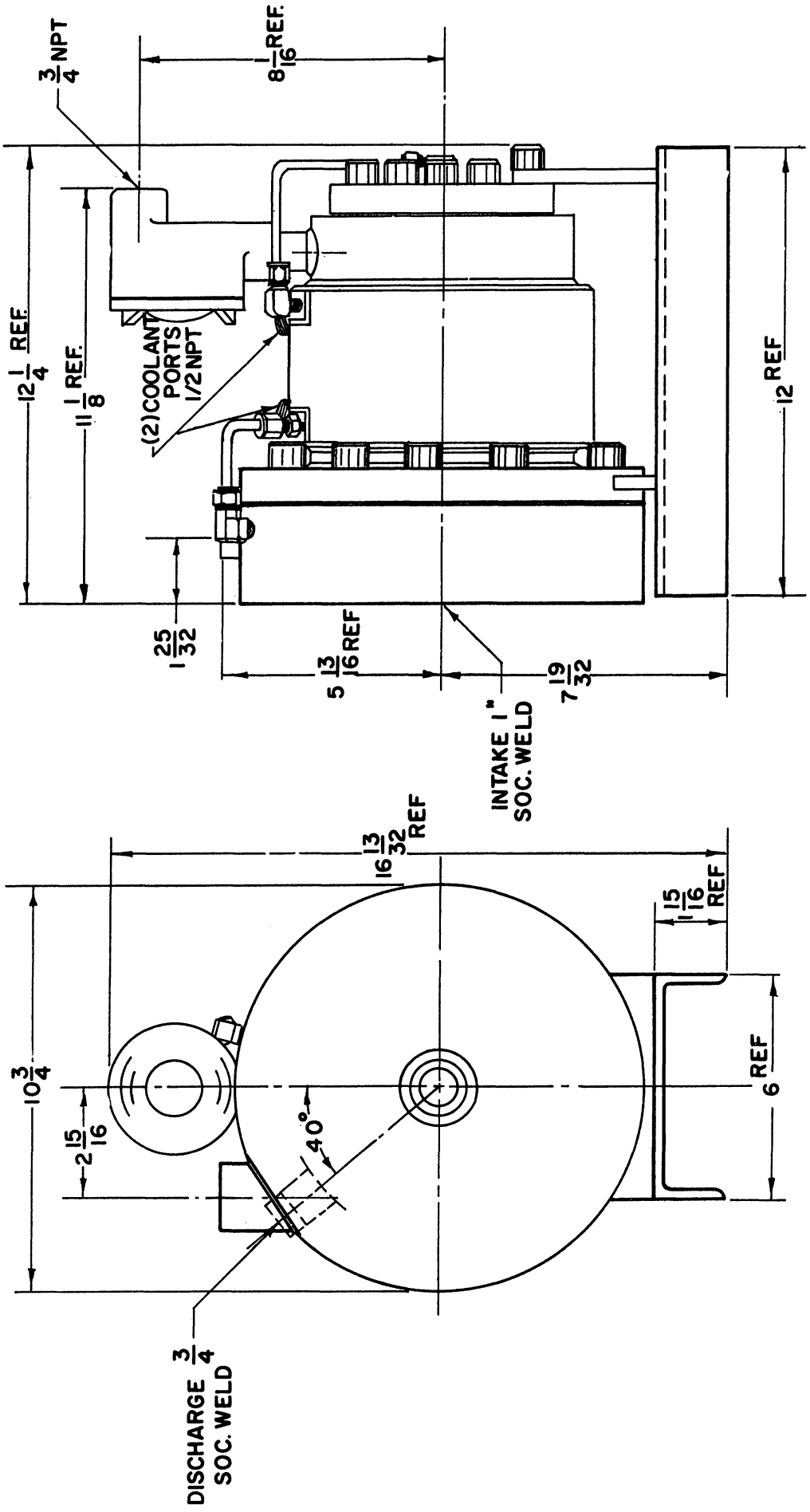

Figure 14. Circulation Pump

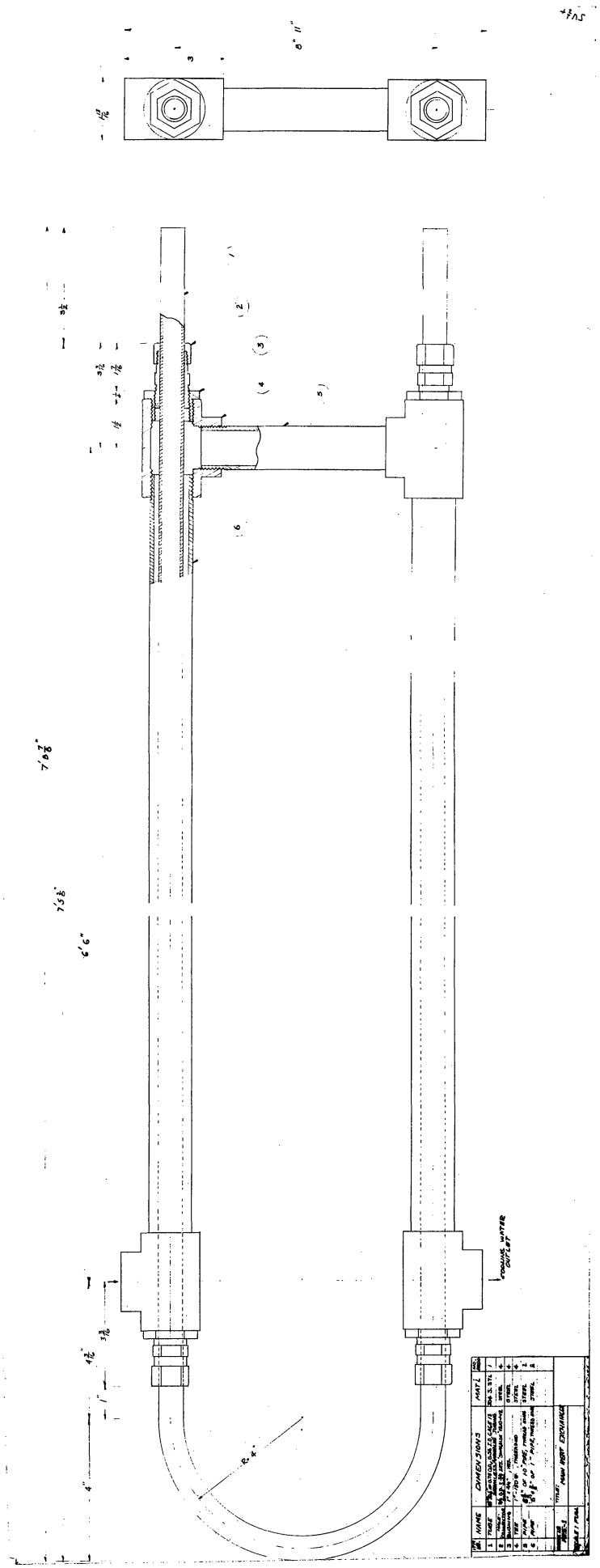

Figure 15. Main Loop Heat Exchanger Drawing

The regenerator and cooler were designed such that the flow rate through the ion-exchanger is approximately 0.85 gpm. This corresponds to 20% of the flow rate through the test section at maximum velocity. Flow through the ion-exchanger was controlled with a teflon sealed needle valve (Autoclave Part No. TV-6002). 3/8" O.D. gage 16 tubing was used throughout this loop. Figure 16 shows a schematic diagram of the ion-exchanger loop.

a. Ion-exchanger

The monobed ion-exchanger was designed to maintain the electrical resistivity of water above 1 x 10^6 ohm-cm. Approximately seven pounds of Amberlite MB-1 resin were used in the ion-exchanger. This resin is supplied by Rohm and Haas Co., Philadelphia, Pa. Incorporated in the design of the ion-exchanger are two filters. A "Neva-Clog" filter is placed at the inlet to the resin bed. It is made out of 347 stainless steel and manufactured by Multi-Metal Wire Cloth Co., New York,N.Y. A porous stainless steel filter (Micr-Metalic" Grade H, 5 micron mean-port opening) is placed at the outlet of the resin bed. This filter is supplied by Micro Metalic Division, Pall Corp., Glen Cove, N.Y. Figure 17 is an illustration of the ion-exchanger assembly.

b. Cooler

Because the maximum operating temperature of the resin is 140°F it was necessary to provide a method

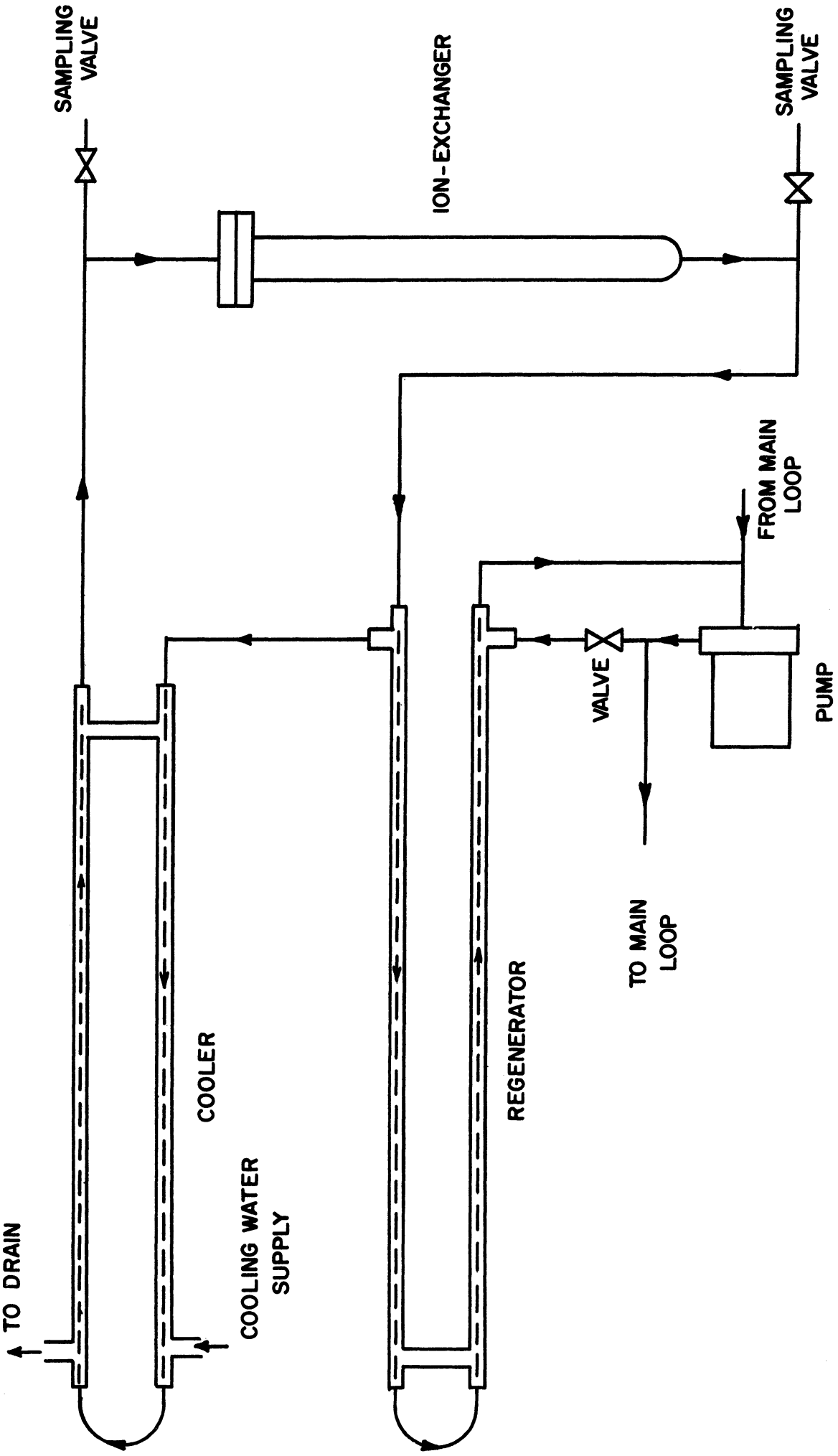

Figure 16. Schematic Diagram of the Ion-Exchanger Loop

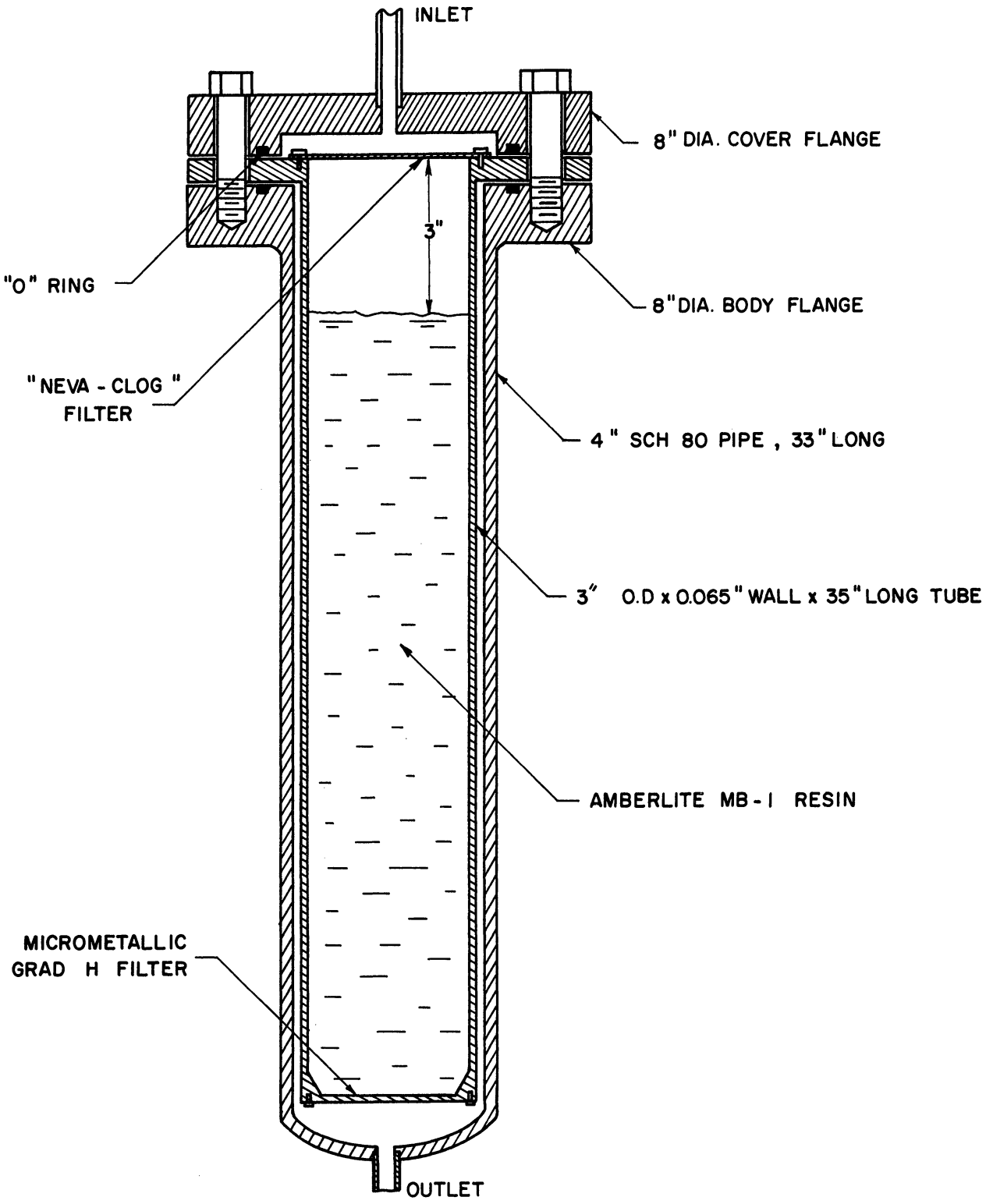

Figure 17. Ion-Exchanger Assembly Drawing

for cooling the water before entering the ion-exchanger. The cooling is accomplished by a cooler and a regenerator. The cooler consists of 13½ ft of 3/8" O.D. gage 16 stainless steel tube bent into a U-shape and two 3/4" pipe shells. A detail drawing of the cooler is shown in Figure 18.

c. Regenerator

The regenerator is U-shaped shell-tube heat exchanger. It consists of 10½ ft. of 3/8" O.D. gage 16 stainless steel tube and two shells made out of 3/4" schedule 40 stainless steel pipe. A detail drawing of the regenerator is shown in Figure 19.

3. Degassification Loop

A degassification system was installed to provide the means for water deaeration prior to each test. Degassification is accomplished by vigorously boiling the water in the degassifier tank and continuously circulating it through the main loop and the ion-exchanger loop. At the same time air is vented to the atmosphere at the top of the degassifier. The degassifier was located 12 ft. above floor level so that the system can be filled by gravity. Because it was intended to degassify the water prior to each test only, this loop was designed to withstand working pressures up to 70 psia. Two valves were provided to cut off the degassification loop

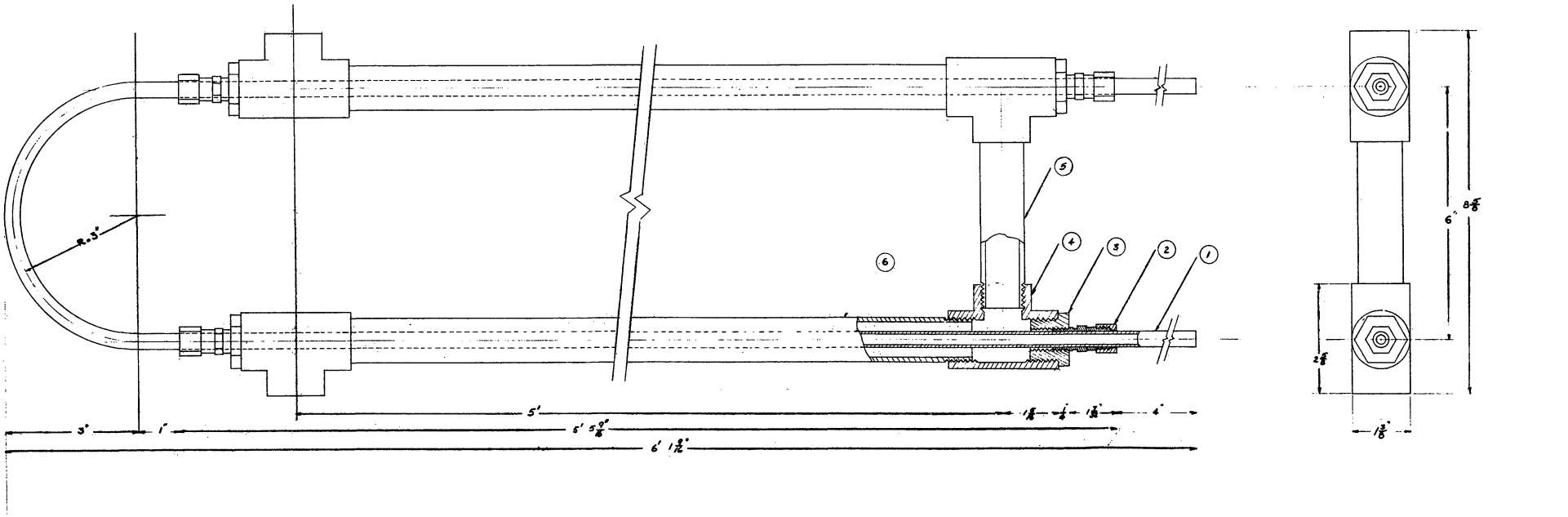

ITM NO.	NAME	DIMENSIONS	MAT'L	NO. REQ'D
1	TUBE	13' 5 7/16" OF 3/8" O.D., 0.555 I.D. GAGE 16 SEAMLESS ANNEALED	304 S. STEEL	1
2	PIPE CONN.	3/8 O.D x 1/8 IPS "SWAGELOK" 600-1-4 ST.	STEEL	4
3	BUSHING	3/4 x 1/4, HEX.	STEEL	4
4	TEE	THREADED 3/4" - 150 lb	STEEL	4
5	PIPE	4 1/2" OF 3/4" PIPE, THREAD BOTH ENDS	STEEL	1
6	PIPE	4" 10 1/2" OF 3/4" PIPE, THREAD BOTH ENDS	STEEL	2
DRAW. NO.	TEHE-L	TITLE ION EXCHANGER COOLER		
SCALE:	FULL			

Figure 18. Ion-Exchanger Cooler

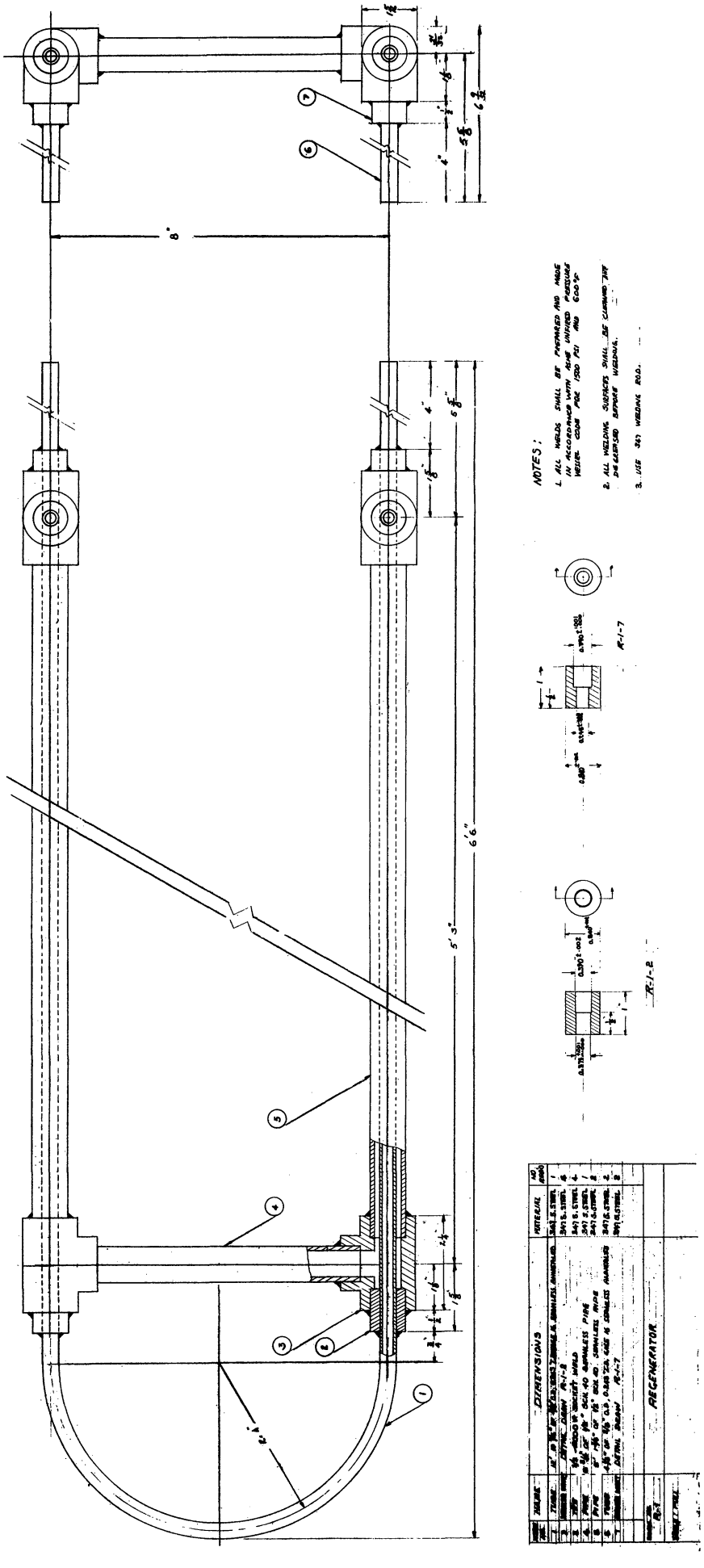

Figure 19. Ion-Exchanger Regenerator

from the rest of the system before pressurizing. 3/8" O.D. gage 20 stainless steel tubing was used throughout the loop. Figure 20 shows the degassification system which consists of the following components.

a. Degassification Tank

A 15 gal. stainless steel tank was used for storage and degassification. It was equipped with a liquid level gage and a filling port. The tank was insulated to minimize the loss of heat to the surroundings.

b. Electric Heater

A 2.5 kw stainless steel electric immersion heater was installed at the bottom of the degassifier tank. The heater, Chromalox catalog No. MTS-225 B, is manufactured by the Edwin L. Wiedgand Co., Pittsburgh, Pa. It was controlled by a General Radio Variac.

c. Condenser

To prevent steam from being vented with the air, a condenser was installed in the degassifier. The condenser consists of 8 ft of 1/8" O.D. gage 22 stainless steel tubing. It is housed inside a one ft. long size 2" stainless steel pipe welded to the top of the degassification tank. City water was used as the cooling fluid in the condenser.

4. Pressurizing System

A nitrogen charged hydraulic accumulator was employed to pressurize the system. A 5 gal. "Bladder"

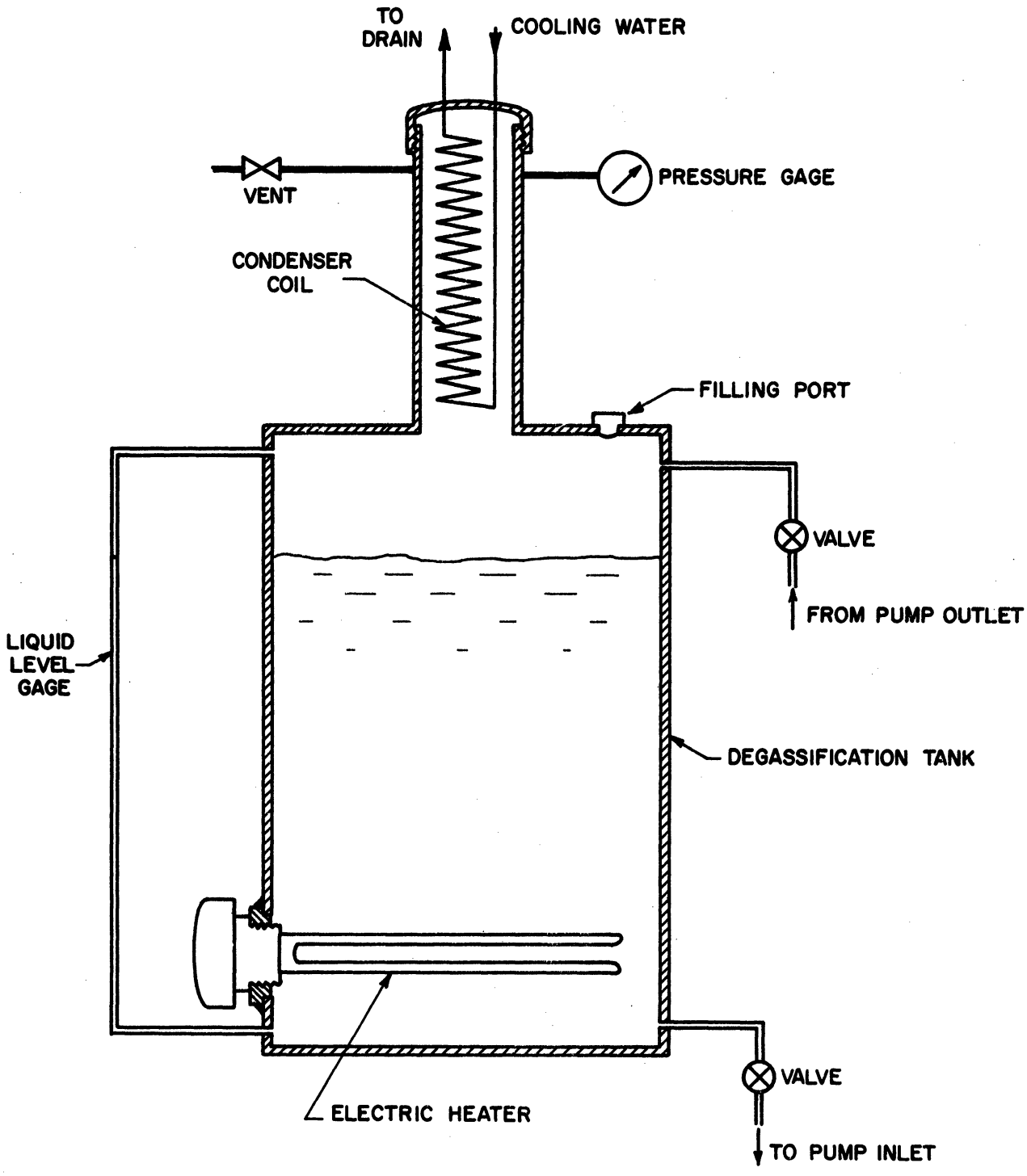

Figure 20. Degassification System

type, 3000 psi water service Greer Hydraulic accumulator (Model 30"-5WS) was selected for this purpose. This type of accumulator has a separator bag made of synthetic compound (Buna N) which separates the nitrogen from system fluid. The discharge port assembly is made of stainless steel while the shell is made of alloy steel (SAE 4130) coated on the inside with Lithcote LC-24. This material is a phenol-formaldehyde, spirit-soluble resin suitable for distilled water applications.

The accumulator was equipped with a valve and gage assembly for charging it when it is desired to pressurize the system. A relief valve was used to discharge the nitrogen to lower system pressure. Figure 21 shows how the accumulator is constructed and Figure 22 is a schematic diagram of the pressurizing system.

5. Safety System

Several safety devices were incorporated in the system. A stainless steel rupture disc assembly (American Instrument Co., Cat. No. 45-9106) was assembled with the main loop. The disc was designed to rupture if system pressure exceeds 1500 psi. A pressure relief valve (Farris Engineering Corp. Type 2745) was connected to the nitrogen line and was adjusted to relieve the nitrogen if system pressure (or nitrogen line pressure) exceeds a pre set limit. This limit was usually set at

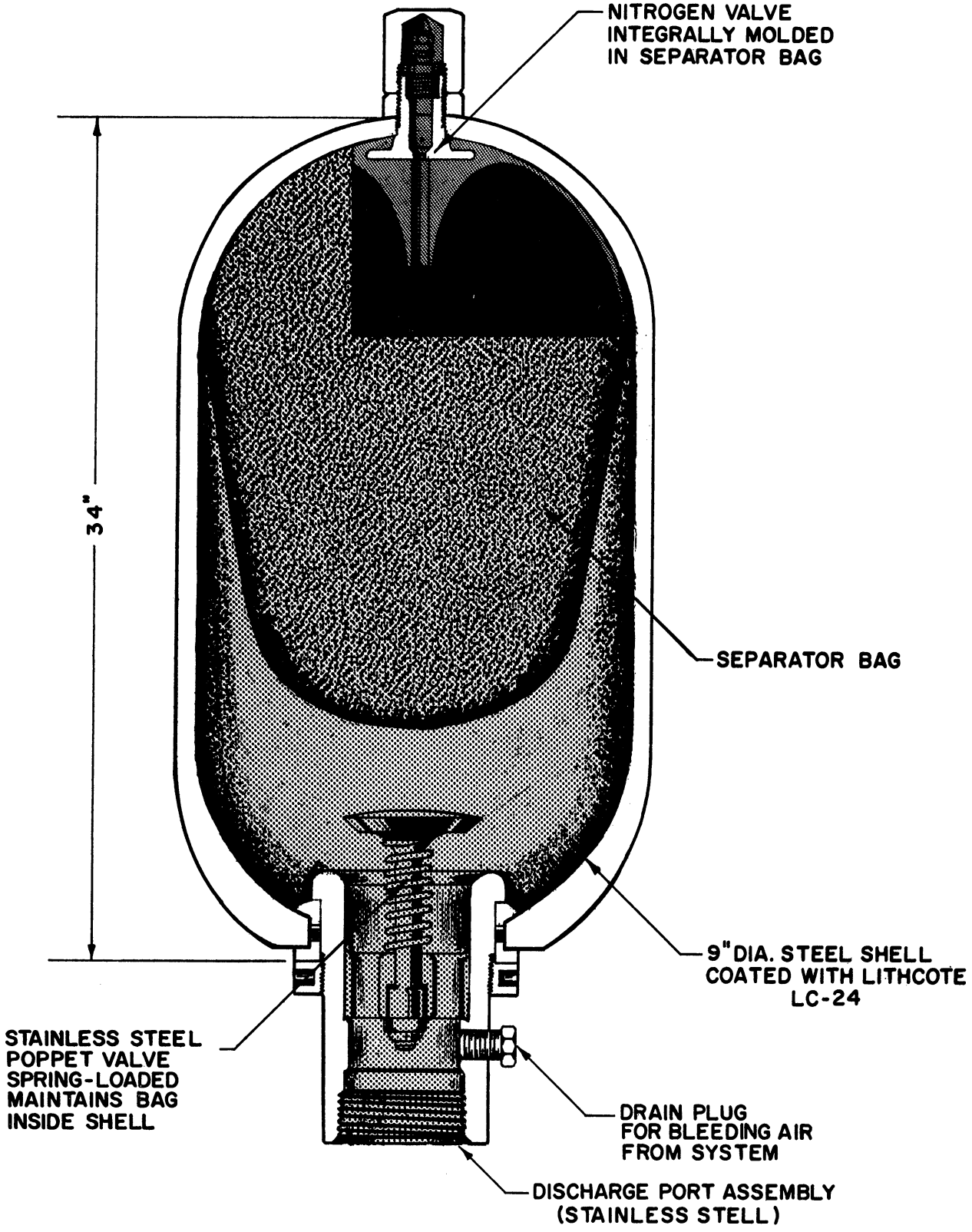

Figure 21. Accumulator

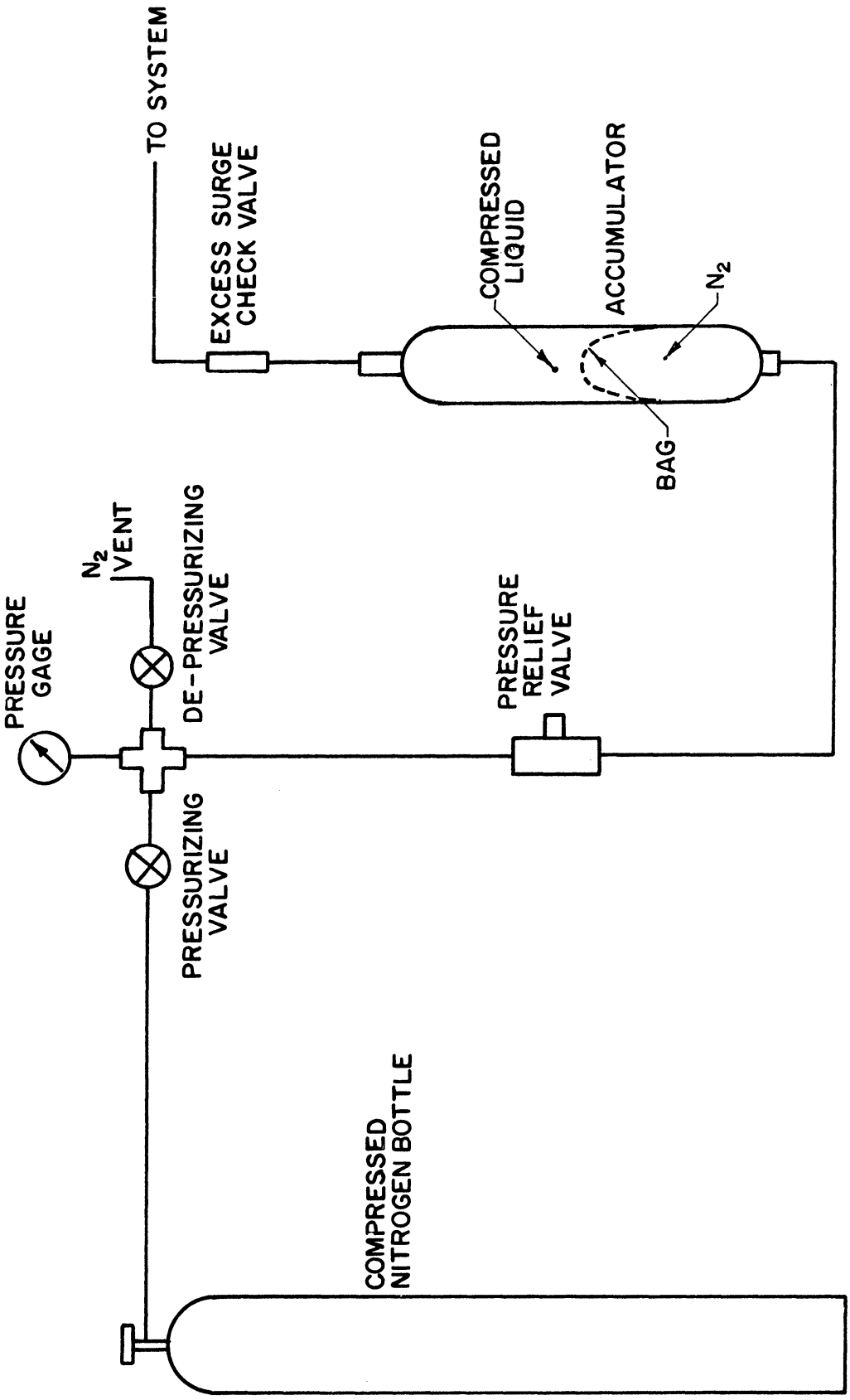

Figure 22. Schematic Diagram of the Pressurizing System

approximately 100 psi above test pressure.

An excess surge check valve (Autoclave Part No. 10K-6602) was installed at the accumulator liquid discharge line. The purpose of this valve was to prevent the compressed liquid within the accumulator from discharging when a sudden drop in system pressure takes place (such as a sudden leak, disc rupture or test section glass breakage).

A removable steel guard 1/8" thick was placed around the test section. This guard has two 9" x 14" glass windows to permit observation of the test section. Each window was made of two glass layers; a $\frac{1}{2}$" auto safety plate glass and a $\frac{1}{2}$" "Tuf-Flex" (Libbey-Owens-Ford) glass.

6. Power Supply

The strip was supplied with D.C. electric power by a 50 kw transformer-rectifier manufactured by Hansen-Van Winkle Munning Co. Rated maximum continuous output of this unit is 2000 amp at 25 volts. It is equipped with a remote control apparatus which is used to control the power supply to the strip.

7. Photographic Apparatus

Photographs of the test section channel were taken with a 4" x 5" Graphex camera. Camera setting of f = 11 and Kodak Royal Pan pahchromatic film were used

for all photographs. The test section channel was back lighted with two General Electric Photolights (cat. No. 9364688G). It was found necessary to use two photolights in order to photograph the whole channel. These photolights have an effective light duration of 2×10^{-6} sec. A 12" x 16" opaque plate glass was placed between the photolights and the test section to diffuse the light and give uniform brightness throughout the channel.

C. Instrumentation and Measurements

1. Heat Flux

The heat flux was calculated from measurements of current and voltage. Current through the strip was measured by means of a current shunt rated at 50 mv at 2000 amp. Voltage leads were taken from the strip end blocks at two points as close as possible to the leading and exit ends of the strip. By means of a bridge circuit the voltage drop between these two points was reduced by a factor of 2000. This voltage was measured with a precision potentiometer (Leeds and Northrup Model 8662). The two voltage lead wires, shown in Figure 9, were discharge-welded to the strip end blocks after the strip was assembled inside the test section. Two stainless steel packing glands with Teflon sealant were used to seal the wires and pass them through the test section. Because it was not possible to weld the lead

wires exactly at the leading and exit ends of the strip, it was necessary to estimate the small voltage drop through the end blocks. This drop, which amounted to 1.3% of the strip voltage drop, was calculated from the measured current and the resistivity of blocks.

2. Inlet Velocity

The inlet velocity to the strip was calculated from the continuity equation. The flow rate was measured with a stainless steel turbine type flowmeter (Potter Model 1/4 - 1029A) located in the main loop. The flowmeter output frequency, which is proportional to the volumetric flow rate, was measured with an electric counter (Hewlett-Packard Model 522B).

3. Inlet Pressure

The pressure at the inlet to the test section was measured with a 12" dial, 0-1500 psi Heise Gage manufactured by the Heise Bourdon Tube Co., Inc., Newtown, Conn. This gage has 750 graduations and is accurate to within 0.1 of 1% of full scale at any point on the dial.

4. Temperature Measurements

a. Thermocouples

The test section was instrumented with ten thermocouples all of which, except the outlet thermocouple, were designed to traverse the flow channel. The inlet thermocouple was placed 1/16" upstream of the leading edge

of the strip while the outlet thermocouple was installed approximately 6" downstream of the exit end of the strip. It was found that sufficient mixing of the fluid was not achieved at the exit thermocouple and it was decided to install two other exit thermocouples, one 12" downstream from the exit end of the strip and another at 30". Eight traversing thermocouples, assembled one inch apart, were located in the heated channel. The first thermocouple was placed 1" downstream from the leading edge of the strip. Figure 23 shows the location of these thermocouples. Chromel-constantan 30 gage thermocouple probes were used for all temperature measurements in the test section. The wires are ceramic insulated within a stainless steel sheath 1/16" O.D. The hot junction is exposed for a length of 9/16" to obtain fast response and to minimize flow disturbance. The thermocouple probes (Aeropack Thermocouples) were supplied by Aero Research Instrument Co., Inc., Chicago, Ill. Figure 24 is a drawing of the thermocouple probe.

Since all thermocouples were made from the same spools of wire only one was calibrated by the manufacturer. Table I gives the manufacturer calibration data. A laboratory check at the steam point for all thermocouples showed a maximum deviation emf of 0.005 mv. An isothermal

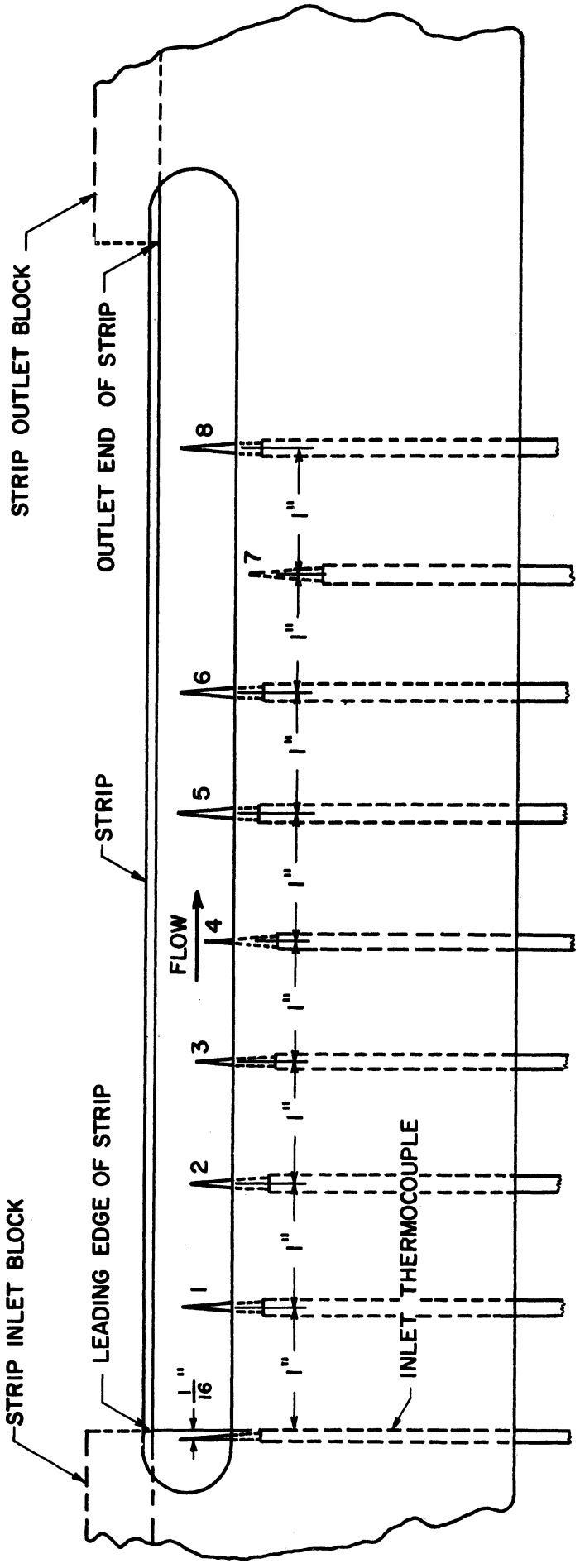

Figure 23. Test Section Traversing Thermocouple Locations

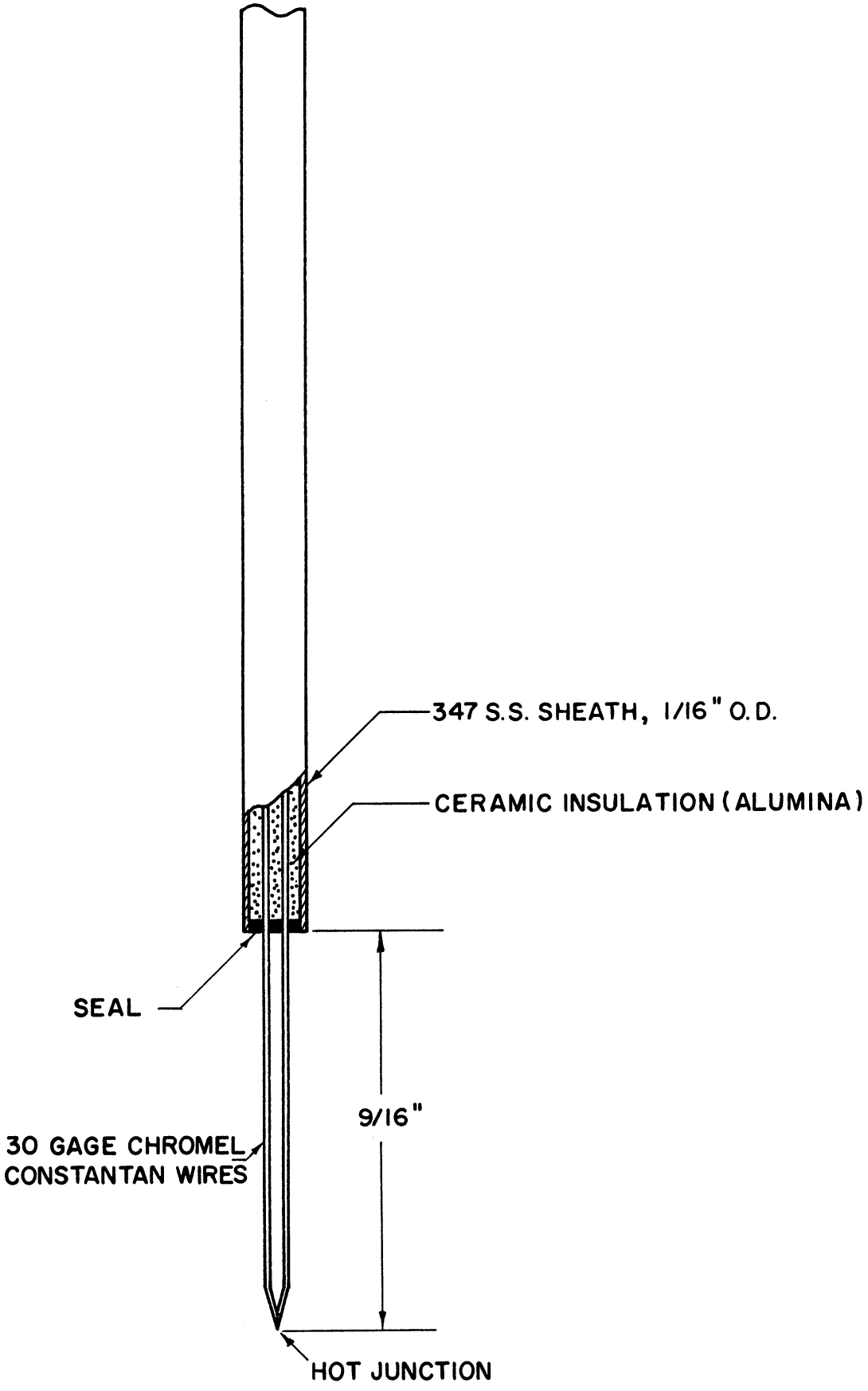

Figure 24. Thermocouple Probe

test was carried out to check the thermocouples at 300°F. All readings checked to within 0.2 per cent.

TABLE I

CALIBRATION DATA FOR THE TRAVERSING THERMOCOUPLES

Observed temperature (°F)	Observed emf (mv)	Standard emf (mv)	Deviation emf (mv)
211.2	6.294	6.331	0.037
544.1	19.835	19.836	0.001
800.8	31.125	31.158	0.033

b. Thermocouple Traversing Mechanism

To make temperature profile measurements of the fluid in the test section channel, a mechanism was designed to traverse each thermocouple individually from the unheated side of the channel to the strip surface. Figure 25 illustrates how the thermocouple probe was sealed while traversing the channel. A stainless steel packing gland with Teflon sealant was used for this purpose. With this arrangement it was possible to traverse the thermocouple probe assembly without any leakage at pressures up to 800 psia. A set screw was used to drive the probe toward the strip surface while system pressure

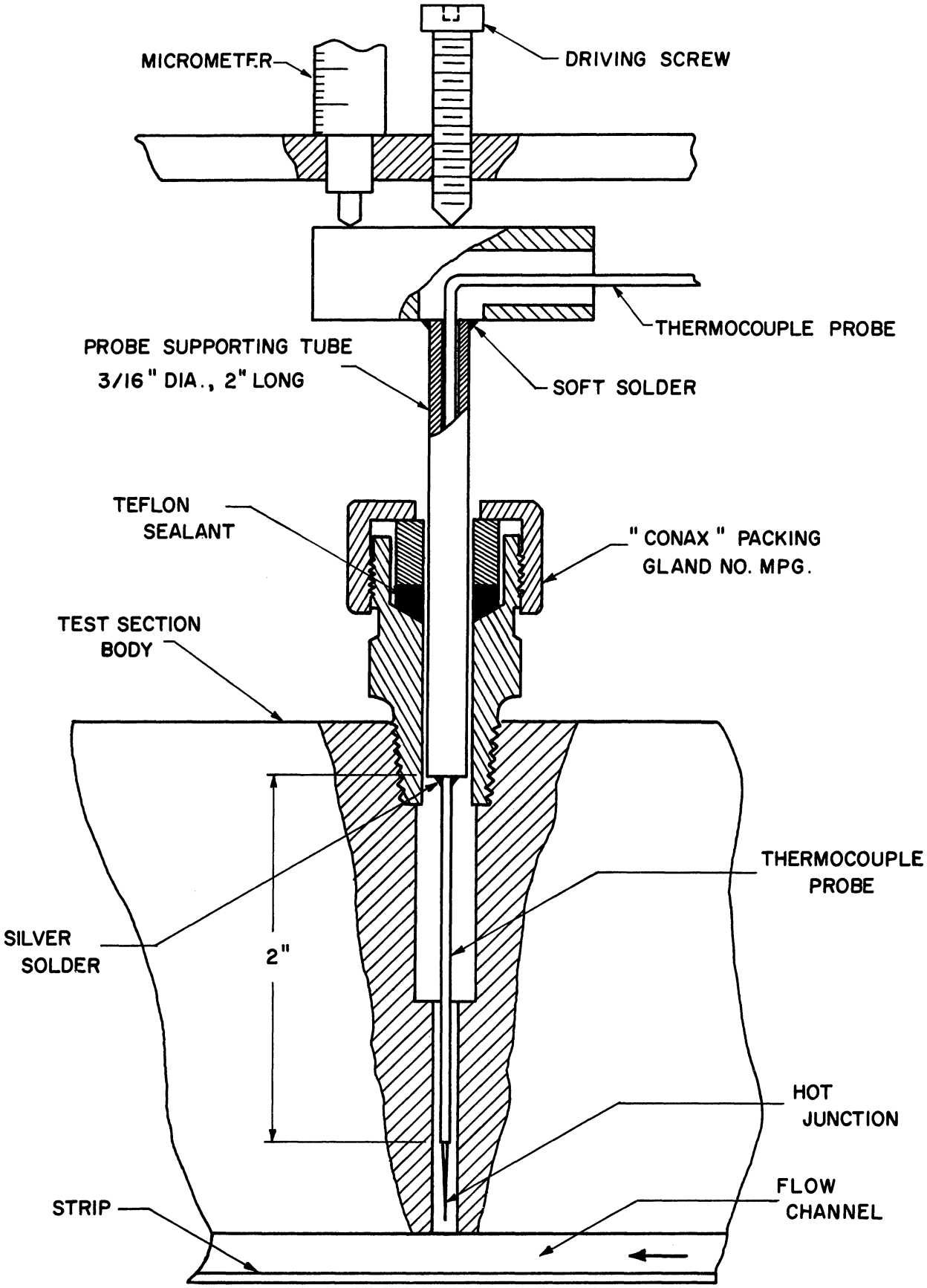

Figure 25. Driving Mechanism and Sealing Gland for the Traversing Thermocouples

was utilized in forcing the probe away from the strip surface. Each driving mechanism was equipped with a micrometer to indicate the position of the hot junction with respect to the strip surface.

c. Measuring and Recording Instruments

Thermocouple emfs were measured with a Leeds and Northrup Model 8662 potentiometer. Double pole, double throw copper knife switches were used so that all test section thermocouples can also be recorded with a recording galvanometer (Minneapolis-Honeywell Visicorder Model 1012). The galvanometers used were Heiland type No. 40-120 with a voltage sensitivity of approximately 1.0 in/mv. This corresponds to approximately 25°F/in.

5. Bubble Boundary Layer Measurements

To minimize inaccuracies in bubble boundary layer measurements each photograph was projected on a screen and enlarged by a factor of approximately 3. A trace of the bubbles and the channel was made from the projected image and a best fit curve was drawn to describe the bubble boundary. The thickness of the bubble boundary was then measured with a scale from the enlarged trace.

6. Electric Resisitivity

A portable conductivity cell and bridge were used to measure the electric resistivity of the water. This

instrument has a resolution of approximately ± 5% at 1×10^6 ohm-cm.

7. Control Panel

To facilitate operation of the system all valves, switches and gages were mounted on an 8' x 10' panel. A photograph of the control panel is shown in Figure 26 and a schematic diagram is shown in Figure 27.

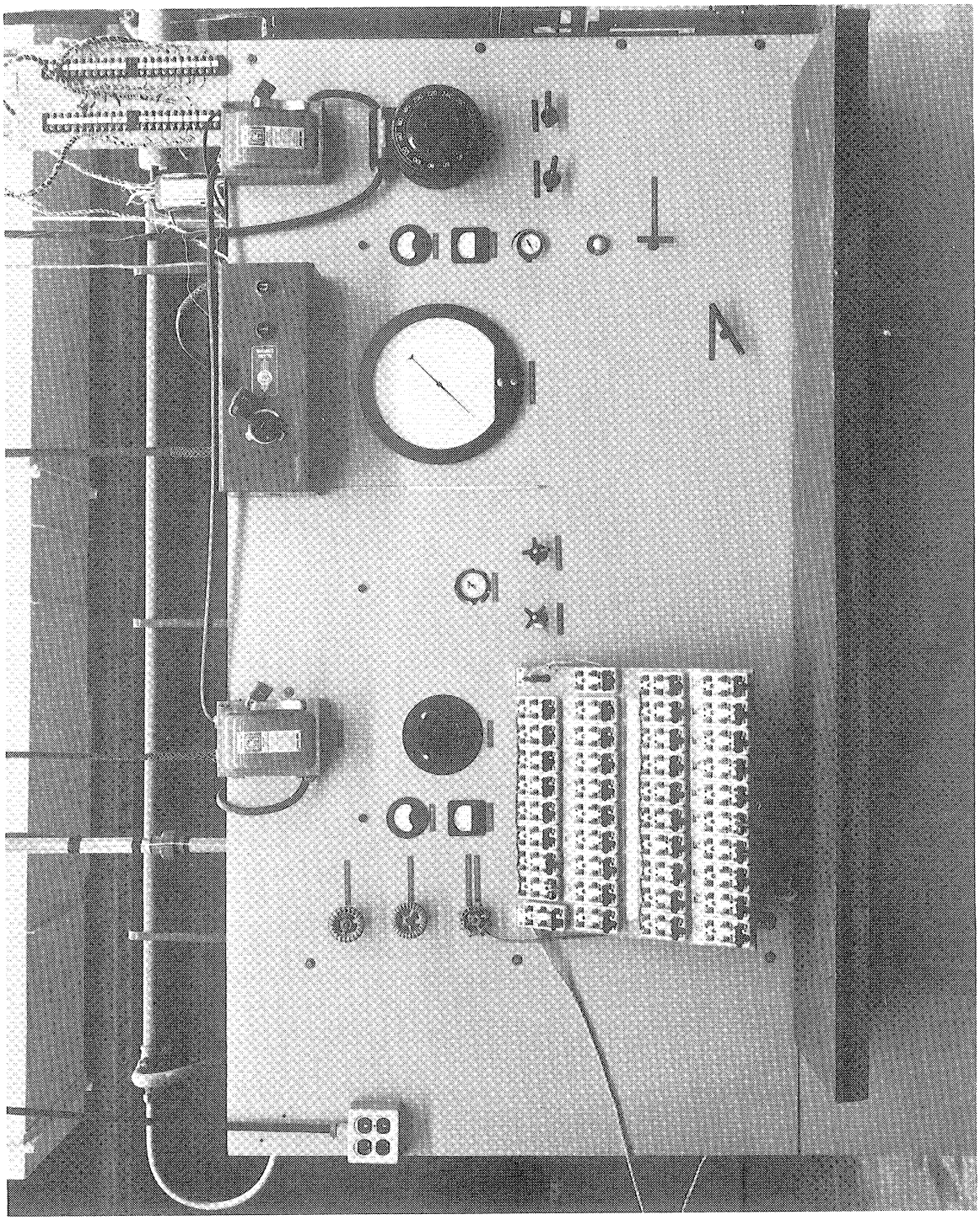

Figure 26. Photograph of the Control Panel

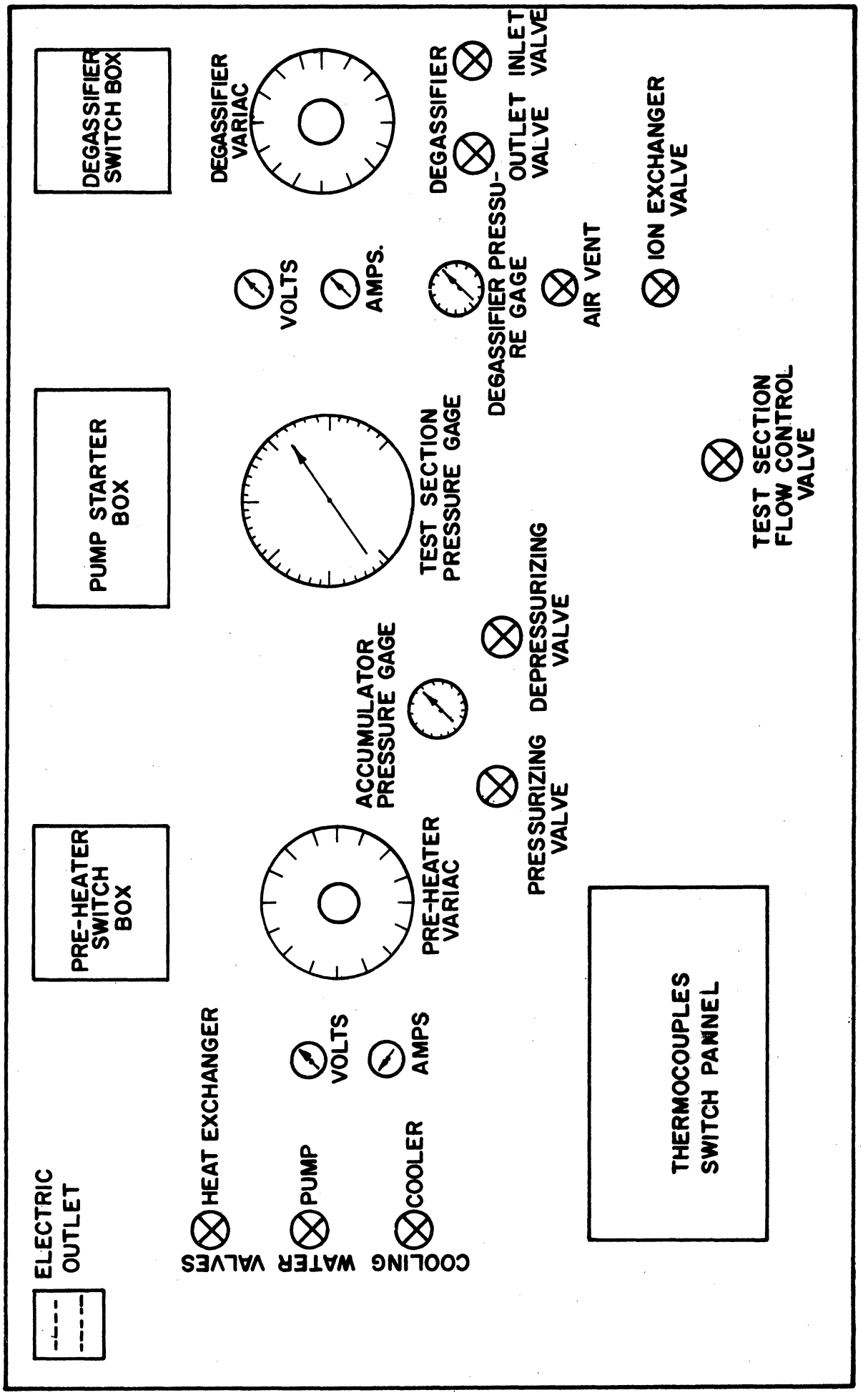

Figure 27. Schematic diagram of the Control Panel

CHAPTER IV

TEST PROCEDURE

A. Preliminary Preparations

The system was filled with distilled water and then pressurized to approximately 60 psig. After turning the circulation pump on, the inlet pressure was then maintained at 40 psig. Cooling water to the ion-exchanger cooler was turned on to maintain the inlet temperature to the ion-exchanger below 140°F. Maximum flow was maintained through the main loop and ion-exchanger loop (flow control valves fully open) while the flow through the degassifier loop was shut-off. The preheater was then turned on and adjusted to maintain the system at approximately 210°F. The degassifier heater was turned on while the air vent valve was left open. After all the air in the degassifier was vented, the valve was closed and the degassifier pressure was allowed to build up to approximately 30 psig. Degassifier flow control valve was then opened and degassification of system water was continued for approximately 2½ hours. In another boiling investigation Clark and Rohsenow (6) found that a period of 3/4 hours was sufficient to reduce the oxygen content to approximately 1.5 ml air/l. The degassifier loop was then shut-off from the main system by closing the two degassification valves.

Power to the strip was turned on after the desired test pressure, velocity, and subcooling were established. By controlling the preheater, the inlet temperature to the strip was maintained at the desired test value.

A 4" x 5" Polaroid photograph was taken to detect boiling. If no bubbles could be detected the heat flux was increased and another photograph was taken. This process was repeated until bubbles appeared at the exit end of the strip.

B. Measurements and Data Recording

After steady state was reached the pressure, flowmeter frequency, voltage, current, inlet and outlet temperatures were recorded and a photograph was taken. Each traversing thermocouple was individually moved through the channel and temperature measurements were made at eleven locations. Because the temperature gradient is high near the strip surface, measurements were made at 0.01", 0.025" and 0.05" from the surface. The other eight measurements were made at 0.05" intervals. At each location the temperature was first recorded on the "Visicorder" and then measured with the potentiometer.

At the end of each test a water sample was taken from the system and its electrical resistivity was measured and recorded.

C. Range of Variables

To determine the effect of pressure, velocity, subcooling and heat flux on incipient boiling and the bubble boundary layer, tests were conducted such that the pressure, velocity, and subcooling were held constant while the heat flux was varied. The range of variables covered is listed in Table II.

TABLE II

RANGE OF VARIABLES COVERED IN EXPERIMENTAL TESTS

Pressure (psia)	Subcooling (°F)	Velocity (ft/sec)	Heat flux range (BTU/hr-ft^2)
200	50,100,200	1,3,5,6	0.19×10^6 - 1.5×10^6
500	100,200,300	1,3,5,6	0.14×10^6 - 1.4×10^6
800	100	1,3,5	0.16×10^6 - 0.73×10^6
1000	200	1	0.26×10^6 - 0.92×10^6

In all tests the electrical resistivity ranged between 1 and 2 megohm.

CHAPTER V

RESULTS

A. Incipient Boiling

1. Introduction

Incipient boiling as defined here shall mean the initial appearance of observable bubbles over a heated surface. The point of incipient boiling is the location along the surface where bubbles first appear. The distance from the leading edge to this point is referred to as the incipient distance. The point of incipient boiling was detected by visual inspection of full scale photographs of the boiling liquid. While this point was not sharply defined, nevertheless, it was possible, in general, to ascertain its location to within $\pm \frac{1}{2}$ in. Typical photographs are shown in Figures 28 and 29 in which the incipient distance X_I is 4.5 and 0.9 in. respectively. These are photographs of two tests in which all variables were held constant except the heat flux. It is noted that increasing the heat flux causes the point of incipient boiling to move towards the leading edge.

2. Comparison with Theoretical Incipient Heat Flux

For each test the incipient distance was measured from the photograph and the corresponding heat flux was

P_i = 500 Psia

V_i = 3.5 ft/sec

$T_{sat}-T_i$ = 200°F

$q/A = 0.848 \times 10^6$ BTU/hr-ft^2

X_I = 4.5 in.

Scale: Distance between thermocouples = 1 in.

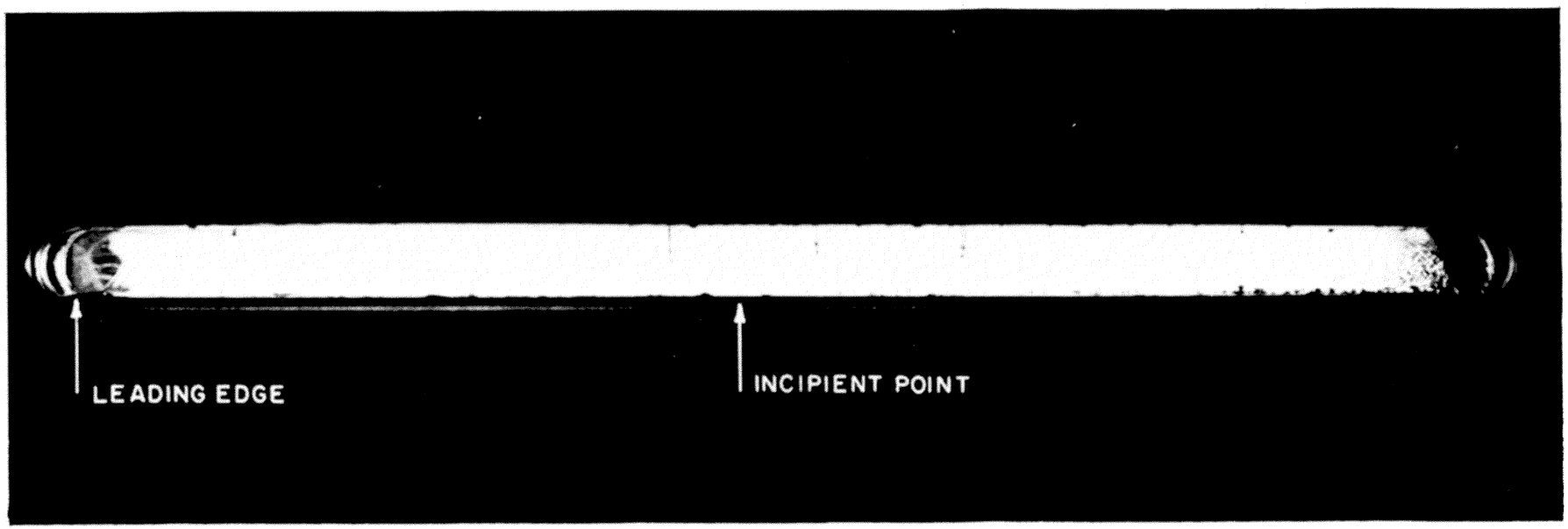

Figure 28. Typical Photograph Showing the Incipient Point at X_I = 4.5 in.

P_i = 500 psia

V_i = 3.5 ft/sec

$T_{sat}-T_i$ = 200°F

$q/A = 1.382 \times 10^6$ BTU/hr-ft^2

X_I = 0.9 in.

Scale: Distance between thermocouples = 1 in.

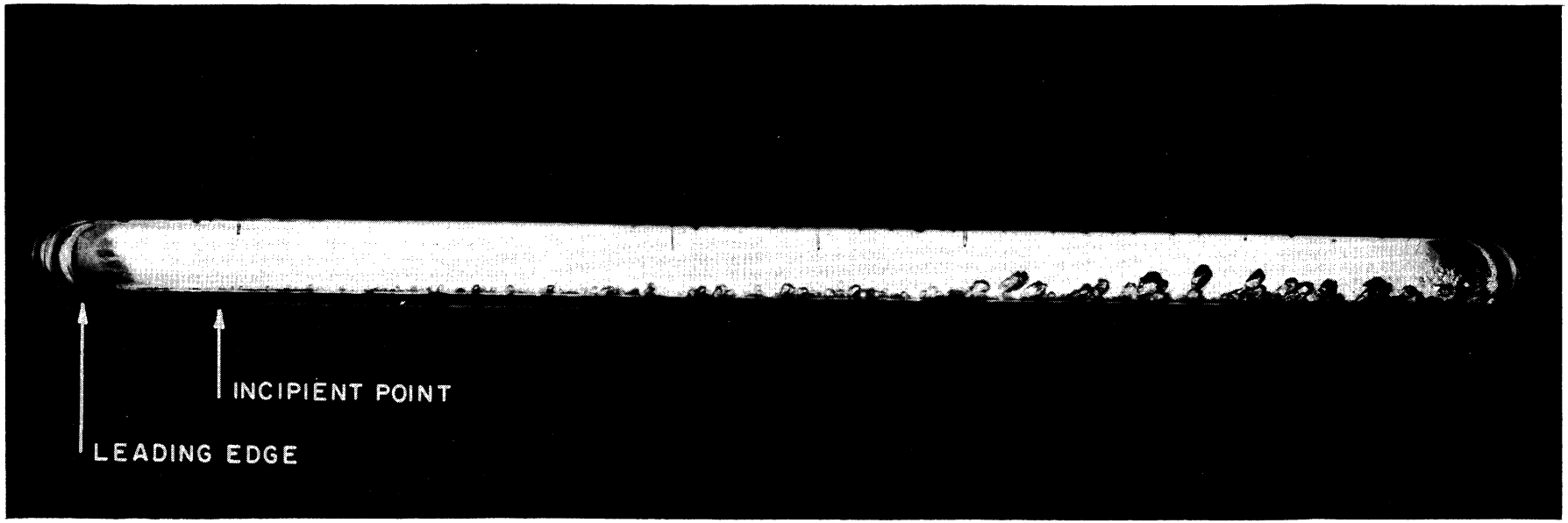

Figure 29. Typical Photograph Showing the Incipient Point at X_I = 0.9 in.

calculated. Equation (5) was then used to calculate the theoretical heat flux, for the same test conditions, which will initiate boiling at the same point. This was done for all tests and it was found that the theoretical heat flux, as predicted by Equation (5), is always less than the actual heat flux. In general, Equation (5) under estimates the incipient heat flux by a factor of approximately 3. Figure 30 is a plot of the ratio of actual to theoretical incipient heat flux vs. incipient distance for all tests. This ratio is approximately equal to 4 at X_I = 0.5 in. and 2.8 at X_I = 7 in. Because of this discrepancy it was decided to investigate the extent to which the assumption that the surface temperature at the point of incipient boiling is equal to saturation temperature may have contributed to this disagreement.

Jens and Lottes (49) summarized experiments by Rohsenow and Clark (12) and Buchberg, et al.(41) on surface boiling of water flowing in vertical stainless steel tubes and correlated their data on surface temperature by the following dimensional equation

$$T_w = T_{sat} + \frac{1.9\ (q/A)^{\frac{1}{4}}}{e^{P/900}} \qquad (8)$$

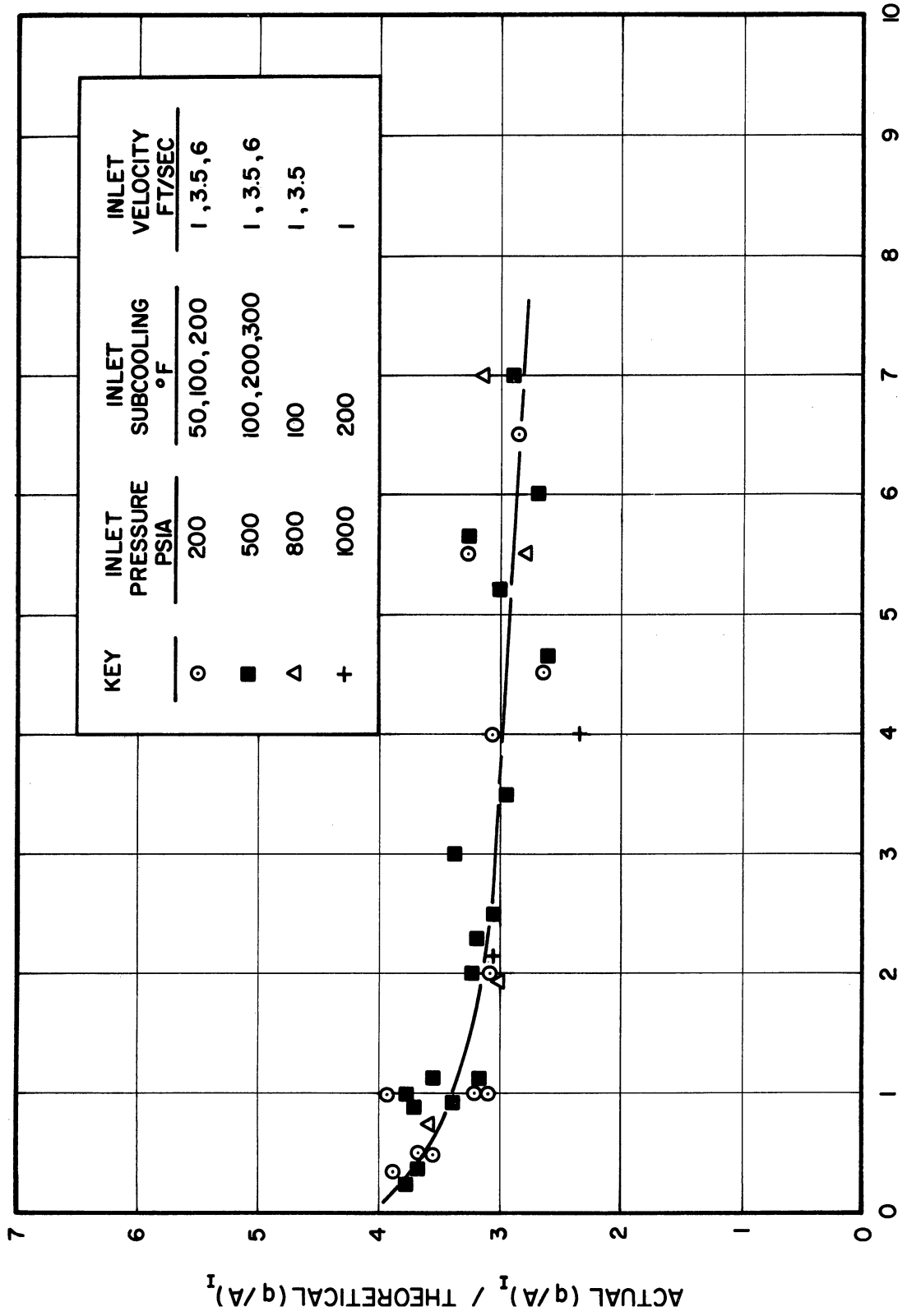

Figure 30. Comparison Between Actual Incipient Boiling Heat Flux and the Theoretical Flux Based on Surface Temperature Equal to Saturation Temperature

While the assumption that at the inception of boiling the surface temperature is equal to saturation temperature is a conservative estimate of T_w , Equation (8) over estimates it. When Equations (3) and (8) are substituted in Equation (2) the following is obtained

$$(q/A)_I = \frac{h_x(T_{sat} - T_i)}{1 + h_x \frac{b X_I}{C_p W}} + \frac{1.9 h_x \, e^{-P/900}}{1 + h_x \frac{b X_I}{C_p W}} (q/A)_I^{\frac{1}{4}} \qquad (9)$$

Figure 31 shows the effect of assuming a higher surface temperature than saturation on the incipient heat flux for a typical inlet state. The incipient heat flux $(q/A)_I$ for every test was calculated from Equation (9) and compared with the actual flux. The result is plotted in Figure 32 as the ratio of the two fluxes vs. X_I. While the overall effect of assuming a surface temperature which is greater than the saturation temperature is an improvement in predicting $(q/A)_I$, Equation (9) still under estimates the incipient heat flux by a factor of approximately 2.5 (as compared with 3 for $T_w = T_{sat}$). This indicates that the large discrepancy between actual and predicted $(q/A)_I$

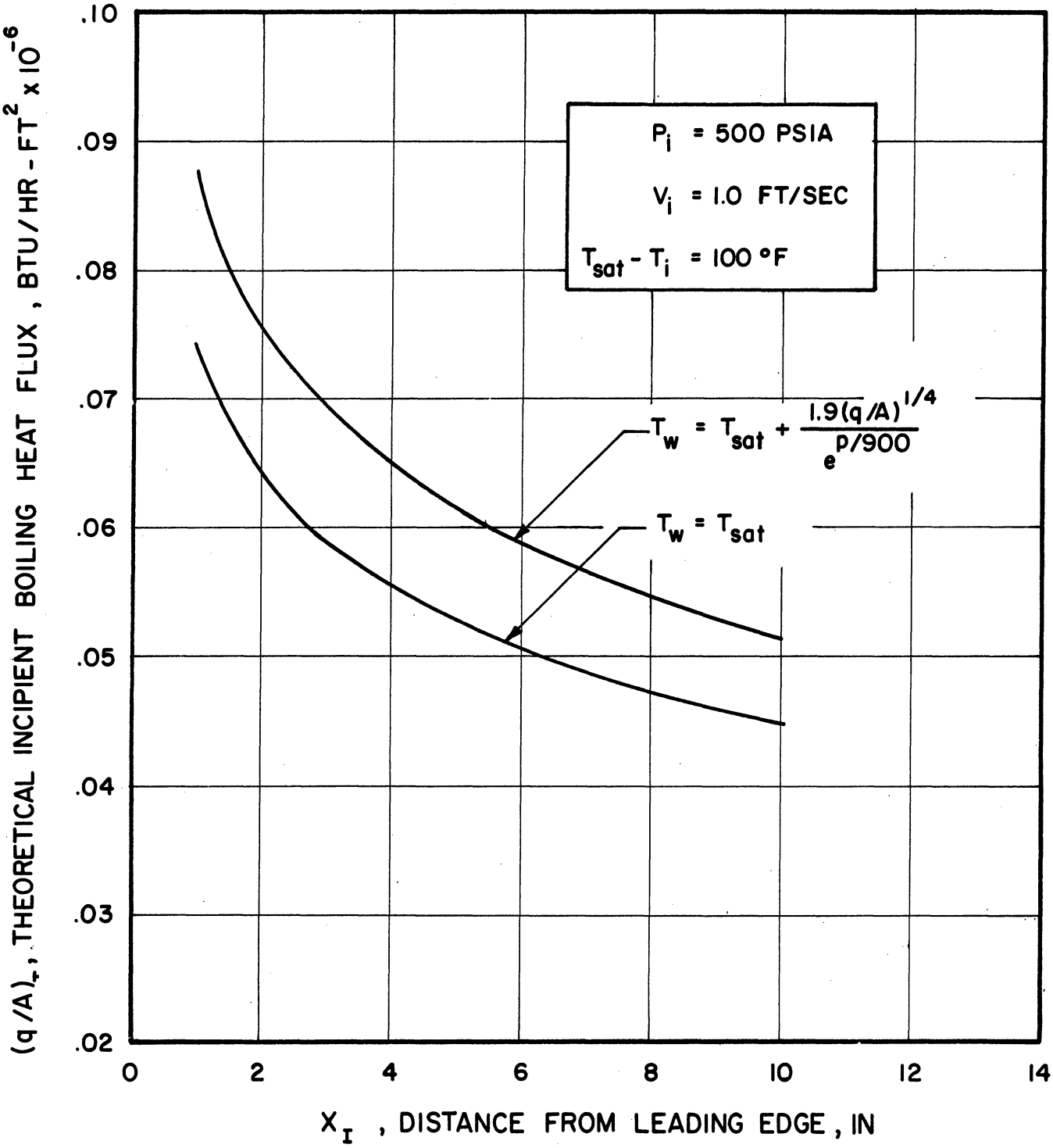

Figure 31. The Effect of Assumed Surface Temperature on Incipient Boiling Heat Flux

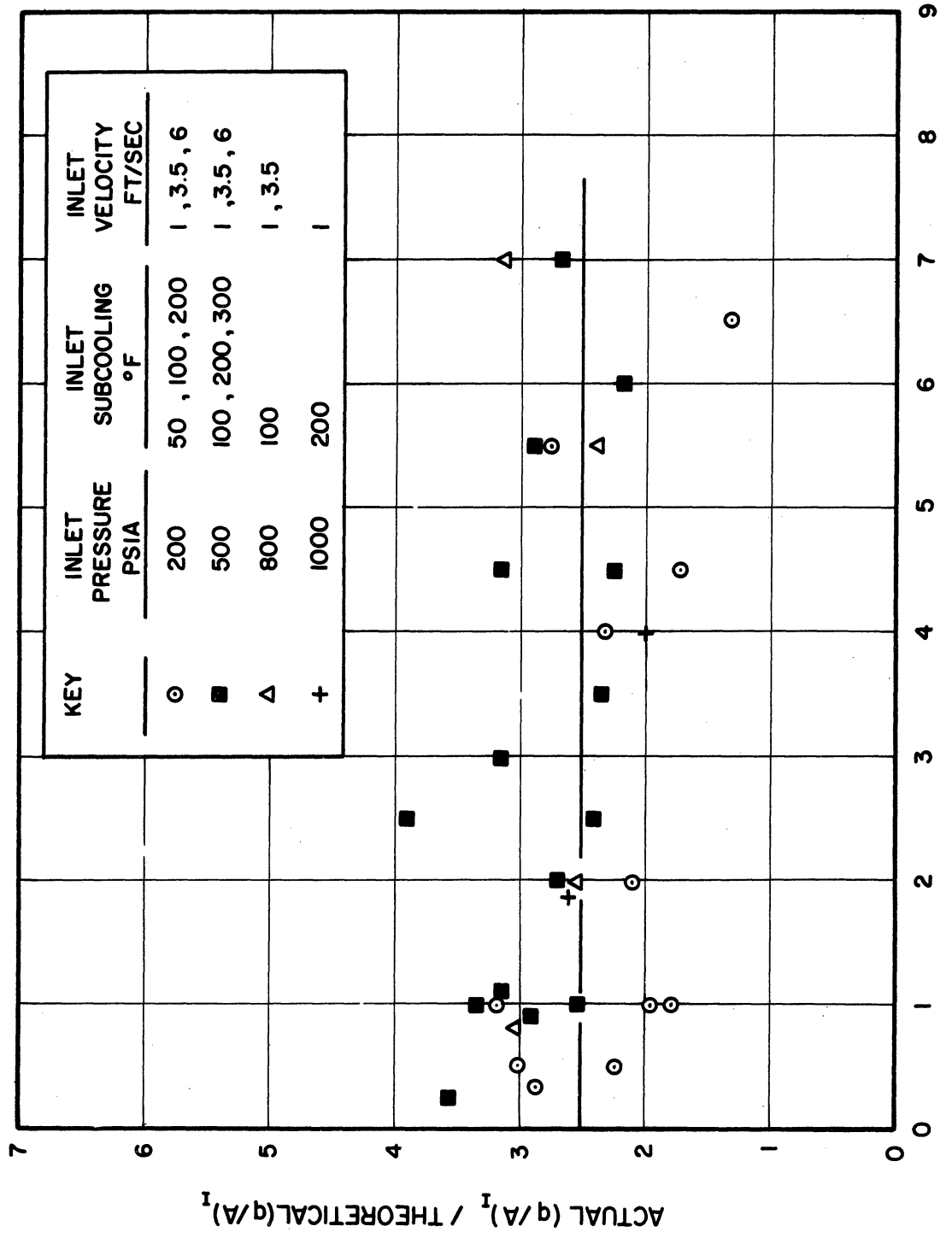

Figure 32. Comparison Between Actual Incipient Boiling Heat Flux and Theoretical Flux Based on Jens and Lottes Surface Temperature Correlation

cannot be attributed to an erronious assumption of the surface temperature. The disagreement is due to the fact that a higher flux is required to facilitate detection of bubbles by visual observation than that which is necessary to initiate them. It is therefore possible that nucleation of bubbles actually does take place at the flux predicted by Equation (5) but in order to detect the bubbles by visual observation this flux must be increased by a factor of approximately 3.

3. Correlation of Incipient Boiling Heat Flux

Examination of Figure 30 suggests that even though Equation (5) under estimates $(q/A)_I$, a simple relation exists between theoretical and actual incipient heat flux.

Since bubbles may be present but cannot be observed at $0 < X < X_I$, it follows that the actual heat transfer coefficient h_x is greater than that described by Equation (6). It was found that a reasonably good correlation for incipient boiling data is obtained when this value of h_x is multiplied by a factor of 3.33. Further refinement in the correlation equation was obtained when the factor $(X_I/4H)^{0.08}$ was introduced into Equation (5). H is the height of the channel, or the spacing between the heated and the adiabatic surface. Thus, the physical significance of $(X_I/4H)$ is that it represents the number

of equivalent diameters for the flow between two heated plates with a spacing of 2H. The resulting correlation equation is therefore

$$\left(q/A\right)_I = \frac{3.33\, h_x (T_{sat} - T_i)}{1 + 3.33 h_x \frac{bX_I}{\omega C_p}} \left(\frac{X_I}{4H}\right)^{-0.08} \qquad (10)$$

where h_x is given by Equation (6). Equation (10) correlates the incipient boiling heat transfer data for all tests to within $\pm$ 15 per cent as shown in Figure 33. Comparison between actual incipient heat flux and that predicted by correlation equation (10) for several tests is shown in Figures 34 through 41.

B. Bubble Boundary Layer

1. Introduction

The bubble boundary layer is defined as the two-phase region adjacent to a heated surface in forced convection boiling. The boundary of this region is defined by a line which separates the single-phase liquid core from the bubble boundary layer as shown in Figure 42. The bubble boundary thickness δ is the distance from

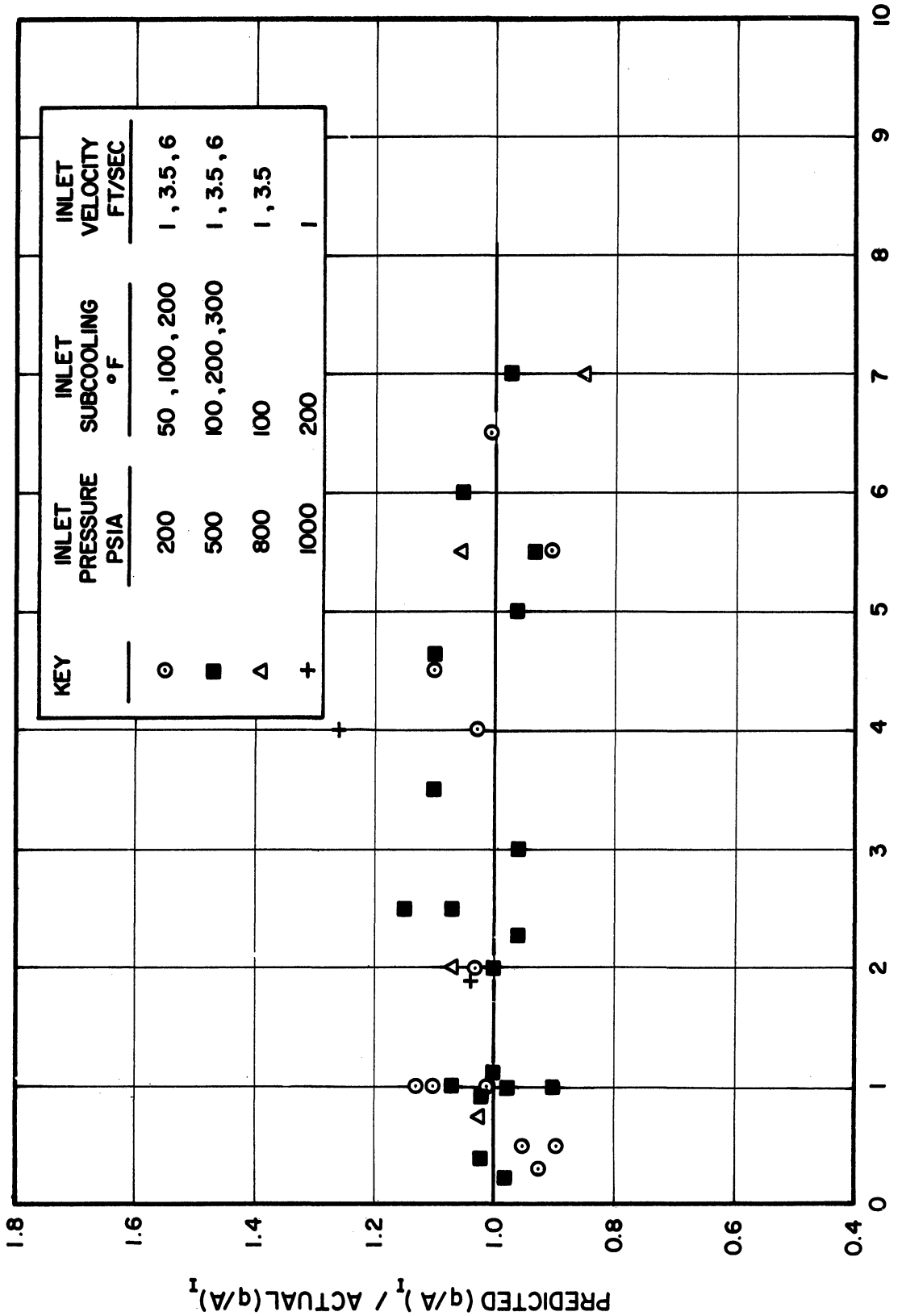

Figure 33. Comparison Between Predicted and Actual Incipient Boiling Heat Flux

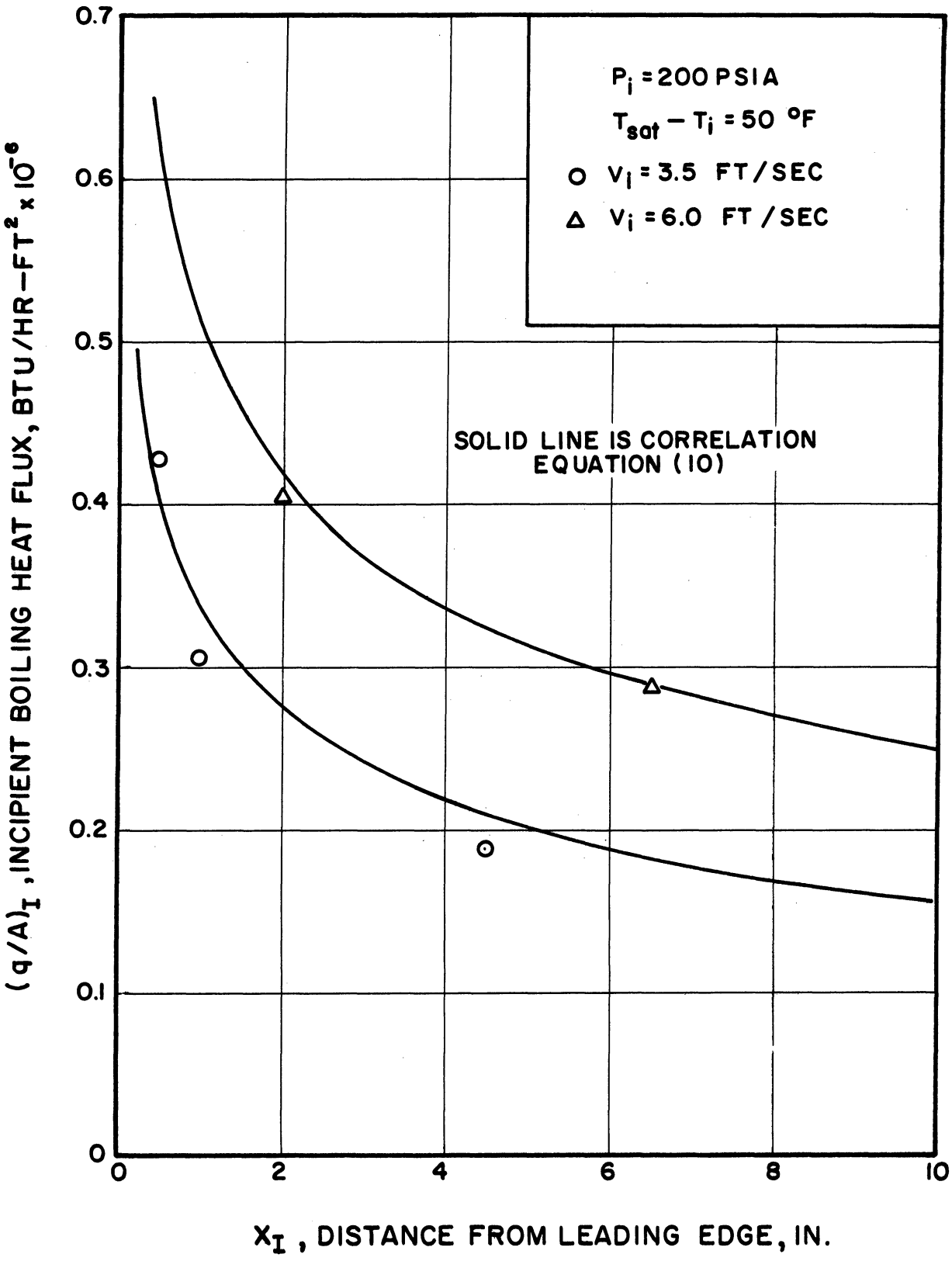

Figure 34. Incipient Boiling Heat Flux vs. Incipient Distance

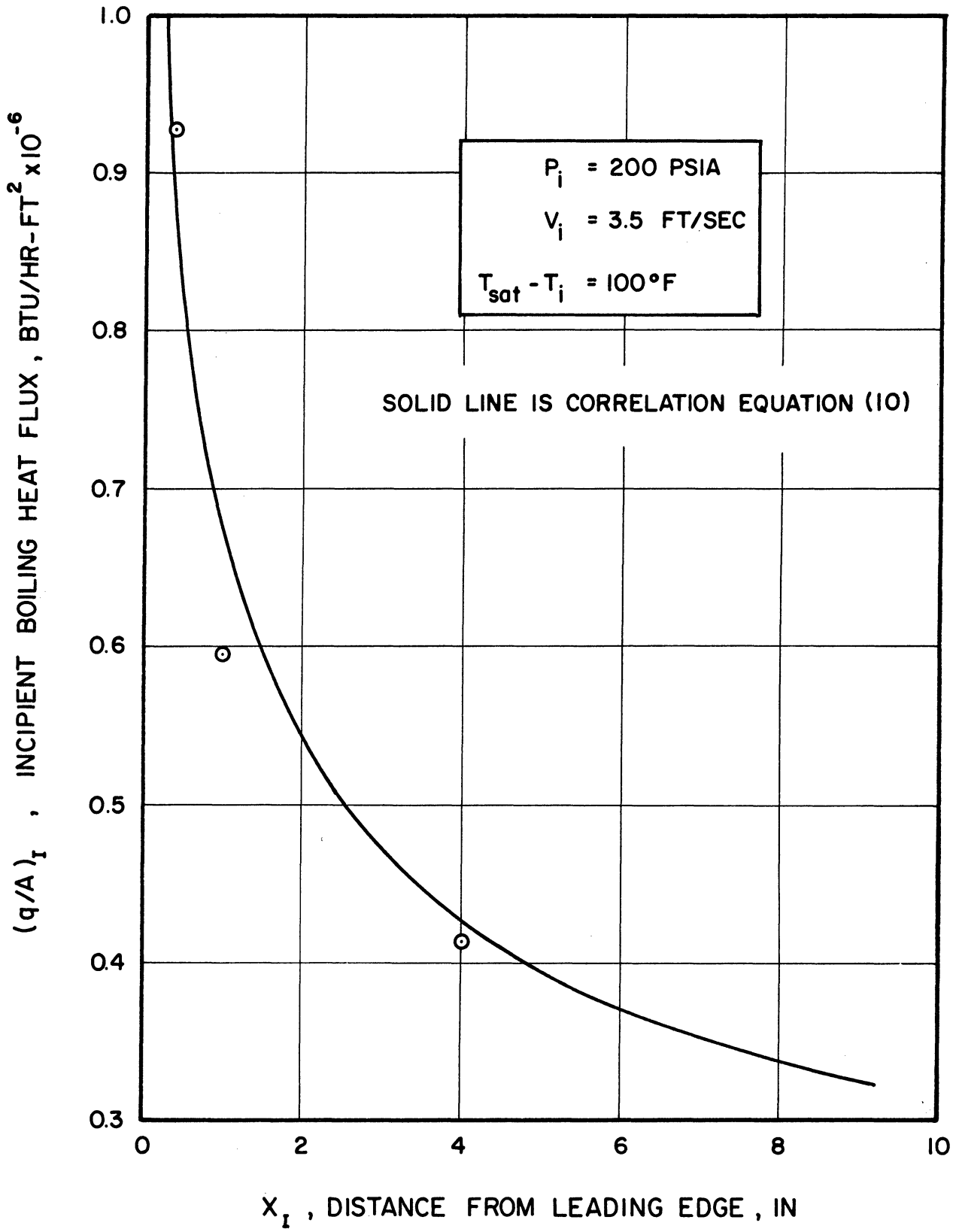

Figure 35. Incipient Boiling Heat Flux vs. Incipient Distance

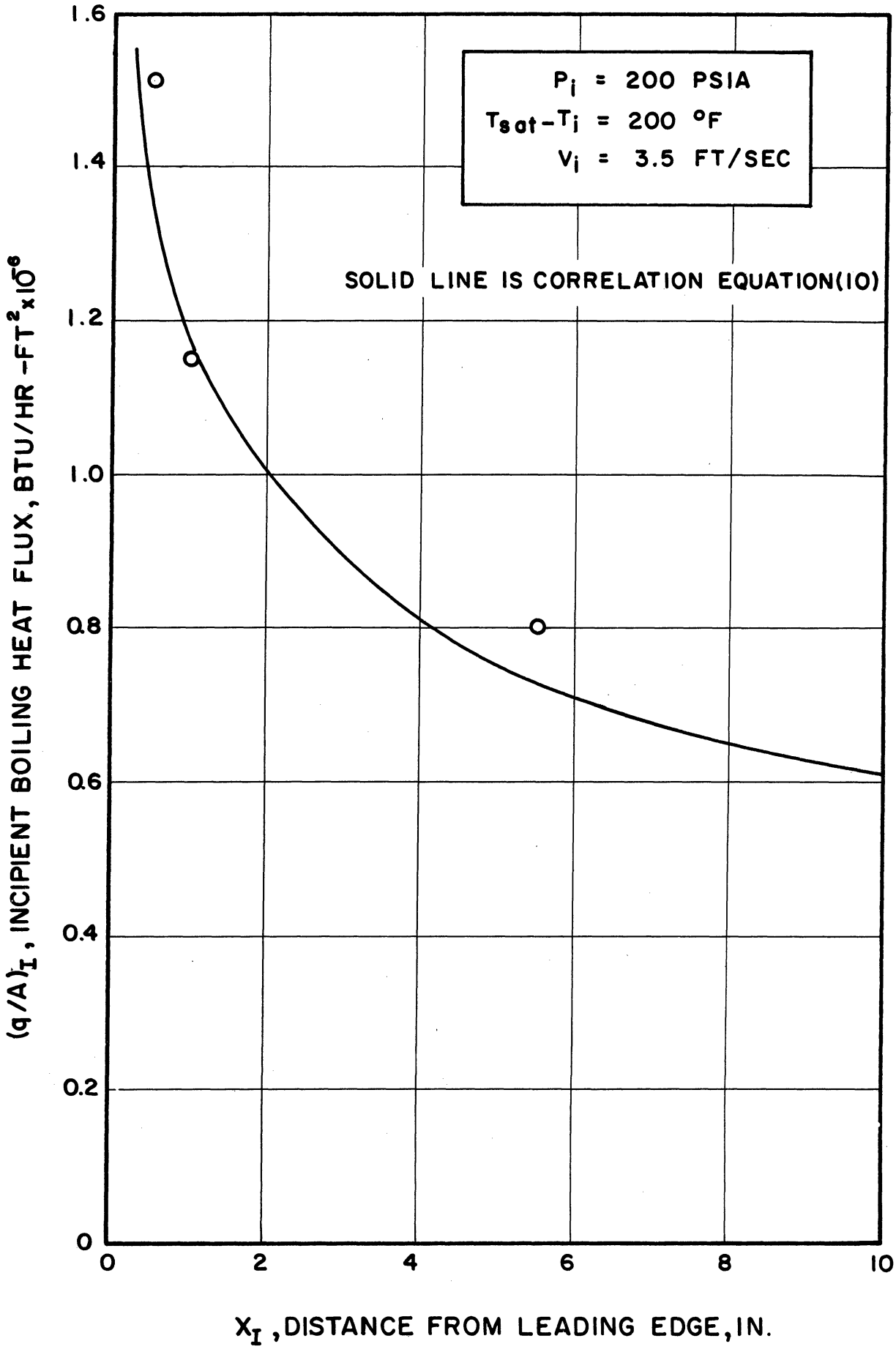

Figure 36. Incipient Boiling Heat Flux vs. Incipient Distance

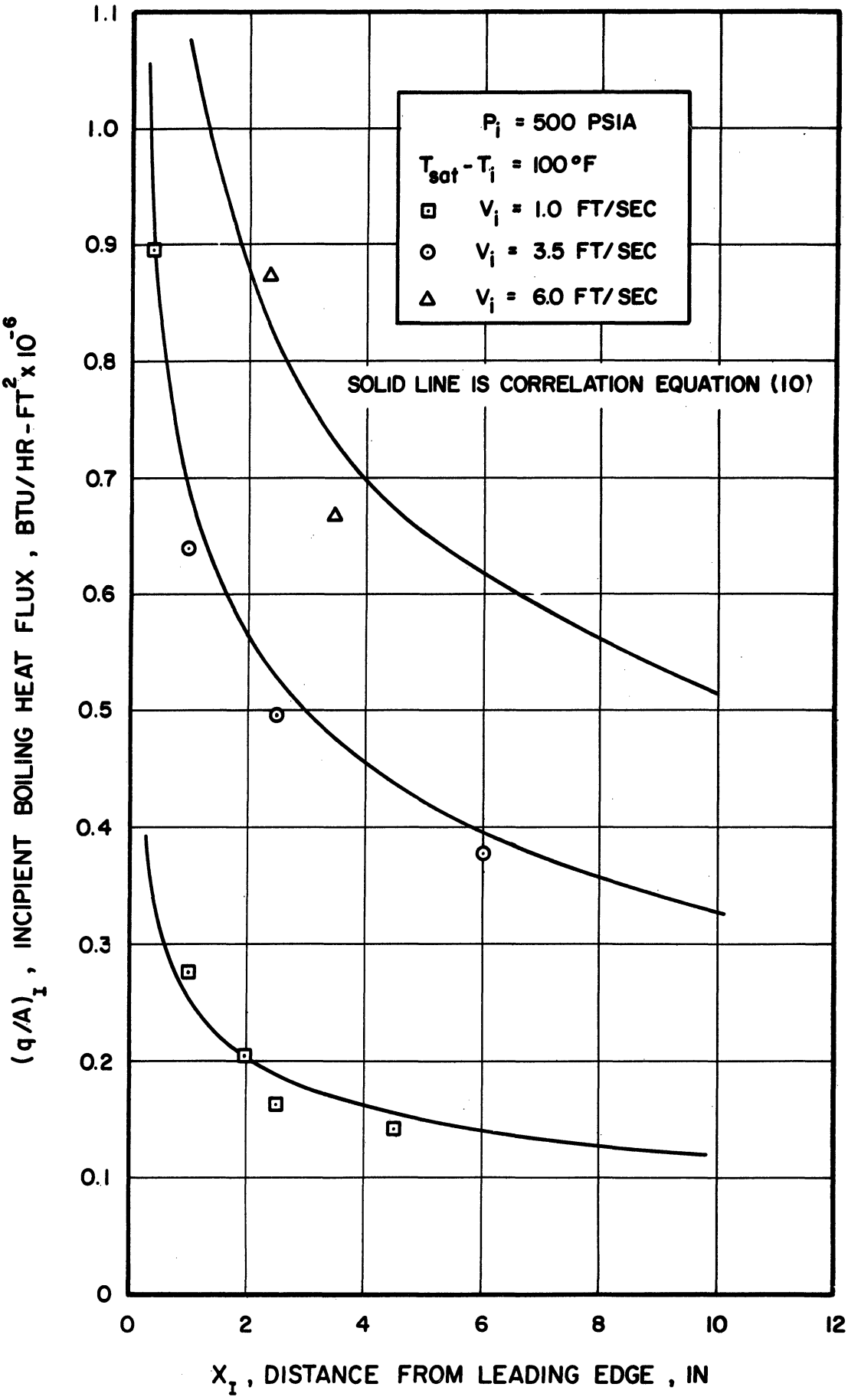

Figure 37. Incipient Boiling Heat Flux vs. Incipient Distance

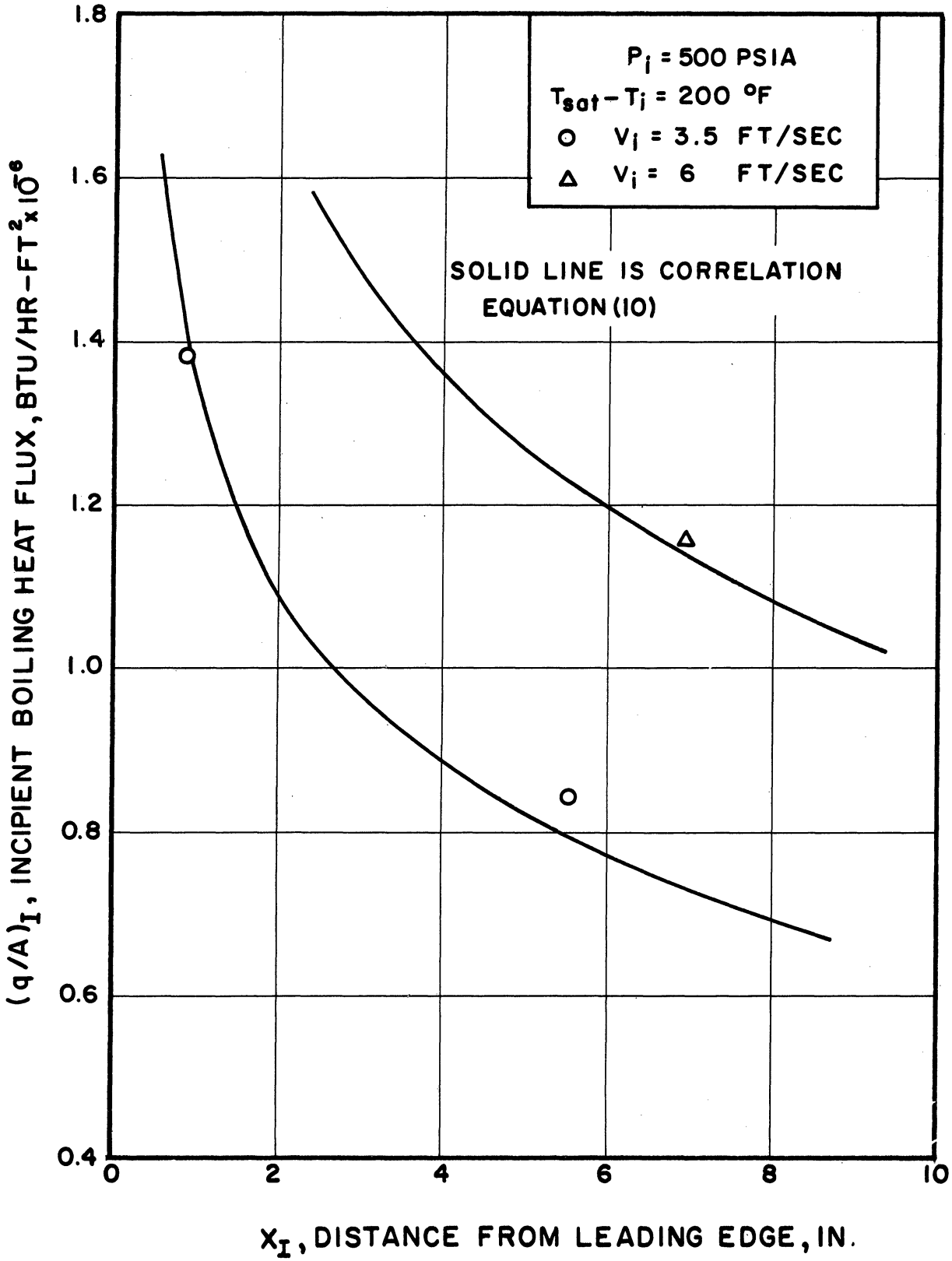

Figure 38. Incipient Boiling Heat Flux vs. Incipient Distance

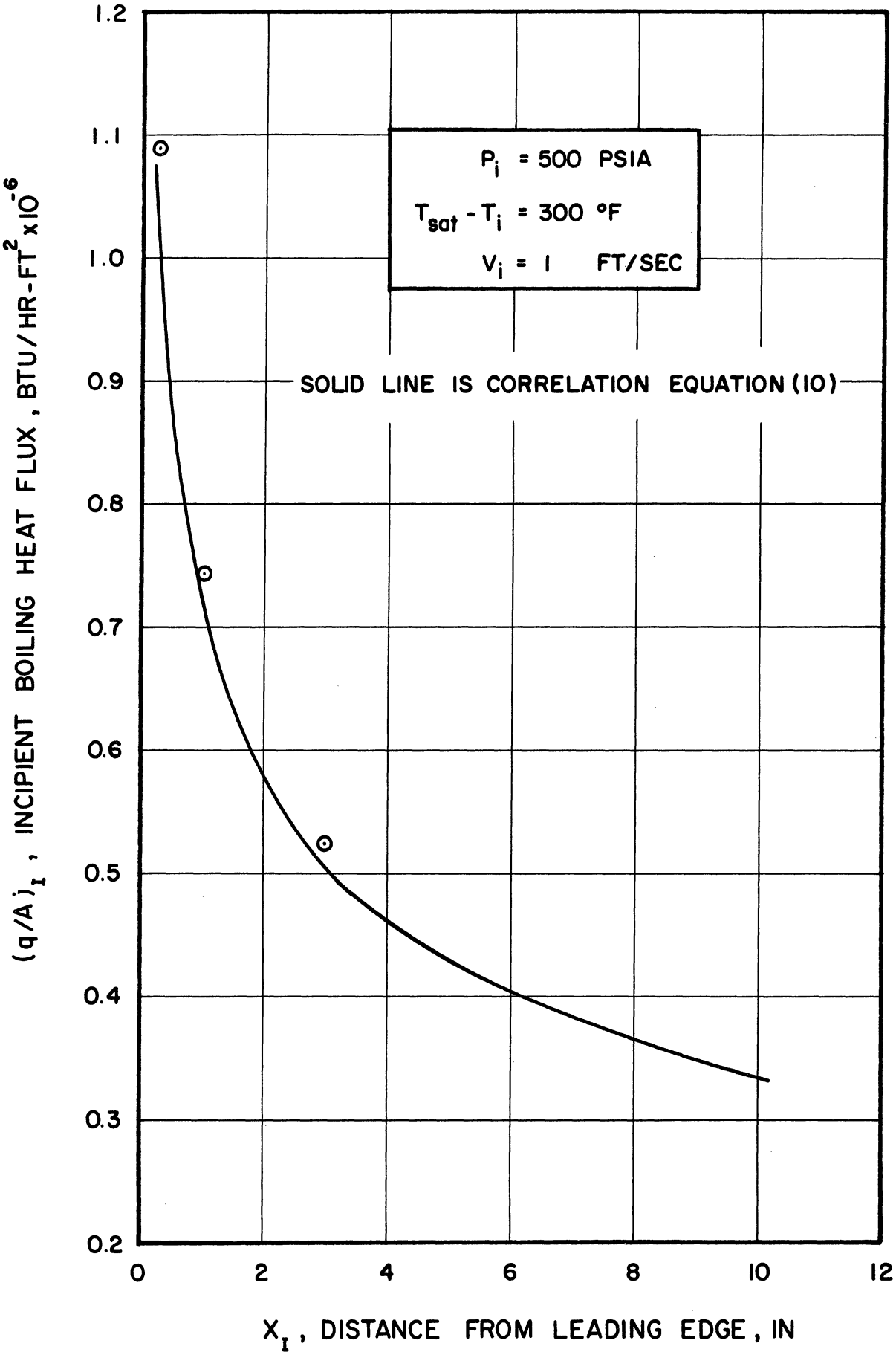

Figure 39. Incipient Boiling Heat Flux vs. Incipient Distance

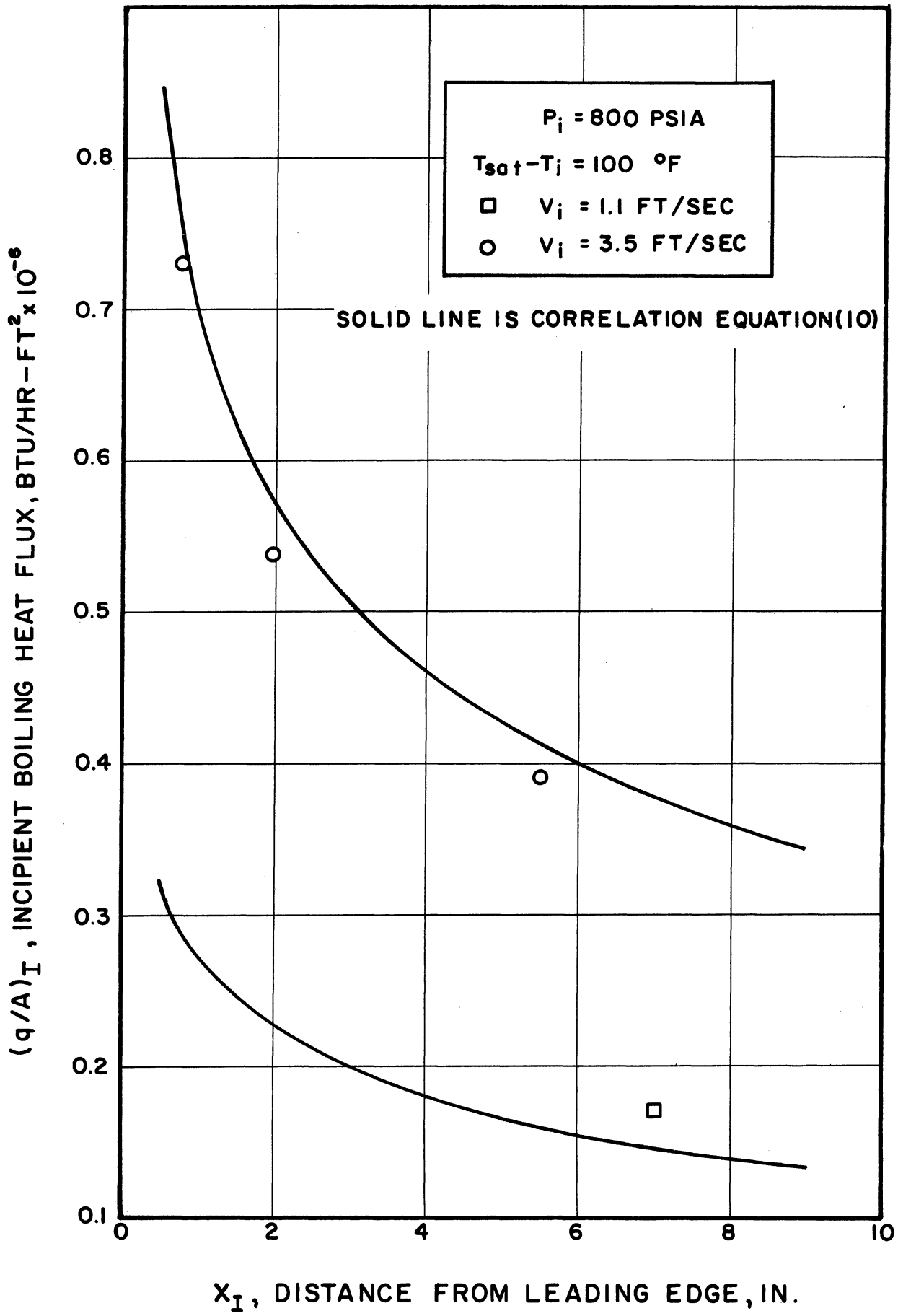

Figure 40. Incipient Boiling Heat Flux vs. Incipient Distance

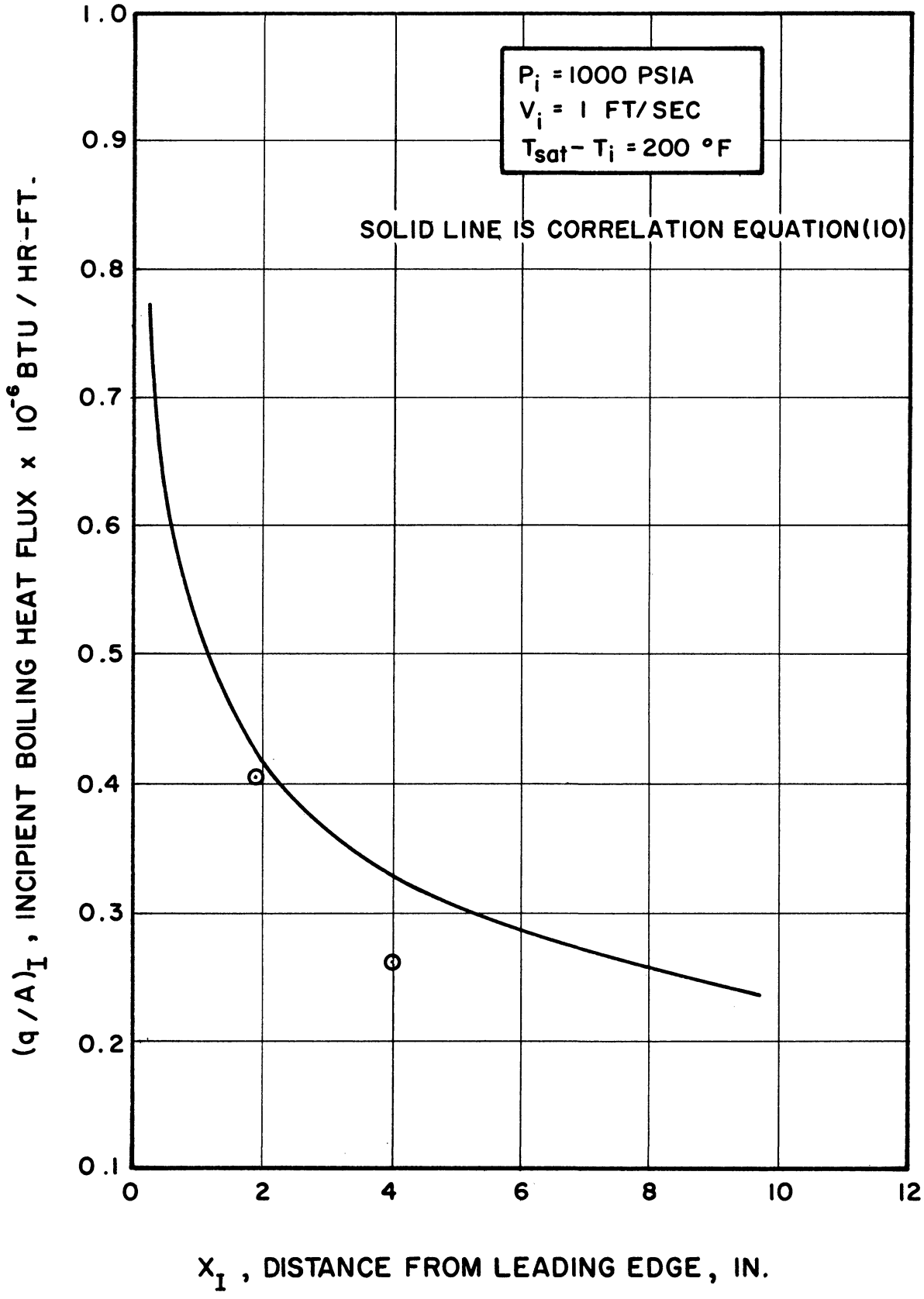

Figure 41. Incipient Boiling Heat Flux vs. Incipient Distance

P_i = 500 psia

V_i = 1 ft/sec

$T_{sat}-T_i$ = 200°F

$q/A = 0.804 \times 10^6$ BTU/hr-ft^2

Scale: Distance between thermocouples = 1 in.

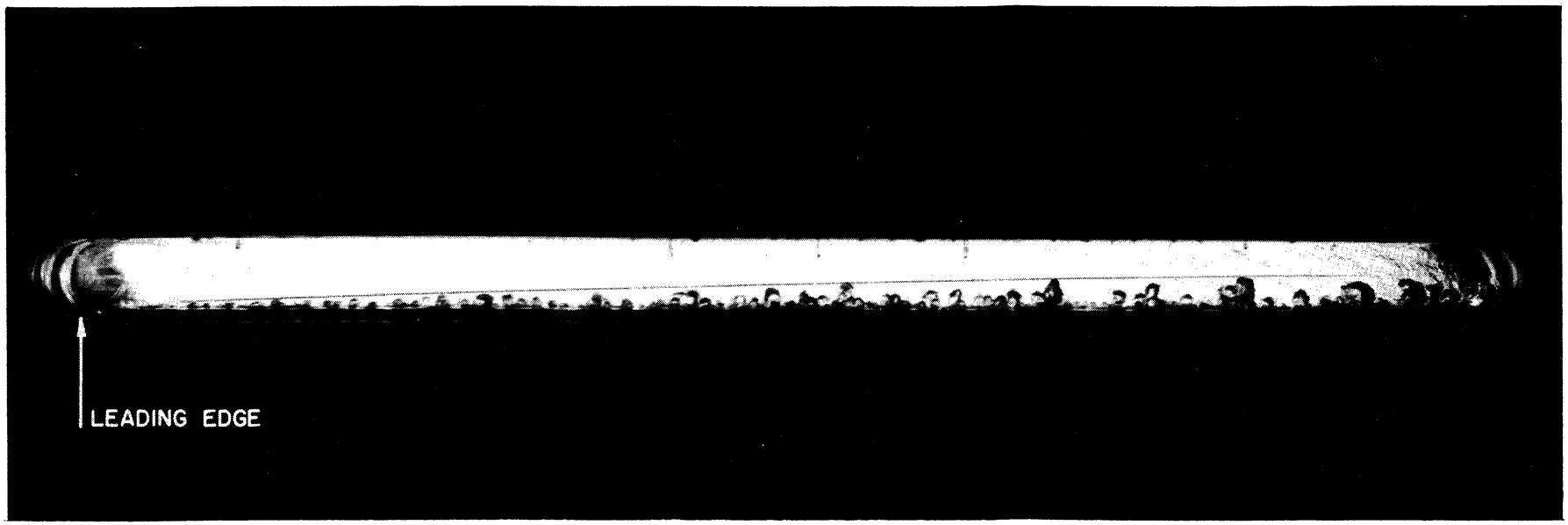

Figure 42. A typical Photograph Showing how the Bubble Boundary Layer is Defined

the heated surface to this line. Other photographs showing nucleation of bubbles and the development and growth of the bubble boundary layer over the heated surface are found in Appendix B.

To avoid burnout of the strip the maximum heat flux was limited to 50 per cent of burnout heat flux as calculated from Jens and Lottes (49) correlation equations. This, in turn, limited the maximum bubble boundary layer thickness to approximately 0.35 inches which corresponds to 75 per cent of channel height.

2. Effect of Heat Flux, Velocity, Subcooling and Pressure on the Bubble Boundary Layer Thickness

To study the effect of heat flux, velocity, subcooling and pressure on the bubble boundary layer, measurements of δ at various distances from the leading edge were made for all tests and plots of δ vs X were constructed. In these plots a solid line was used to define the outline of the bubble boundary layer.

a) The Effect of Heat Flux

When all variables are held constant an increase in the heat flux causes an increase in the bubble boundary layer thickness as shown in Figures 43 to 47. This is expected since larger bubbles can be maintained at higher flux.

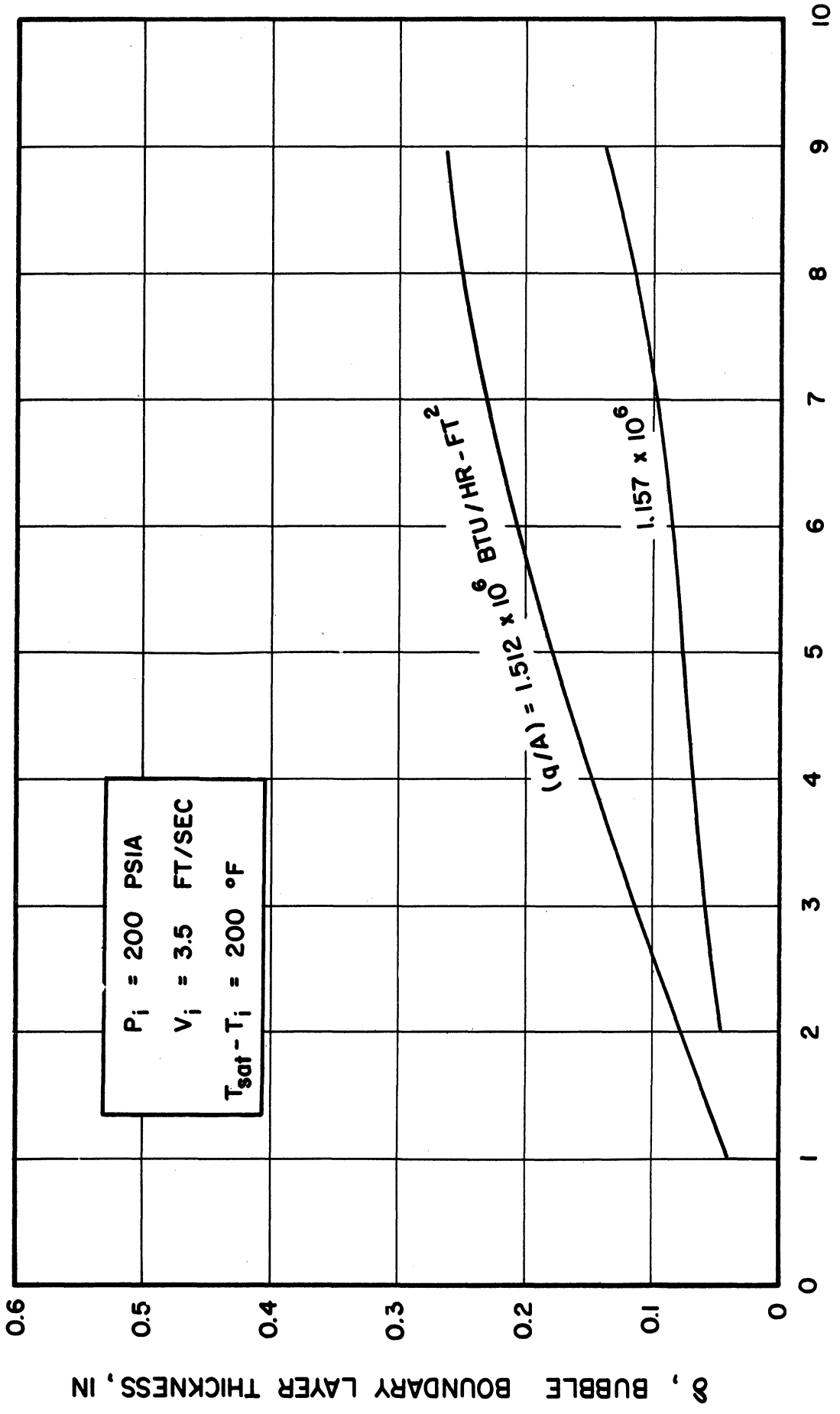

Figure 43. The effect of Heat Flux on the Bubble Boundary Layer Thickness

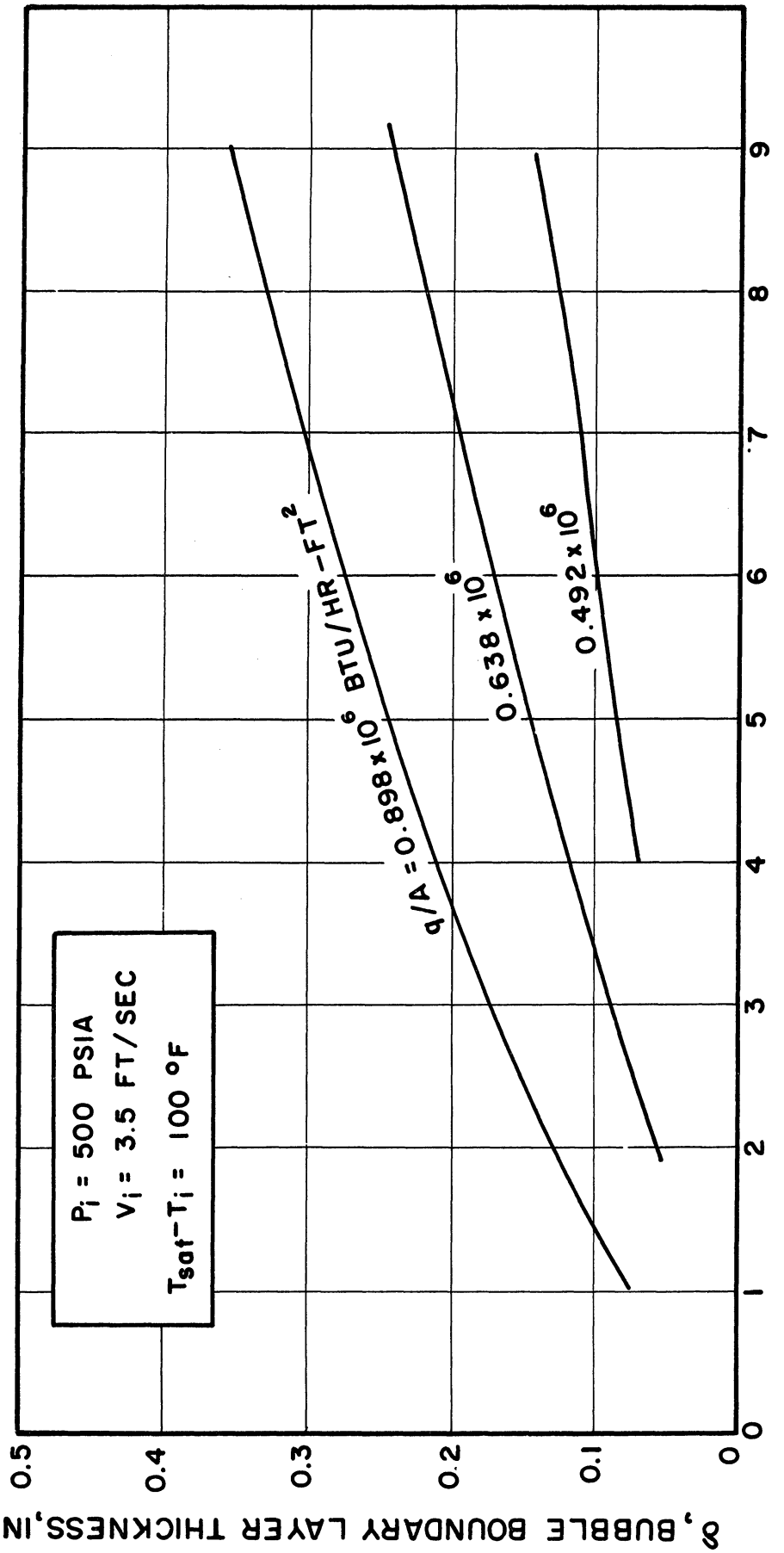

Figure 44. The Effect of Heat Flux on the Bubble Boundary Layer Thickness

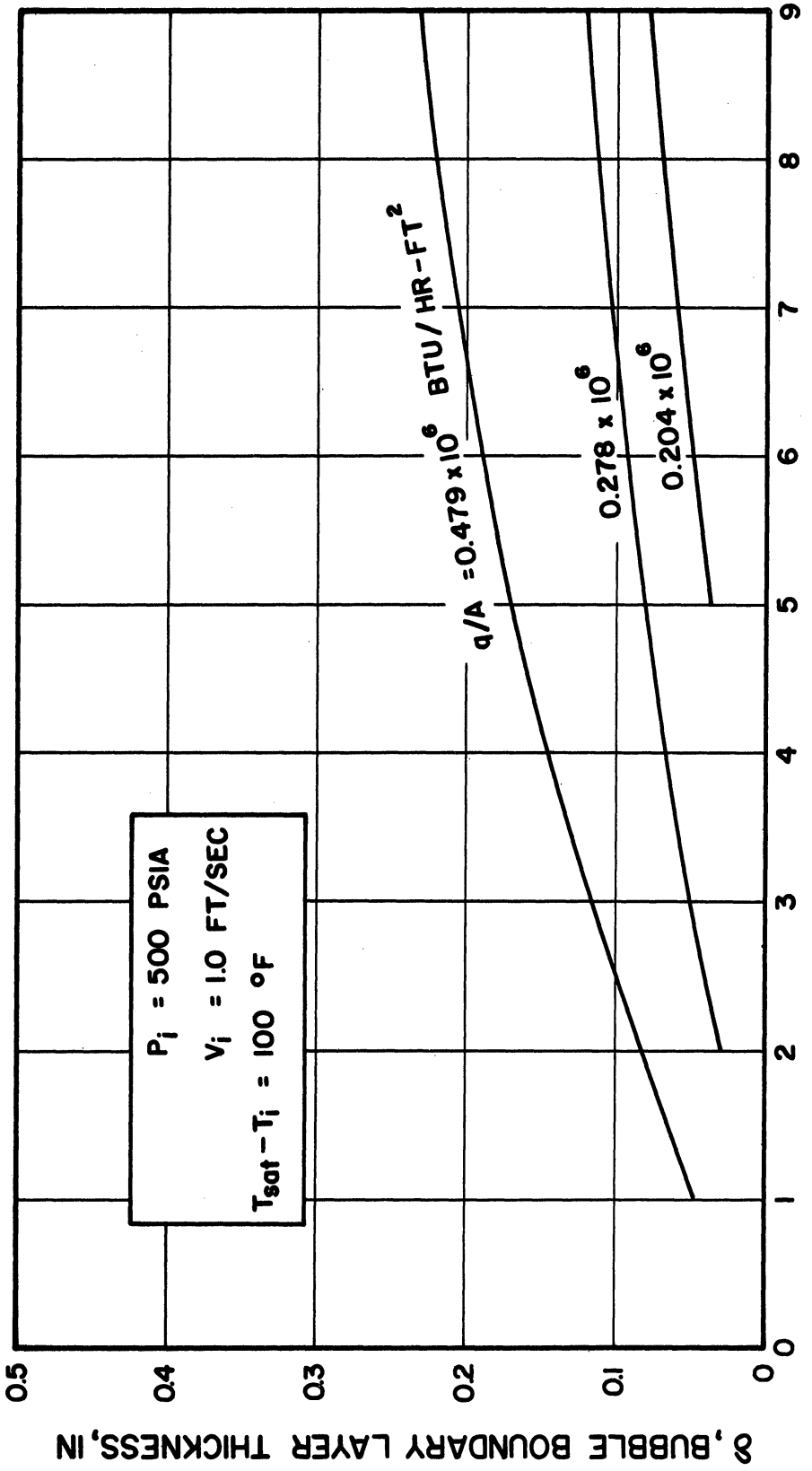

Figure 45. The Effect of Heat Flux on the Bubble Boundary Layer Thickness

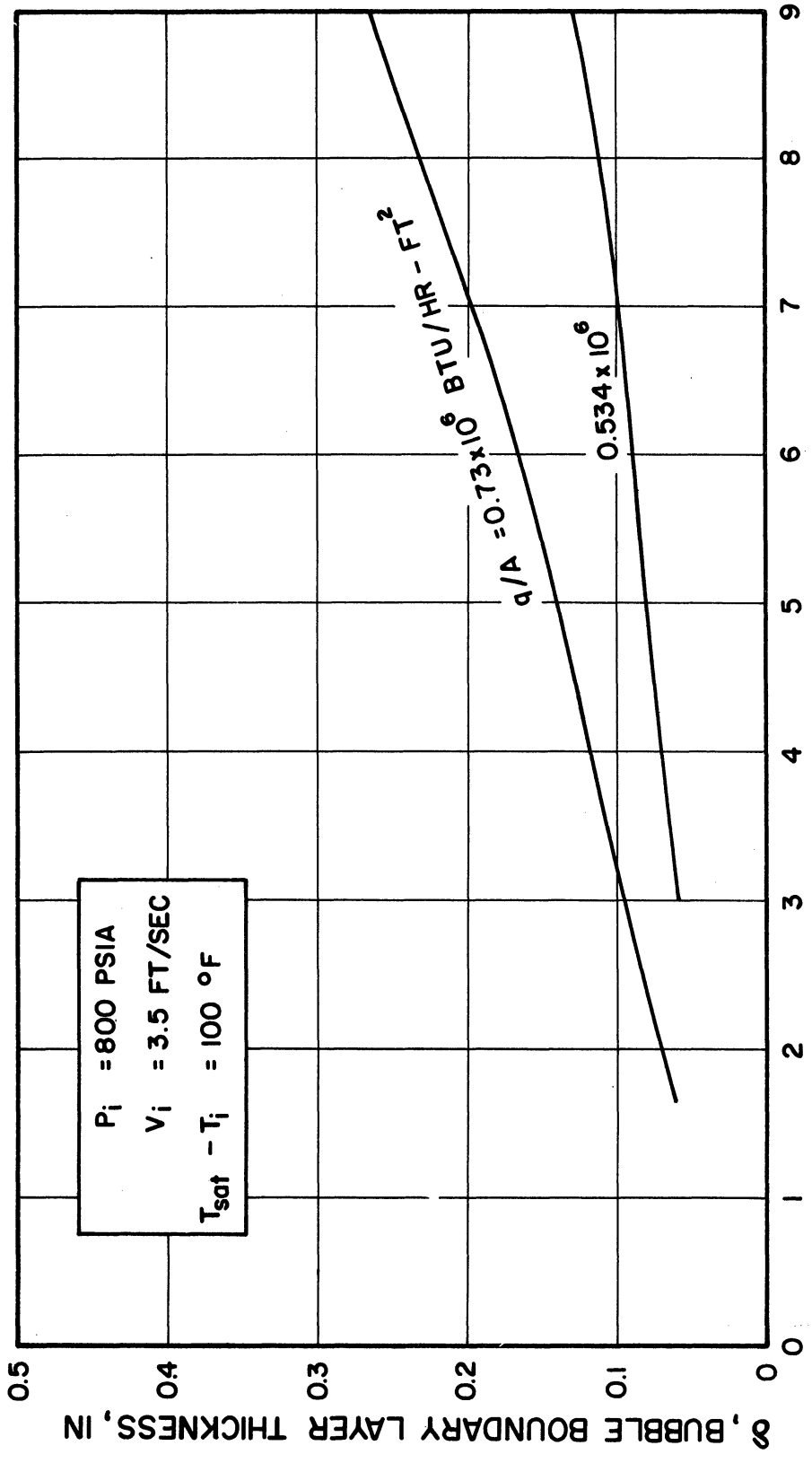

Figure 46. The Effect of Heat Flux on the Bubble Boundary Layer Thickness

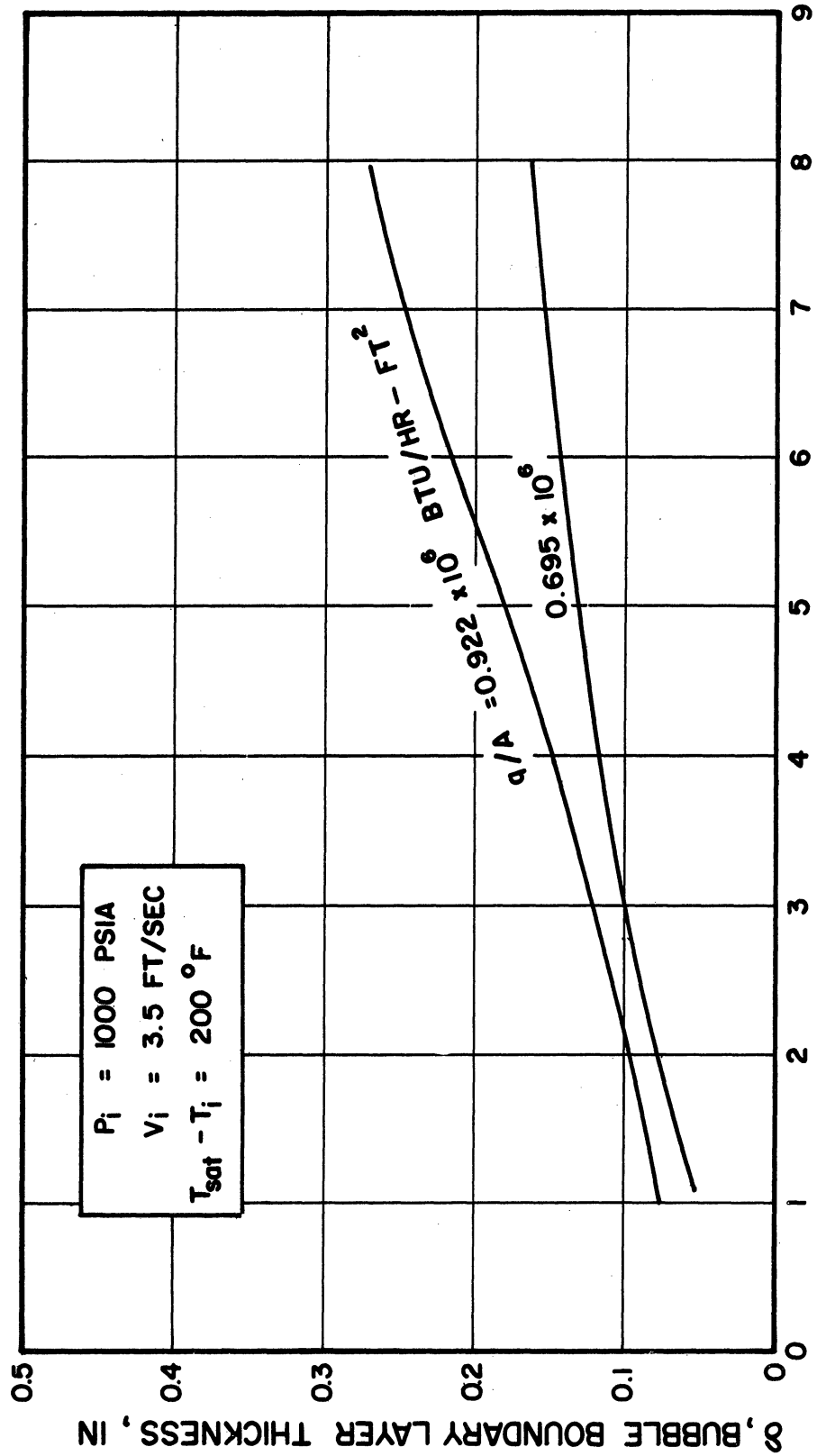

Figure 47. The Effect of Heat Flux on the Bubble Boundary Layer Thickness

b) Effect of Inlet Velocity

For constant pressure, subcooling and heat flux, increasing the velocity causes a decrease in the bubble boundary layer as illustrated in Figures 48 and 49.

c) Effect of Subcooling

An increase in inlet subcooling for constant pressure, velocity and flux decreases the bubble boundary layer thickness as shown in Figure 50. This is an expected behavior since the higher the subcooling the greater the rate of bubble condensation.

d) Effect of Pressure

Comparison of the bubble boundary layer thickness for various tests in which the inlet velocity, subcooling, and heat flux were kept constant while the pressure was varied show that the bubble boundary layer thickness is not affected by the pressure in a simple manner. Figure 51 shows that the bubble boundary layer thickness is greater at 500 psia than at 200 psia. On the other hand, Figure 52 shows that the bubble boundary layer thickness is larger at 500 psia than 800 psia. Thus it cannot be concluded that the higher the pressure the smaller is the bubble boundary layer thickness.

3. Correlation of the Bubble Boundary Layer Thickness

To correlate the experimental data for the bubble

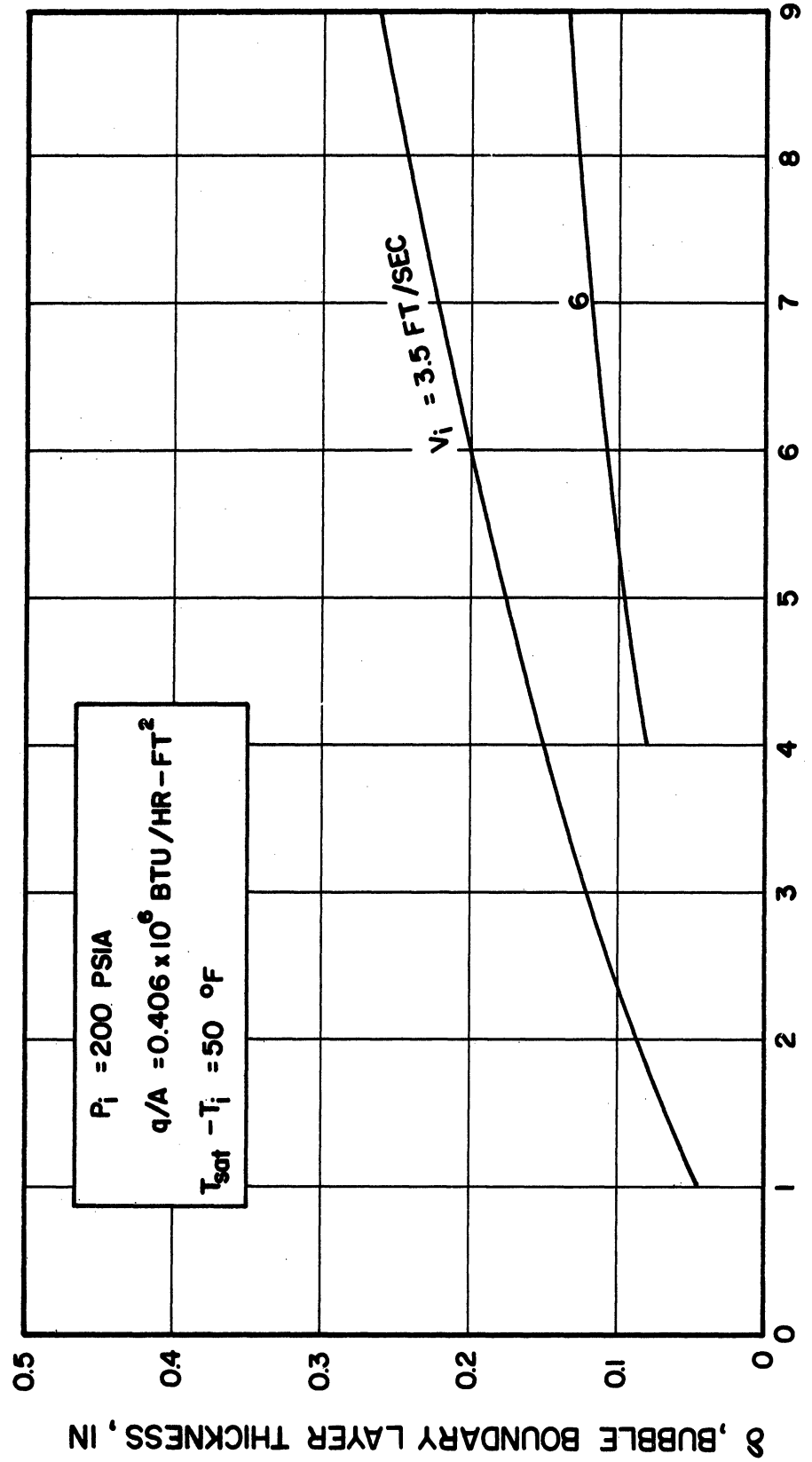

Figure 48. The Effect of Velocity on the Bubble Boundary Layer Thickness

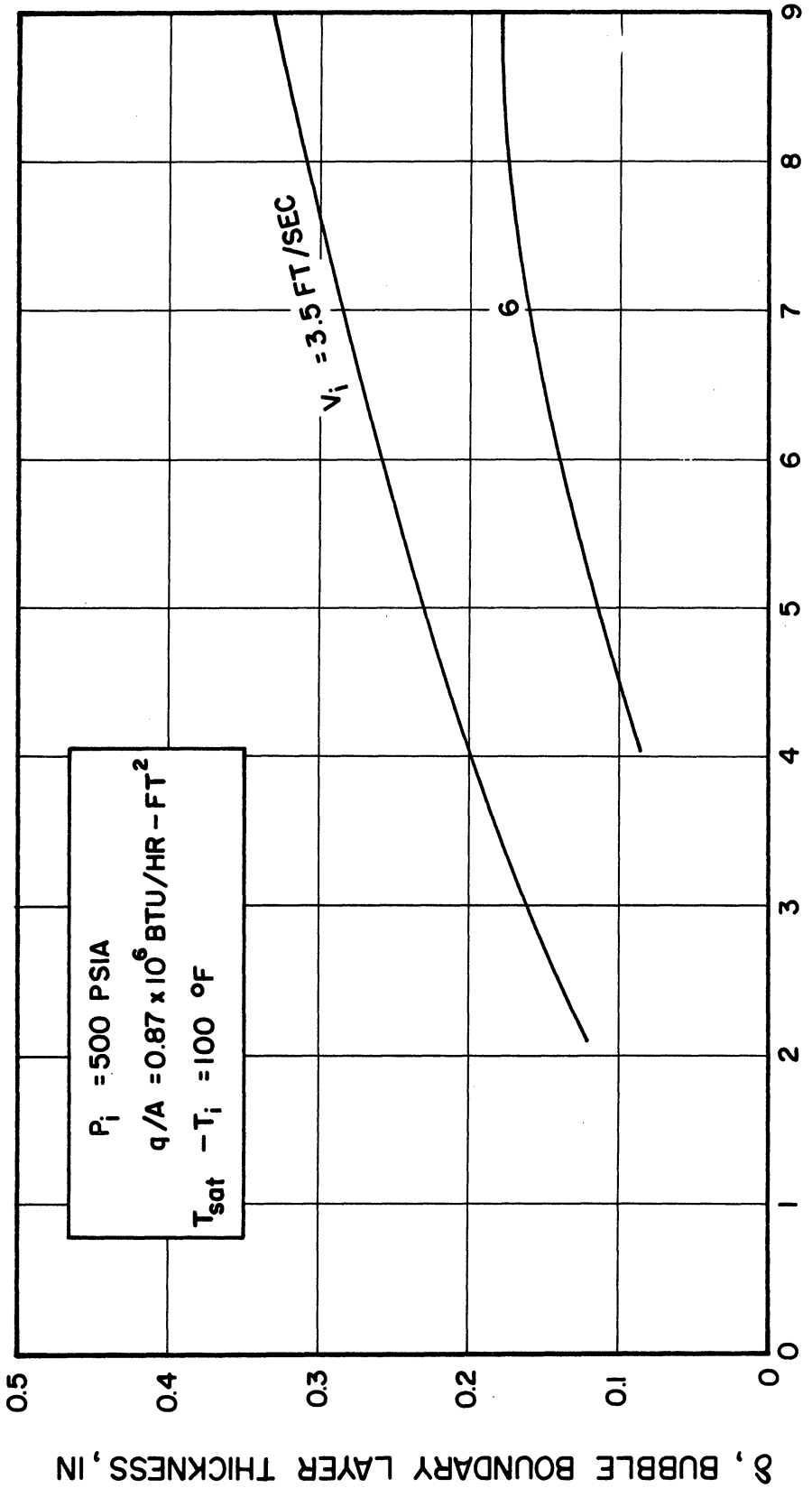

Figure 49. The Effect of Velocity on the Bubble Boundary Layer Thickness

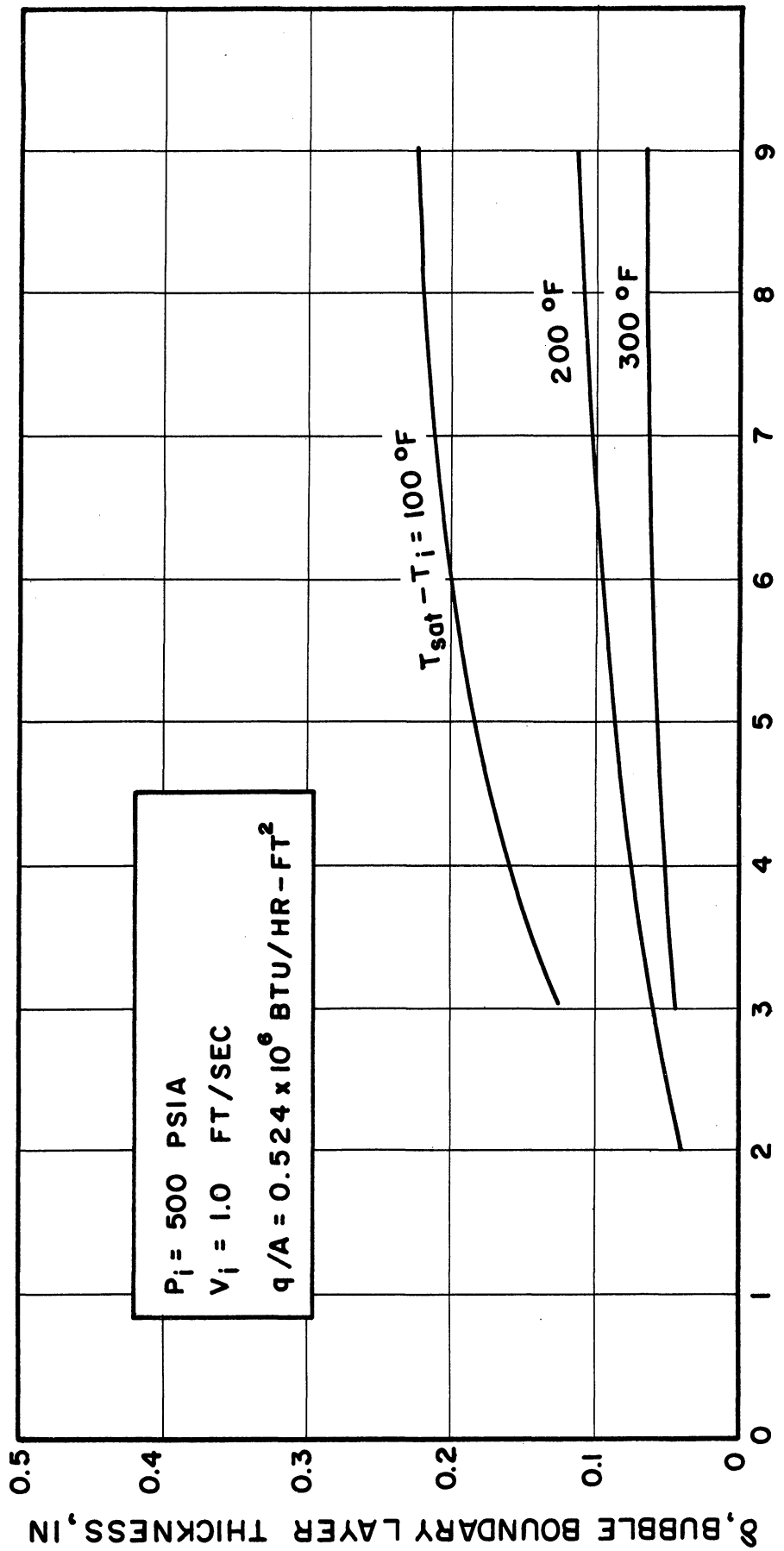

Figure 50. The Effect of Subcooling on the Bubble Boundary Layer Thickness

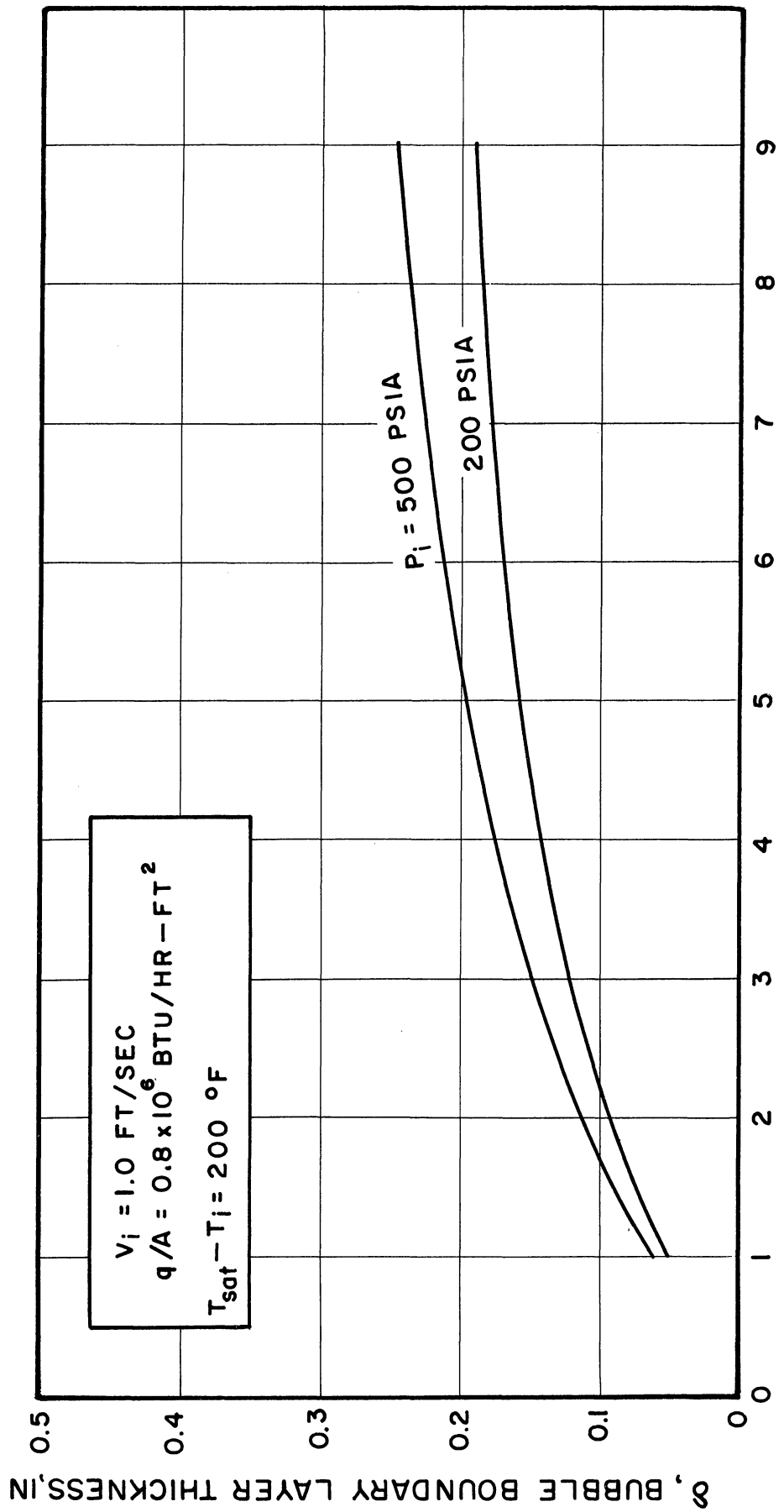

Figure 51. The Effect of Pressure on the Bubble Boundary Layer Thickness

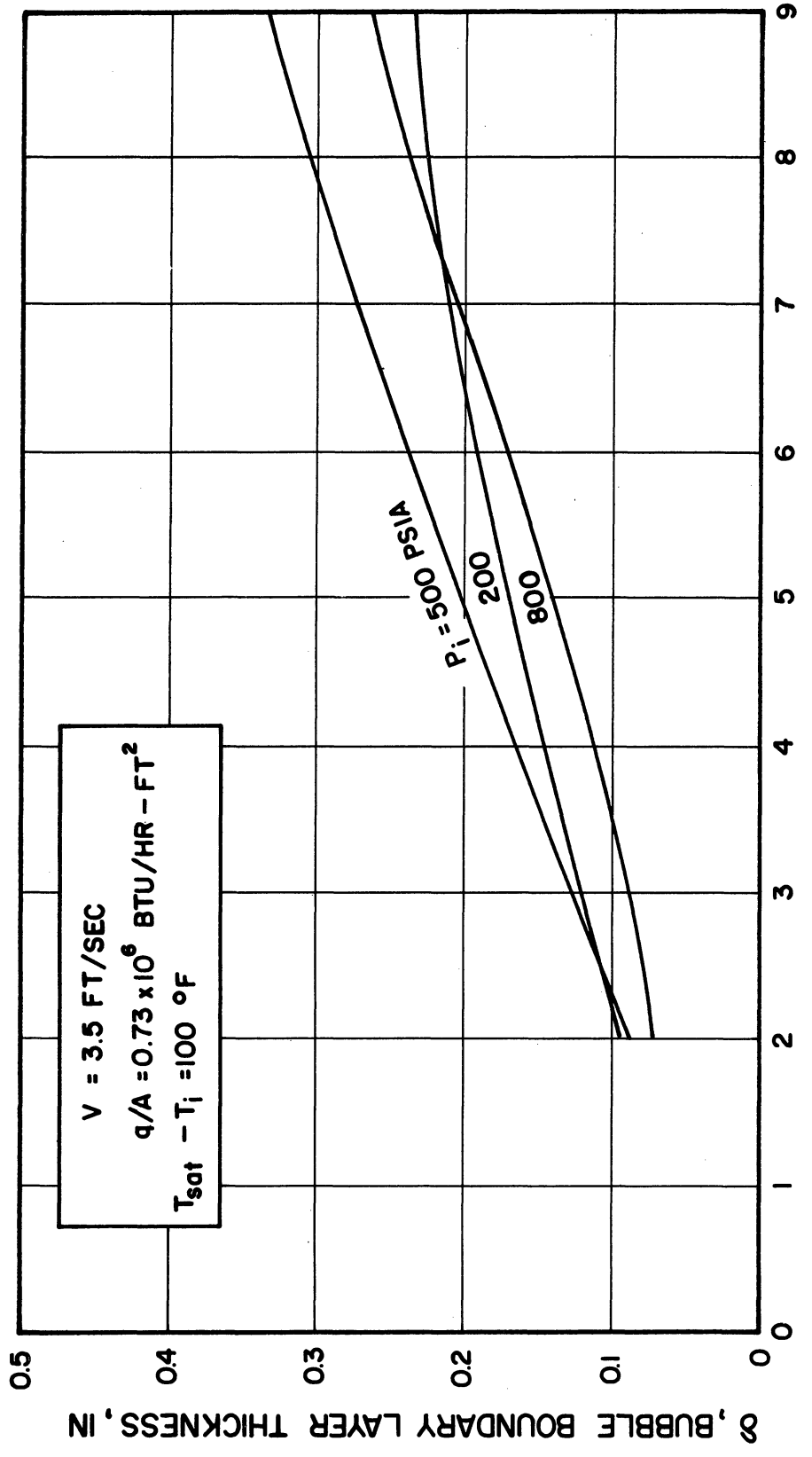

Figure 52. The Effect of Pressure on the Bubble Boundary Layer Thickness

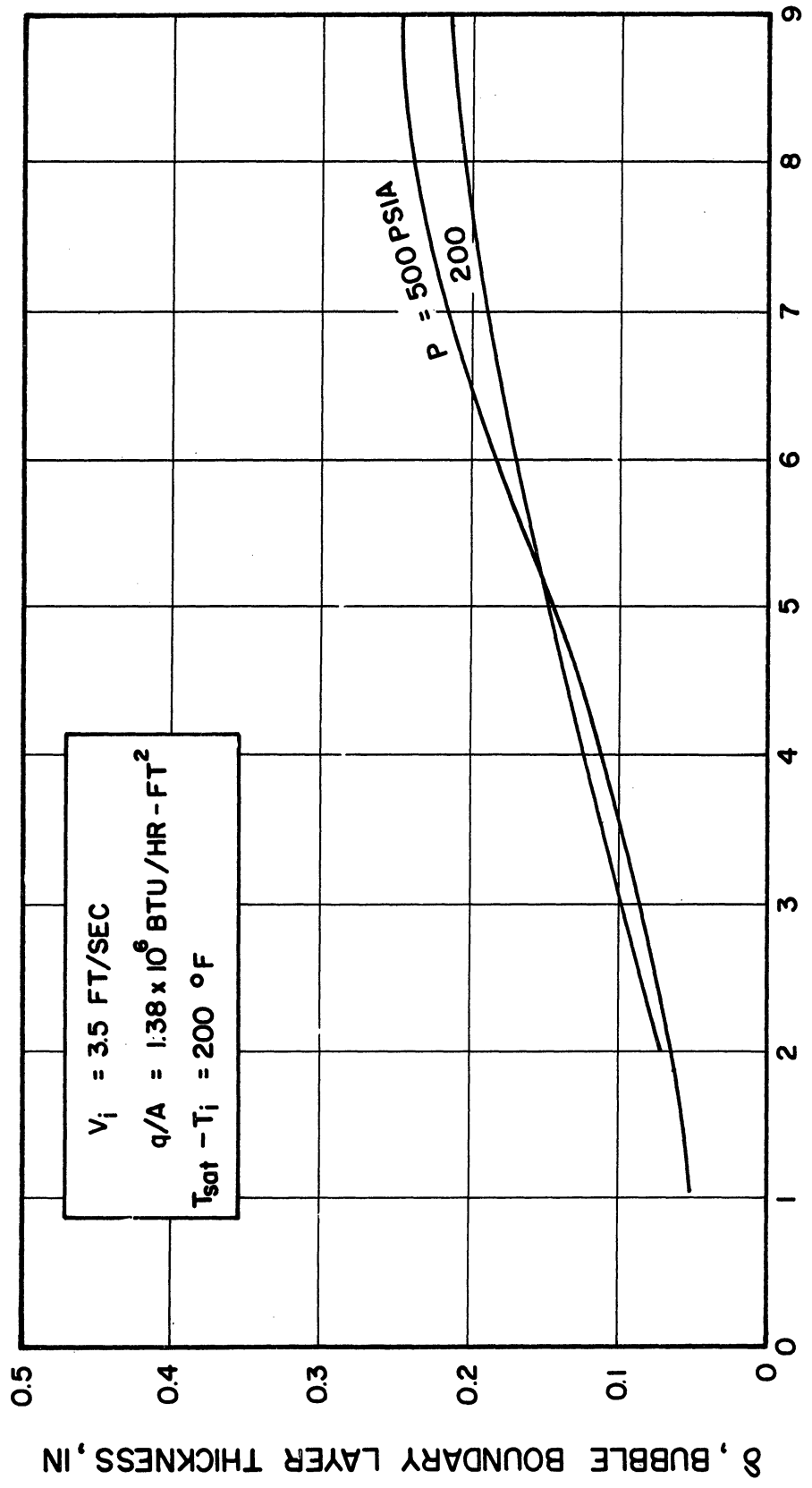

Figure 53. The Effect of Pressure on the Bubble Boundary Layer Thickness.

boundary layer thickness, a regression analysis program was carried out on the IBM 709 Computor. In this program the sum of the squares of the differences between observed and predicted values of δ is minimized. The correlation equation was assumed to be of the form

$$\delta = \alpha_o \, Z_1^{\alpha_1} \, Z_2^{\alpha_2} \, Z_3^{\alpha_3} \cdots Z_n^{\alpha_n} \tag{11}$$

where $Z_1, Z_2, Z_3, \ldots, Z_4$ are independent variables which affect δ and $\alpha_o, \alpha_1, \alpha_2, \alpha_3, \ldots, \alpha_n$ are constants to be determined by the method of least squares. Using this method two correlation equations were determined which adequately predict the bubble boundary layer thickness.

a) Dimensional Correlation Equation

Equation (12) was found to predict δ to within $\pm$ 20 per cent for the range of variables listed in Table II.

$$\delta = 6\times10^{-4} \left(T_{sat}-T_i\right)^{-1.163} \left(G\right)^{-0.504} \left(q/A\right)^{1.256} \left(X-X_I\right)^{0.534} \tag{12}$$

Equation (12) is plotted in Figure 54 together with experimental data on the bubble boundary layer thickness. For each test the thickness δ at four locations along the strip is compared with the predicted value.

b) Dimensionless Correlation Equation

Another correlation equation in terms of significant dimensionless groups was also obtained. Equation (13) predicts the bubble boundary layer thickness δ to within $\pm$ 20 per cent.

$$\frac{\delta P}{\sigma} = 8.54\times10^{-4}\left[\frac{C_p\mu}{k}\right]^{1.742}\left[\frac{\rho_L}{\rho_V}-1\right]^{-0.6}\left[\frac{(q_b/A)}{C_pG(T_{sat}-T_i)}\right]^{0.448}\left[\frac{(q_b/A)(X-X_I)}{\mu h_{fg}}\right]^{0.302}\left[\frac{P(X-X_I)}{\sigma}\right]^{0.237} \qquad (13)$$

The fluid properties C_p, μ and k are evaluated at the film temperature while the surface tension σ is evaluated at the saturation temperature.

A plot of Equation (13) is given in Figure 55 and experimental points on the bubble boundary thickness are shown.

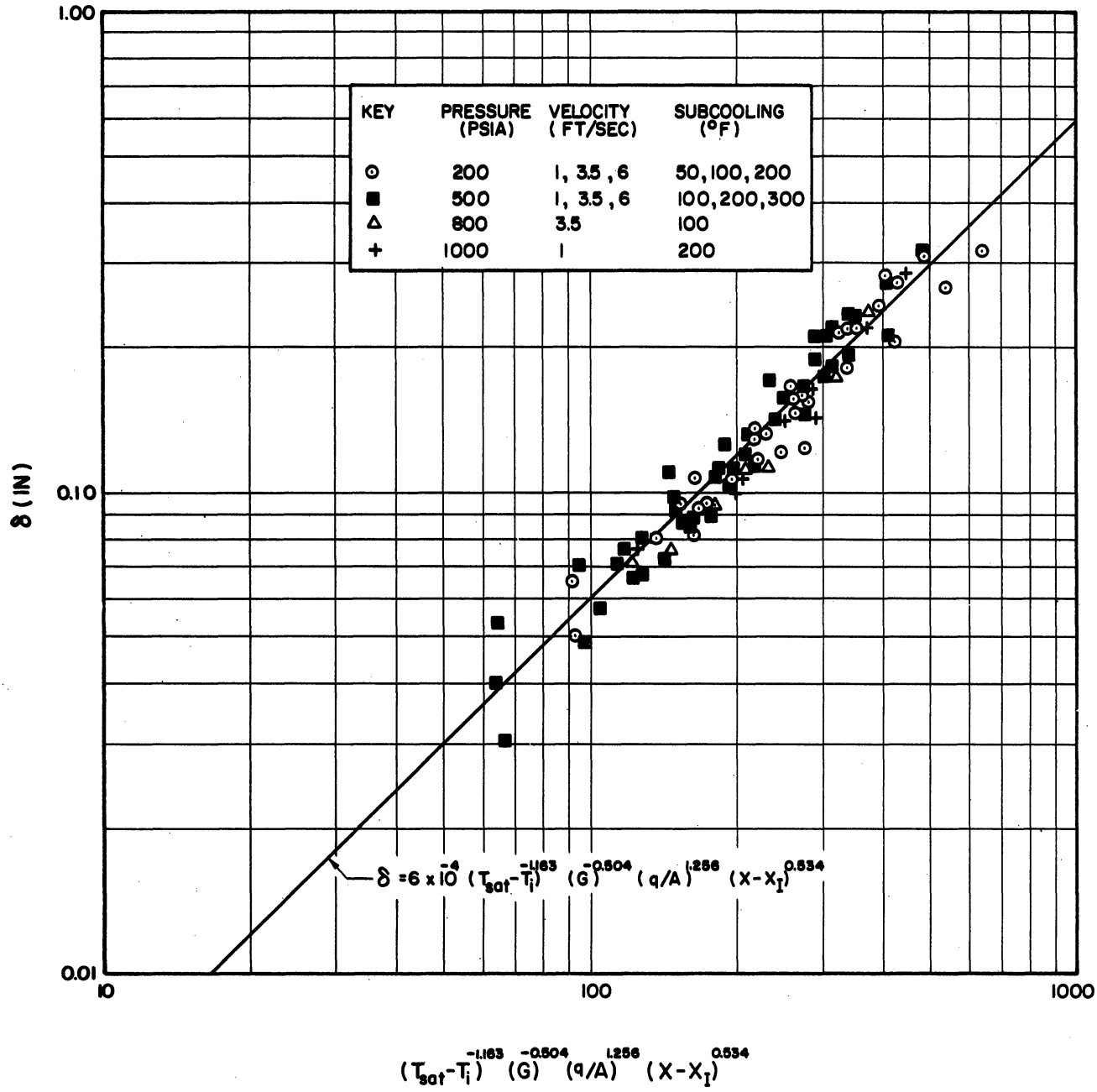

Figure 54. Dimensional Correlation of the Bubble Boundary Layer Thickness

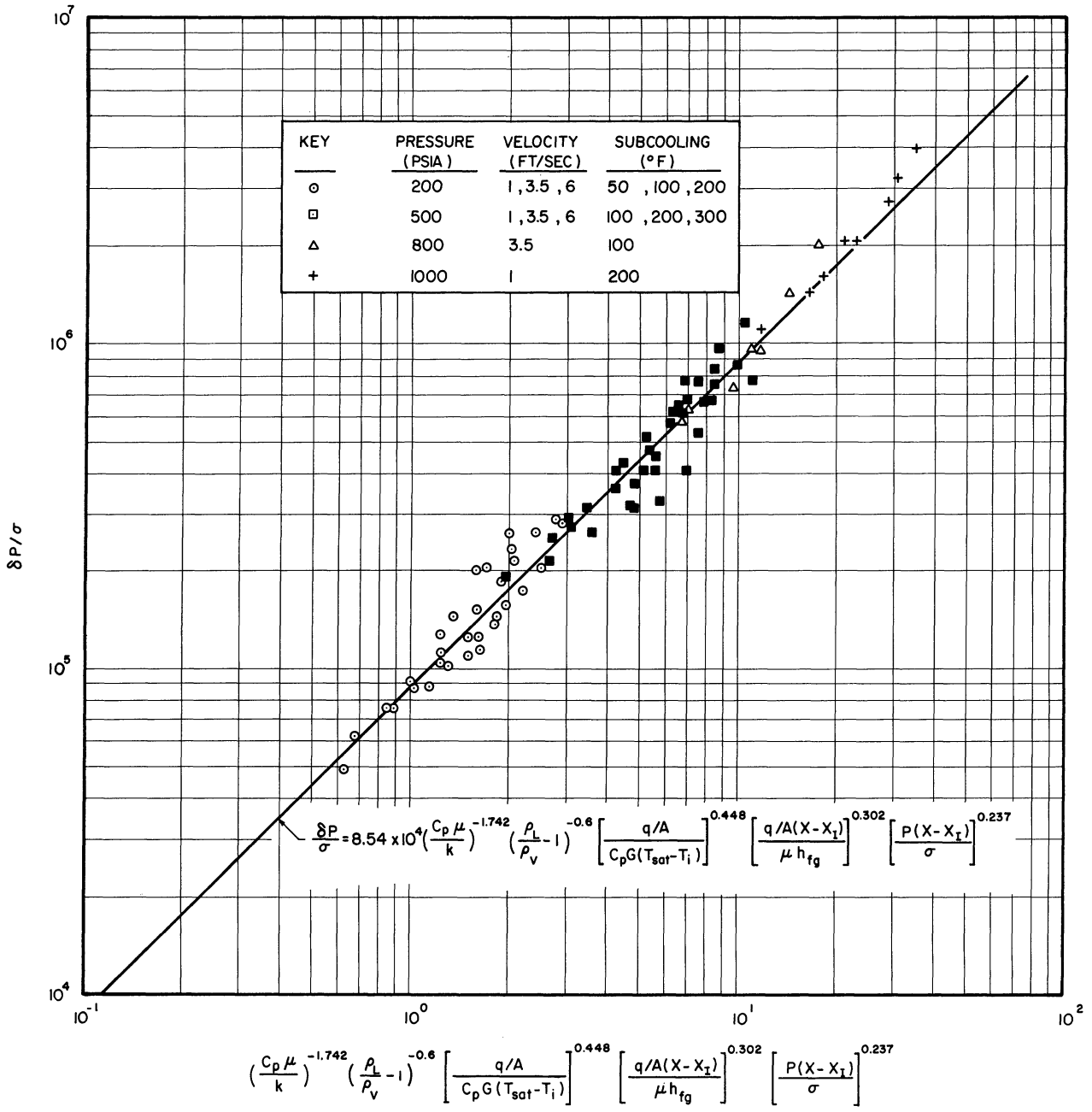

Figure 55. Dimensionless Correlation of the Bubble Boundary Layer Thickness

C. Results of Temperature Measurements

1. Introduction

"Visicorder" traces of the traversing thermocouple signals indicated considerable fluctuations in temperature within the turbulent boundary layer as well as the bubble boundary layer. These fluctuations, as illustrated in Figure 56, suggested the definition of the following temperature terms:

a) "Minimum Temperature"

The lowest extreme of temperature fluctuations as indicated by the "Visicorder" is referred to as the "minimum temperature" as illustrated in Figure 56.

b) "Maximum Temperature"

The upper level of temperature fluctuations is referred to as the "maximum temperature". This temperature is also determined from the "Visicorder" record.

c) "Mean Temperature"

The mean temperature is the time average of the temperature fluctuations. It is measured by the potentiometer after damping out fluctuations in thermocouple output signal.

Because the "Visicorder" has a finite time response, certain amount of damping in temperature fluctuations is expected. This means that the lowest temperature level

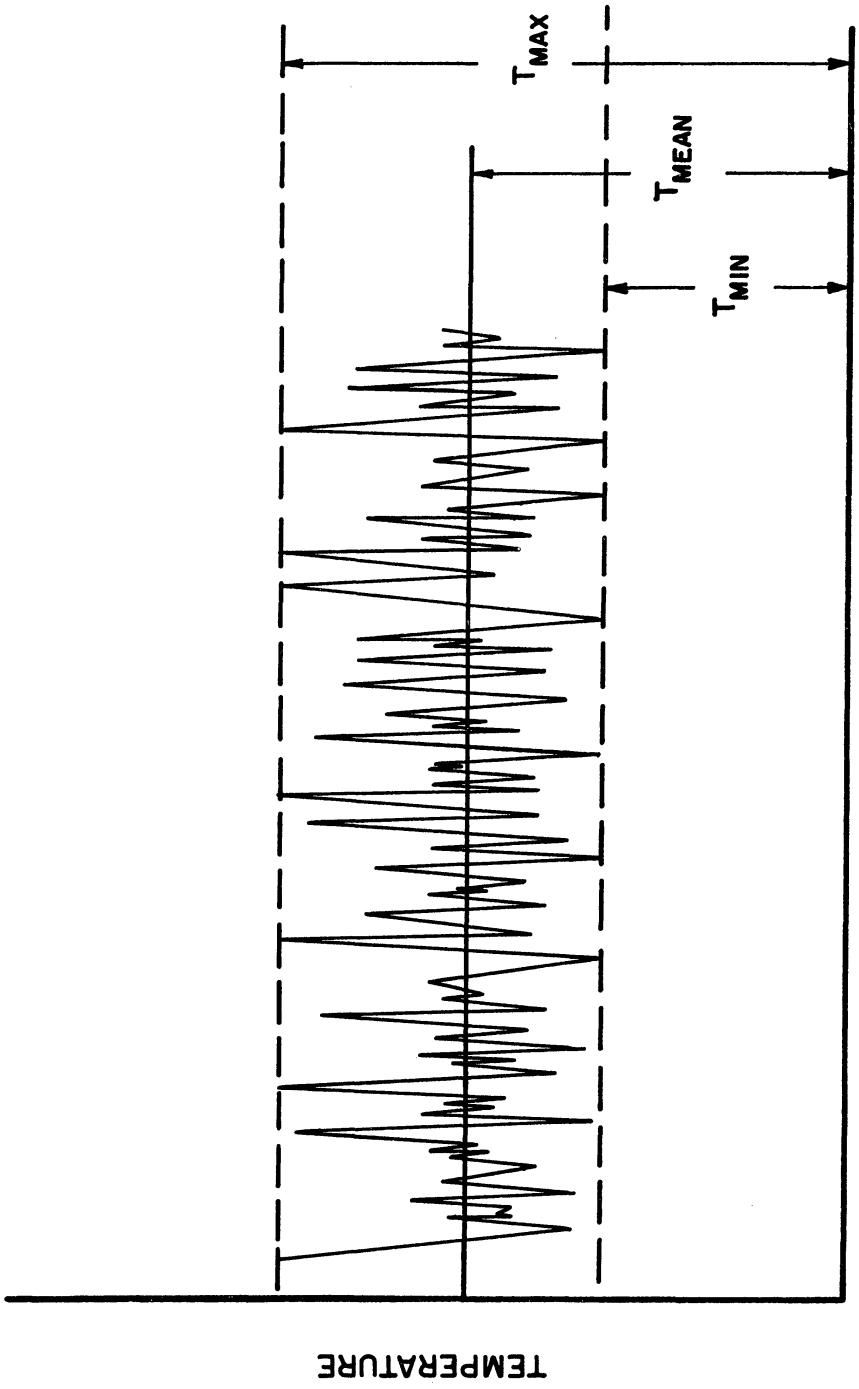

Figure 56. Fluctuations in Traversing Thermocouple Signal

existing at the thermocouple hot junction is less than T_{MIN} and the highest level is greater than T_{MAX}. Typical plots of maximum, minimum and mean temperature profiles for various conditions are shown in Figures 57 and 58.

2. Fluid Temperature Profiles

"Mean temperature" profile plots for various tests are shown in Figures 59 through 69. In no case was the measured mean temperature near the surface greater than saturation temperature. Furthermore, it is noted that the temperature gradient within the bubble boundary layer at a given distance from the heated surface decreases with increasing heat flux.

"Maximum temperature" profiles are shown in Figures 70 through 76. While temperatures as high as saturation were recorded near the surface it is observed that superheated vapor was seldom detected at locations as close to the surface as 0.01 inches. However, because of "Visicorder" damping, this does not rule out the existence of a superheated film near the surface. Referring to Figure 74, the temperature at X = 6" and y = 0.01" is 477°F, which corresponds to 10°F superheat. The surface temperature, as approximated by equation (8), is 498°F which indicates that a maximum superheat of 31°F may exist near the surface.

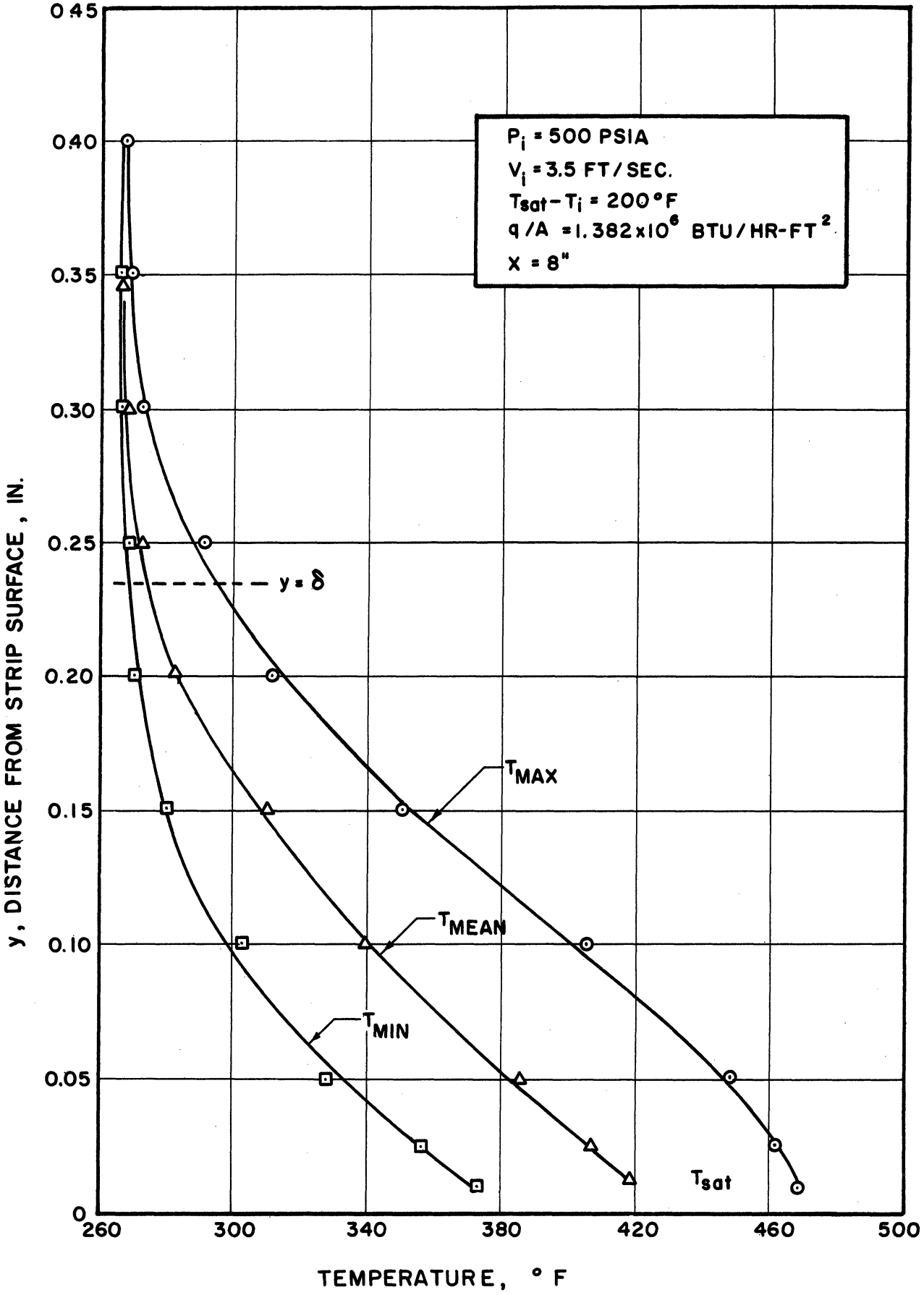

Figure 57. Maximum, Minimum and Mean Temperature Profiles

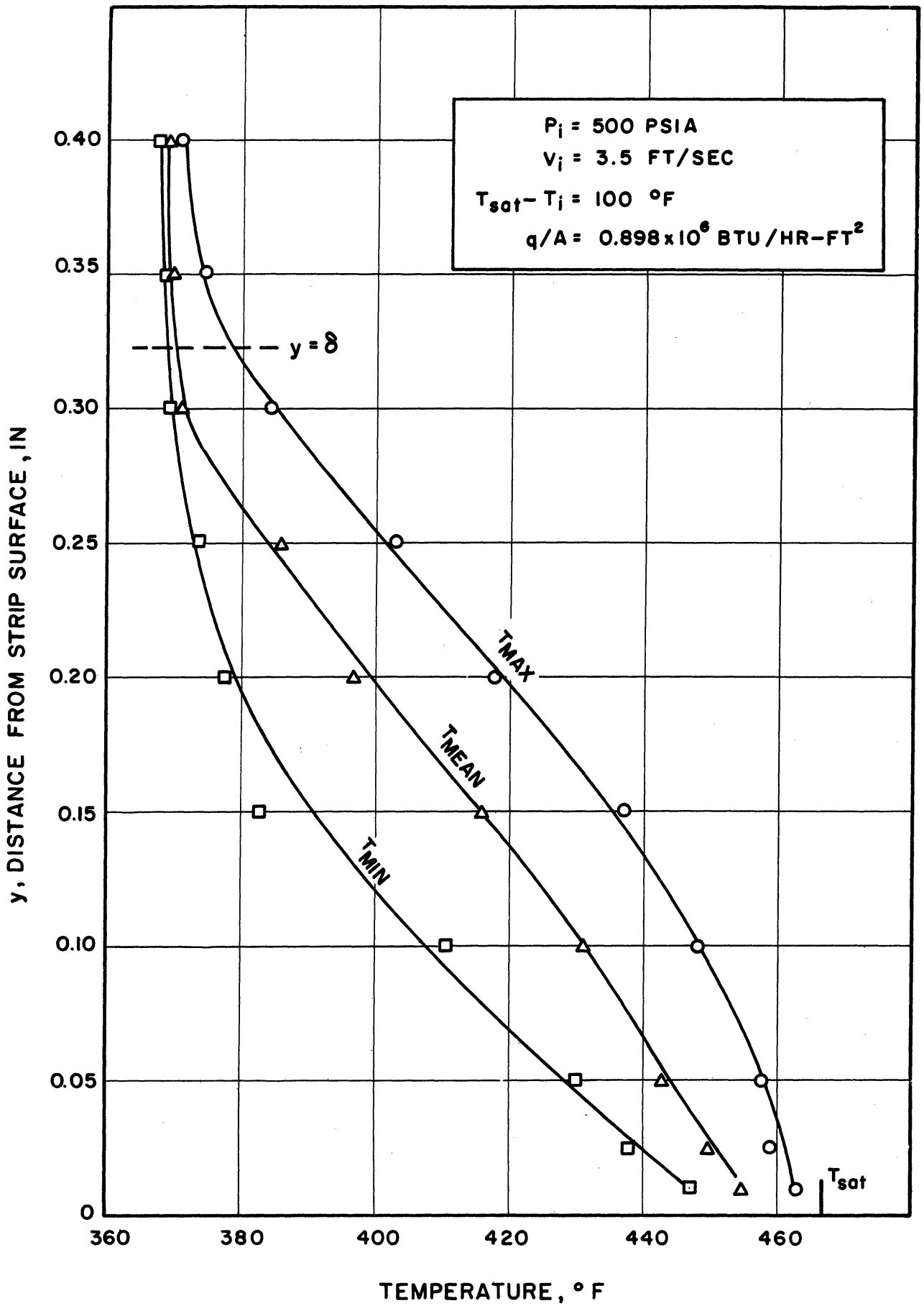

Figure 58. Maximum, Minimum and Mean Temperature Profiles

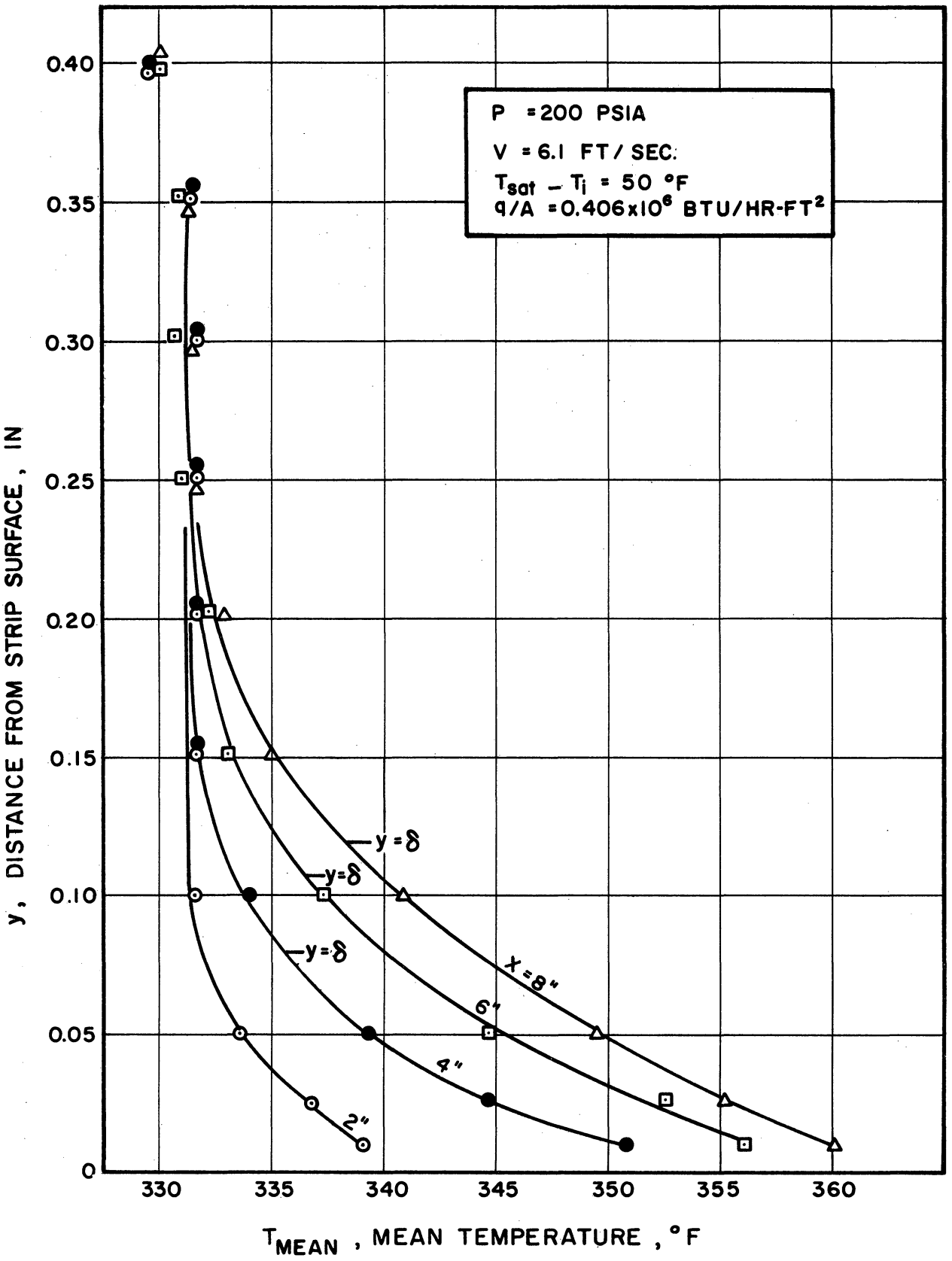

Figure 59. Mean Temperature Profile

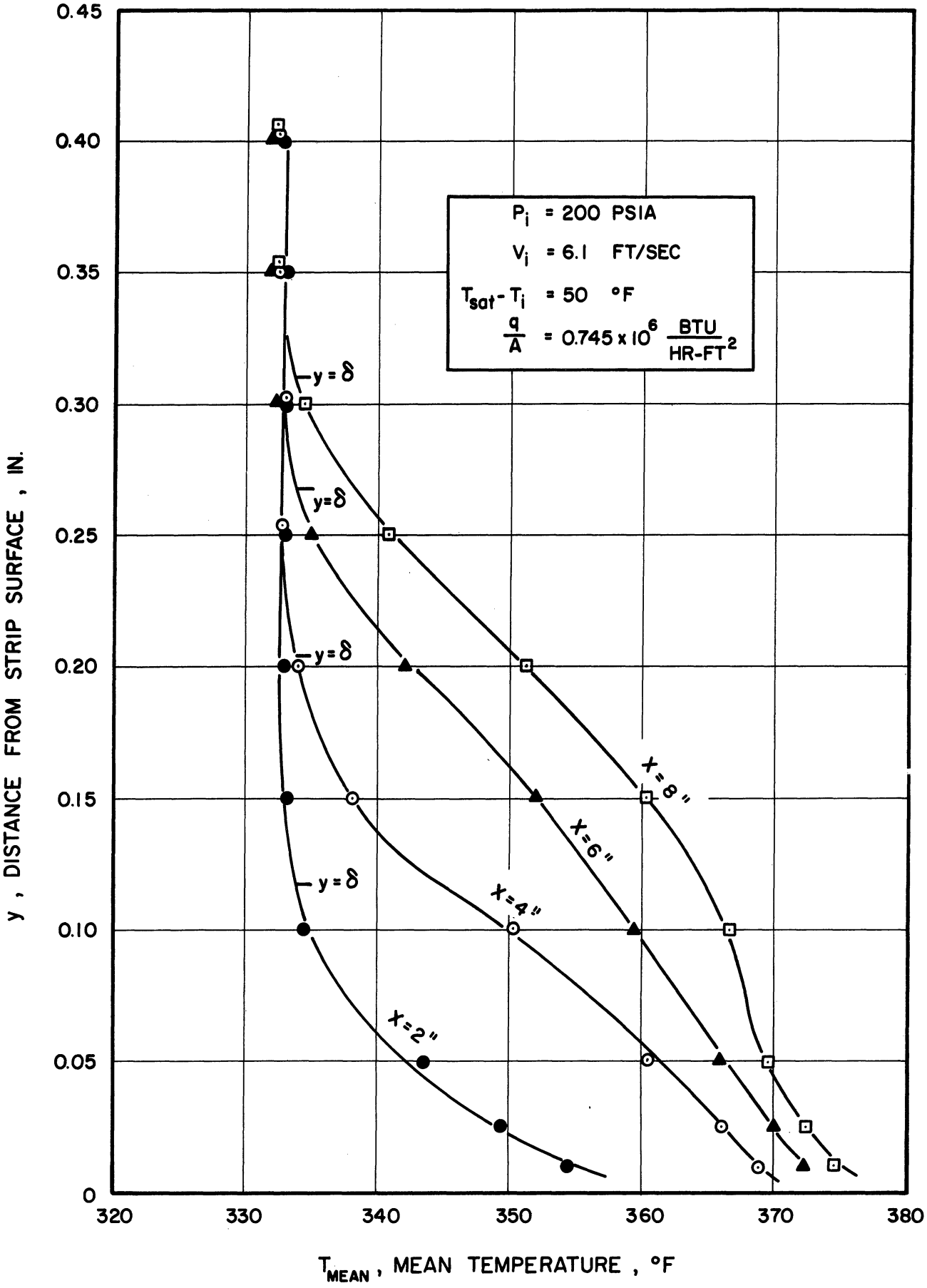

Figure 60. Mean Temperature Profile

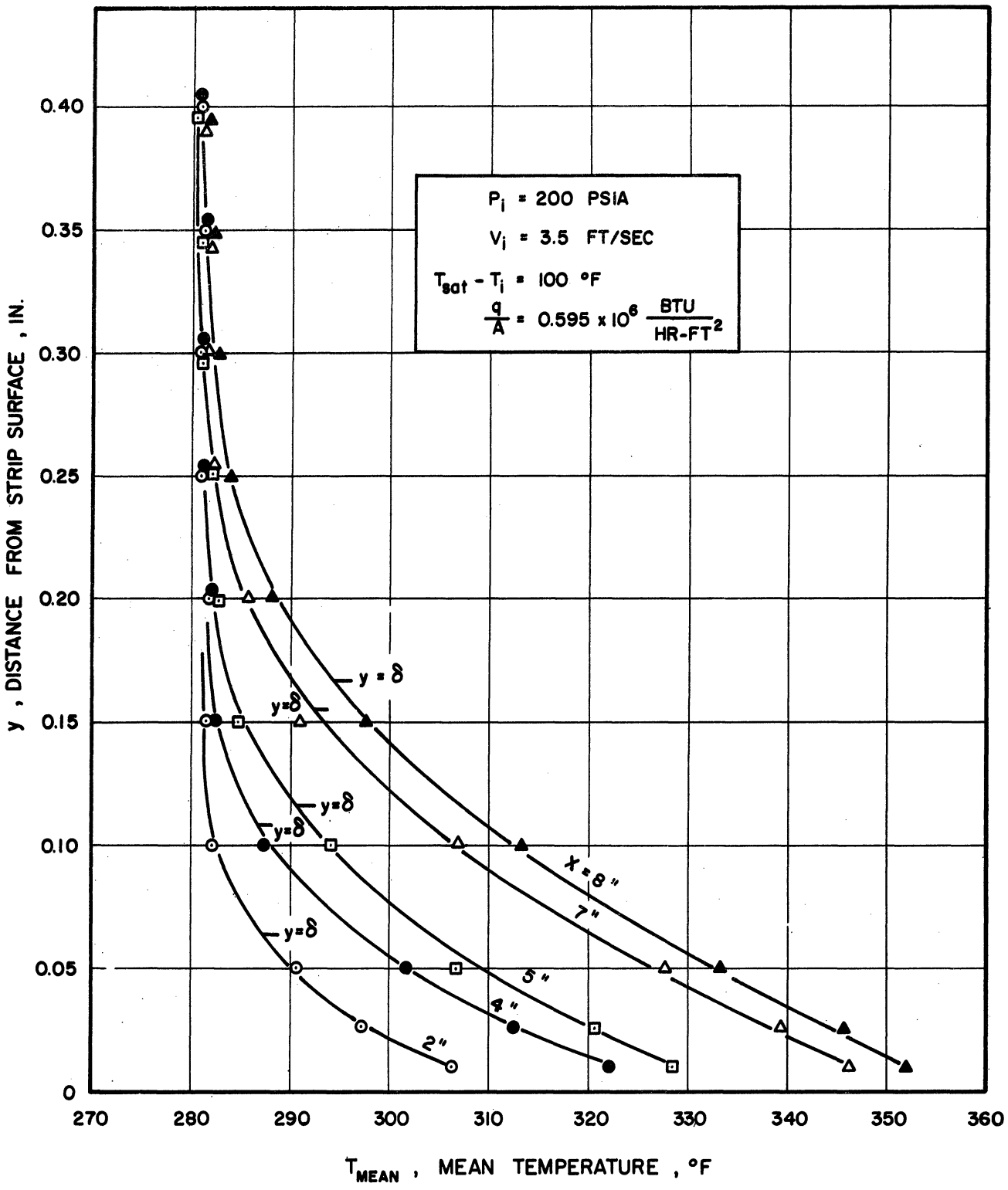

Figure 61. Mean Temperature Profile

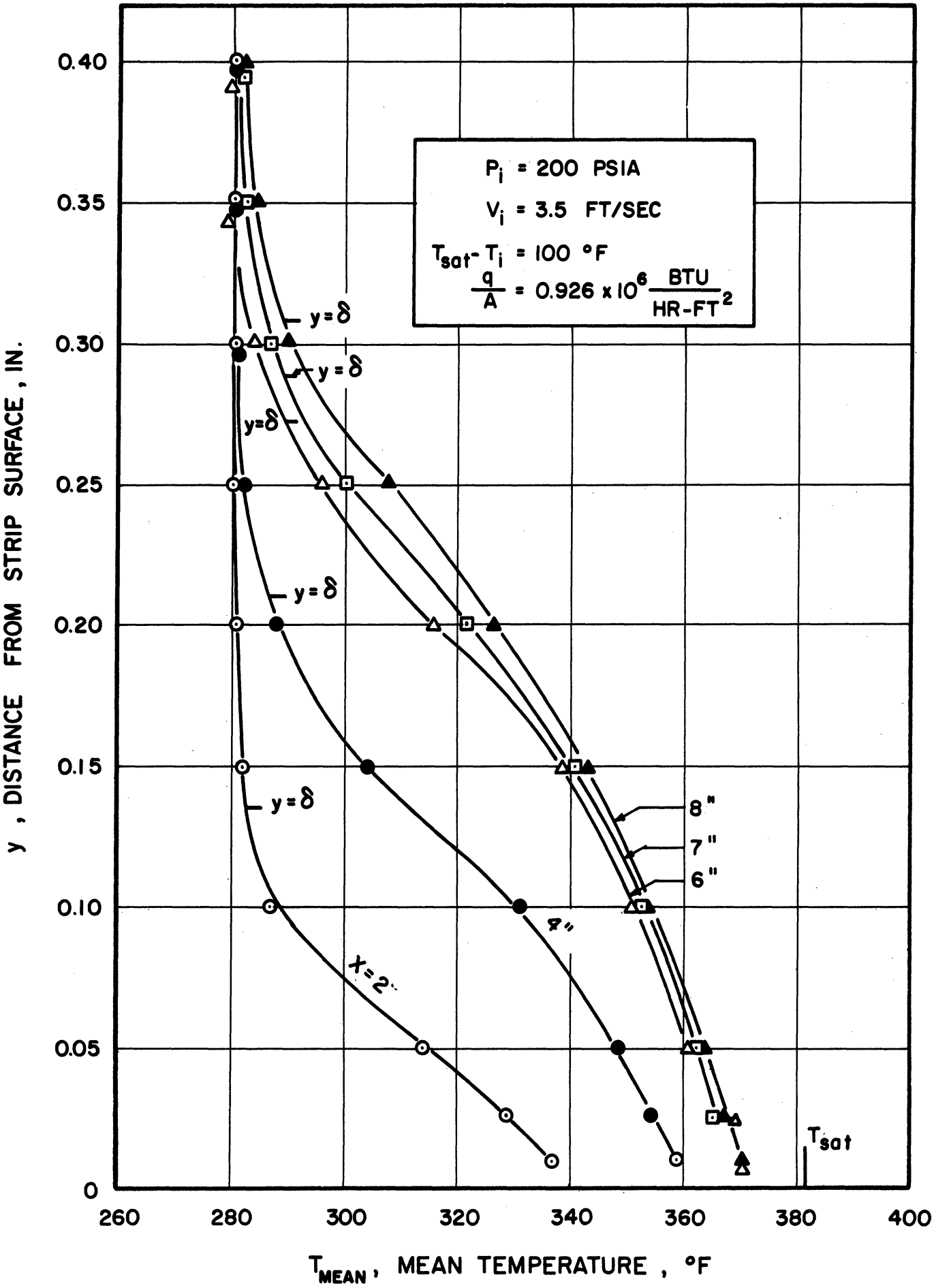

Figure 62. Mean Temperature Profile

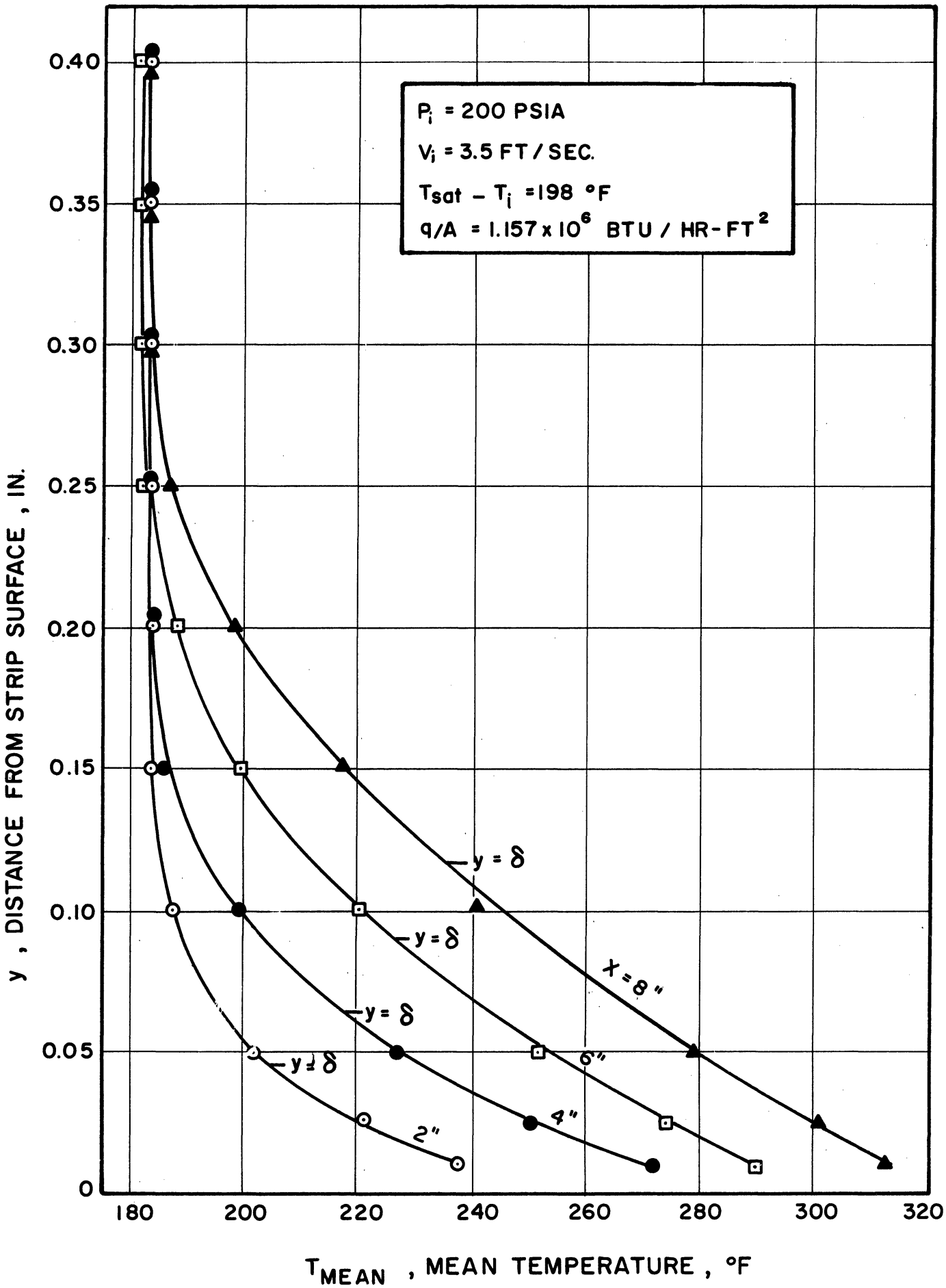

Figure 63. Mean Temperature Profile

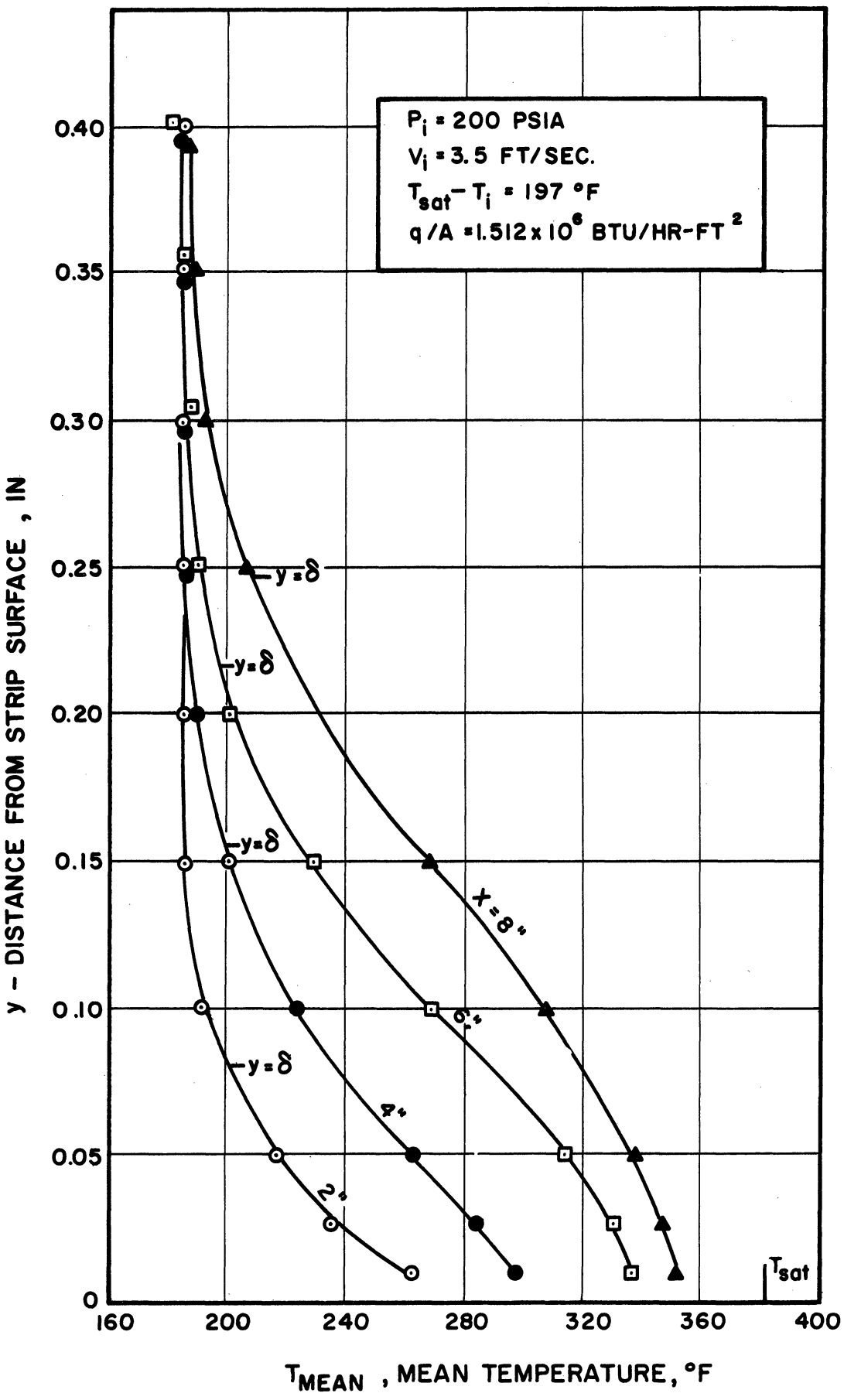

Figure 64. Mean Temperature Profile

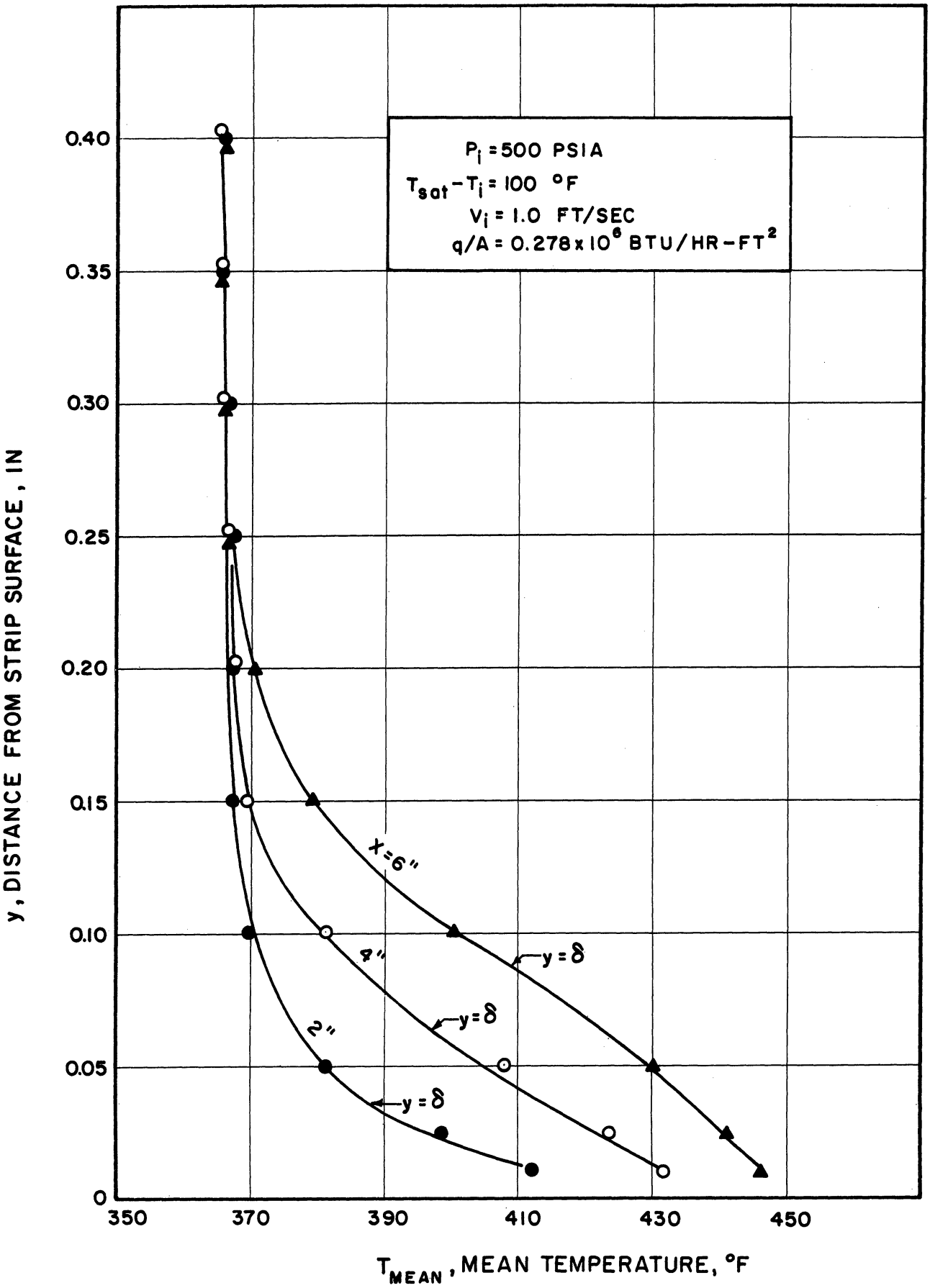

Figure 65. Mean Temperature Profile

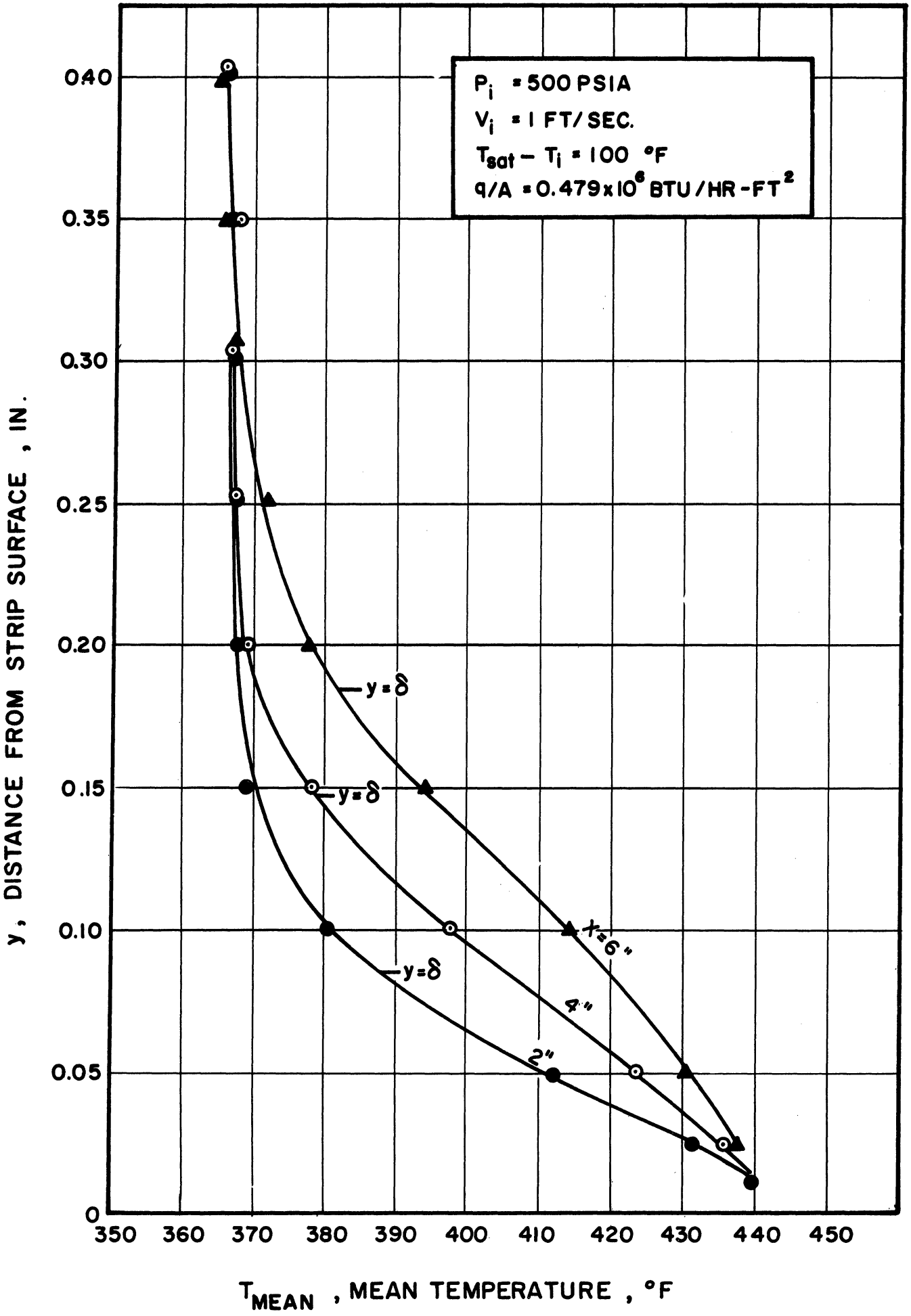

Figure 66. Mean Temperature Profile

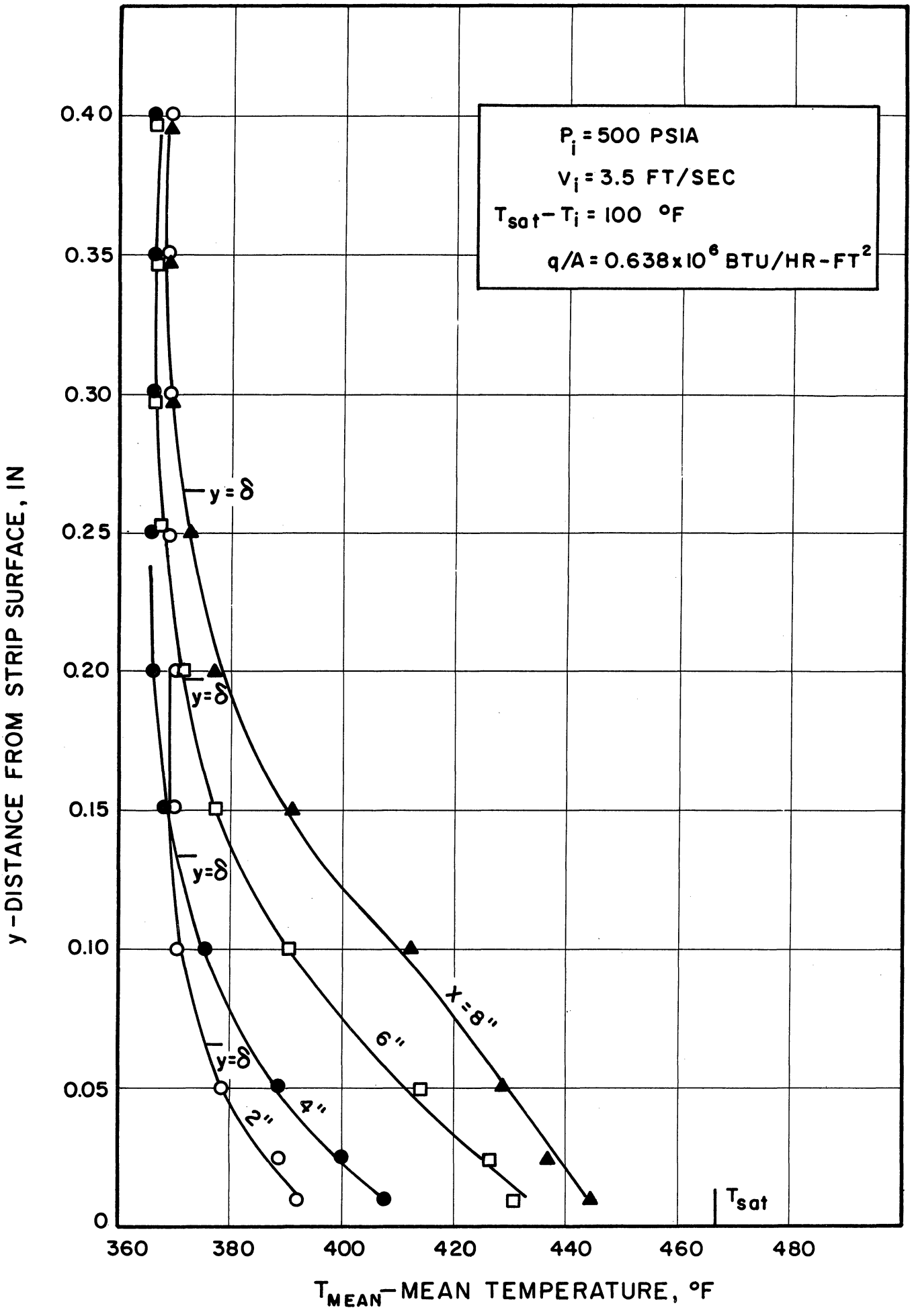

Figure 67. Mean Temperature Profile

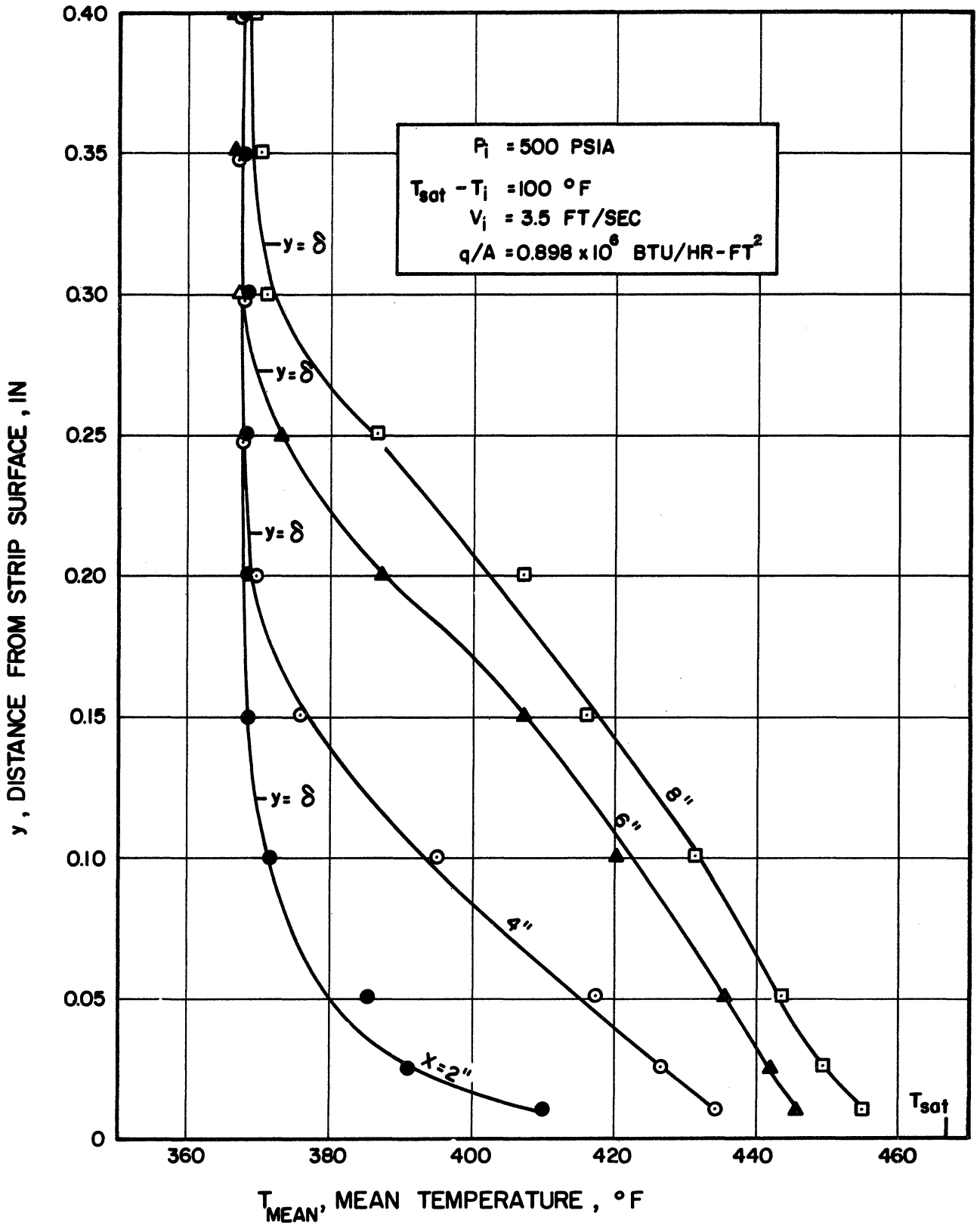

Figure 68. Mean Temperature Profile

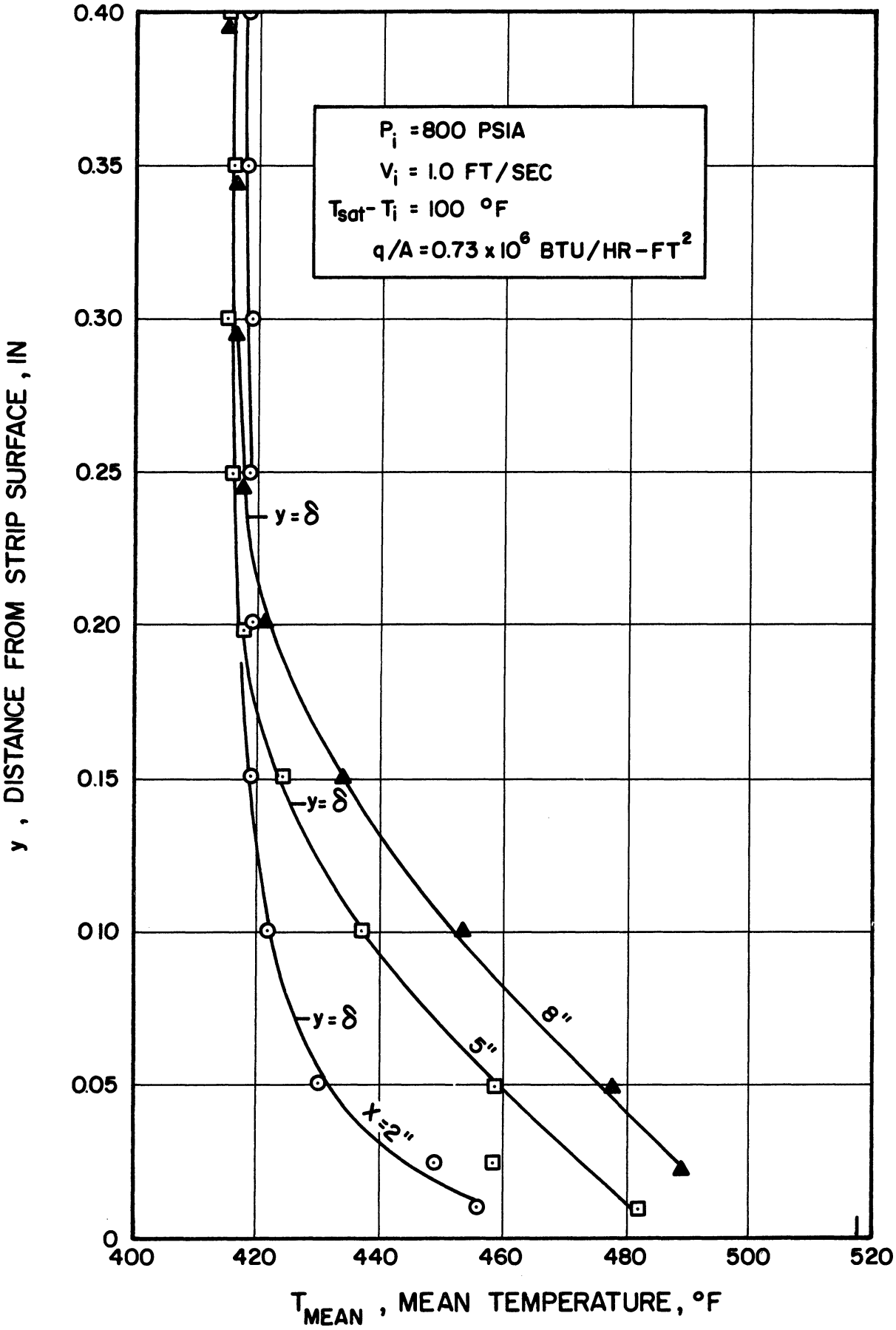

Figure 69. Mean Temperature Profile

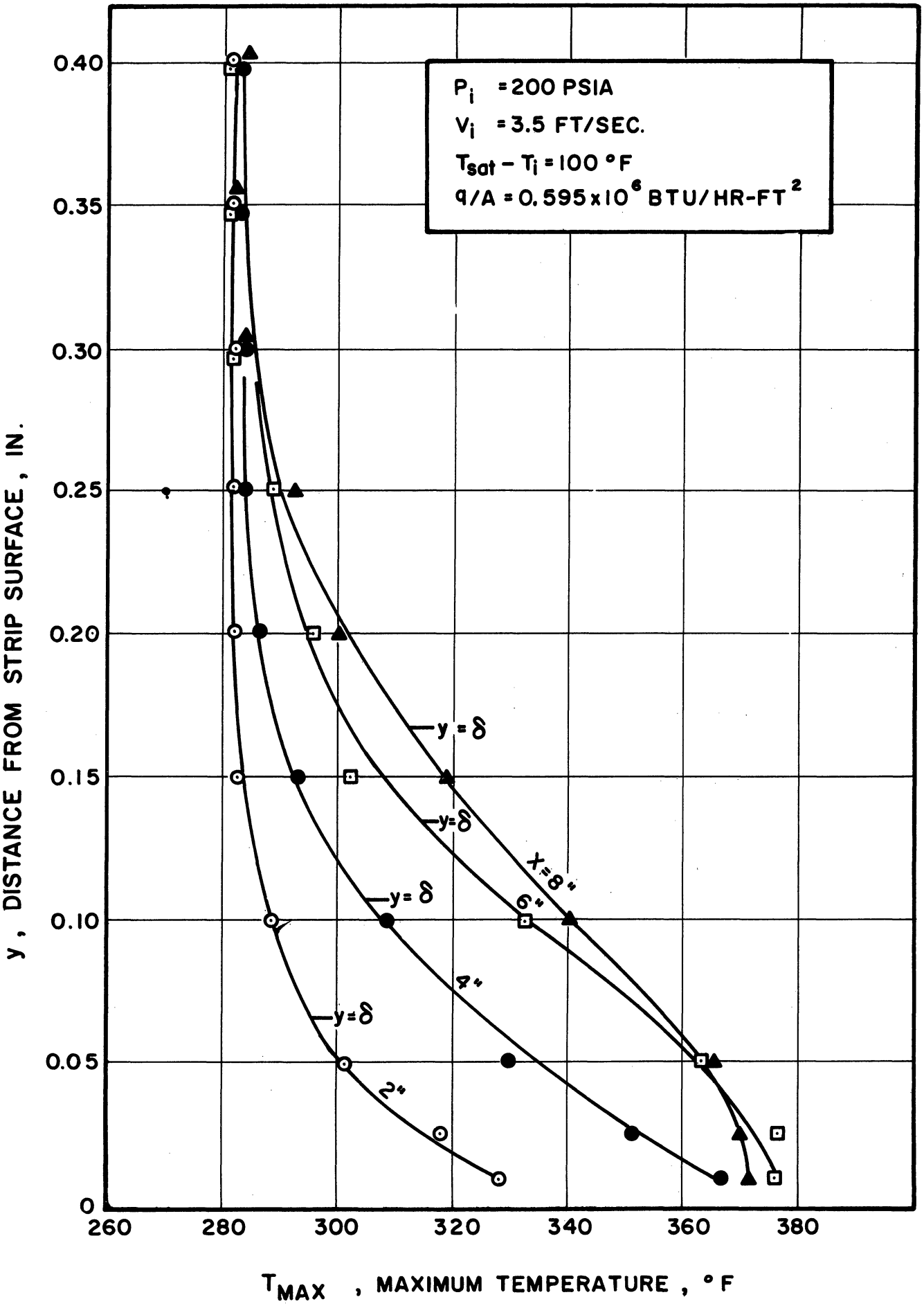

Figure 70. Maximum Temperature Profile

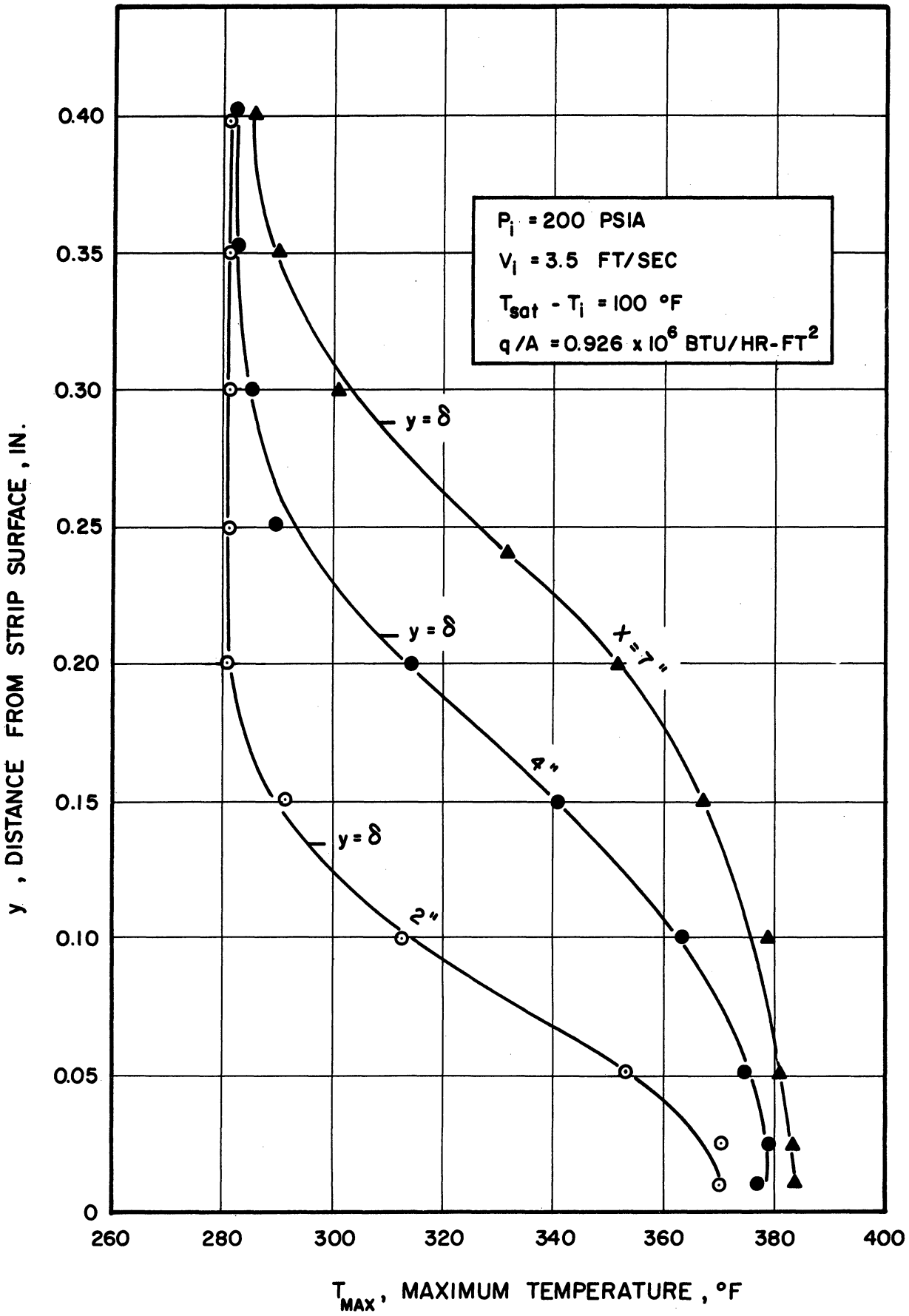

Figure 71. Maximum Temperature Profile

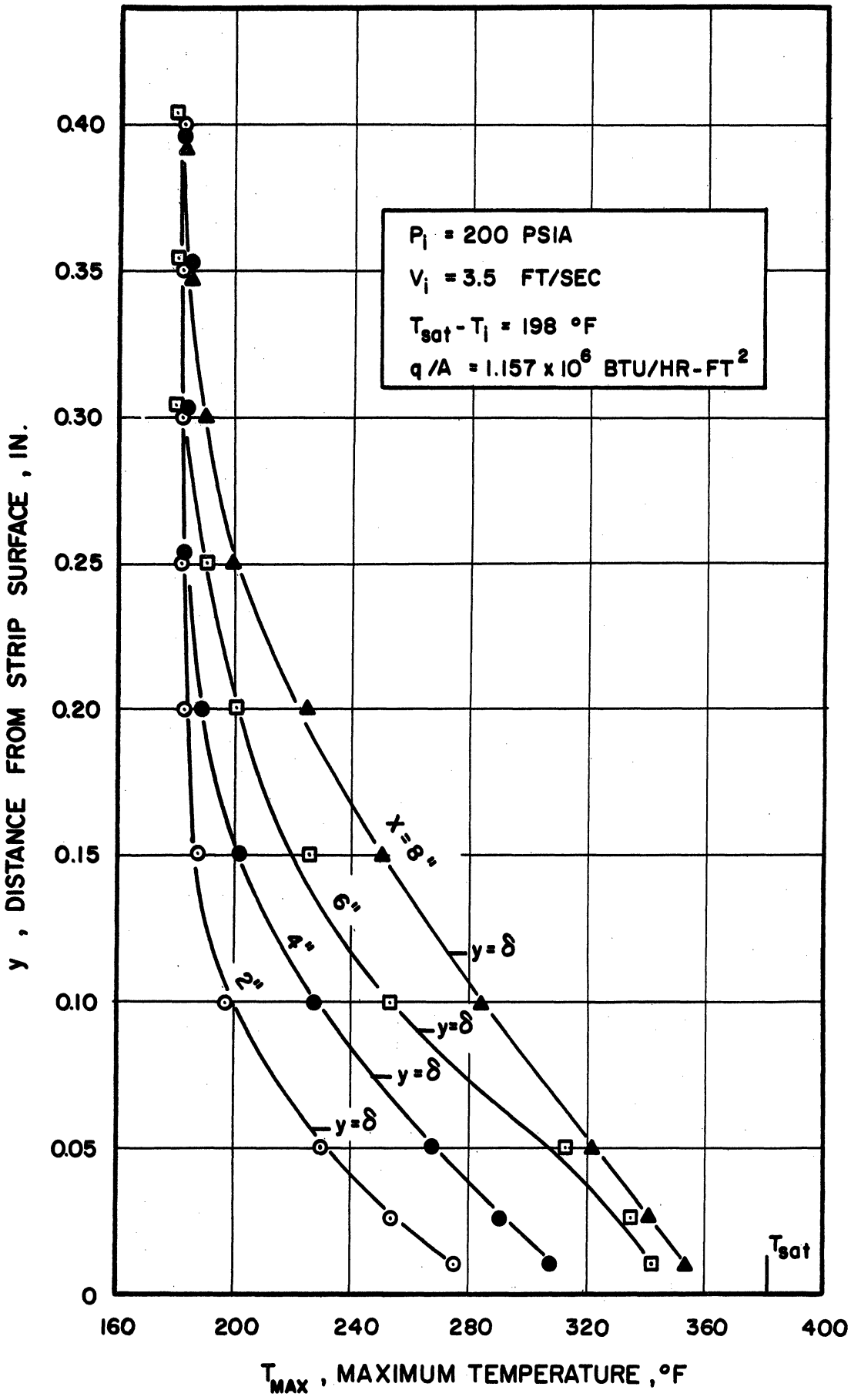

Figure 72. Maximum Temperature Profile

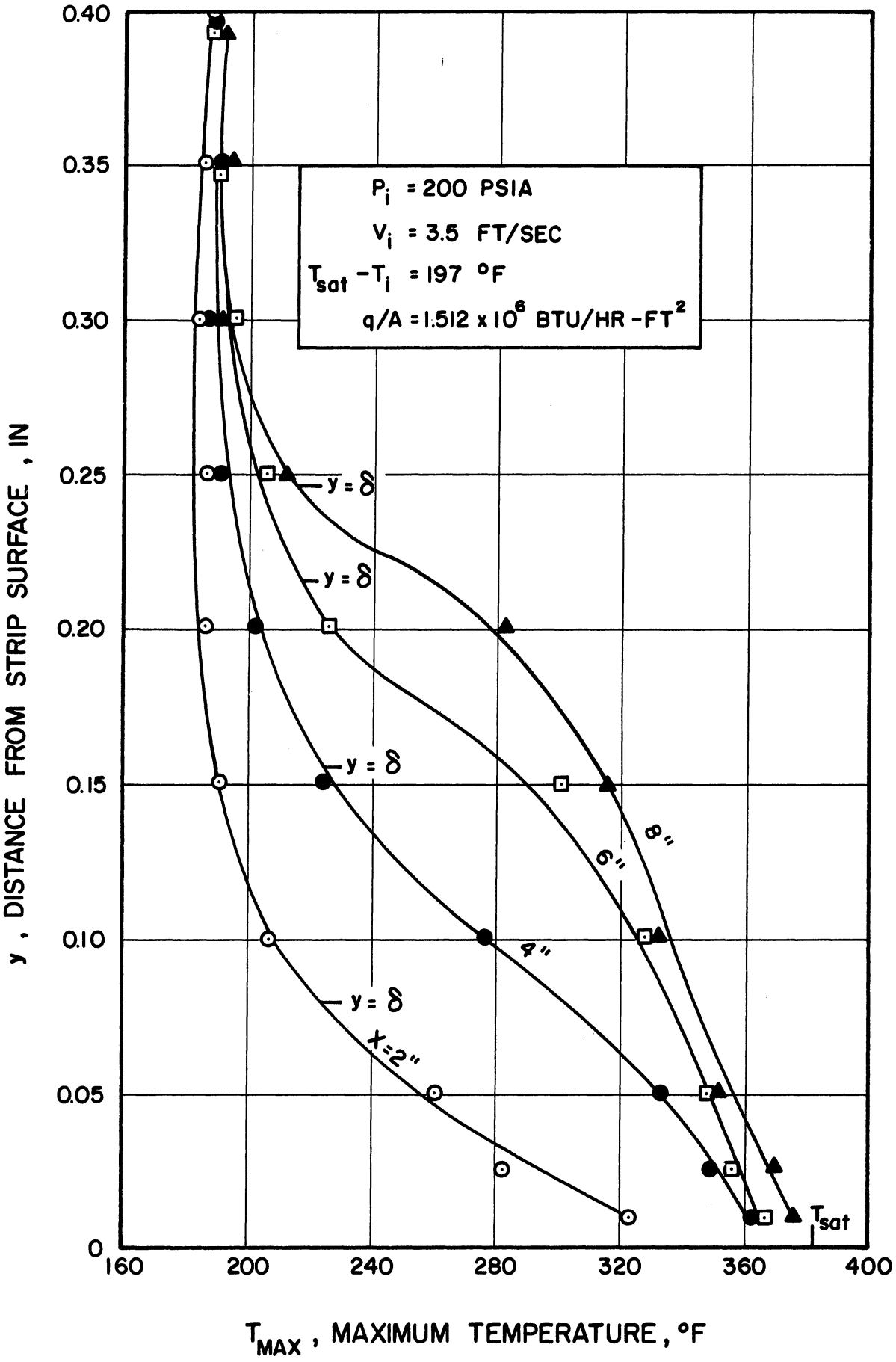

Figure 73. Maximum Temperature Profile

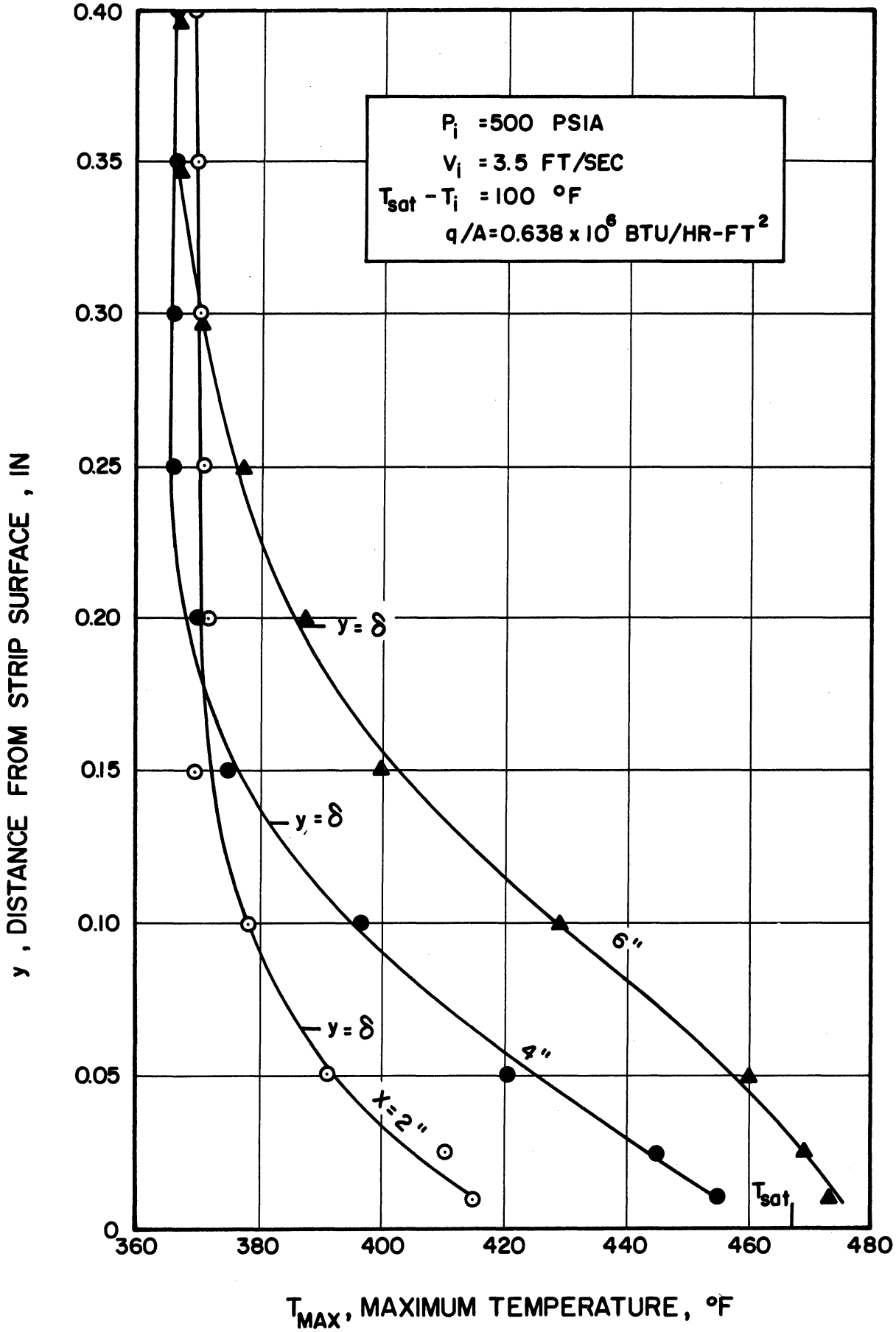

Figure 74. Maximum Temperature Profile

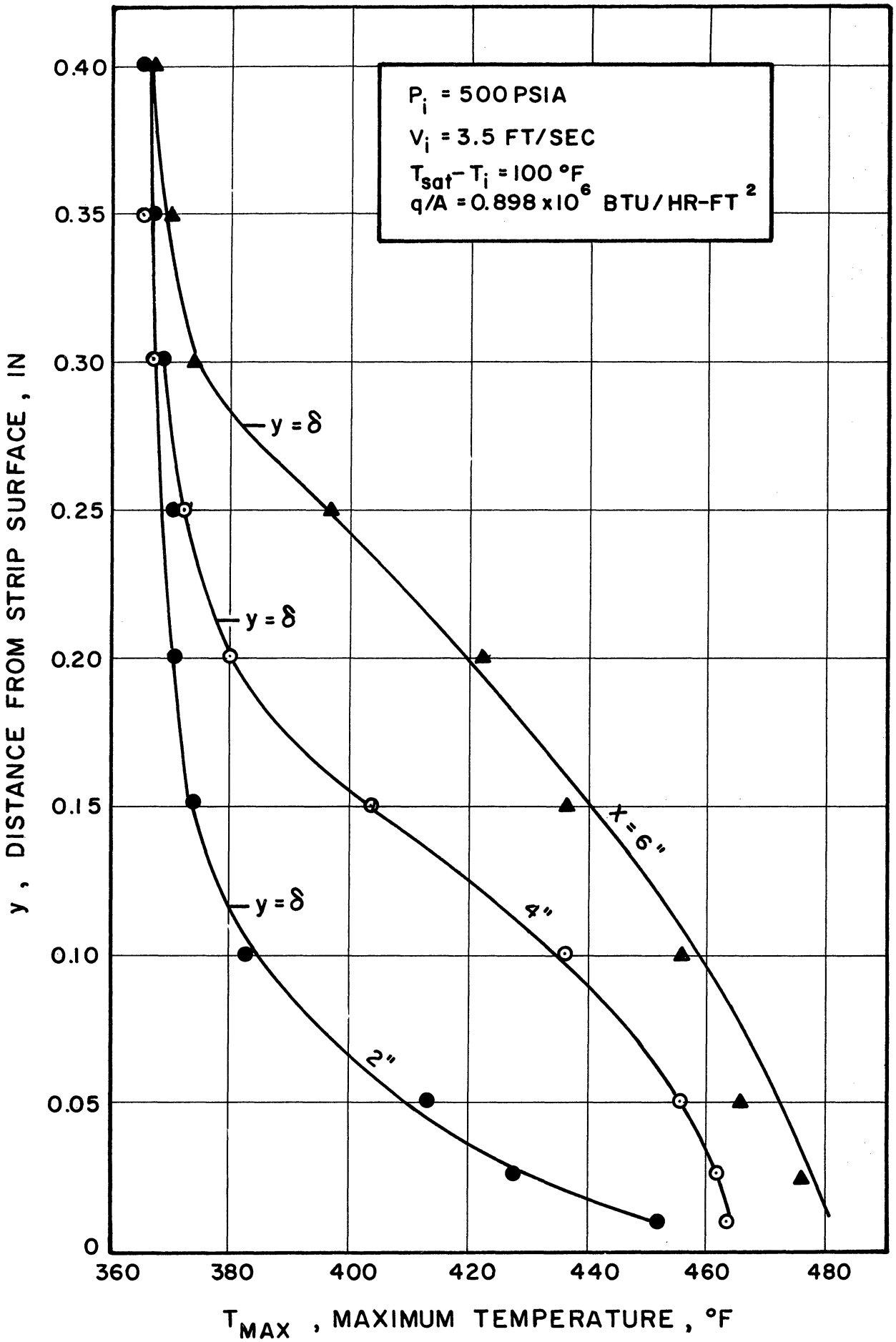

Figure 75. Maximum Temperature Profile

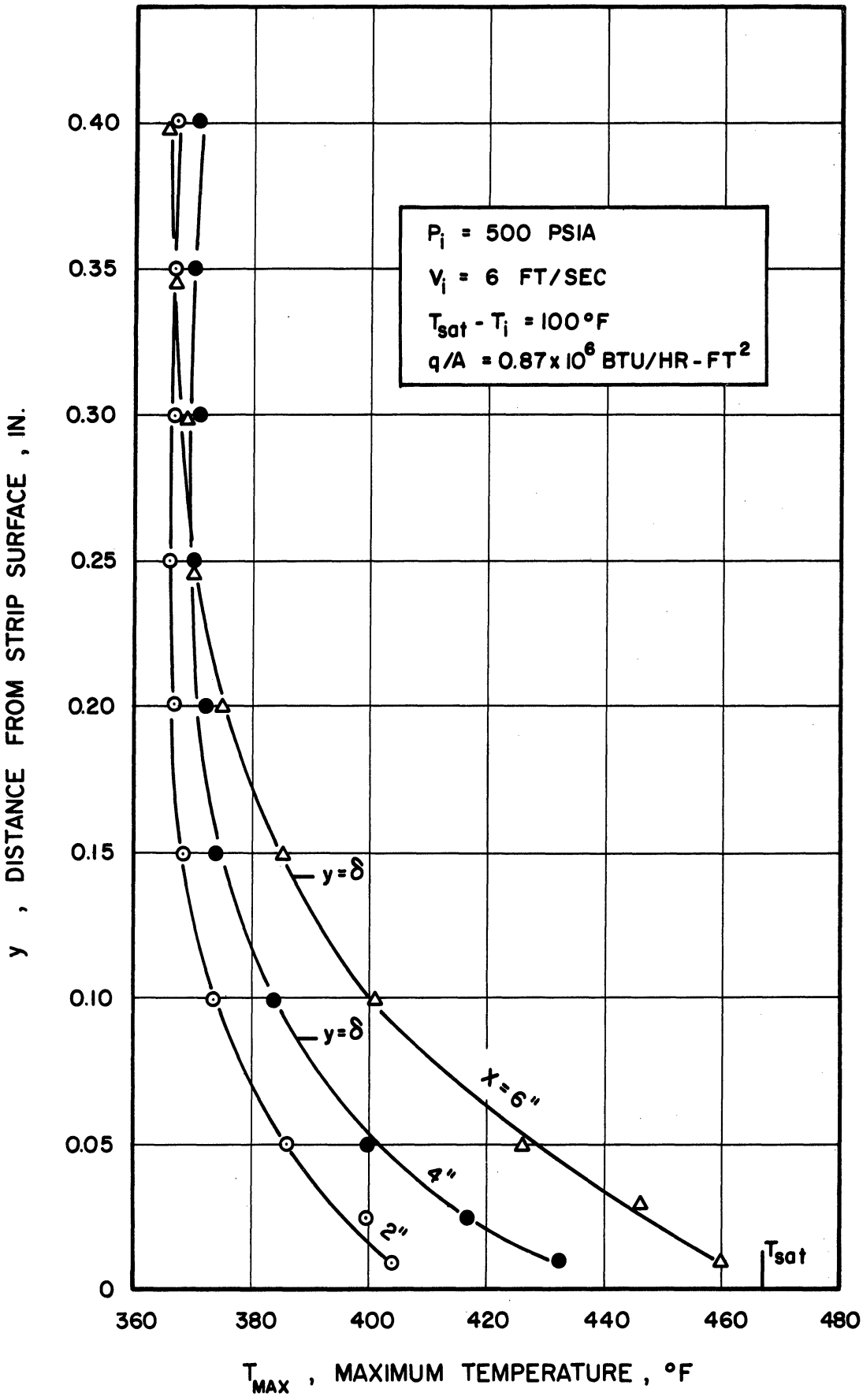

Figure 76. Maximum Temperature Profile

"Minimum temperature" profiles are shown in Figures 77 through 83. The bubble boundary layer thickness is shown on these plots to point out the existence of highly subcooled liquid well within the two phase region.

3. Temperature Distribution at the Single-phase Core-Bubble Boundary Interface

To investigate the extent to which subcooled liquid exists along the bubble boundary layer (i.e. at $y=\delta$), plots of $(T_{sat} - T_{MIN})_{y=\delta} / (T_{sat} - T_i)$ vs. y were constructed. This dimensionless temperature ratio is an indication of the degree to which inlet subcooling is maintained along the bubble boundary layer. A ratio of unity means that liquid particles at the inlet temperature exist along the bubble boundary layer. These plots are shown in Figures 84 through 88. It is noted that in some tests a temperature ratio of unity was maintained as far downstream as 6 inches from the leading edge. Furthermore, it is observed that for the same inlet pressure, velocity and subcooling, this temperature ratio increases with increasing heat flux.

Bankoff (43) derived an approximate expression for estimating the mean temperature at the single-phase core-bubble boundary interface. Using Gunther's (25) data he found that this temperature rises steeply towards

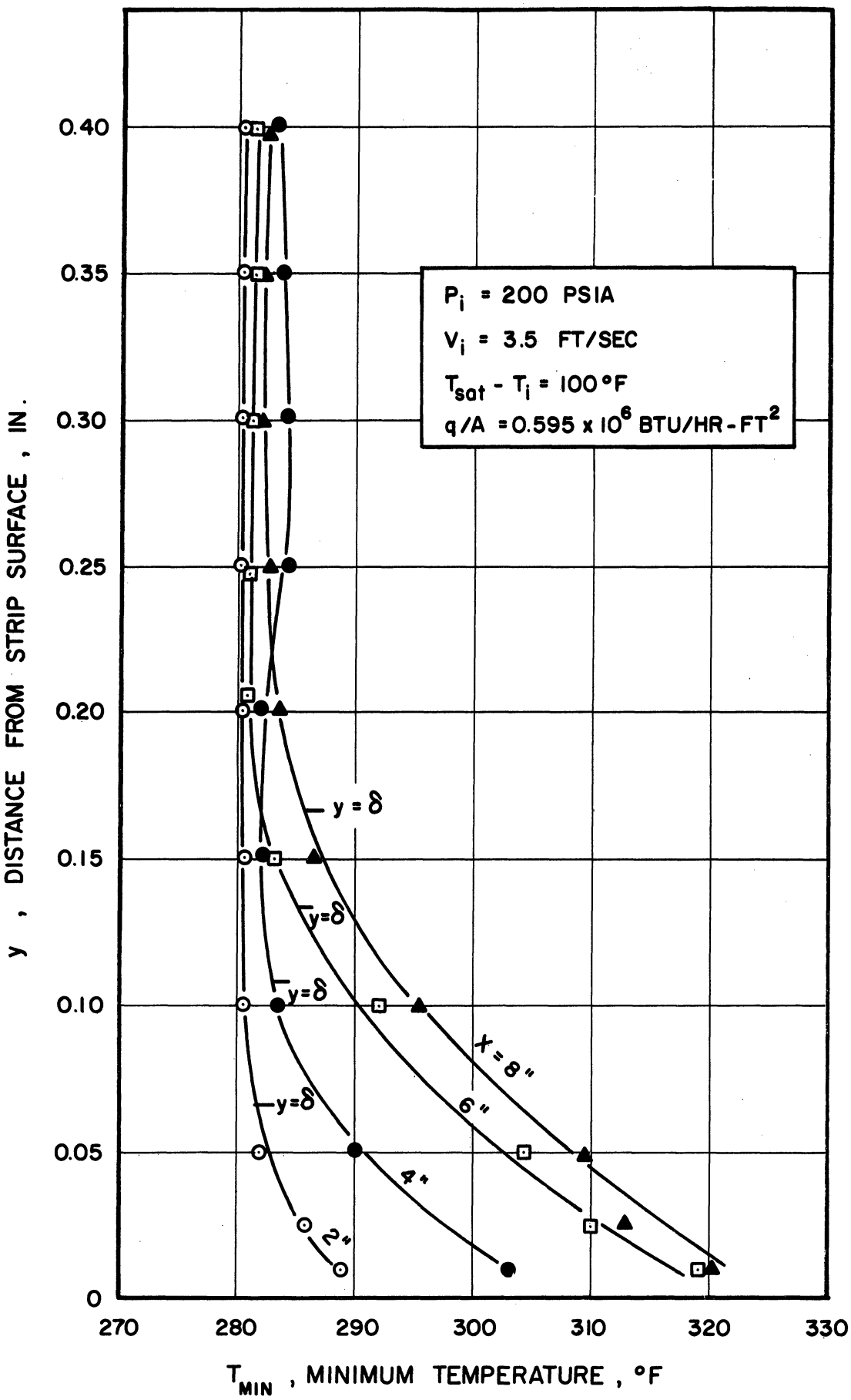

Figure 77. Minimum Temperature Profile

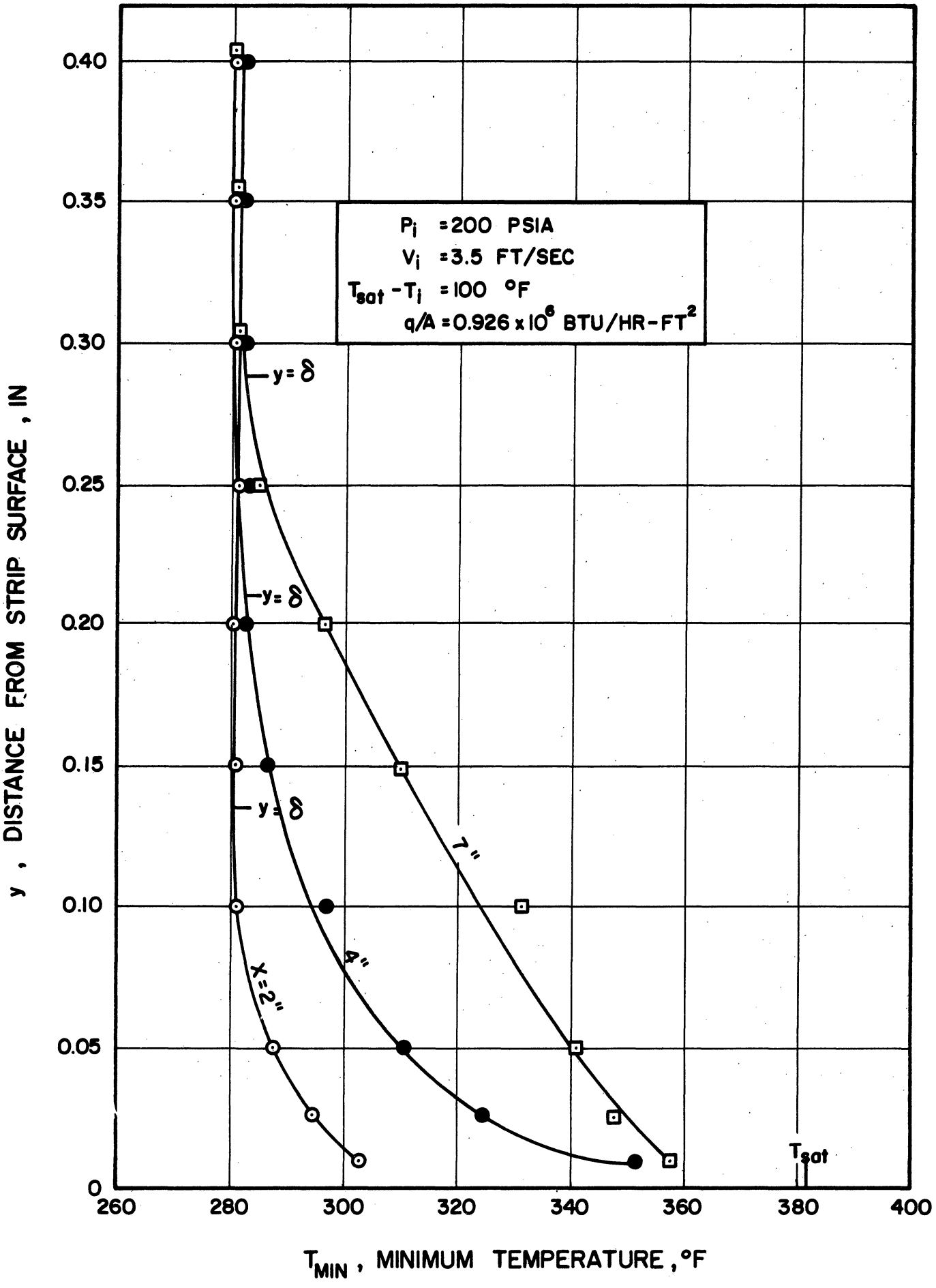

Figure 78. Minimum Temperature Profile

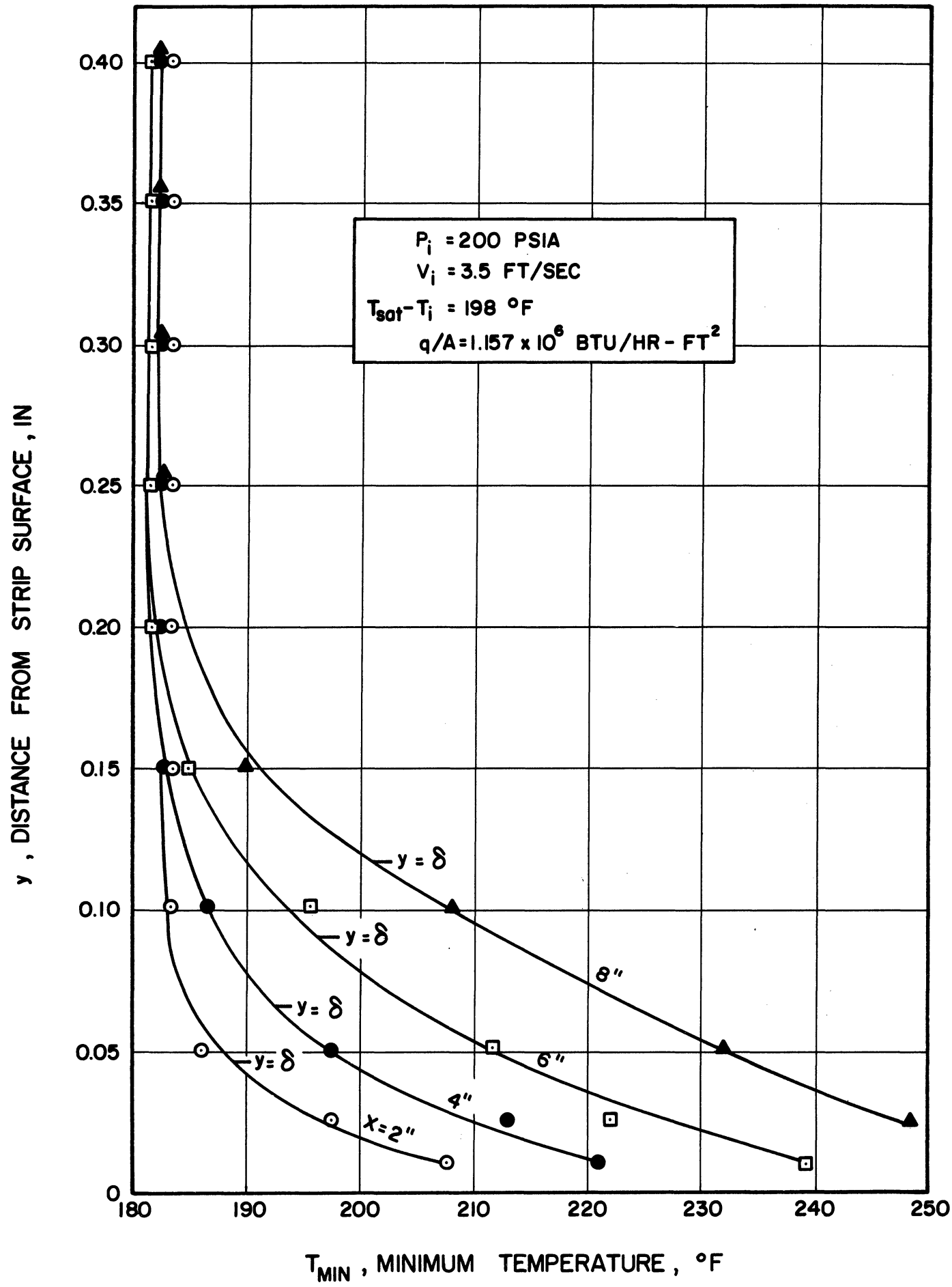

Figure 79. Minimum Temperature Profile

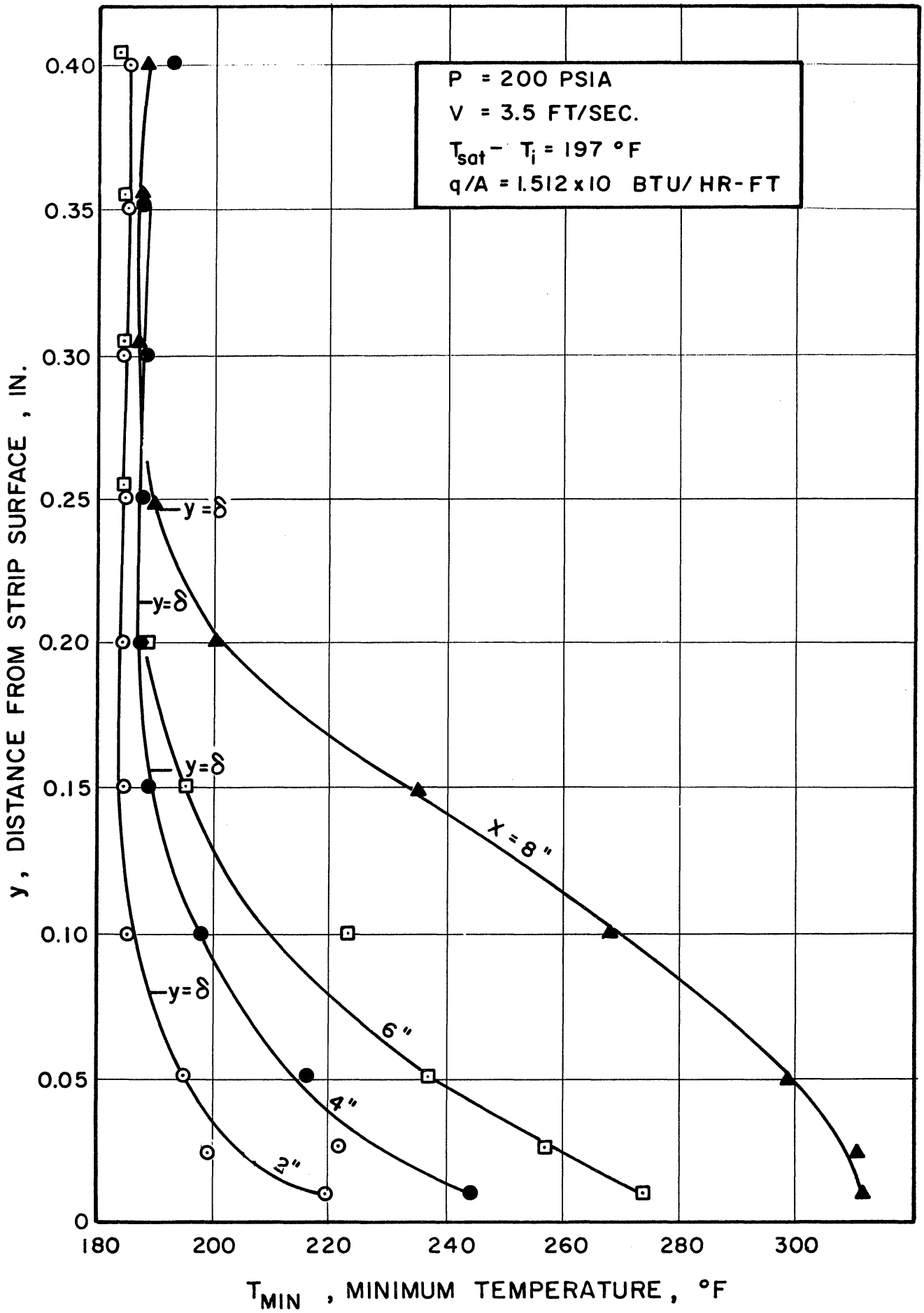

Figure 80. Minimum Temperature Profile

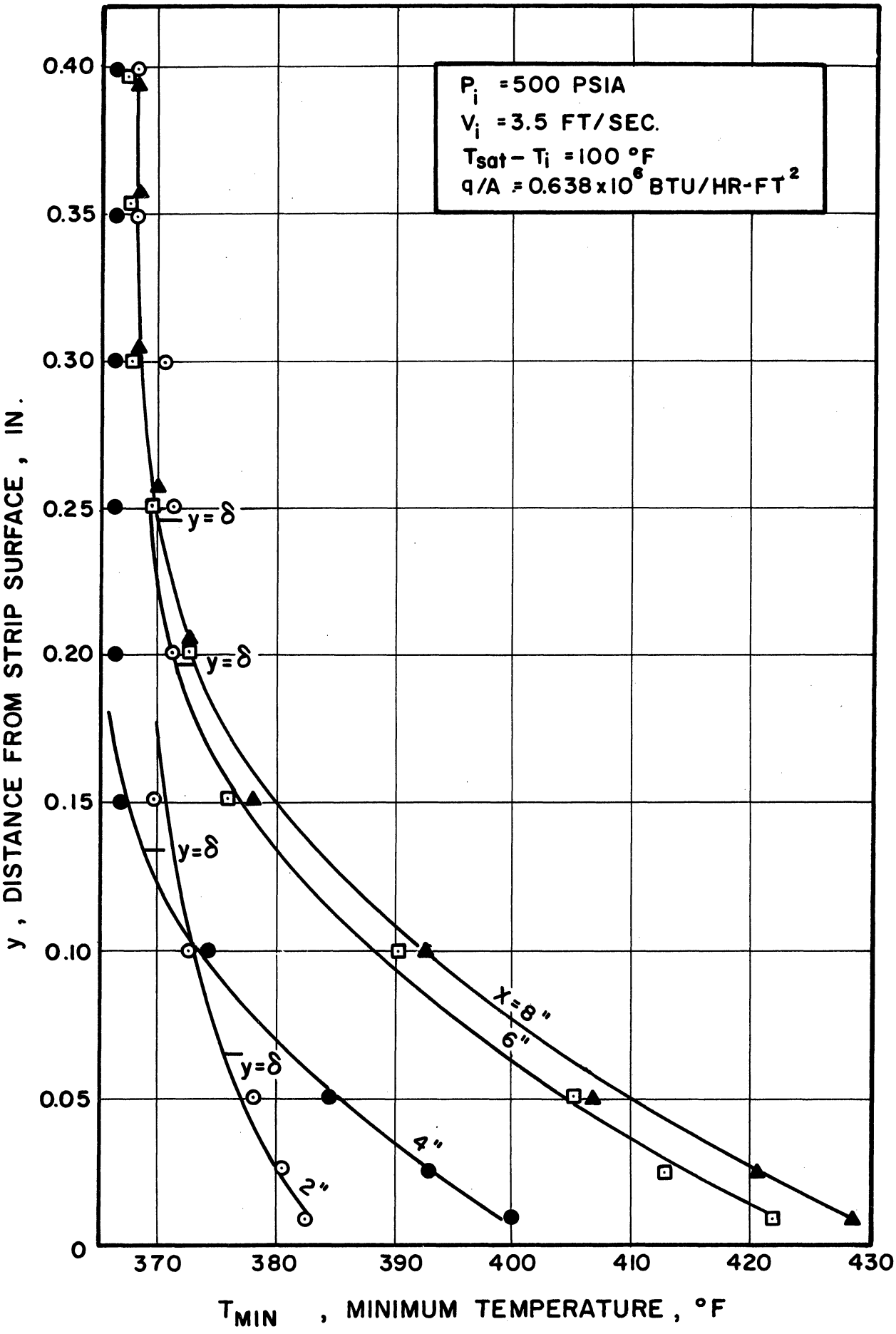

Figure 81. Minimum Temperature Profile

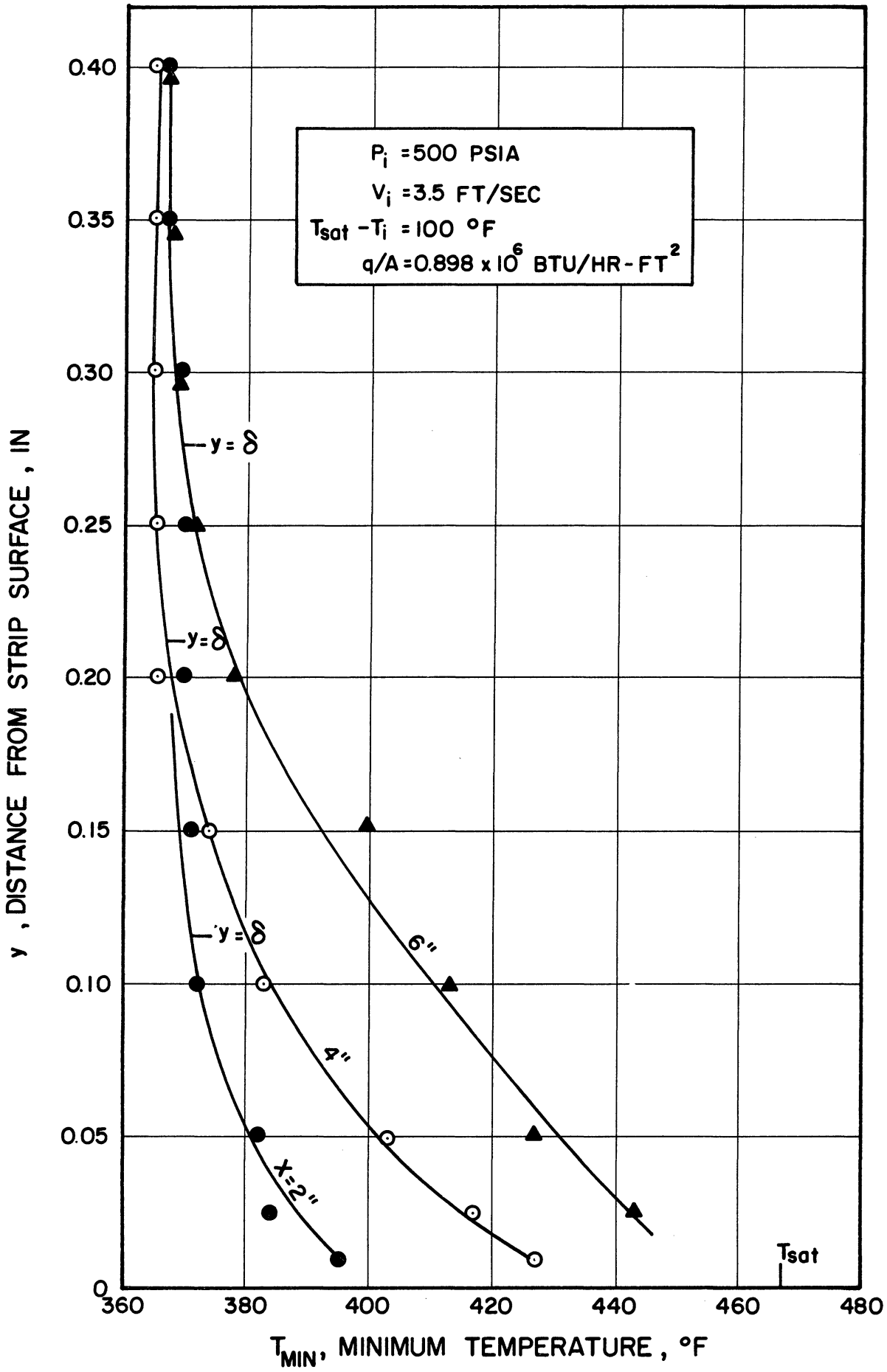

Figure 82. Minimum Temperature Profile

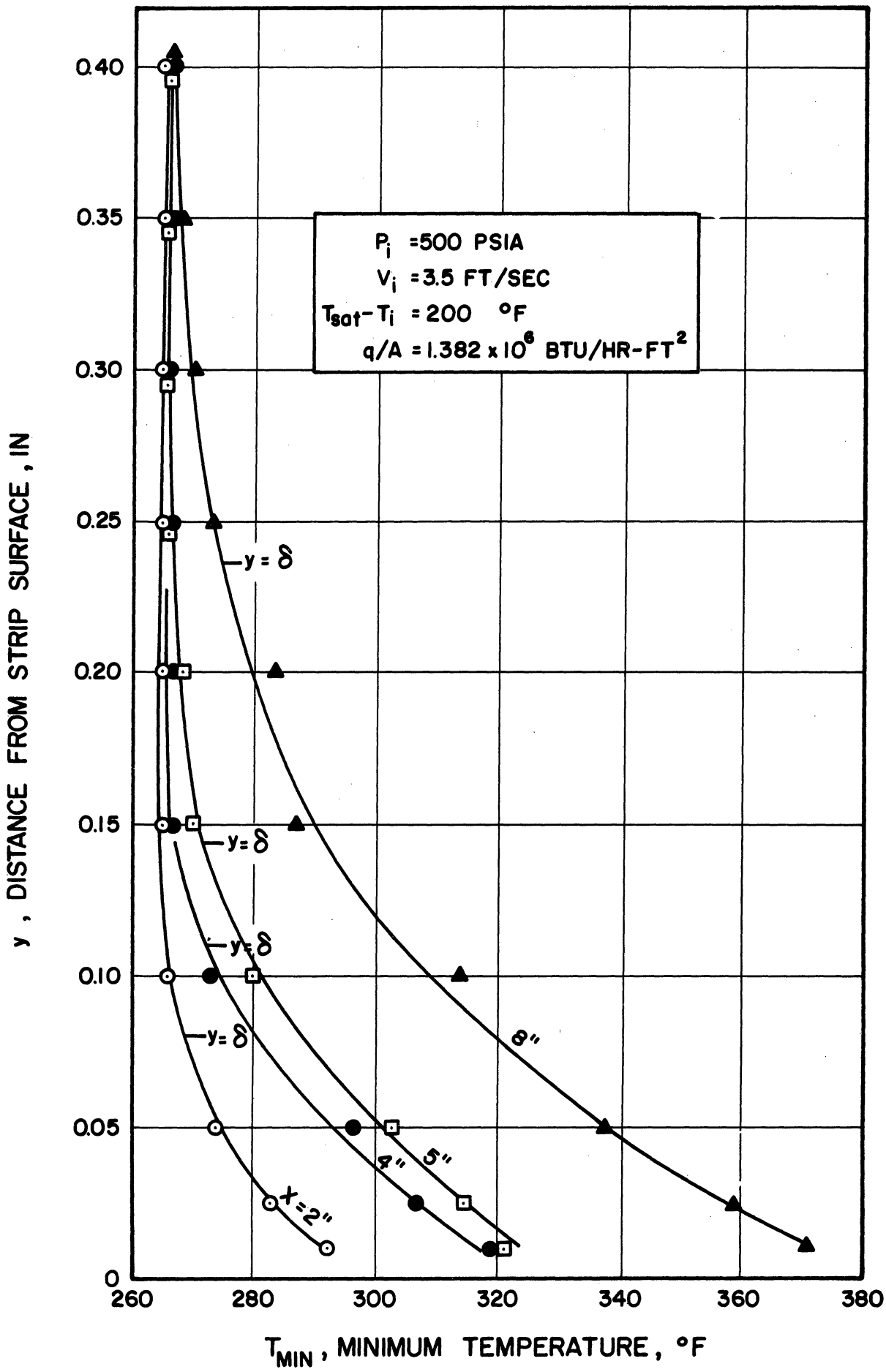

Figure 83. Minimum Temperature Profile

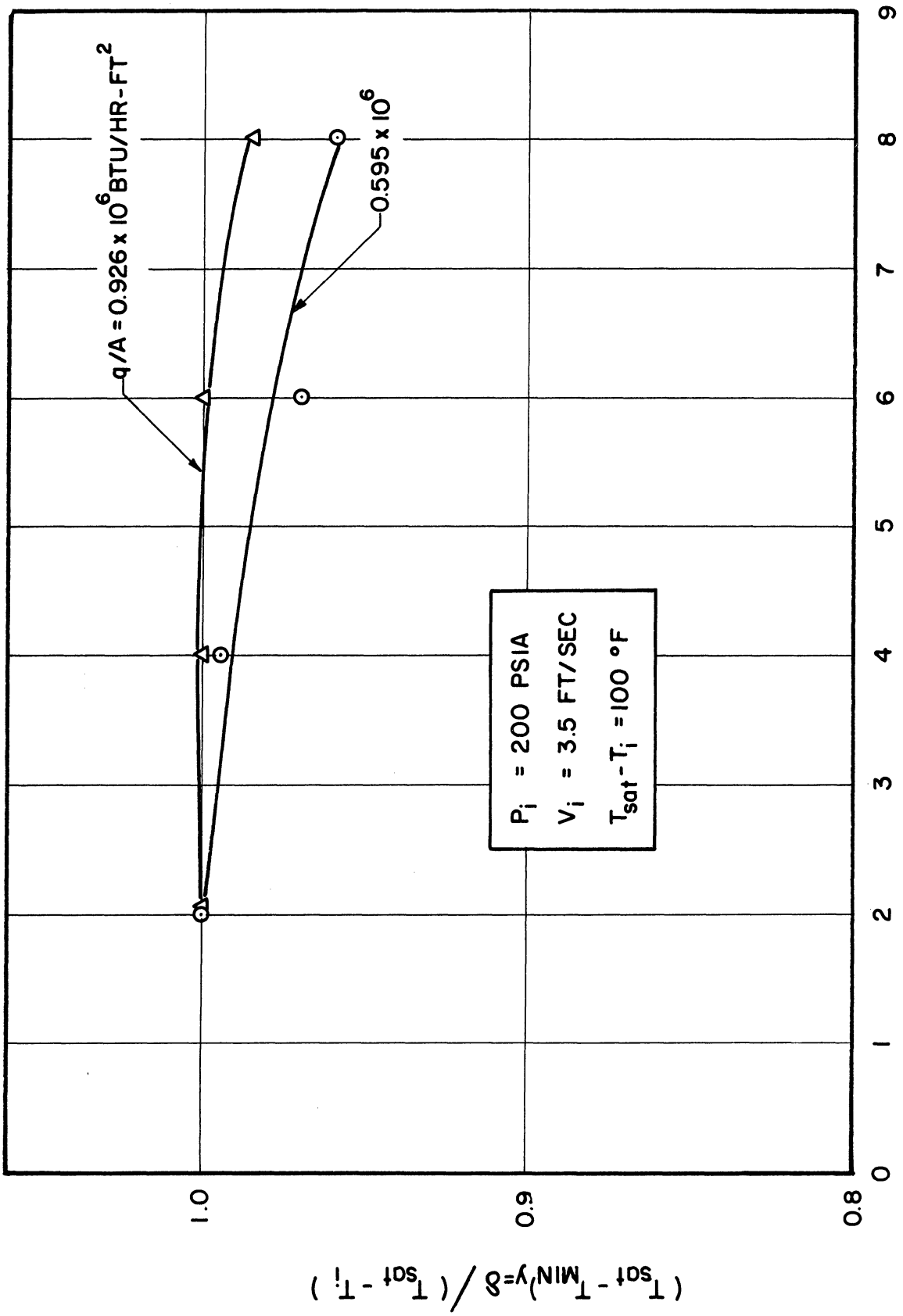

Figure 84. Minimum Temperature Distribution at the Single-Phase Core-Bubble Boundary Interface

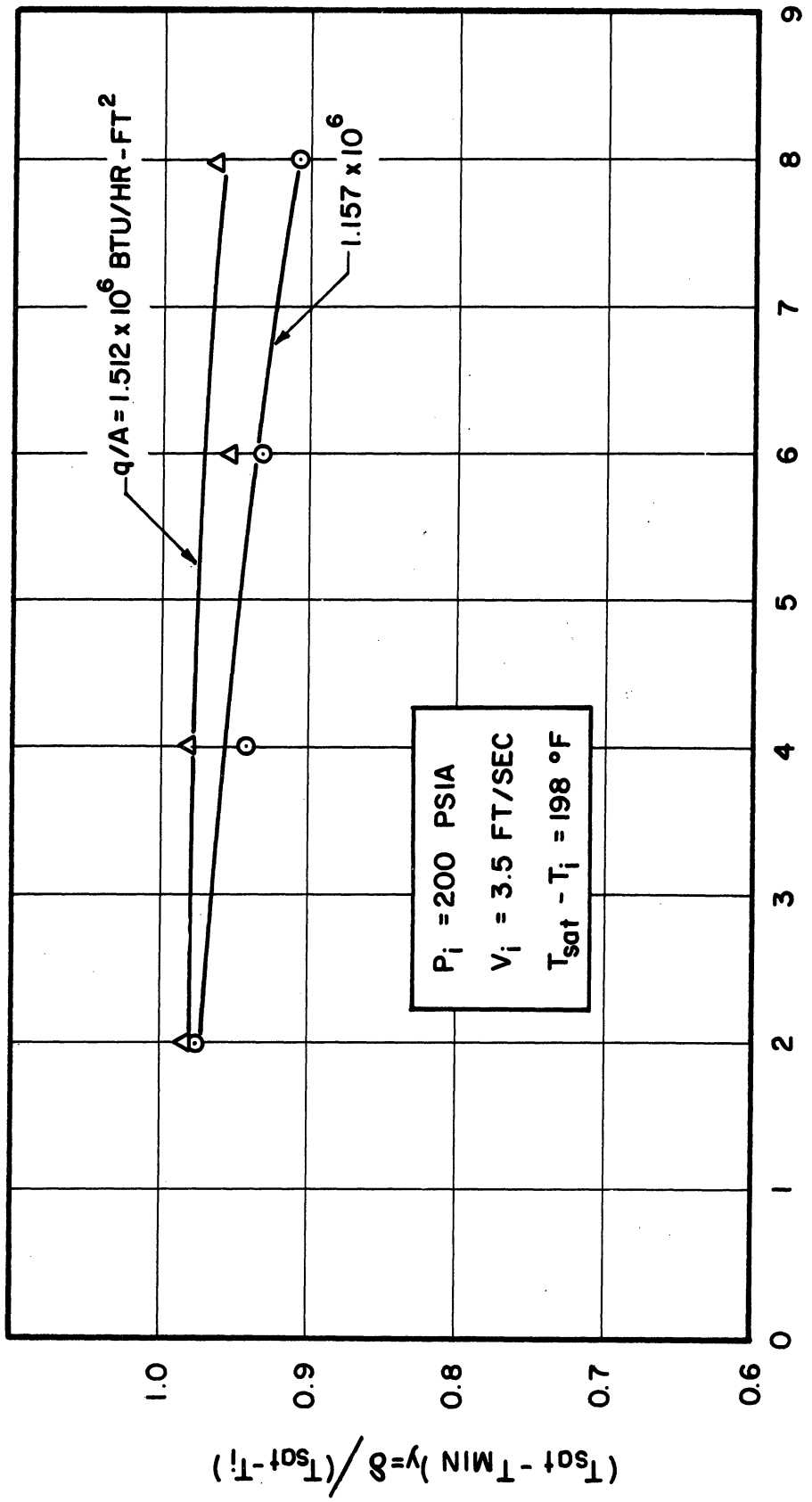

Figure 85. Minimum Temperature Distribution at the Single-Phase Core-Bubble Boundary Interface

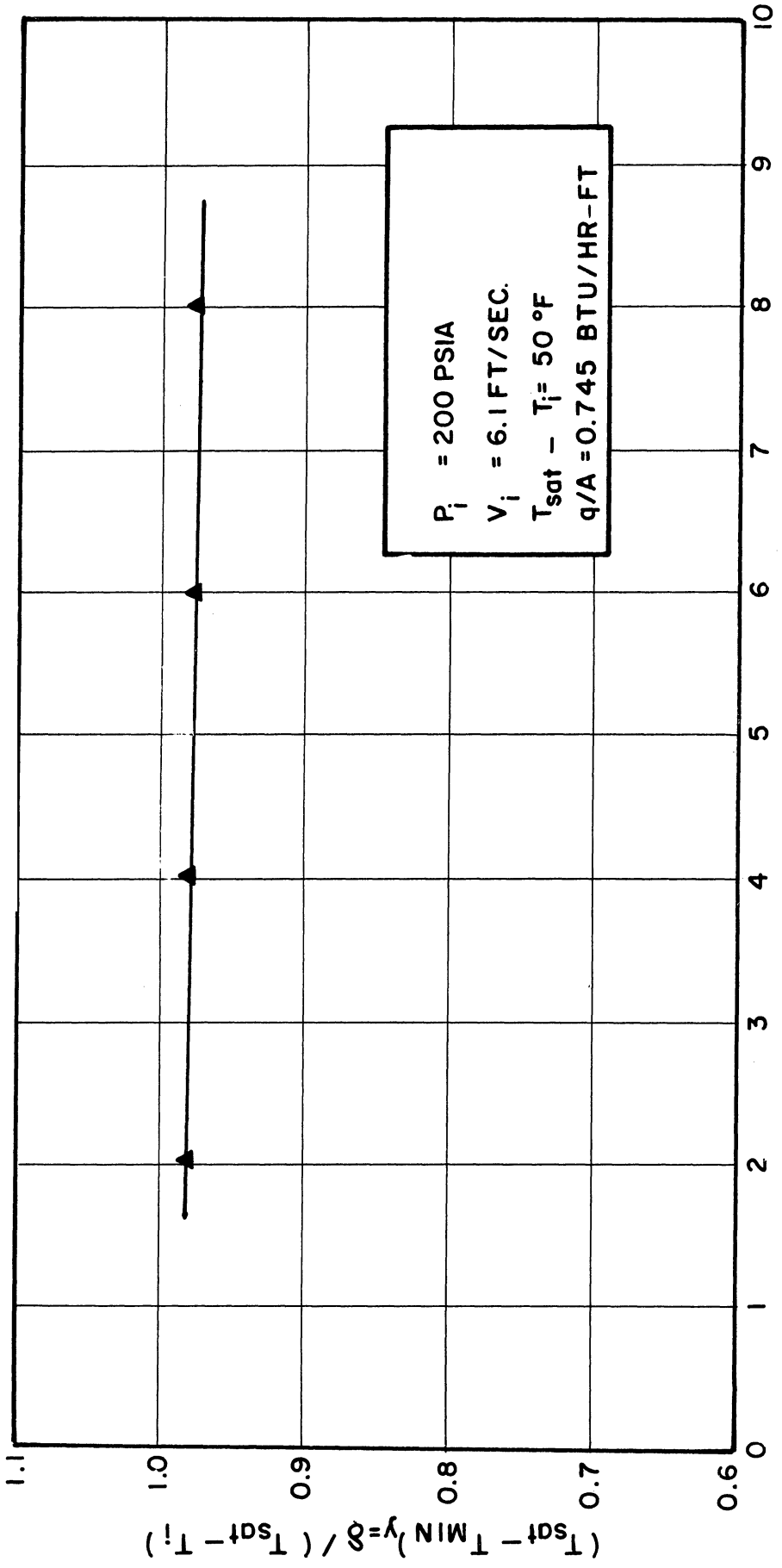

Figure 86. Minimum Temperature Distribution at the Single-Phase Core-Bubble Boundary Interface

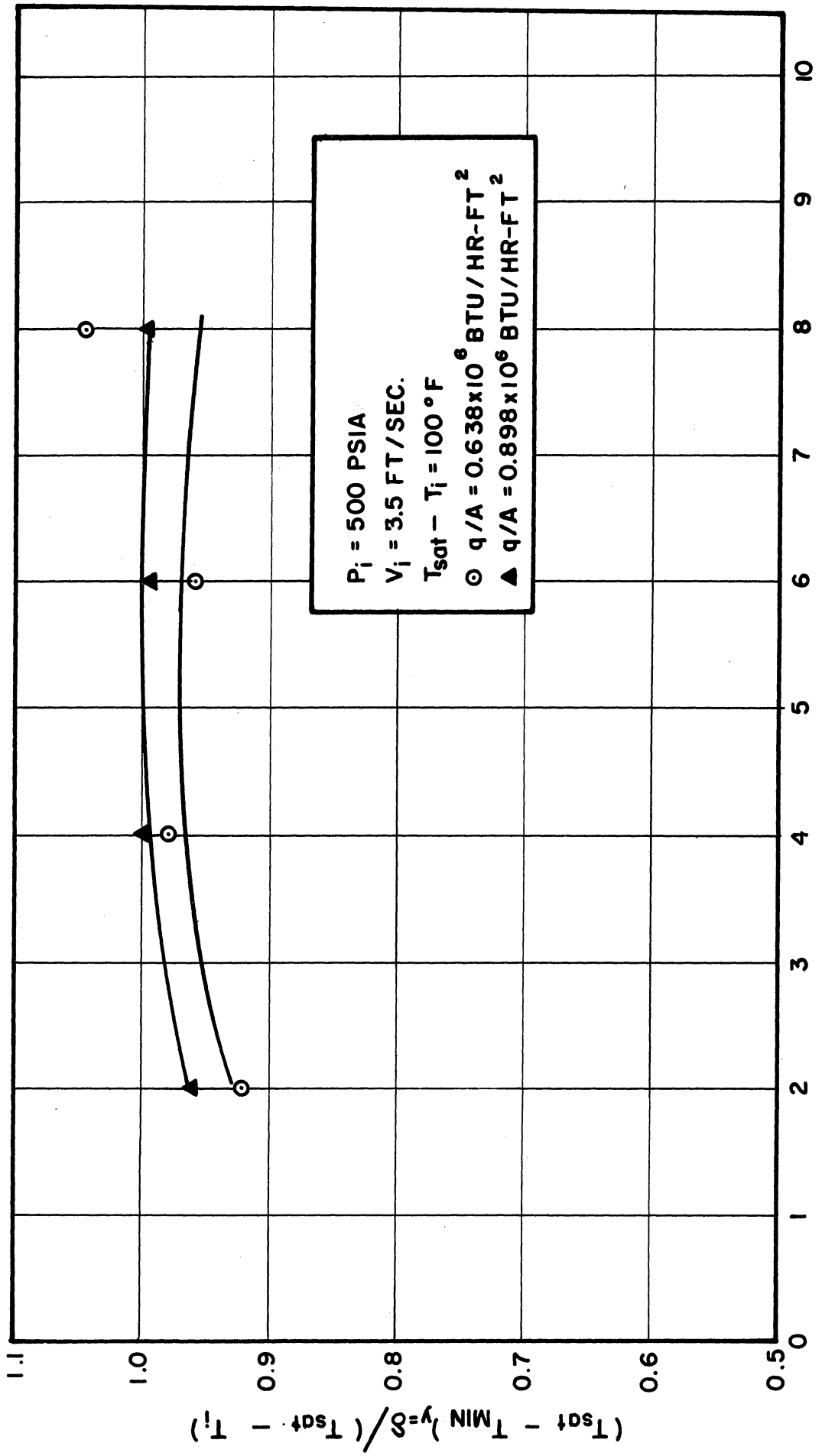

Figure 87. Minimum Temperature Distribution at the Single-Phase Core-Bubble Boundary Interface

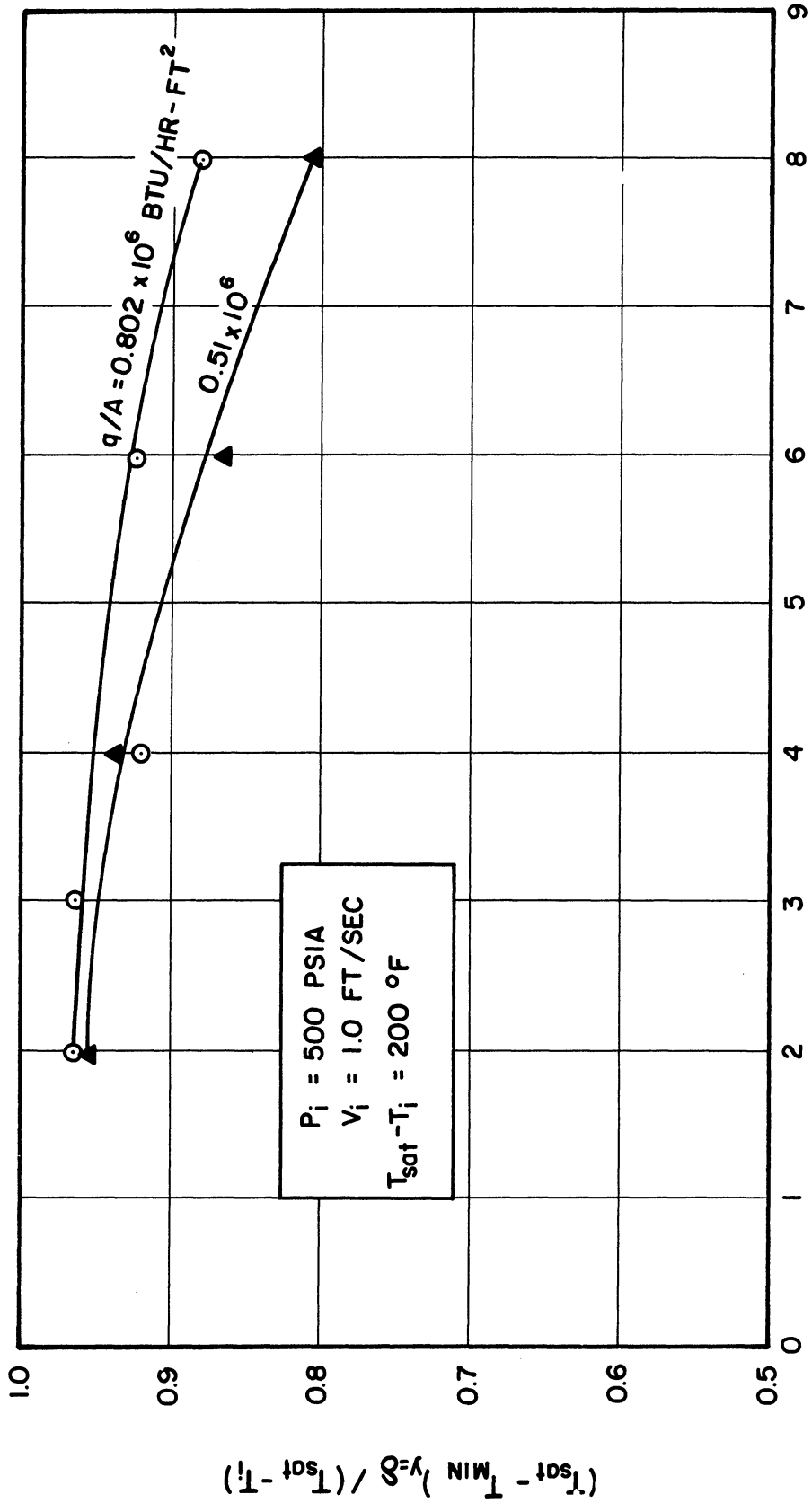

Figure 88. Minimum Temperature Distribution at the Single-Phase Core-Bubble Boundary Interface

saturation temperature as burnout is approached. To compare Bankoff's analysis with the findings of this investigation, plots of $(T_{sat} - T_{MEAN})_{y=\delta} / (T_{sat} - T_i)$ vs. y are shown in Figures 89 through 93. These plots show that as the heat flux is increased the dimensionless temperature ratio approaches unity. Or, in other words, the mean temperature at the interface approaches the inlet temperature as the heat flux is increased. This appears to contradict Bankoff's predictions.

4. Temperature Fluctuations

A typical "Visicorder" trace showing the temperature fluctuations at various distances from the strip surface is reproduced in Figures 94 and 95. It is noted that the amplitudes of temperature fluctuations are random. Their frequency, however, remains virtually constant throughout the single-phase core as well as the bubble boundary layer. This frequency is estimated to be 20 cycles/sec. In general, the amplitude of temperature fluctuations decreases with increasing distance from the heated surface. To investigate the behavior of temperature fluctuations, plots of $(T_{MAX} - T_{MIN})$ vs. y for various tests were constructed. These plots are shown in Figures 96 through 101. It is noted that the amplitude of temperature fluctuations

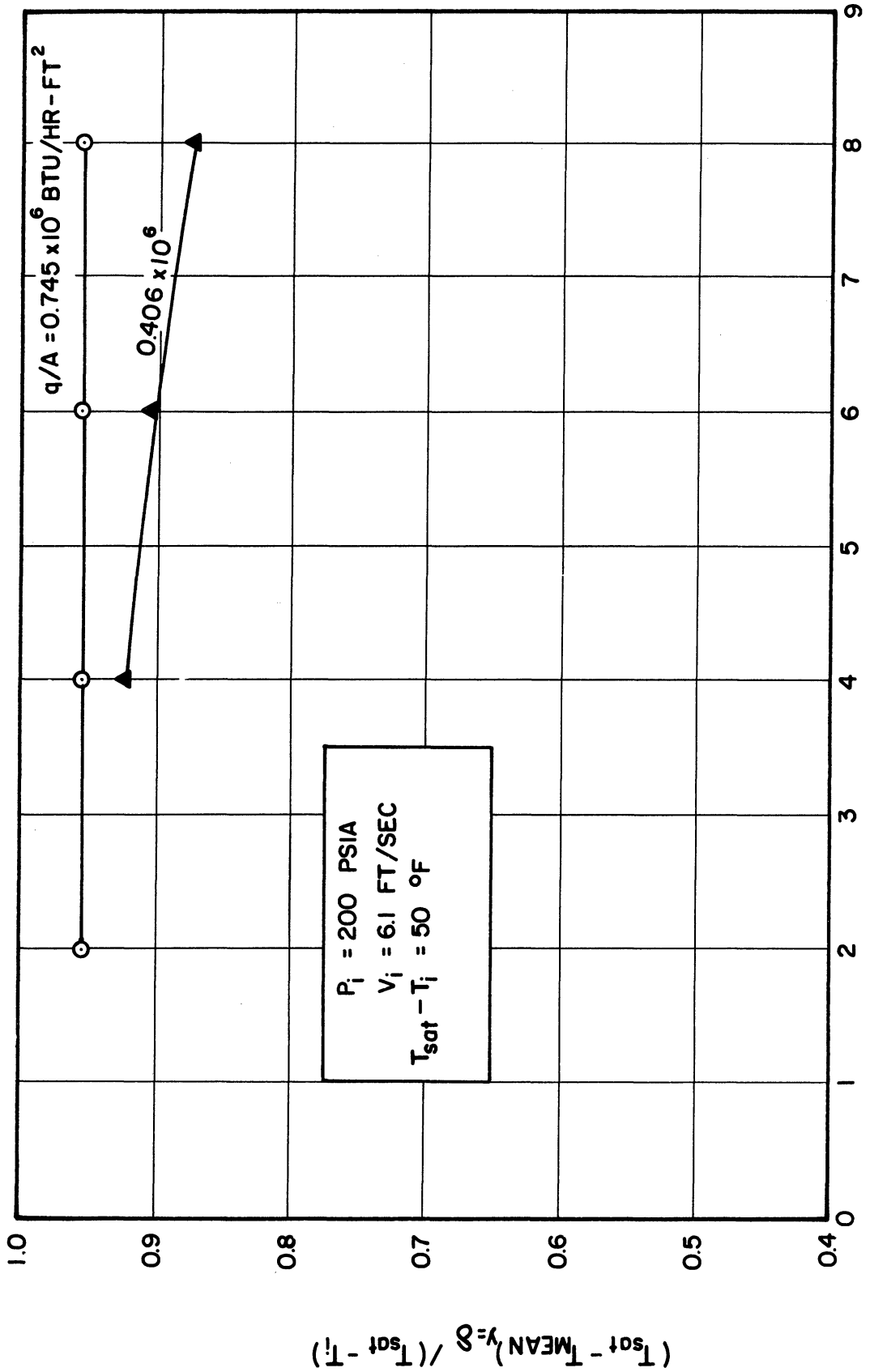

Figure 89. Mean Temperature Distribution at the Single-Phase Core-Bubble Boundary Interface

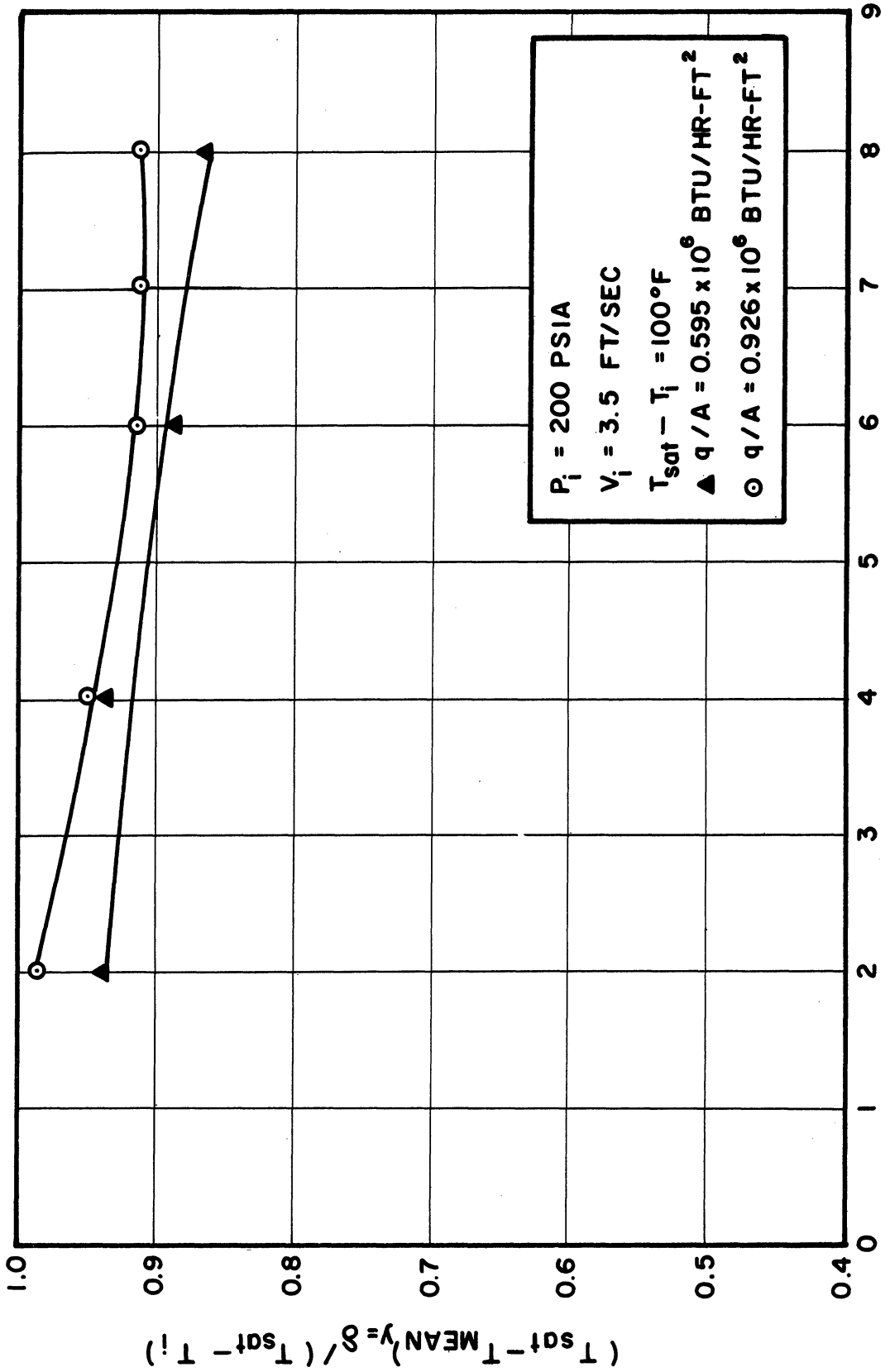

Figure 90. Mean Temperature Distribution at the Single-Phase Core-Bubble Boundary Interface

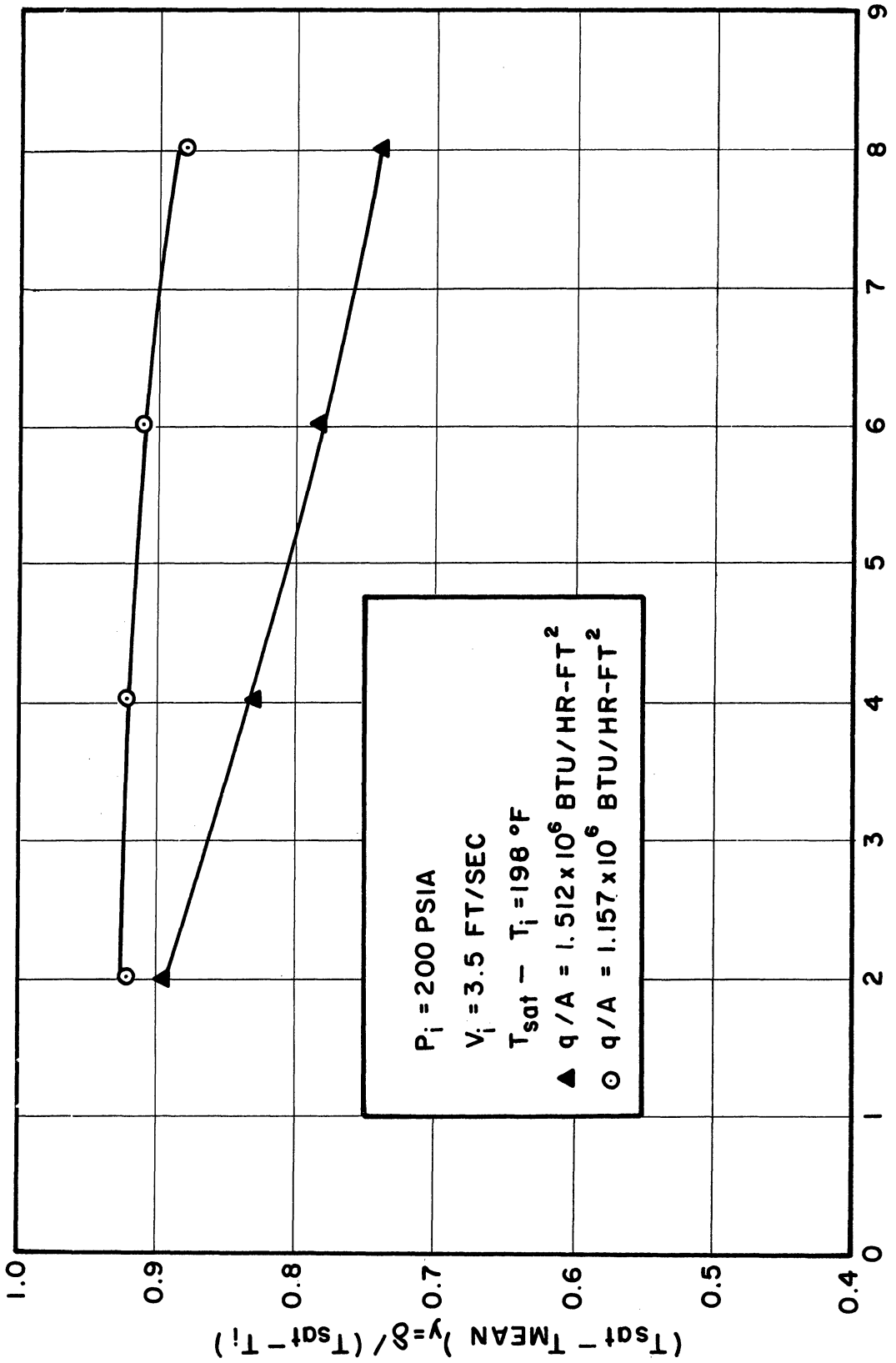

Figure 91. Mean Temperature Distribution at the Single-Phase Core-Rubble Boundary Interface

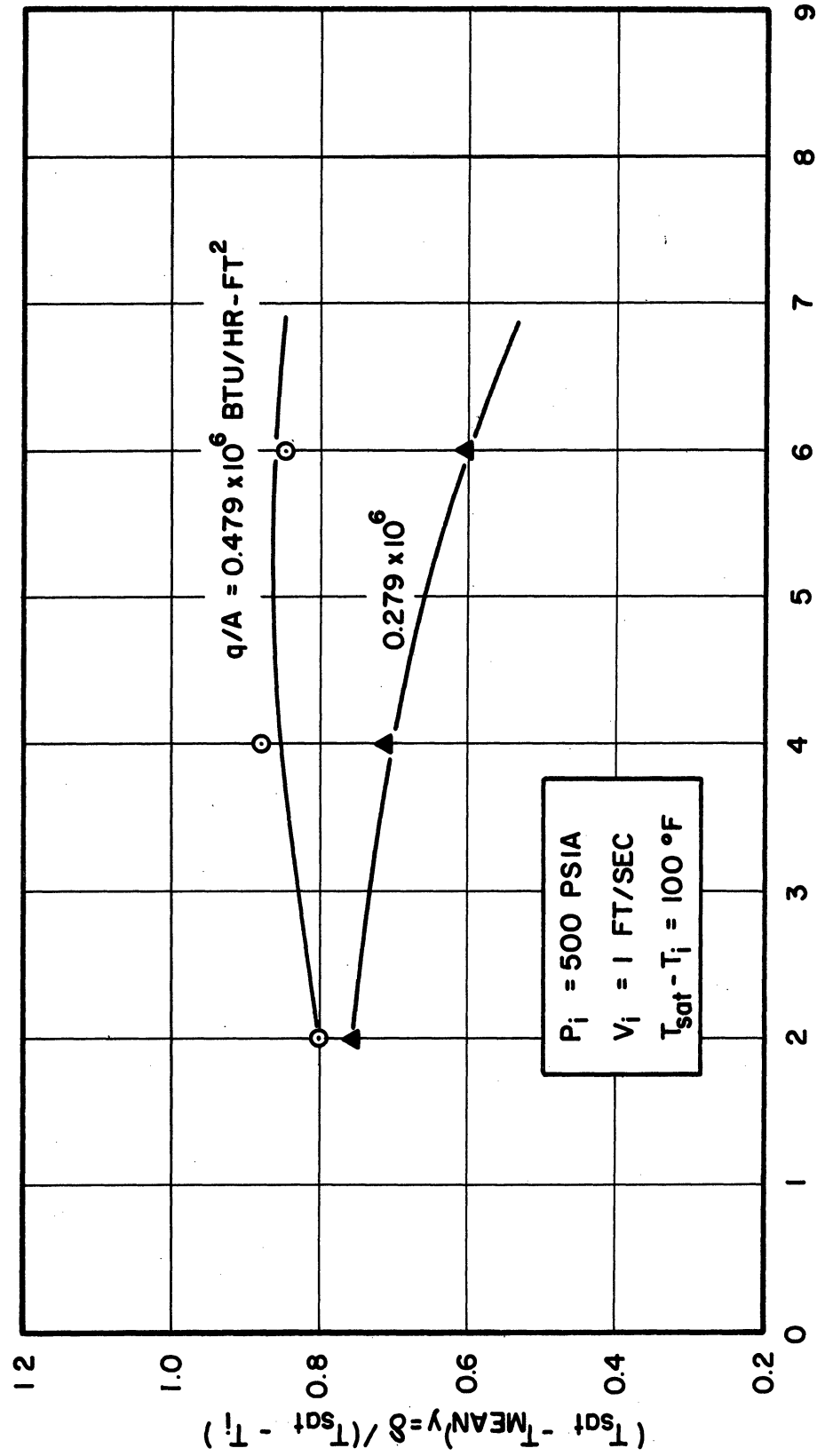

Figure 92. Mean Temperature Distribution at the Single-Phase Core-Bubble Boundary Interface

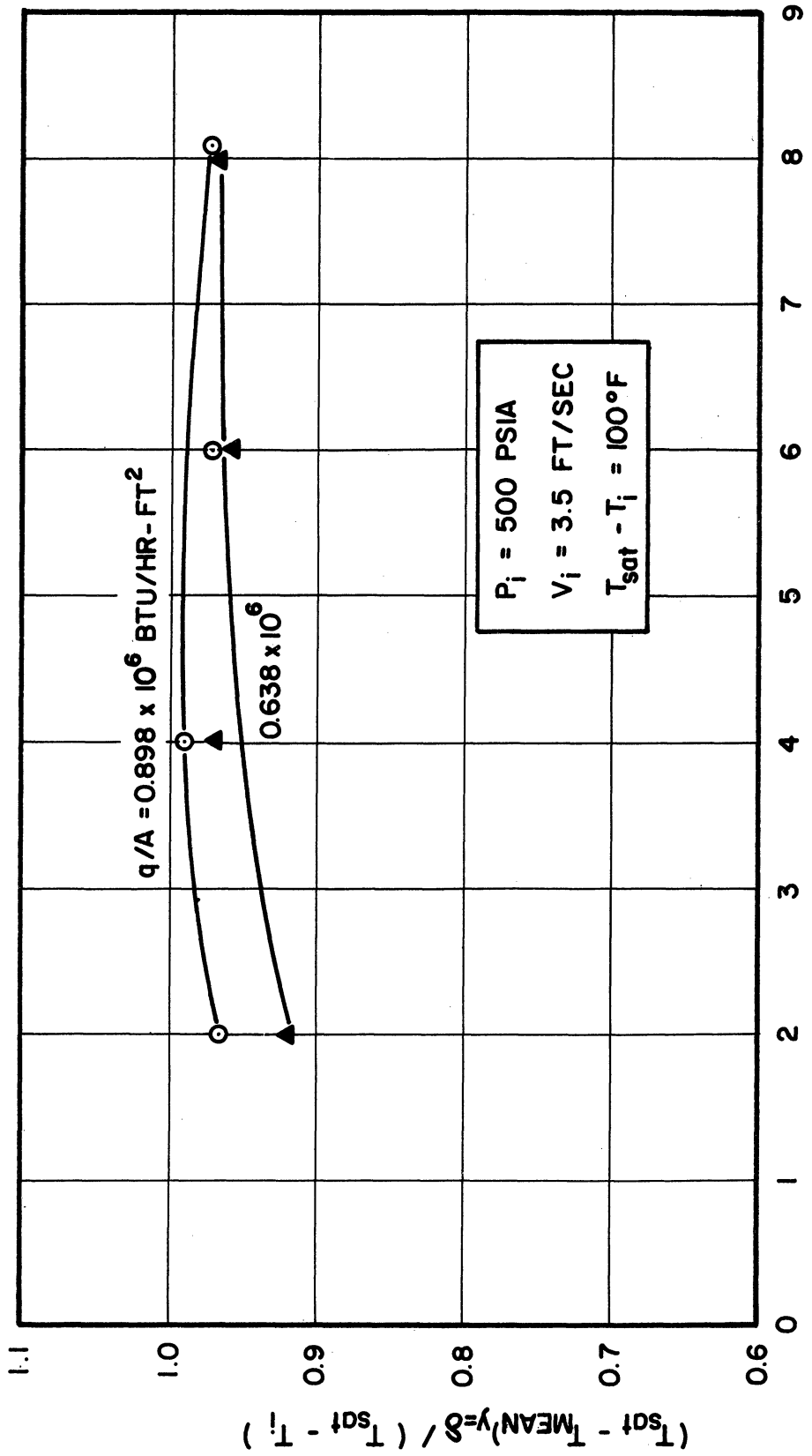

Figure 93. Mean Temperature Distribution at the Single-Phase Core-Bubble Boundary Interface

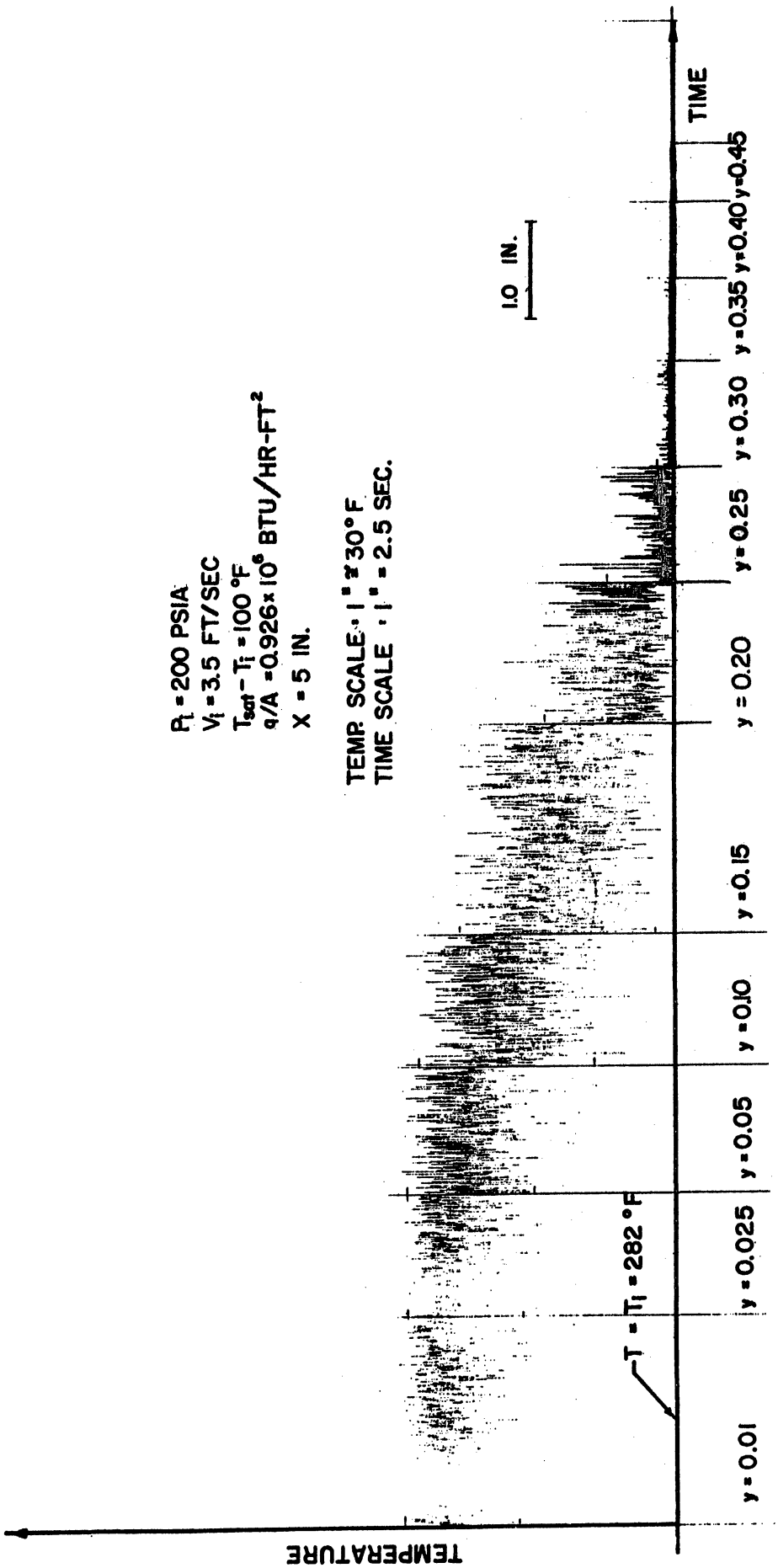

Figure 94. Typical "Visicorder" Record of Temperature Fluctuations.

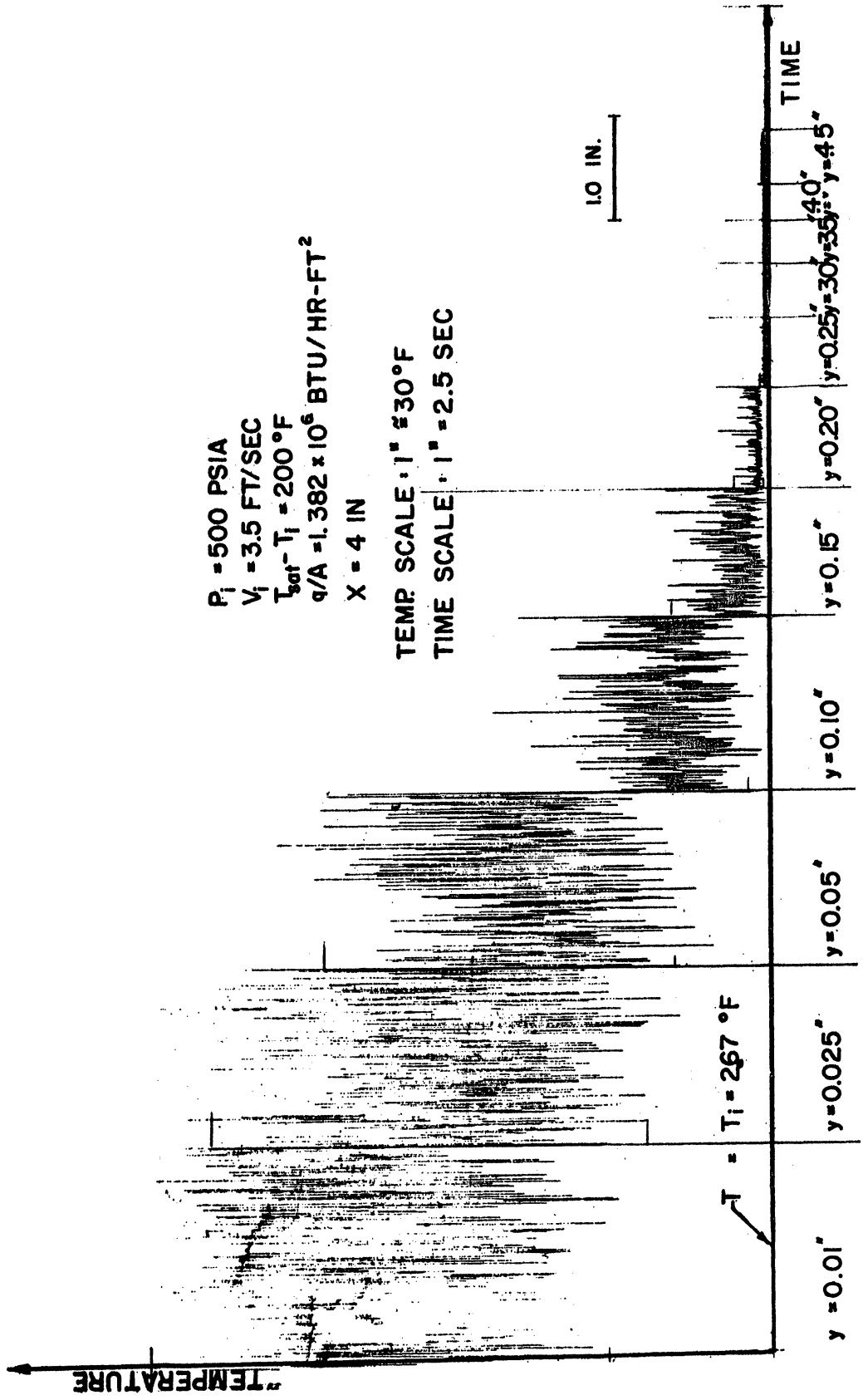

Figure 95. Typical "Visicorder" Record of Temperature Fluctuations.

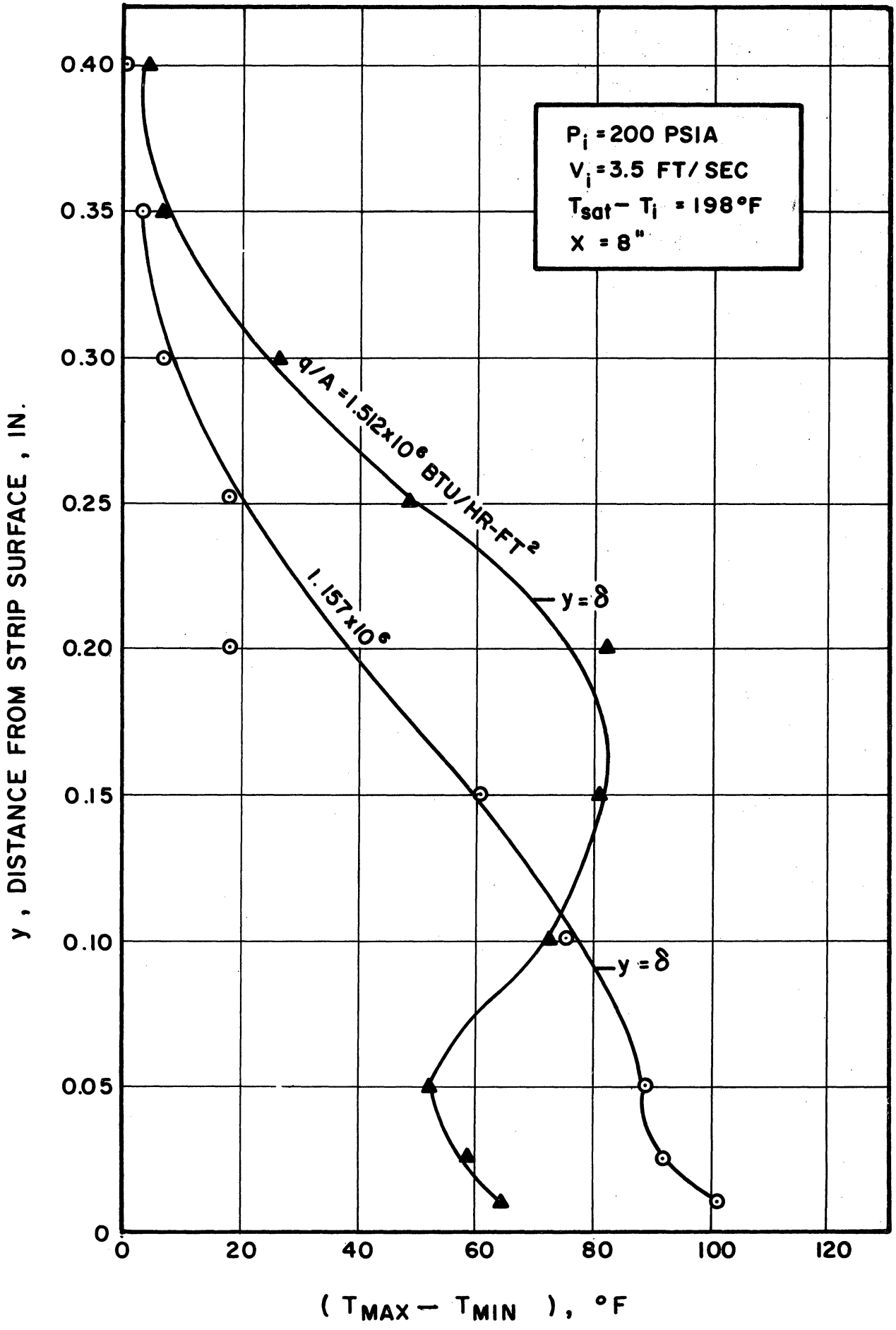

Figure 96. The Effect of Heat Flux on Temperature Fluctuations

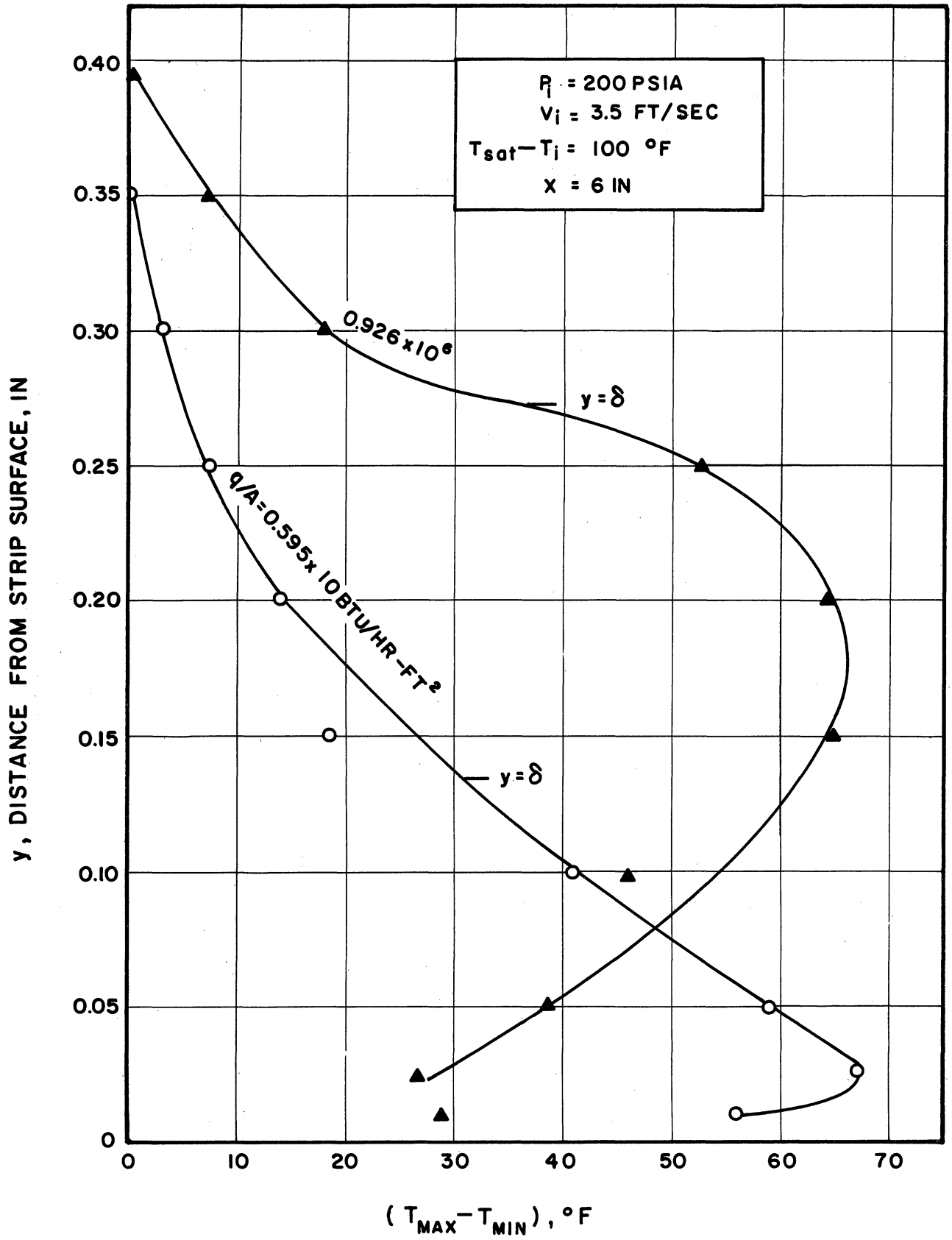

Figure 97. The Effect of Heat Flux on Temperature Fluctuations

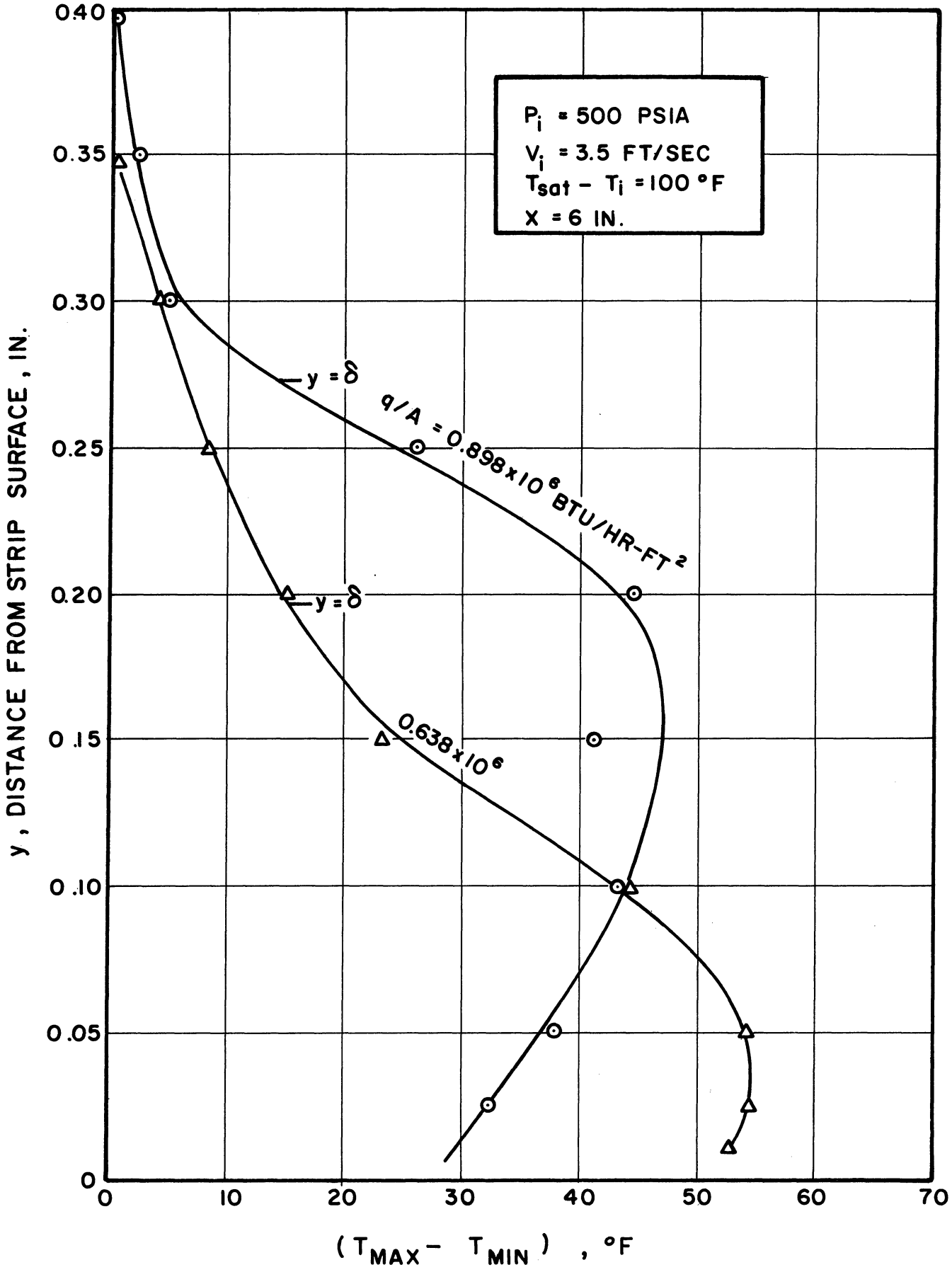

Figure 98. The Effect of Heat Flux on Temperature Fluctuations

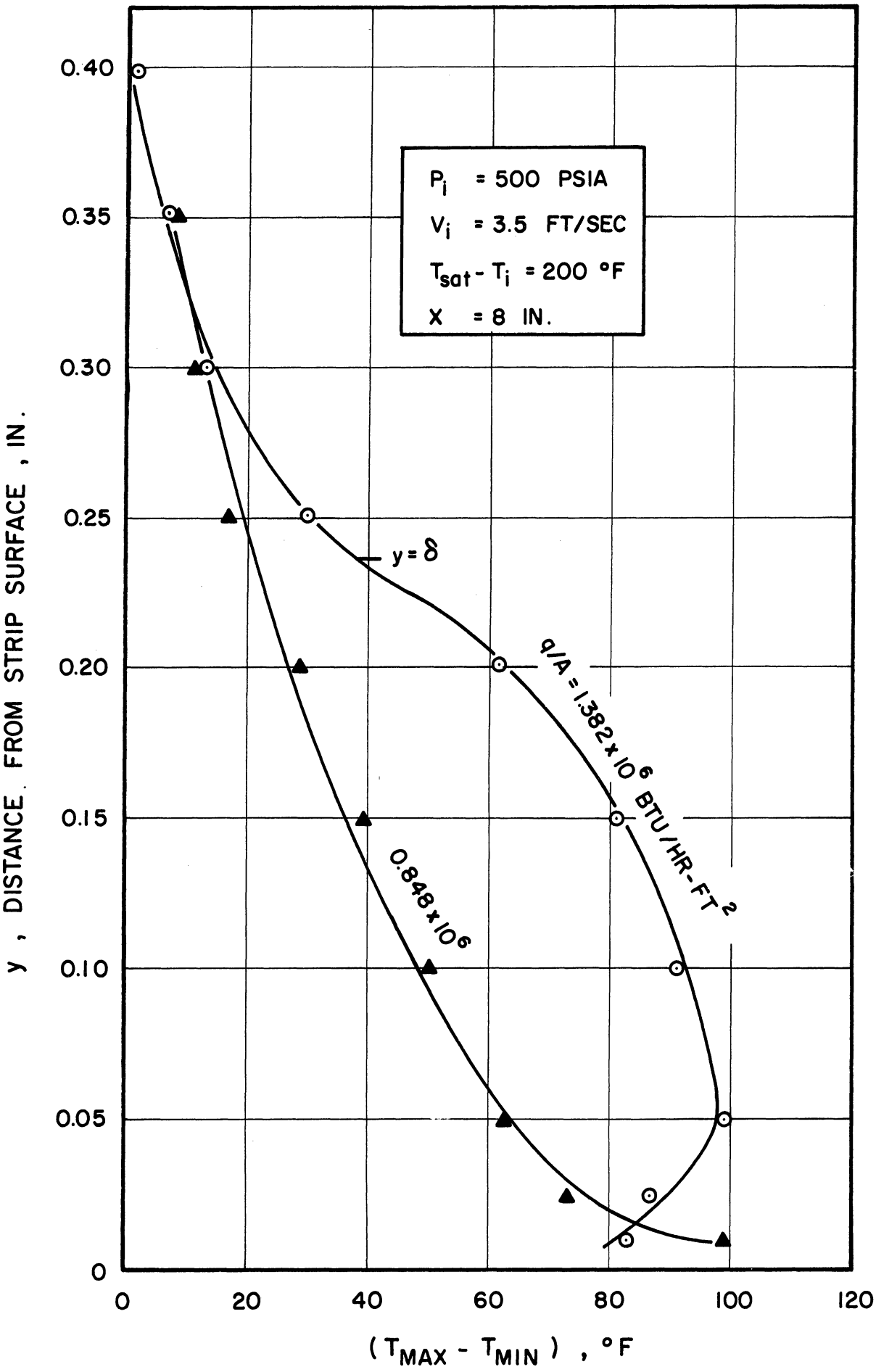

Figure 99. The Effect of Heat Flux on Temperature Fluctuations

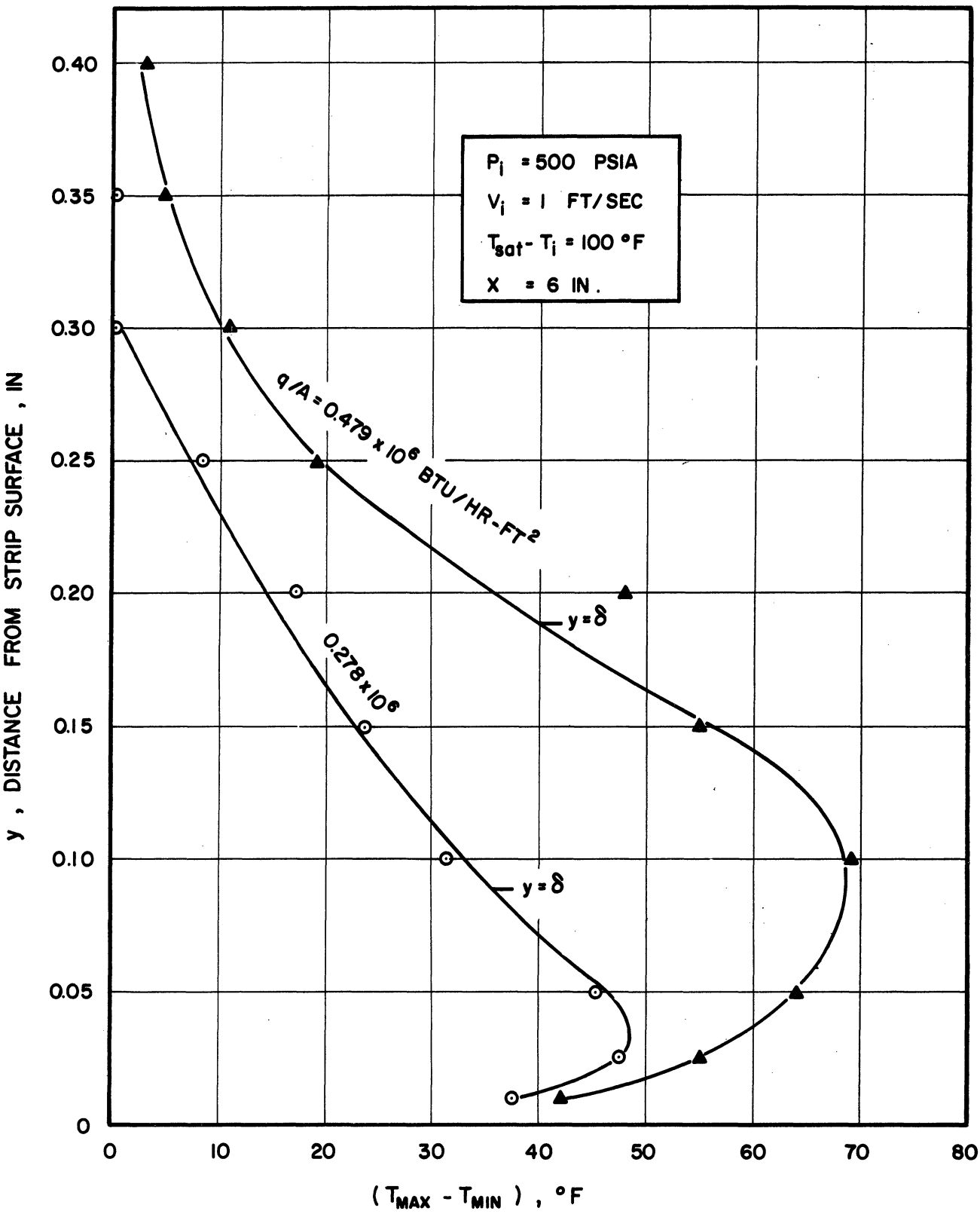

Figure 100. The Effect of Heat Flux on Temperature Fluctuations

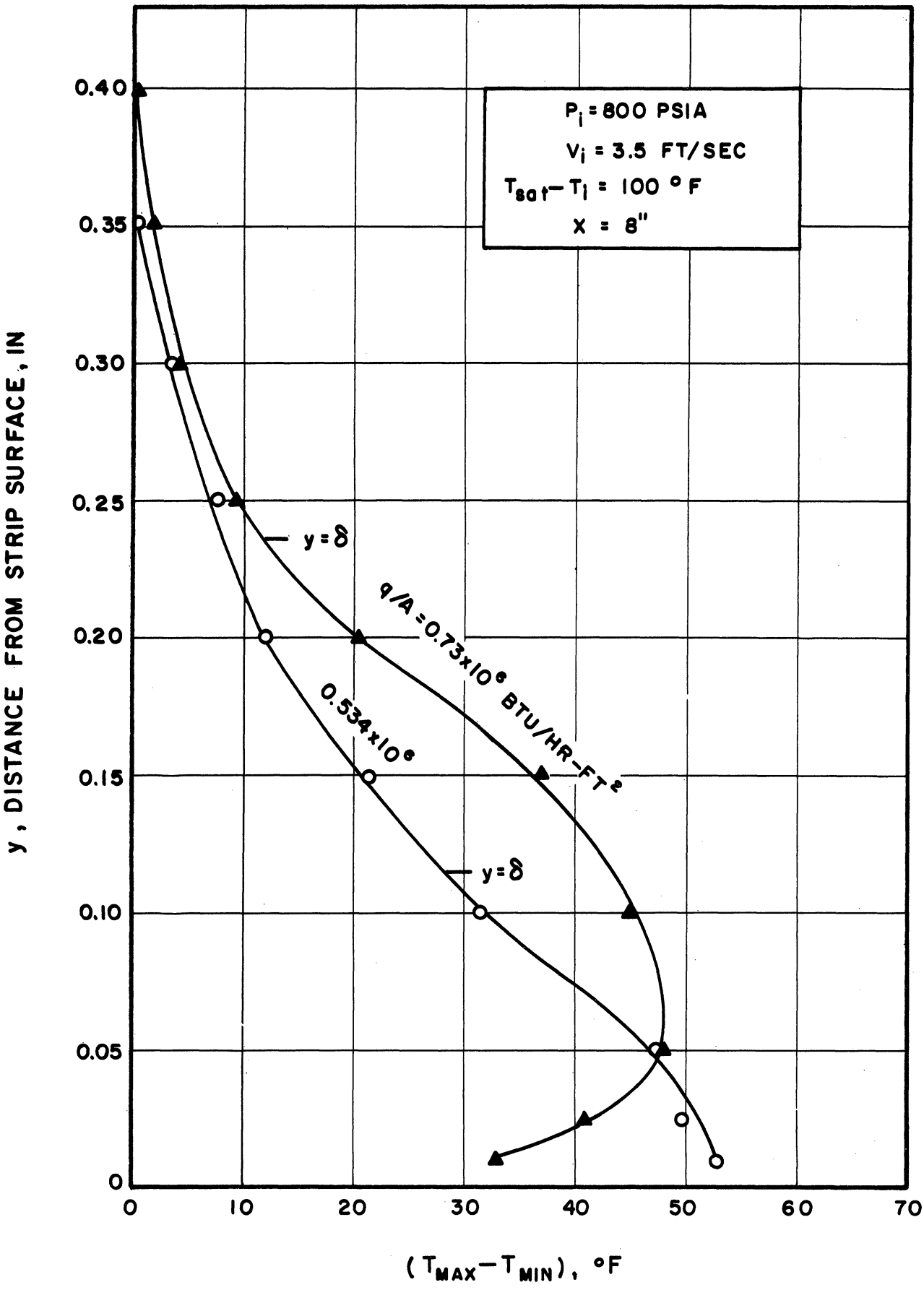

Figure 101. The Effect of Heat Flux on Temperature Fluctuations

first increases and then decreases as the thermocouple is traversed away from the heated surface. This suggests that a thin film may exist near the surface in which temperature fluctuations are partially damped out. It is possible, however, that the decrease in magnitude of temperature fluctuations near the surface may be partially due to changes in the time response of the thermocouple, owing to the presence of an increased vapor fraction there. Based on the method outlined by Clark (73), an approximate value for the ratio of the damped amplitude of temperature fluctuations to the undamped amplitude was obtained. For a typical test this ratio was estimated to be 0.99 in the single phase core and 0.91 near the surface at y = .01", where it was assumed that the fluid is all vapor flowing at the same mass velocity as the liquid core. Another important observation is that within this film the amplitude of measured temperature fluctuations decreases as the heat flux is increased. It is reasonable to assume that the decrease in the indicated amplitude is primarily the result of an actual reduction in temperature fluctuations of the fluid itself rather than a change in the thermocouple time response, since in this process the hot junction is surrounded by predominately saturated vapor. Table III summarizes the temperature measurements at 0.01"

from the heated surface and 6" from the leading edge for two tests at 500 psia, 3.5 ft/sec and 100° subcooling and varying heat flux. The amplitude of temperature fluctuations is 53°F at 0.638×10^6 BTU/hr-ft^2 while it is 30°F at 0.898×10^6 BTU/hr-ft^2.

TABLE III

TYPICAL TEMPERATURE DISTRIBUTION AT $y = 0.01$"

(q/A) BTU/hr-ft^2	T_{MIN} (°F)	T_{MAX} (°F)	$(T_{MAX} - T_{MIN})$°F
0.638×10^6	422	475	53
0.898×10^6	450	480	30

Table III also shows that at 0.638×10^6 BTU/hr-ft^2 the superheat, based on T_{MAX}, is 8°F while at 0.898×10^6 BTU/hr-ft^2 it is 13°F. Based on these observations one may postulate that as burnout heat flux is approached a thin layer of superheated steam is formed over the surface with a characteristically low heat transfer coefficient. Burnout takes place when the rate of heat transfer through this layer becomes less than the rate at which heat is added at the surface.

Figure 102 shows the behavior of temperature fluctu-

ations at various locations along the strip. The amplitude of temperature fluctuations near the surface decreases as the distance from the leading edge is increased. This trend is shown in Figure 103 where (T_{MAX} - T_{MIN}) at $y = 0.01$ in. is plotted against the distance from the leading edge.

5. Surface Temperature Measurements

Several attemps were made to measure the adiabatic surface temperature of the strip. The first attempt was to weld the thermocouple wires to the adiabatic surface of the strip. Because it was difficult to weld the two thermocouple wires on an equipotential line, considerable D.C. voltage was picked up. The "Visicorder" was used to calibrate this D.C. pick-up and it was found that it is of the same order of magnitude as the thermal emf. Therefore, to make accurate surface temperature measurements, extremely accurate calibration of the D.C. voltage was necessary.

Because of the presence of liquid next to the adiabatic side of the strip, it is expected that local boiling does take place whenever the adiabatic surface temperature reaches saturation. The boiling of the liquid around the hot junction influenced the indicated thermocouple temperature, resulting in severe fluctuations of emf.

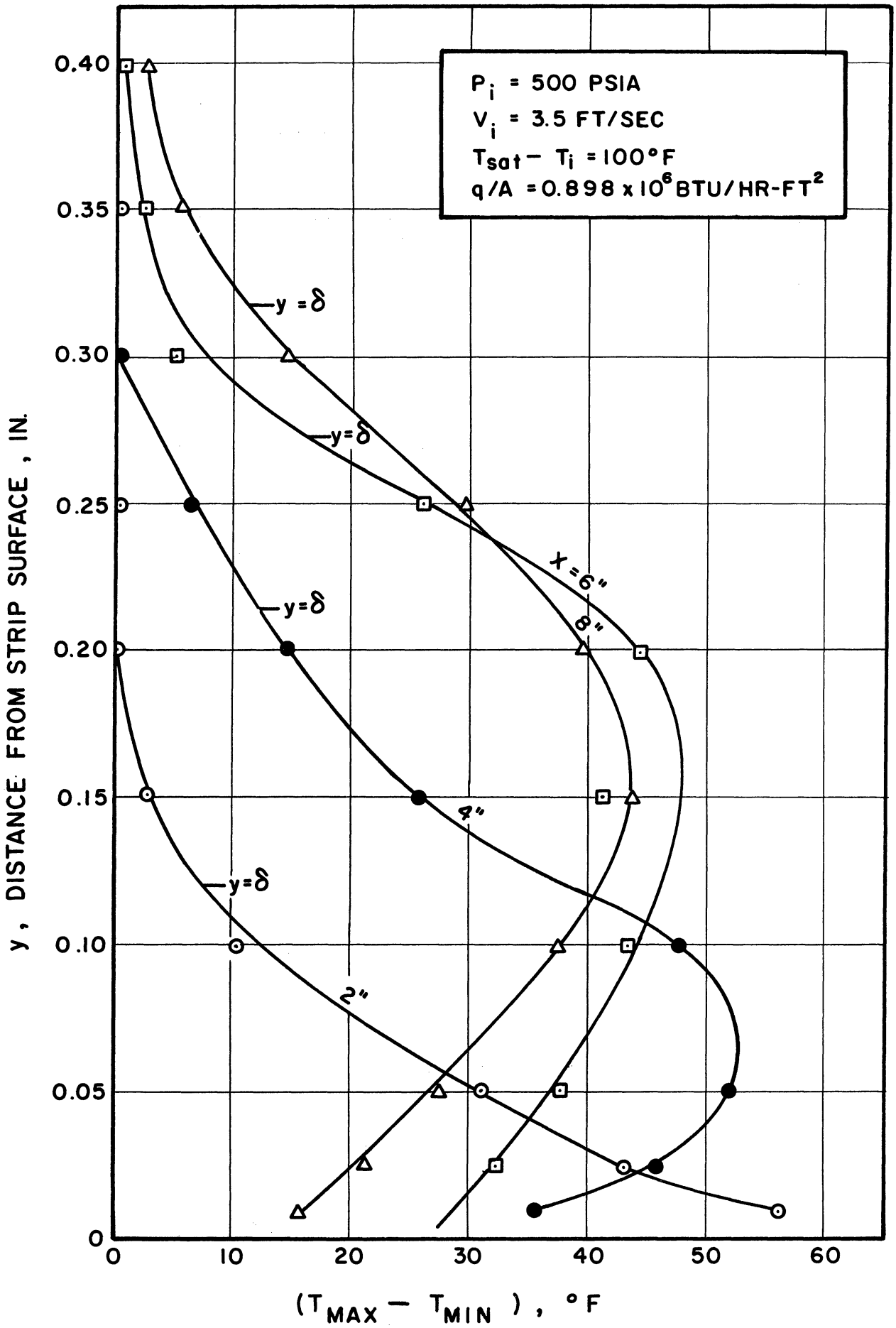

Figure 102. Fluid Temperature Fluctuation Profiles at Various Locations Along Heated Surface

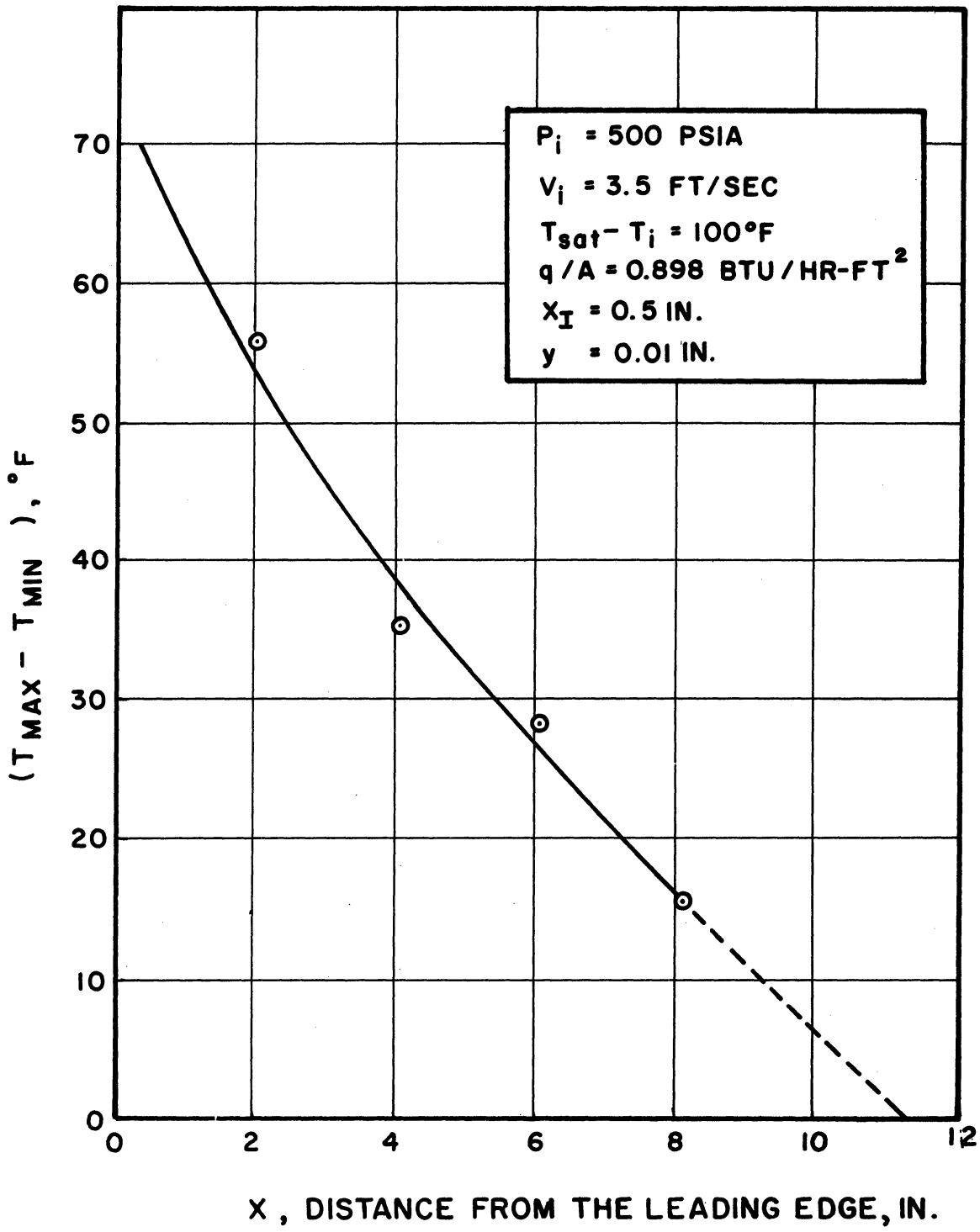

Figure 103. Temperature Fluctuations vs. Distance from the Leading Edge

In a second attempt to measure the surface temperature, the D.C. voltage pick-up was eliminated by electrically insulating the hot junction with a thin (0.002") mica sheet. Because of poor mechanical contact between the hot junction and the heated surface, the thermocouple gave low surface temperature readings. In several tests during boiling the recorded surface temperature did not exceed saturation temperature.

In a third method, to obtain a good mechanical contact between the hot junction and the strip, a 1/16" O.D. thermocouple probe, with the hot junction welded integrally with the sheath ("Aeropack" - Design No. T-14, junction No. 8), was used. The probe was forced against the strip surface by means of a spring mounted outside the test section. D.C. pick-up was eliminated by insulating the hot junction with a 0.002" mica sheet. Test during boiling showed that the recorded surface temperature did not exceed saturation temperature.

Because of the various difficulties experienced in attempting to measure the surface temperature no satisfactory data was obtained and these measurements were abandoned.

CHAPTER VI

CONCLUSIONS

1. Within the range of variables investigated the assumption that nucleation takes place when the surface temperature is equal to saturation temperature appears to be reasonable for the purpose of correlating experimental data on incipient boiling.

2. For the same velocity and subcooling, the pressure does not appreciably affect the relationship between incipient heat flux and incipient distance.

3. High speed movies (7500 frames per second) showed that bubbles move along the heated surface and that they are seldom detached from the surface.

4. No systematic relation exists between pressure and the bubble boundary layer thickness. It does not always follow that the thickness decreases with increasing pressure for the same velocity, subcooling, and heat flux.

5. The bubble boundary layer thickness increases with increasing distance from the leading edge. The increase in bubble boundary layer thickness is primarily the result of an increase in bubble size. Furthermore, since the bubble boundary layer thickness at a given point along the strip is determined by the size of an individual bubble at that location, it follows that

correlation equation (12) or (13) may be used to predict bubble size.

6. The mean temperature at the single-phase core-bubble boundary interface approaches inlet temperature as the heat flux is increased towards burnout.

7. It is speculated that as burnout heat flux is approached a stagnant layer of superheated vapor is formed over the heated surface. This layer is characterized by small temperature fluctuations and consequently by a decrease in the rate of heat transfer. Burnout takes place when the rate of heat transfer through this layer becomes less than the rate at which heat is generated within the surface.

8. The amplitude of temperature fluctuations near the heated surface decreases as the distance from the leading edge is increased.

9. A simplified model for forced convection boiling is one in which the flow regime is divided into two regions; a single-phase core, which is at the inlet temperature, and a two phase bubble boundary layer region.

APPENDIX A

ESTIMATION OF ERRORS

A. Introduction

Since uncertainties in experimental measurements propagate into the results, it is essential to estimate the extent to which these uncertainties affect the accuracy of the results. The method used to determine the uncertainties in the results is outlined by Kline and McClintock (71) and is briefly discussed here.

If the result R is a linear function of n independent variables, then the uncertainty interval, W_R, of the result is related to the uncertainty interval of the variables, W_n, according to the following equation

$$W_R = \left[\left(\frac{\partial R}{\partial V_1} W_1\right)^2 + \left(\frac{\partial R}{\partial V_2} W_2\right)^2 + \cdots + \left(\frac{\partial R}{\partial V_n} W_n\right)^2\right]^{\frac{1}{2}} \qquad (14)$$

where V_n is the independent variable. Each variable is described by the mean of the readings M_n and an uncertainty interval based on certain odds. This may be expressed as $M_n \pm W_n$. A "confidence limit" is placed on the value of M_n which is based on specific odds that the true value of M_n lies within $M_n \pm W_n$. A 95% confidence limit means that the odds are 19:1 that the true value of M_n lies within $M_n \pm W_n$. To estimate the

uncertainties in the results it is necessary to specify the uncertainty, W_n, of each measured variable.

B. Uncertainties in Measurements

1. Thermocouple Calibration

Since all thermocouples were made from the same spools of wire only one was calibrated by the manufacturer. This calibration showed an average deviation from standard calibration tables of 0.23 per cent. A calibration check was made for all traversing thermocouples at the steam point which agreed to within 0.6 per cent with the manufacturer calibration.

2. Visicorder

a. Calibration

A precision potentiometer (L & N No. 8662) was used to calibrate the galvanometer deflection vs. applied emf. All galvanometers were found to be linear to within 2 per cent over a deflection range of four inches.

b. Steady state deflection measurements

Galvanometer deflections are traced on the "Visicorder" paper and can be measured to within 0.015 inch. Since this error is constant, it follows that the per cent error decreases with increasing deflections. Since in all tests the galvanometers were bucked by a constant voltage which corresponds to the inlet thermo-

couple emf and since this represents approximately a deflection of 3.5 inches at the lowest inlet temperature, it follows that the maximum error in deflection measurements is approximately 0.43 per cent.

c. Maximum and minimum deflections due to temperature fluctuations

Temperature fluctuations in the turbulent boundary layer as well as in the bubble boundary layer were recorded by the "Visicorder" as fluctuations in galvanometer deflection. Maximum and minimum deflection levels were observed in all such traces as shown in Figure 94. Since these two deflection levels were not, in general, clearly defined limits some error was involved in specifying the maximum and minimum deflections. This error is estimated to be 0.10". Since in all tests the galvanometers were bucked by a constant voltage which corresponds to the inlet thermocouple emf and since for a typical test this represents approximately 8 inches of galvanometer deflection it follows that a typical per cent error in estimating the minimum deflection level is 1.25 and the corresponding error in the maximum deflection level is 1.0 per cent.

3. Potentiometer

a. Sensitive Scale

The L & N No. 8662 potentiometer can be read to within $\pm$ 0.005 mv on the low range scale. When used

to measure thermocouple emf this uncertainty corresponds to 0.1 per cent at the lowest recorded temperature.

b. Damped signal

Because of temperature fluctuations within the thermal boundary layer and the bubble boundary layer it was found necessary to damp out these fluctuations whenever it was desired to obtain a mean reading. A resistor was added in series with the thermocouple circuit which damped out some of the fluctuations but reduced the potentiometer sensitivity. The error due to this is estimated to be $\pm$ 0.03 mv. For a typical reading of 8 mv this corresponds to 0.37 per cent.

c. Fluctuating signal

At high amplitudes of temperature fluctuations it was not possible to completely damp out the thermocouple fluctuating signal. This caused the potentiometer balancing needle to oscillate and made it necessary to estimate the mean value of the oscillating emf. The uncertainty involved in this is estimated to be $\pm$ 0.08 mv. For a typical reading of 8 mv the per cent error is 1.0.

4. Current

The potentiometer was used to measure shunt voltage and the current was then calculated from this measurement. A typical error in such a measurement is 0.2 per cent.

5. Voltage

The voltage was reduced by a factor of 2000 and the potentiometer was used to measure this reduced voltage. A typical error in such a measurement is 0.1 per cent. However, the calculated voltage has a greater uncertainty because the bridge resistors which were used to reduce the voltage are accurate to within $\pm$ 1%.

6. Flowmeter Calibration

The turbine type flowmeter used was calibrated for water at room temperature by the manufacturer. The calibration was checked with a weigh tank at water temperatures up to 160^{o}F. This check agreed to within 0.7 per cent with the manufacturer's calibration.

7. Pressure

The Heise pressure gage, as calibrated by the manufacturer, is accurate to within $\pm$ 1.5 psi anywhere on the scale. The per cent error for a typical pressure of 500 psig is 0.3.

8. Bubble Boundary Thickness Measurement

Two sources of errors are involved in specifying the bubble boundary layer; (1) the inconsistency in drawing a best fit curve which describes the bubble boundary layer and, (2) error in scaling the bubble boundary layer thickness. To estimate the first error, a typical enlarged trace of the bubble boundary was

selected and a flexible plastic spline was used to describe the bubble boundary layer. Twenty five measurements of the bubble boundary layer thickness were made at three different locations along the strip. Each measurement was based on an independent spline fit of the bubble boundary layer. The deviation from the mean bubble boundary thickness for all three locations was found to be approximately 3.8%.

An error of $\pm$ 0.015 in. is involved in scaling the bubble boundary layer thickness. This error is constant, however, the per cent error decreases with increasing bubble boundary layer thickness. For a typical thickness of 0.5 inch, measured on an enlarged trace, the per cent error is 3.0.

Typical uncertainty intervals for various measured quantities are summarized in Table IV.

C. Uncertainty in Experimental Results

Uncertainty intervals for the experimental results were calculated for 95 per cent confidence limit by using Equation (14) and the appropriate uncertainties in measurements.

In determining the uncertainty interval for the heat flux it was assumed that all the energy dissipated in the strip is transferred to the liquid. Actually

TABLE IV

UNCERTAINTY INTERVALS OF MEASUREMENTS

Measurement	Units	M_n Typical mean value	W_n Typical uncertainty interval	W_n/M_n%
1. Thermocouple calibration	Mv	7	.02	0.3
2. "Visicorder" Calibration	Mv/in	2.0	0.02	1.0
3. "Visicorder" deflection				
a) Steady state	in	3.0	0.015	0.5
b) Maximum deflection level	in	10	0.10	1.0
c) Minimum deflection level	in	8	0.10	1.25
4. Potentiometer				
a) Sensitive scale	Mv	5	0.005	0.1
b) Damped	Mv	8	0.03	0.37
c) Fluctuating	Mv	8	0.08	1.0
5. Current	Mv	2.5	0.005	0.2
6. Voltage	Mv	5.0	0.005	0.1
7. Flowmeter	cts/gal	75	1.0	1.3
8. Pressure	psig	500	1.5	0.3
9. Bubble boundary layer thickness (enlarged)	in	0.79	0.03	3.8

some energy is lost to the surroundings by conduction and convection from the test section. Because of the complicated geometry of the test section it is difficult to accurately estimate the heat loss to the surroundings. However, based on simplifying assumptions this loss is estimated at 2 per cent for a typical test.

Typical uncertainty intervals for the experimental results are listed in Table V.

TABLE V

TYPICAL UNCERTAINTY INTERVALS FOR EXPERIMENTAL RESULTS

Results	Uncertainty Interval per cent
1. Inlet temperature	0.3
2. "Mean" temperature	1.0
3. "Minimum" temperature	1.6
4. "Maximum" temperature	1.4
5. Saturation temperature	0.1
6. Inlet pressure	0.3
7. Inlet velocity	2.1
8. Heat flux	1.7
9. Bubble boundary layer thickness	3.8

APPENDIX B

PHOTOGRAPHS SHOWING NUCLEATION OF BUBBLES AND THE FORMATION AND DEVELOPMENT OF THE BUBBLE BOUNDARY LAYER IN FORCED CONVECTION FLOW OVER A HEATED PLATE

P_i = 200 psia

V_i = 3.5 ft/sec

$T_{sat}-T_i$ = 100°F

q/A = 0.595 BTU/hr-ft^2

Scale: Distance between thermocouples = 1"

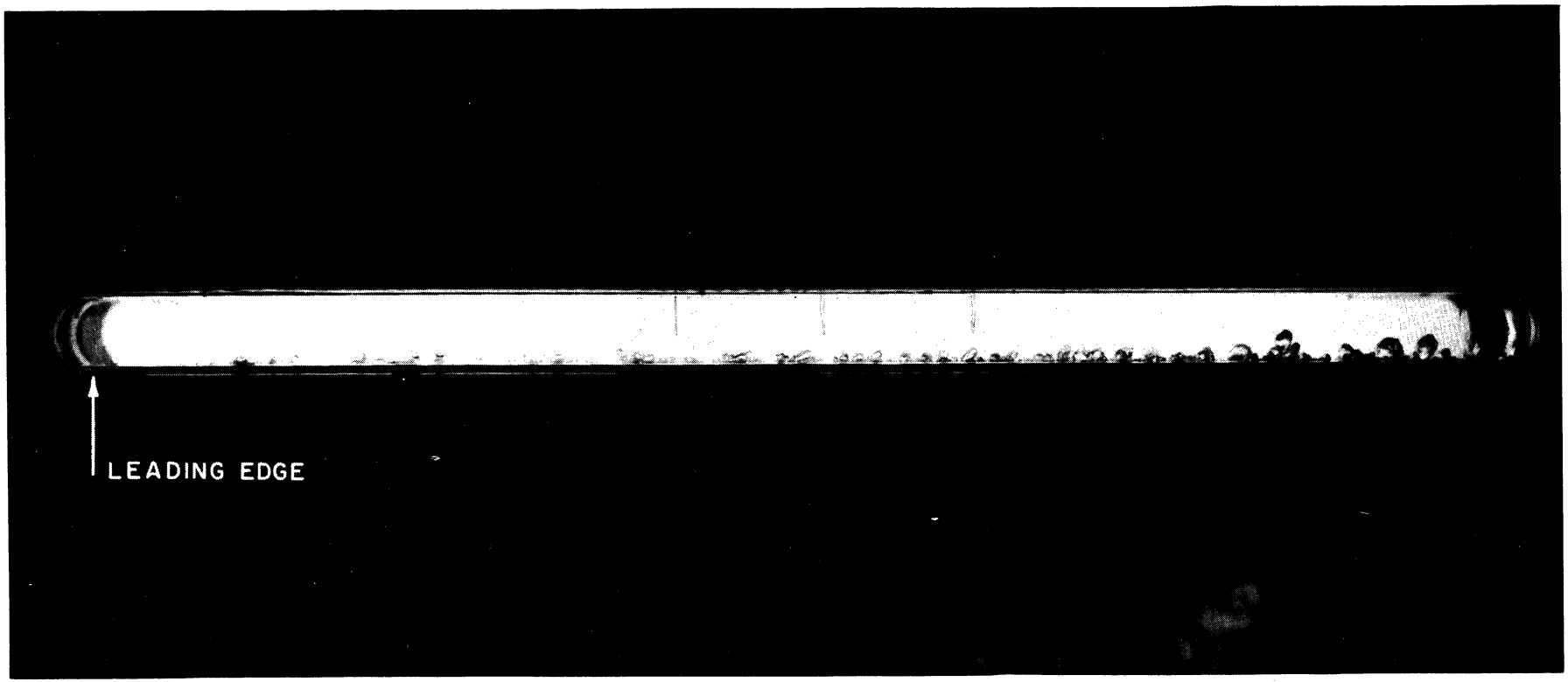

Figure 104. Photograph Showing Nucleation of Bubbles and the Formation and Development of the Bubble Boundary Layer in Forced Convection Flow Over a Heated Plate

P_i = 200 psia

V_i = 3.5 ft/sec

$T_{sat}-T_i$ = 100

$q/A = 0.926 \times 10^6$ BTU/hr-ft^2

Scale: Distance between thermocouples = 1"

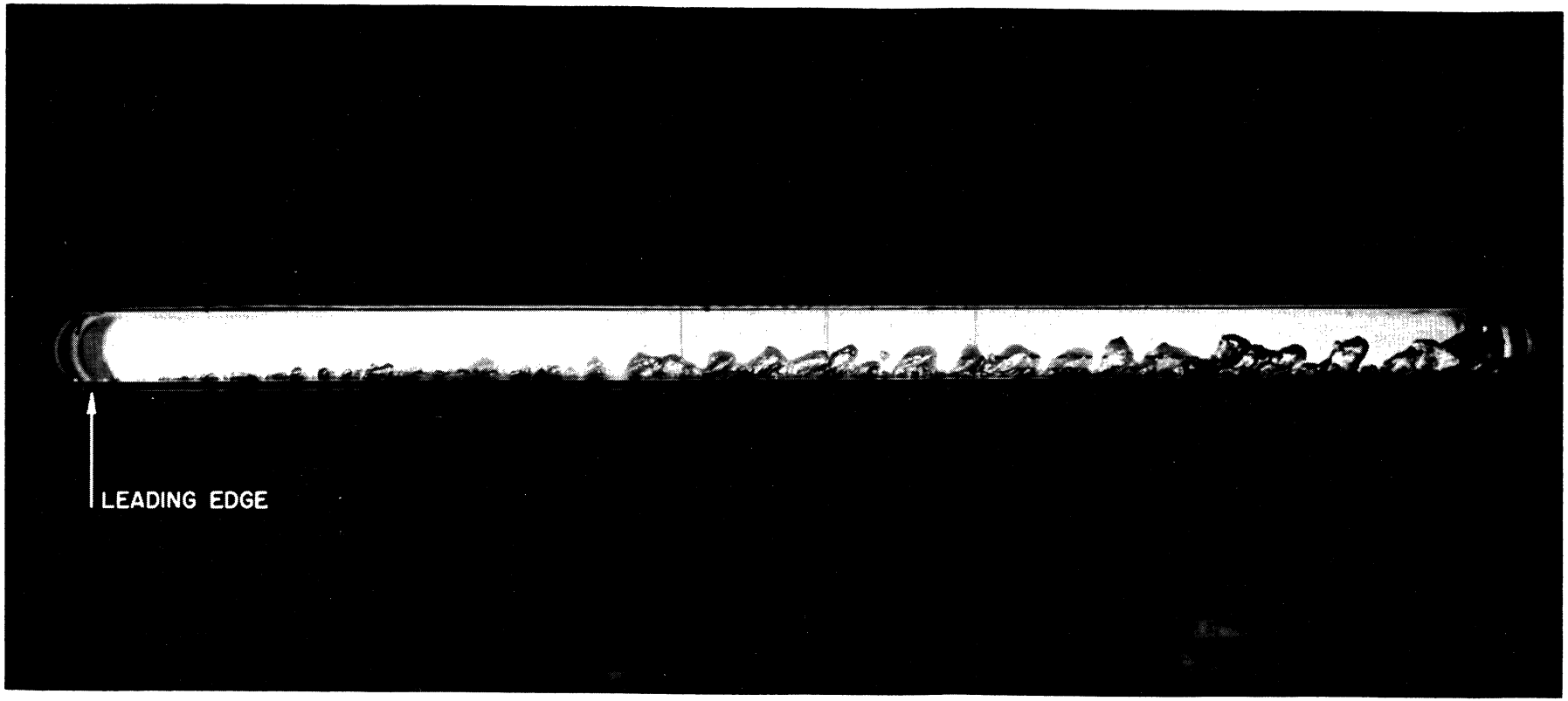

Figure 105. Photograph Showing Nucleation of Bubbles and the Formation and Development of the Bubble Boundary Layer in Forced Convection Flow Over a Heated Plate

P_i = 200 psia

V_i = 1 ft/sec

$T_{sat}-T_i$ = 200°F

$q/A = 0.8 \times 10^6$ BTU/hr-ft^2

Scale: Distance between thermocouples = 1"

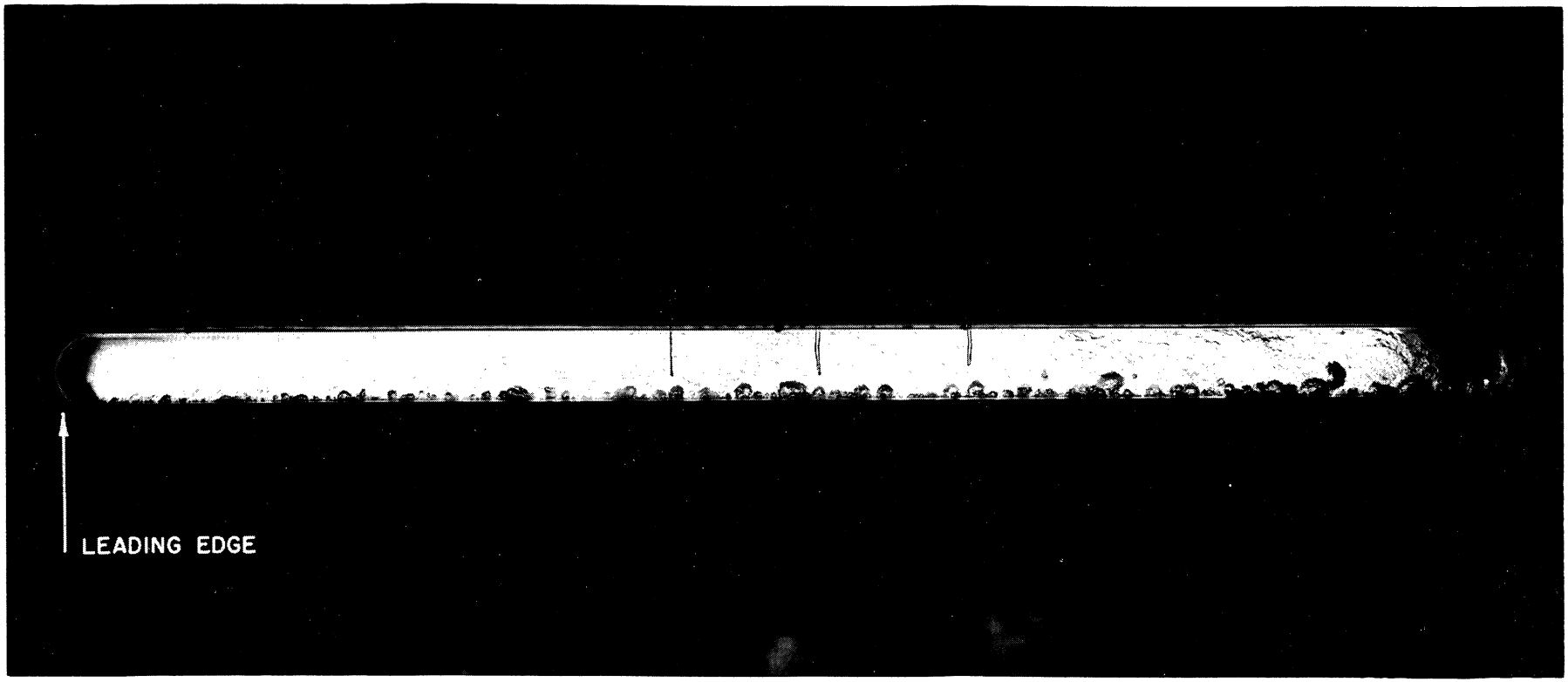

Figure 106. Photograph Showing Nucleation of Bubbles and the Formation and Development of the Bubble Boundary Layer in Forced Convection Flow Over a Heated Plate

P_i = 200 psia

V_i = 3.5 ft/sec

$T_{sat}-T_i$ = 198°F

$q/A = 1.157 \times 10^6$ BTU/hr-ft^2

Scale: Distance between thermocouples = 1 in.

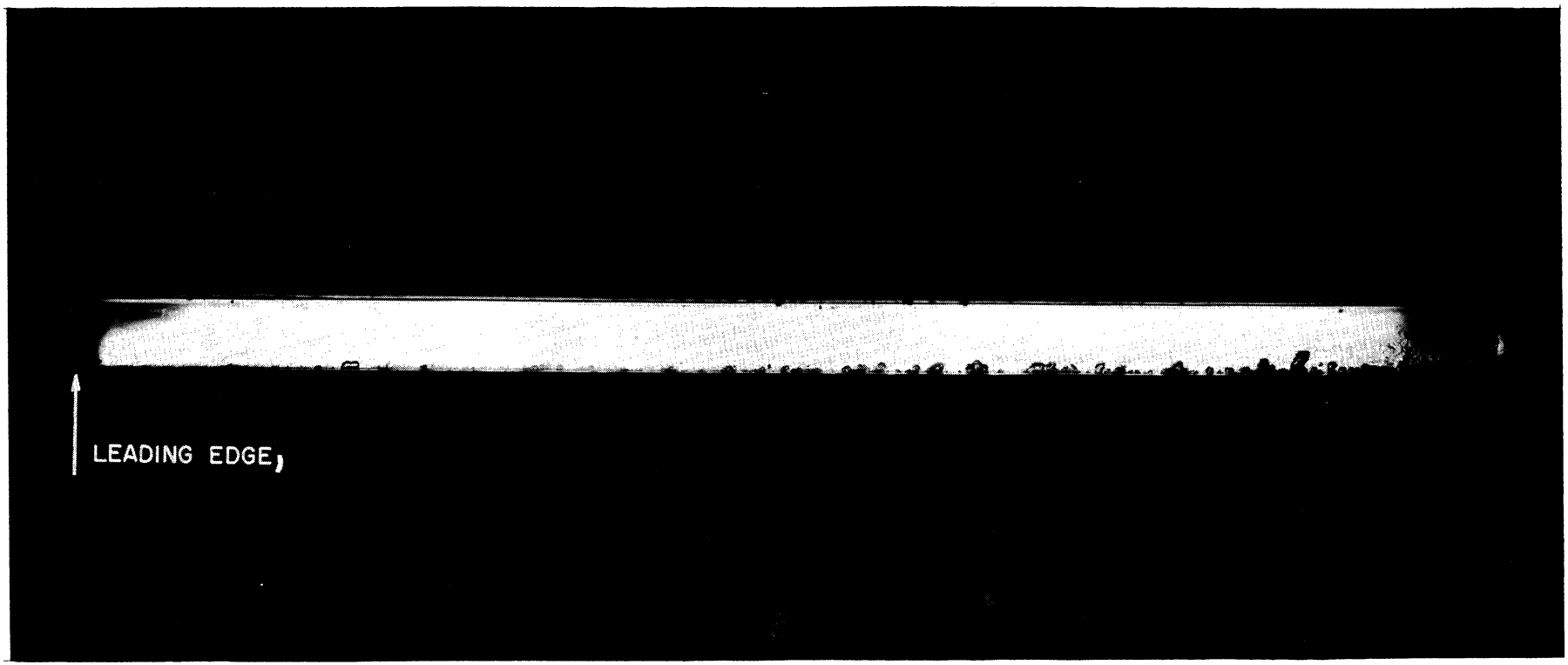

Figure 107. Photograph Showing Nucleation of Bubbles and the Formation and Development of the Bubble Boundary Layer in Forced Convection Flow Over a Heated Plate

P_i = 200 psia

V_i = 3.5 ft/sec

$T_{sat}-T_i$ = 197°F

$q/A = 1.512 \times 10^6$ BTU/hr-ft^2

Scale: Distance between thermocouples = 1"

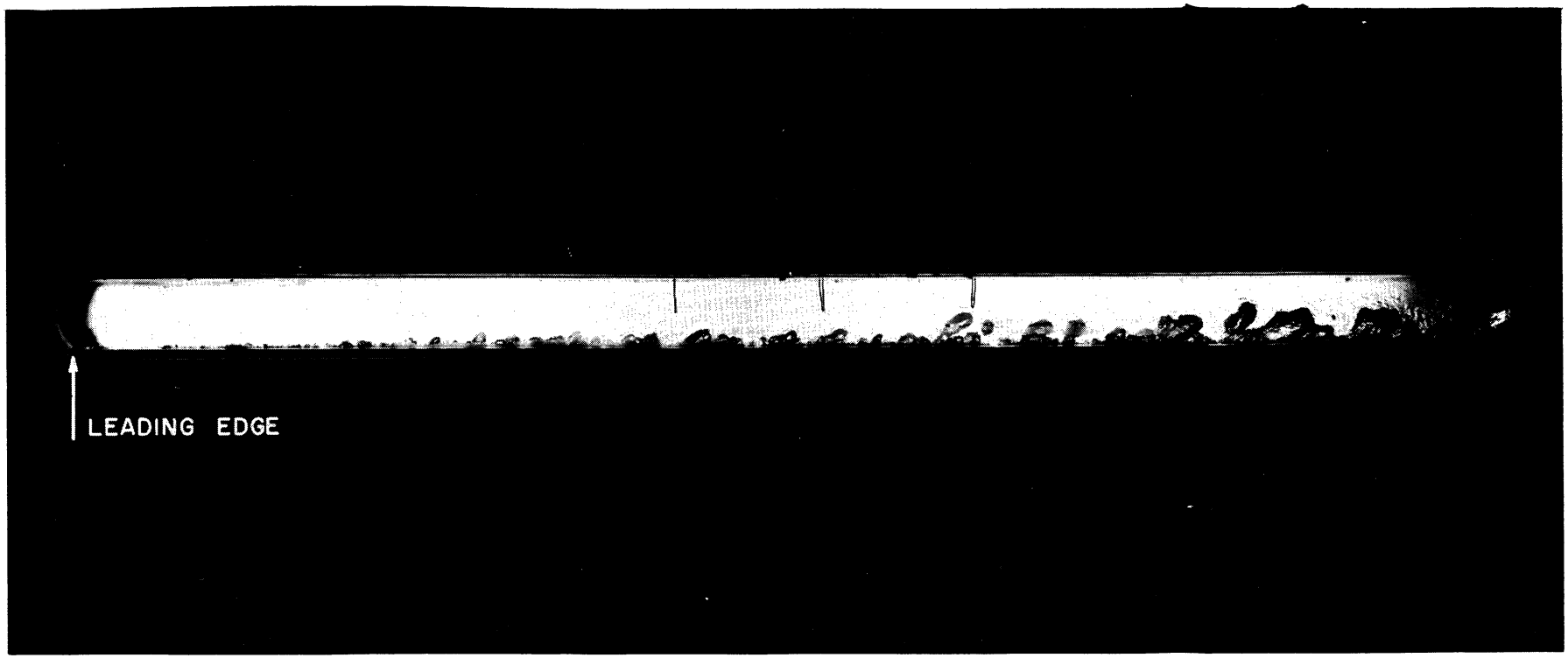

Figure 108. Photograph Showing Nucleation of Bubbles and the Formation and Development of the Bubble Boundary Layer in Forced Convection Flow Over a Heated Plate

P_i = 500 psia

V_i = 1 ft/sec

$T_{sat}-T_i$ = 100°F

$q/A = 0.204 \times 10^6$ BTU/hr-ft^2

Scale: Distance between thermocouples = 1"

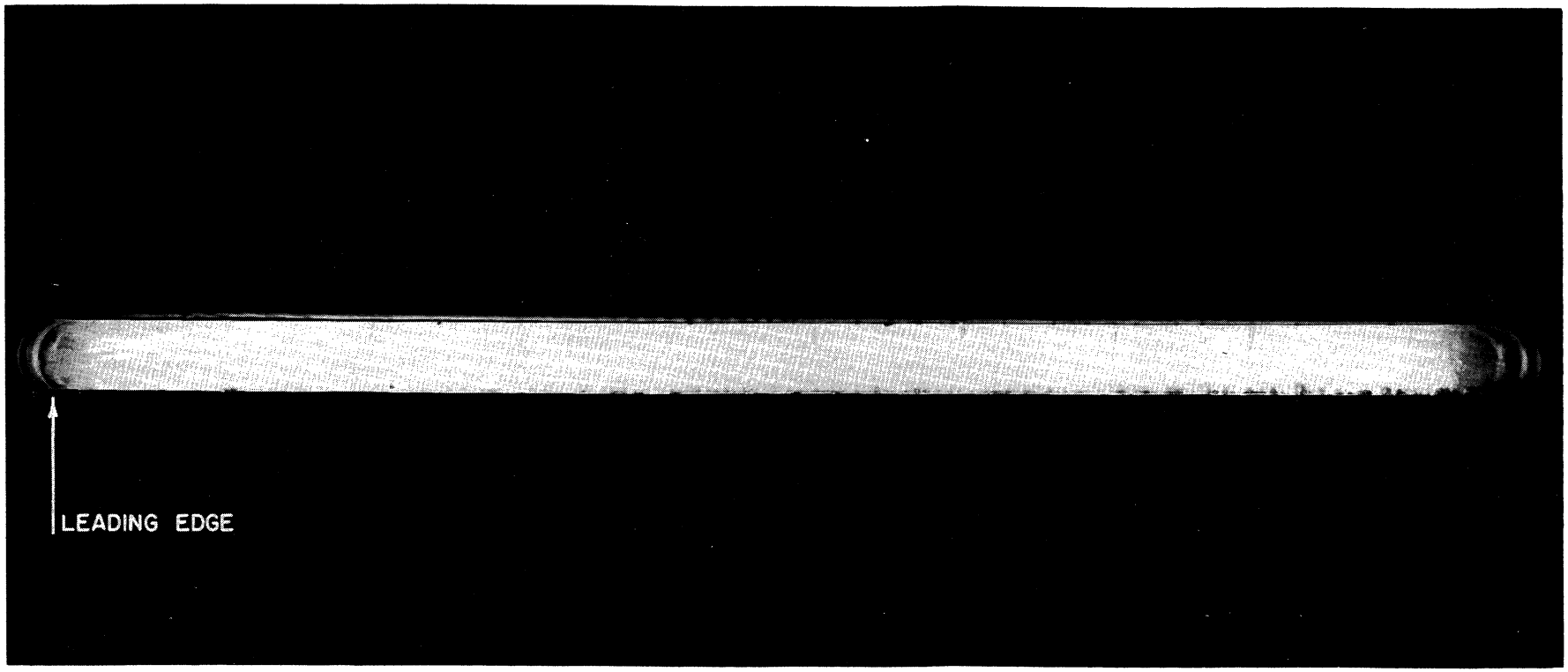

Figure 109. Photograph Showing Nucleation of Bubbles and the Formation and Development of the Bubble Boundary Layer in Forced Convection Flow Over a Heated Plate

P_i = 500 psia

V_i = 1 ft/sec

$T_{sat}-T_i$ = 100°F

q/A = 0.278 BTU/hr-ft^2

Scale: Distance between thermocouples = 1"

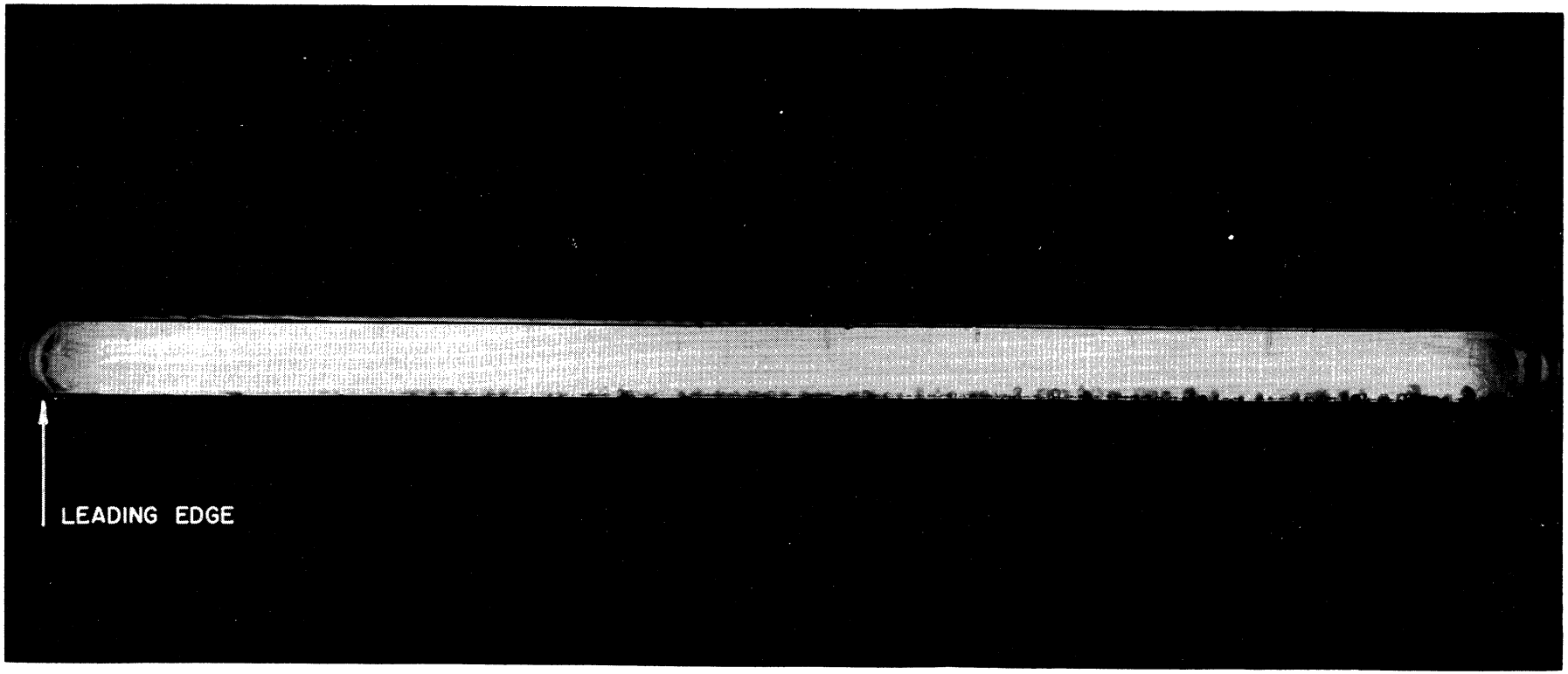

Figure 110, Photograph Showing Nucleation of Bubbles and the Formation and Development of the Bubble Boundary Layer in Forced Convection Flow Over a Heated Plate

P_i = 500 psia

V_i = 1 ft/sec

$T_{sat}-T_i = 100^{o}F$

$q/A = 0.479 \times 10^{6}$ BTU/hr-ft^2

Scale: Distance between thermocouples = 1"

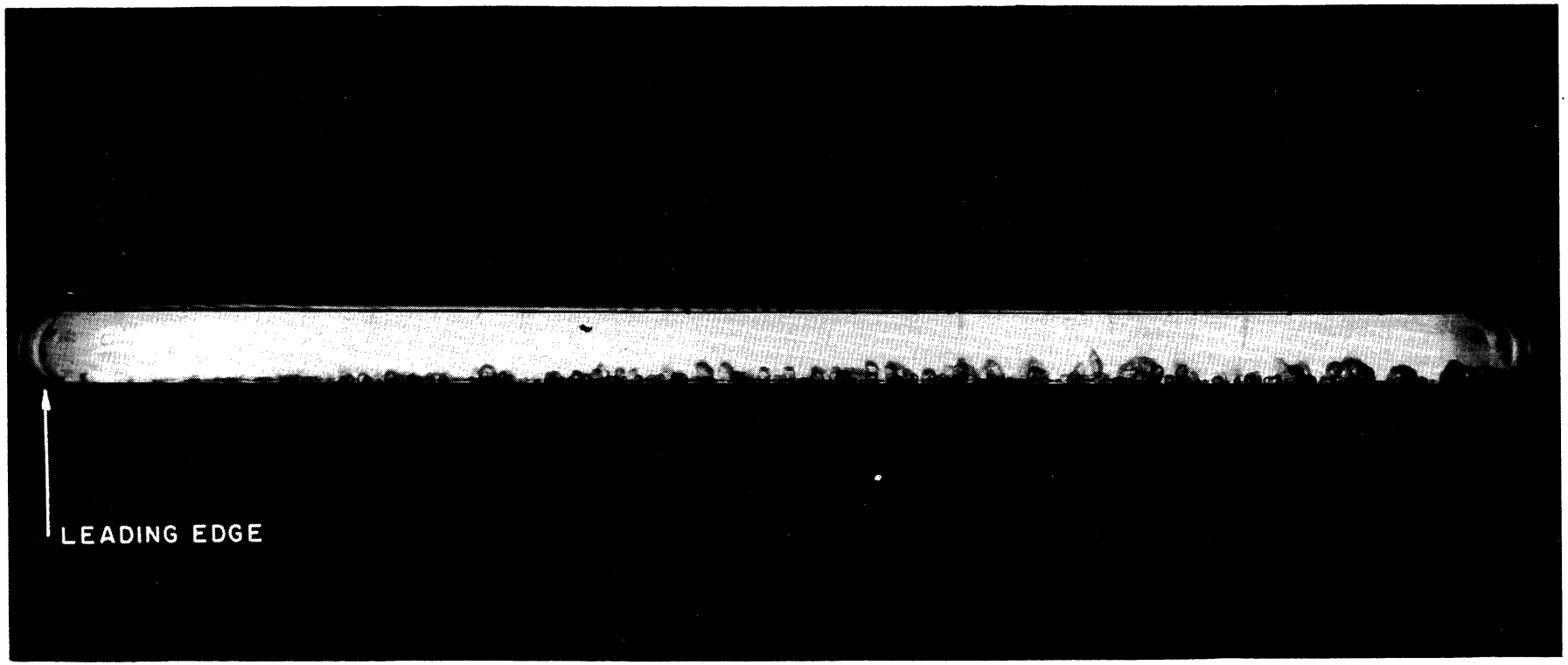

Figure 111. Photograph Showing Nucleation of Bubbles and the Formation and Development of the Bubble Boundary Layer in Forced Convection Flow Over a Heated Plate

P_i = 500 psia

V_i = 3.6 ft/sec

$T_{sat}-T_i$ = 100°F

$q/A = 0.492 \times 10^6$ BTU/hr-ft^2

Scale: Distance between thermocouples = 1 in

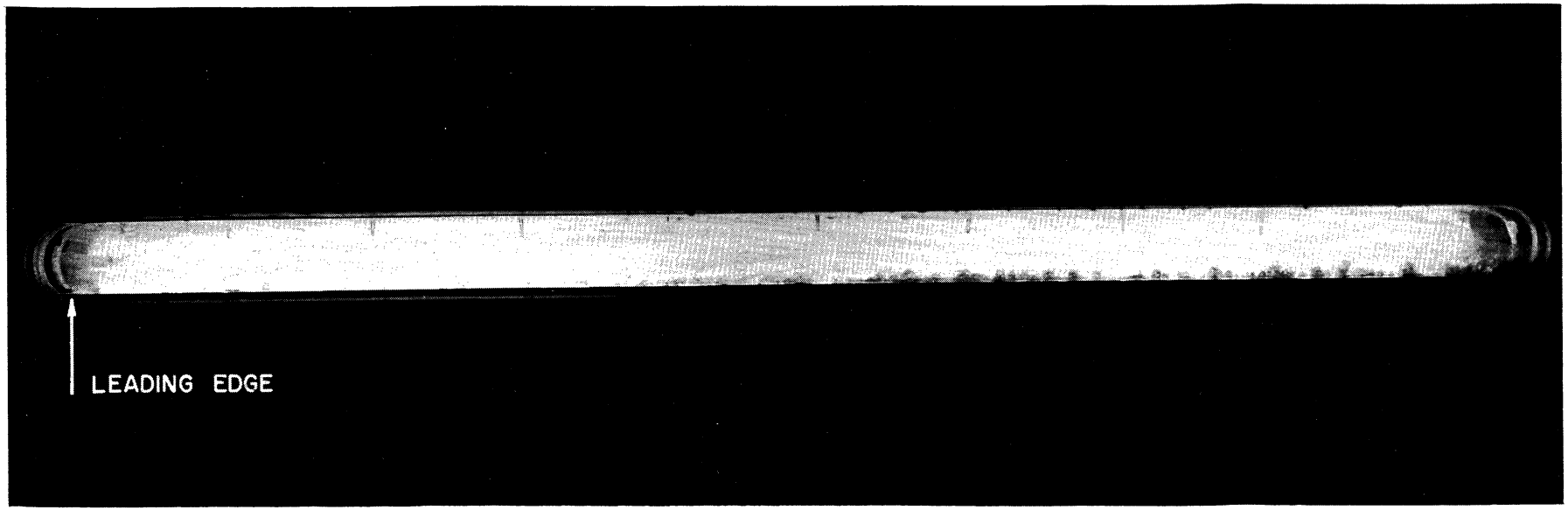

Figure 112. Photograph Showing Nucleation of Bubbles and the Formation and Development of the Bubble Boundary Layer in Forced Convection in Flow Over a Heated Plate

P_i = 500 psia

V_i = 3.5 ft/sec

$T_{sat}-T_i$ = 100°F

$q/A = 0.638 \times 10^6$ BTU/hr-ft^2

Scale: Distance between thermocouples = 1"

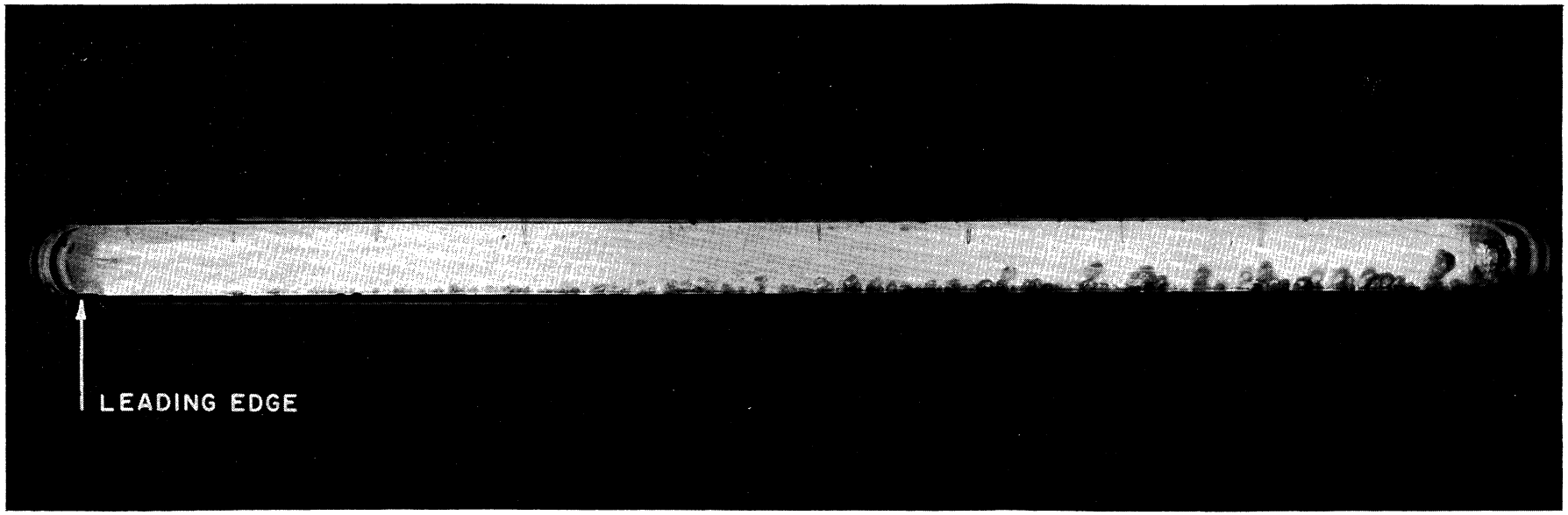

Figure 113. Photograph Showing Nucleation of Bubbles and the Formation and Development of the Bubble Boundary Layer in Forced Convection in Flow Over a Heated Plate

P_i = 500 psia

V_i = 5.9 ft/sec

$T_{sat}-T_i$ = 99°F

$q/A = 0.665 \times 10^6$ BTU/hr-ft^2

Scale: Distance between thermocouples = 1"

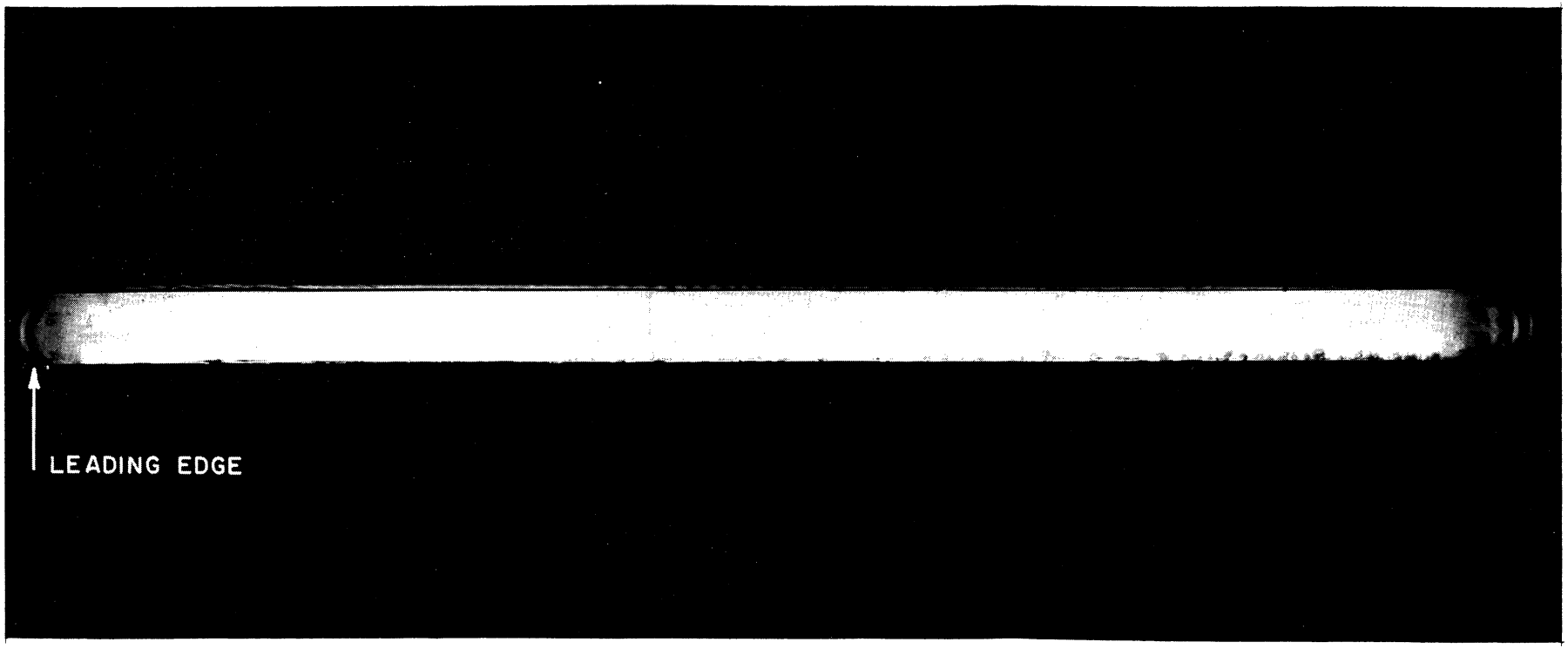

Figure 114. Photograph Showing Nucleation of Bubbles and the Formation and Development of the Bubble Boundary Layer in Forced Convection in Flow Over a Heated Plate

P_i = 500 psia

V_i = 6.1 ft/sec

$T_{sat}-T_i$ = 99°F

$q/A = 0.87 \times 10^6$ BTU/hr-ft^2

Scale: Distance between thermocouples = 1"

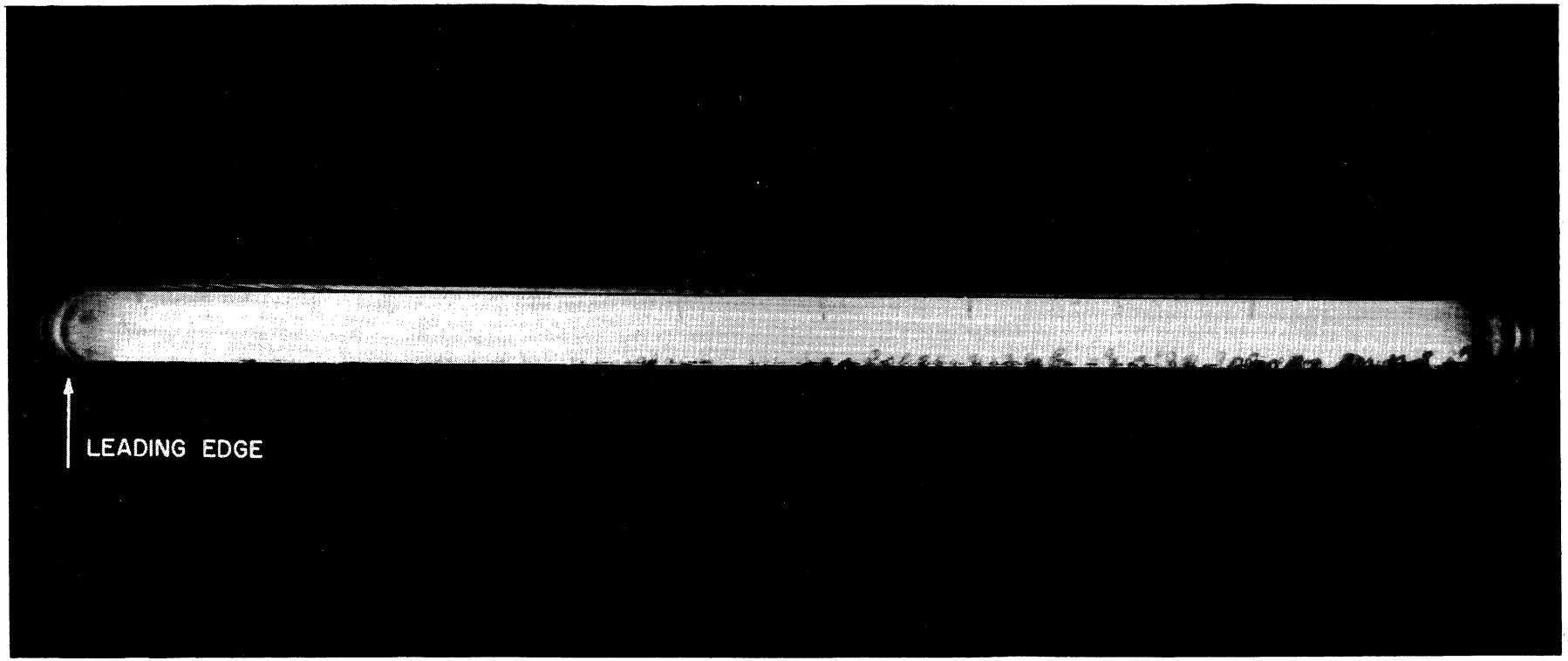

Figure 115. Photograph Showing Nucleation of Bubbles and the Formation and Development of the Bubble Boundary Layer in Forced Convection in Flow Over a Heated Plate

P_i = 500 psia

V_i = 1 ft/sec

$T_{sat}-T_i$ = 300°F

$q/A = 1.09 \times 10^6$ BTU/hr-ft^2

Scale: Distance between thermocouples = 1"

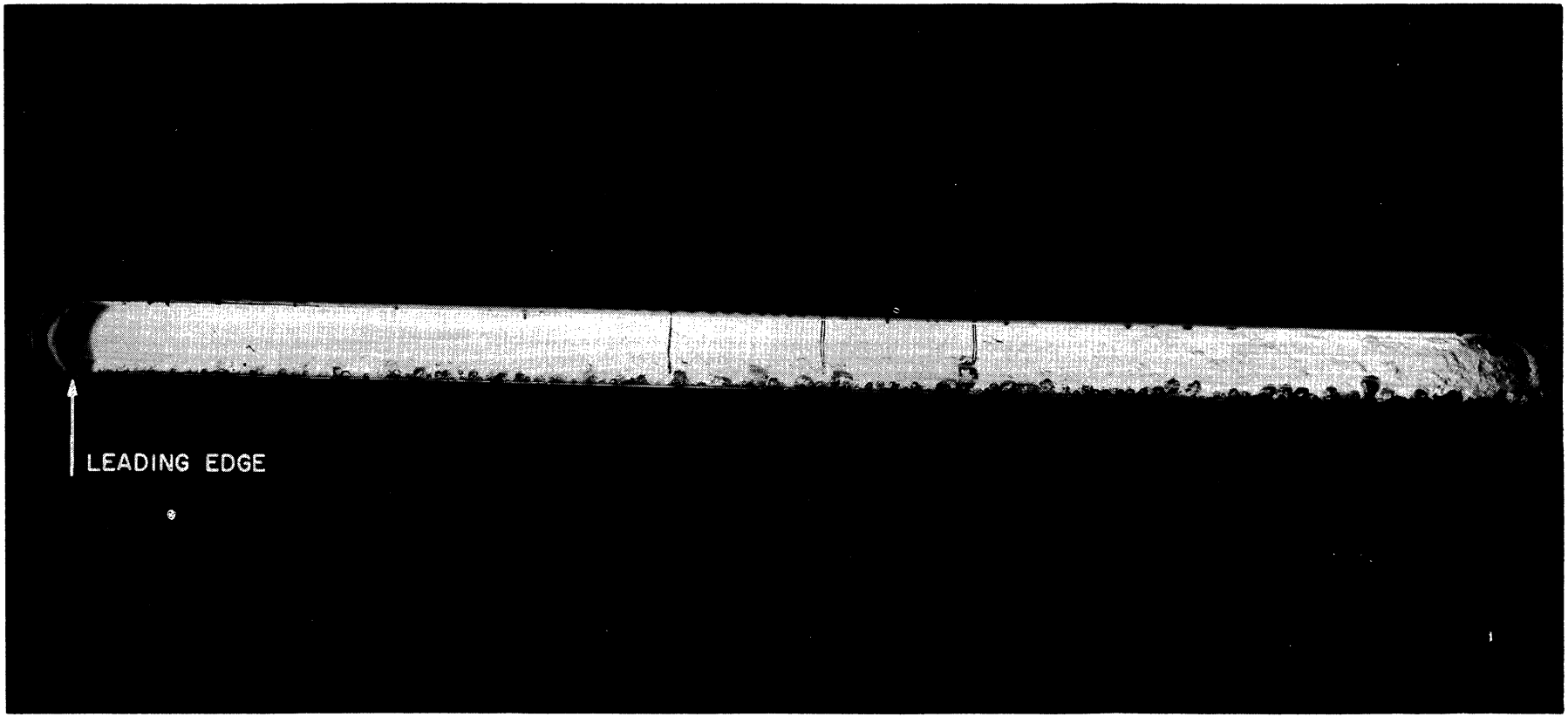

Figure 116. Photograph Showing Nucleation of Bubbles and the Formation and Development of the Bubble Boundary Layer in Forced Convection in Flow Over a Heated Plate

P_i = 800 psia

V_i = 3.5 ft/sec

$T_{sat}-T_i$ = 100°F

$q/A = 0.534 \times 10^6$ BTU/hr-ft^2

Scale: Distance between thermocouples = 1 in

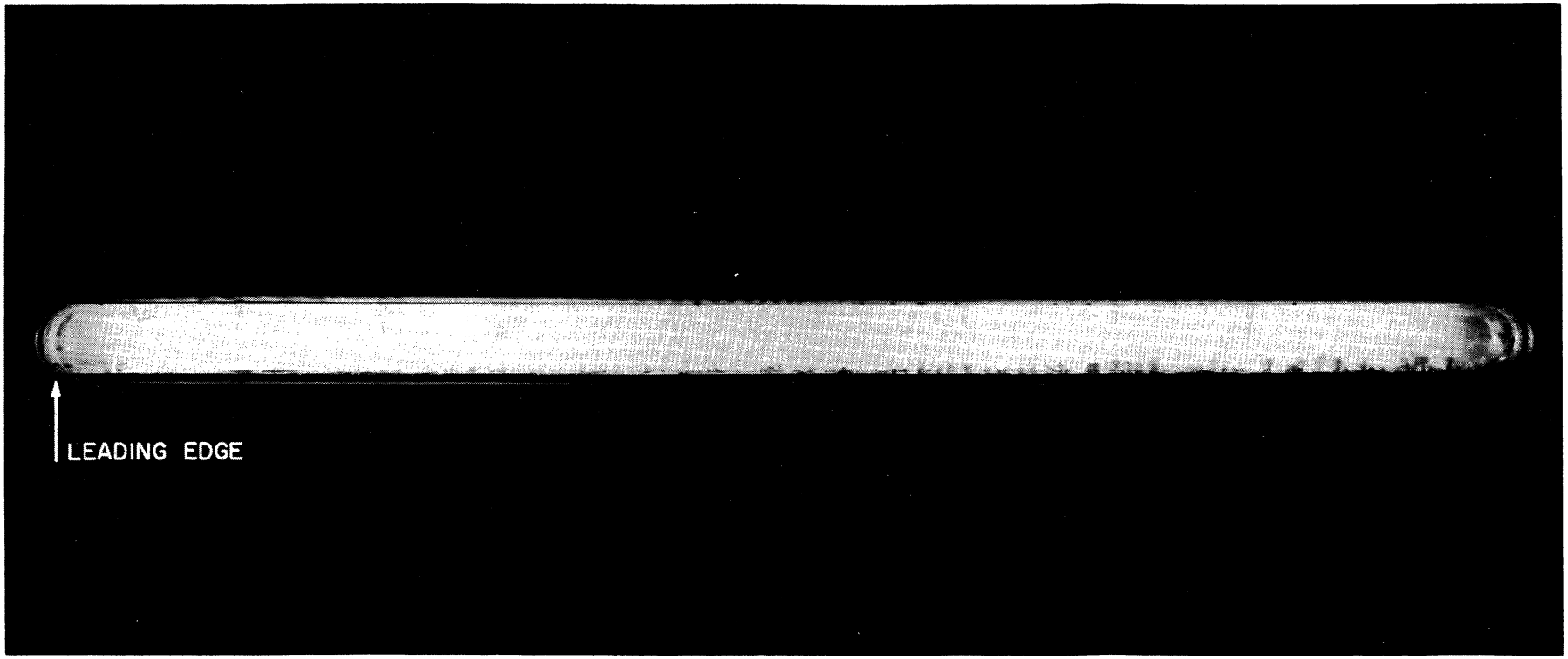

Figure 117. Photograph Showing Nucleation of Bubbles and the Formation and Development of the Bubble Boundary Layer in Forced Convection in Flow Over a Heated Plate

P_i = 800 psia

V_i = 3.5 ft/sec

$T_{sat}-T_i$ = 100°F

$q/A = 0.73 \times 10^6$ BTU/hr-ft^2

Scale: Distance between thermocouples = 1"

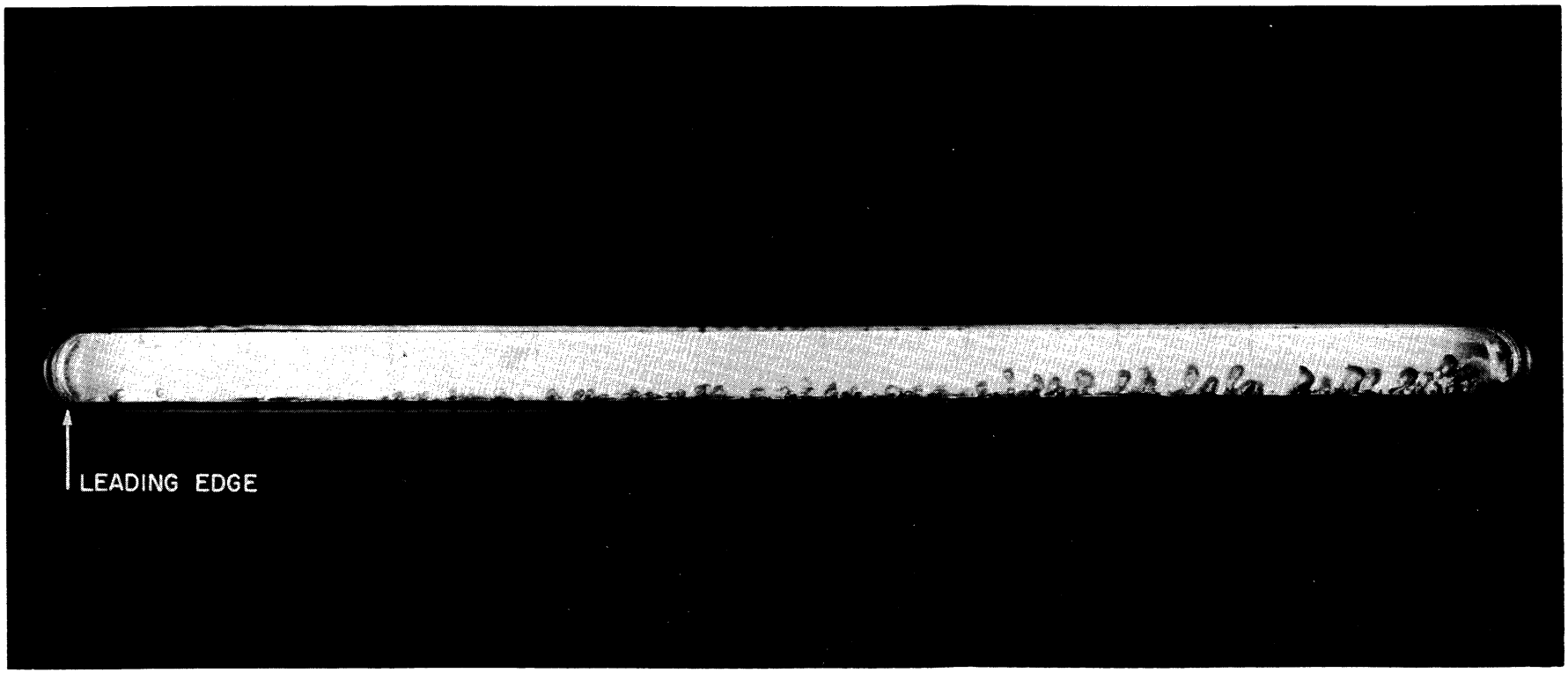

Figure 118. Photograph Showing Nucleation of Bubbles and the Formation and Development of the Bubble Boundary Layer in Forced Convection in Flow Over a Heated Plate

P_i = 1000 psia

V_i = 1 ft/sec

$T_{sat}-T_i$ = 200°F

$q/A = 0.695 \times 10^6$ BTU/hr-ft^2

Scale: Distance between thermocouples = 1"

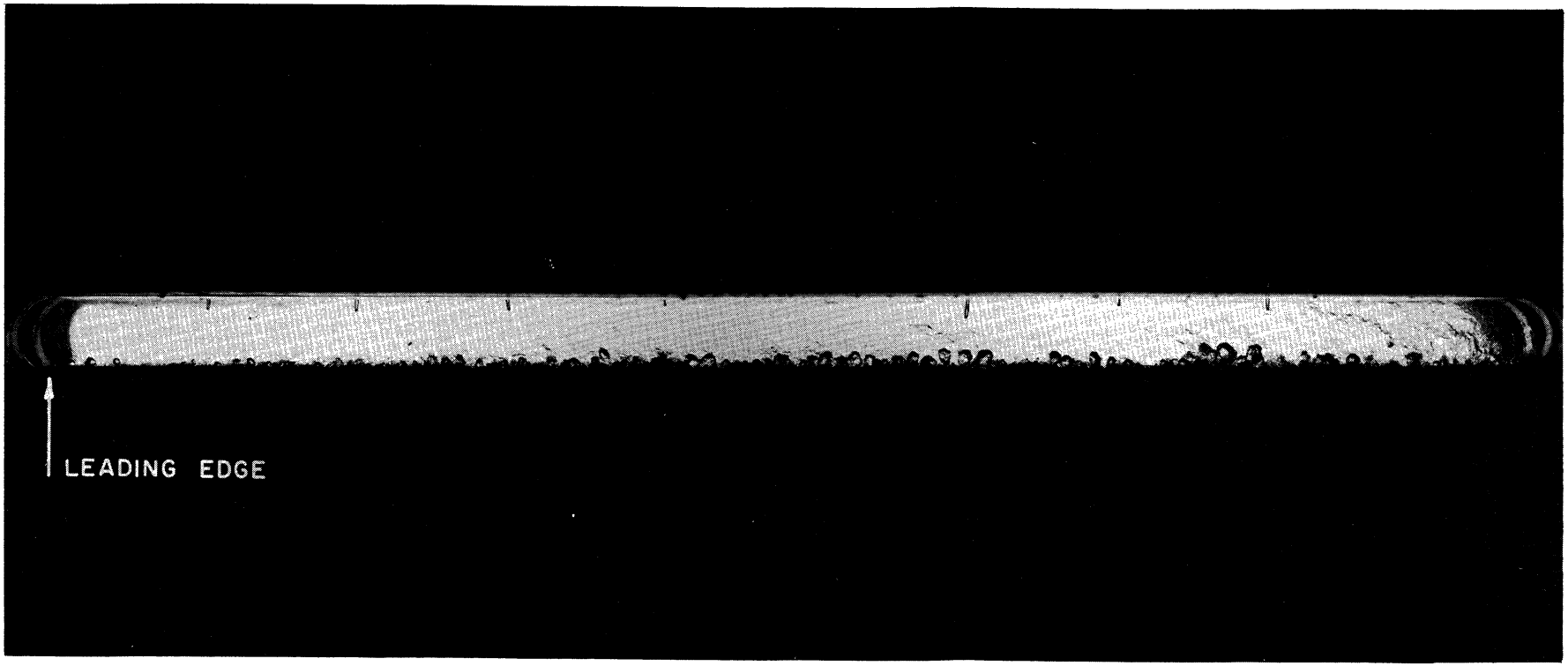

Figure 119. Photograph Showing Nucleation of Bubbles and the Formation and Development of the Bubble Boundary Layer in Forced Convection in Flow Over a Heated Plate

P_i = 1000 psia

V_i = 1 ft/sec

$T_{sat}-T_i$ = 200°F

$q/A = 0.922 \times 10^6$ BTU/hr-ft^2

Scale: Distance between thermocouples = 1"

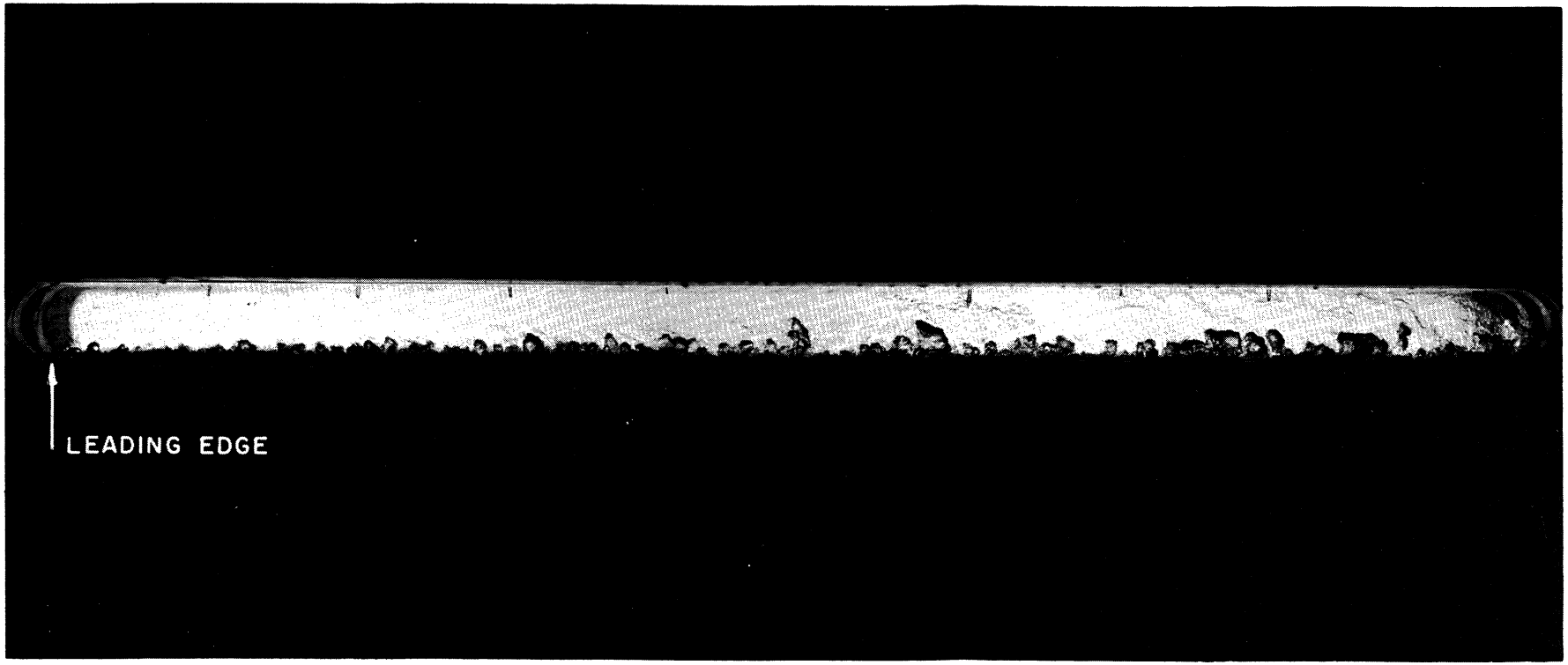

Figure 120. Photograph Showing Nucleation of Bubbles and the Formation and Development of the Bubble Boundary Layer in Forced Convection in Flow Over a Heated Plate

BIBLIOGRAPHY

1. Jens, W.H., "Boiling Heat Transfer", American Society of Naval Engineers - J., 67, 1955, pp 457-466.

2. Jens, W.H. and Leppert, G., "Recent Developments in Boiling Research", Amer. Soc. of Naval Engineers - J. 67, 1955, pp. 137-55.

3. Jens. W.H. and Leppert, G., "Recent Developments in Boiling Research, Part II Pressure Drop" Amer. Soc. of Naval Engineers - J. 67, 1955, pp. 437-56.

4. McAdams, W.H., Addoms, J.N., Rinaldo, P.M. and Day, R.S. "Heat Transfer From Single Horizontal Wires to Boiling Water", Chem. Engineering Progress, 44, No. 8, 1948, pp. 639-646.

5. McAdams, W.H., Kennel, W.E., Minden, C.S., Carl, R., Picornell, P.M., and Dew, J.E., "Heat Transfer at High Rates to Water with Surface Boiling", Industrial and Engineering Chem. 41, Sept. 1949, pp. 1945-1953.

6. Clark, J.A. and Rohsenow, W.M., "Local Boiling Heat Transfer to Water at Low Reynolds Numbers and High Pressures", ASME Trans, 76, May 1954, pp. 553-562.

7. Kreith, F. and Summerfield, M., "Heat Transfer to Water at High Flux Densities with and without Surface Boiling", ASME Trans., 71, No. 7, 1949, pp. 806-815.

8. Jacob, M., Heat Transfer, Wiley, N.Y., 1949, Vol. 1 pp. 614-657.

9. Wilson, R.H., "Literature Survey Re: Bubble Formation", CF-50-4-148, April 1950.

10. Griffith, P., "Bubble Growth Rates in Boiling", ASME Trans, 80, 1958, pp. 721-727.

11. Gunther, F.C. and Kreith, F. "Photographic Study of Bubble Formation in Heat Transfer to Subcooled Water", Heat Transfer and Fluid Mechanic Inst., Berkeley, Calif., 1949, pp. 113-126.

12. Rohsenow, W.M. and Clark, J.A., "Heat Transfer and Pressure Drop Data for High Heat Flux Densities to Water at High Sub-critical Pressures", Heat Transfer and Fluid Mechanics Inst., Stanford, Calif, 1951, pp. 193-207.

13. Kreith, F. and Summerfield, M., "Pressure Drop and Convective Heat Transfer with Surface Boiling at High Heat Flux; Data for Aniline and n-Butyl Alcohol", ASME Trans., 72, No. 6, Aug. 1950, pp. 869-78.

14. Isbin, H.S., Moen, R.Y., and Mosher, D.R., "Two-Phase Pressure Drops", U.S. Atomic Energy Commission, AECU-2994, Nov. 1954.

15. Sher, N.C., "Preliminary Investigation of Pressure Drop and Heat Transfer in Rectangular Channels at 1100 psia", Westinghouse Atomic Energy Div., WAPD-TH-265, 1956.

16. Viscardi, J.E., "Boiling Burnout Progress, "Nuclear Development Corp. of America, NDA-24, No. 8, 1956.

17. Dingee, D.A. Epstein, H.A., Chastain, J.W. and Fawcett, S.L., "Burnout Heat Flux in a Rectangular Channel", Battelle Memorial Inst. BMI-1065, Jan. 10, 1956.

18. Masnovi, R. and Troy, M., "Upflow Burnout Data for 0.101x1x6 in Vertical Rectangular Channels at 2000 psia", Westinghouse Atomic Power Division, WAPD-TH-289, 1957.

19. Troy, M., "Upflow Burnout Data for Water in Rectangular Channels at Pressures from 600 to 1870 psia", Westinghouse Atomic Power Div. WAPD-TH-321, 1957.

20. Egen, R.A., Dingee, D.A. and Chastain, J.W., "Vapor Formation and Behavior in Boiling Heat Transfer", Battelle Memorial Inst. BMI-1163, 1957.

21. Griffith, P., Clark, J.A., and Rohsenow, W.M., "Void Volumes in Subcooled Boiling Systems", ASME Paper No. 58-HT-19.

22. Marchaterre, F.J., "The Effect of Pressure on Boiling Density in Multiple Rectangular Channels," Argonne Nat. Lab. ANL-5522, 1956.

23. Miller, A.I., "Investigation of the Effect of Channel Heigh on the Density of Water Flowing Over a Flat Plate with Surface Boiling", S.M. Thesis, M.I.T., 1954.

24. Dyer, J.C., "An Investigation Into the Growth of a Boiling Boundary Layer in Turbulent Flow", S.M. Thesis, M.I.T., 1956.

25. Gunther, F.C., "Photographic Study of Surface Boiling Heat Transfer to Water with Forced Convection", ASME Trans., 73, 1951, pp. 115-123.

26. Jeffery, R.W., "Visual Study of Water Flowing Over a Flat Plate at High Rates of Heat Transfer with Surface Boiling" S.B. Thesis, M.I.T., 1952.

27. Whitehead, A.D., "An Examination of Bubble Sizes in Local Boiling Heat Transfer Experiments", S.M. Thesis M.I.T., 1952.

28. Rohsenow, W.M, and Clark, J.A., "A Study of the Mechanism of Boiling Heat Transfer", ASME Trans., 73, July 1951, pp. 609-620.

29. De Bortoli, R.A., et al., "Investigation of Burnout Heat Flux", Reactor Heat Transfer Conf. of 1956, TID-7529, Part 1, Book 1.

30. Bettis Subcommittee, "Review of Thermal Design Criteria for Pressurized Water Reactors at 2000 psia", WAPD-SFR-RS-444, 1956.

31. Hooker, H.H., and Popper, G.F., "A Gamma Ray Attenuation Method for Void Fraction Determinations in Experimental Boiling Heat Transfer Test Facilities", Argonne National Lab., ANL-5766, Nov. 1958.

32. McAdams, W.H., Heat Transmission, McGraw-Hill, 1954, pp. 368-408.

33. Rohsenow, W.M., "Heat Transfer, A Symposium," Engineering Research Institute, University of Michigan, Ann Arbor, Mich. 1952.

34. Rohsenow, W.M., "A Method of Correlating Heat Transfer Data for Surface Boiling of Liquids", ASME Trans, 74, 1952, pp. 969-976.

35. Lowery, A.J., and Westwater, J.W., "Heat Transfer to Boiling Mechanol-Effect of Added Agents", Industrial and Engineering Chem, 49, 1957, pp. 1445-1448.

36. Leppert, G., Costello, C.P. and Hoglund, B.M., "Boiling Heat Transfer to Water Containing a Volatil Additive", ASME Trans., 80, No. 7, 1958, pp. 1395-1404.

37. Petrick, M.P., "Two-Phase Air-Water Flow Phenomena", Argonne National Laboratory, ANL-5787, 1958.

38. Galson, A.E., "Steam Slip and Burnout in Bulk Boiling Systems", GEAP-1076, 1957.

39. Boarts, R.M., et al., "Temperature Drops and Liquid-Film Heat Transfer Coefficients in Vertical Tubes", Ind. and Engrg, Chem., 28, 1937, pp. 912-918.

40. Grohse, E.W., Mueller, G.O., and Findley, J.A., "Fundamental Investigation of Boiling Heat Transfer and Two-Phase Flow", Knolls Atomic Power Laboratory, KAPL-M-EWG-1, 1958.

41. Buchberg, H., et al., "Studies in Boiling Heat Transfer", Final Report, AEC COO-24, March 1951.

42. Mueller, G.O., "A Review and Assessment of Boiling Heat Transfer and the Departure from Nucleat Boiling", Knolls Atomic Power Lab. KAPL-M-GOM-2, 1958.

43. Bankoff, S.G., "On the Mechanism of Subcooled Nucleate Boiling", Memorandum No. 30-8, Jet Propulsion Laboratory, Calif. Inst. of Tech., Pasadena, Calif., Feb. 5, 1959.

44. Staniszewski, B.E., "Nucleate Boiling Bubble Growth and Departure", Technical Report No. 16, DSR, Project No. 7-7673, Mass. Inst. of Tech., Cambridge, Mass., Aug. 1959.

45. Richardson, Bobbie L., "Some Problems in Horizontal Two-Phase Component Flow", ANL-5949, Dec. 1958.

46. Marcheterre, J.R. and Petrick, M., "The Prediction of Steam Volume Fractions in Boiling Systems", Nuclear Science and Engineering, Vol. 2, No. 1, Supplement 13-14, 1959.

47. Isbin, H.S., Sher, N.C., Eddy, K.C., "Void Fractions in Two Phase Steam-Water Flow", Journal AIChE, March, 1957.

48. Cook, W.H., "Boiling Density in Vertical Rectangular Multichannel Sections with Natural Circulation", ANL-5621, 1956.

49. Jens. W.H., and Lottes, P.A., "Analysis of Heat Transfer Burnout, Pressure Drop and Density Data for High-Pressure Water," ANL 4627, 1951.

50. Jens, W.H., and Lottes, P.A., "Two Phase Pressure Drop and Burnout Using Water Flowing in Round and Rectangular Channels", ANL-4915, 1952.

51. Reynolds, J.B., "Local Boiling Pressure Drop", ANL-5187, 1954.

52. Jacket, H.S., Roarty, J.E., and Sher, N.C., "Boiling Pressure Drop in Rectangular Channels", WAPD-TH-204, 1956.

53. Johnson, H.A., and Abou-Sabe, H.A., "Heat Transfer and Pressure Drop for Turbulent Flow of Air-Water Mixtures in a Horizontal Pipe", ASME Trans., Vol. 74, 1952, pp. 977-987.

54. Levy, S., "Theory of Pressure Drop and Heat Transfer For Two-Phase Two-Component Annular Flow in Pipes", Ohio State Univ., Engr. Exp. Station Bull. No. 149 Proceedings of the Second Midwestern Conference on Fluid Mechanics, 1952.

55. Larson, R.F., "Factors Affecting Boiling in a Liquid", Industrial and Engineering Chemistry, Vol. 37, 1945, pp. 1004-1009.

56. Faneuff, C.E., McLean, E.A., and Scherrer, V.E., "Some Aspects of Surface Boiling", Journal Applied Physics, Vol. 29, No. 1, 1958, pp. 80-84.

57. Jacobs, James M., Heat Transfer and Fluid Flow. A Bibliography of Selected Report Literature TID-3305 (Supplement 1).

58. Roberts, H.A., "A Review of Net Boiling Heat Transfer and Pressure Drop From the Literature", AERE-ED/M-22, Aug. 1955.

59. Stroebe, G.W., et al. "Boiling-Film Heat Transfer Coefficients in a Long-Tube Vertical Evaporator", Ind. and Engr. Chem, 31, 1939, pp. 200-206.

60. Larson, R.F., "Occurrence of Metastable States of Liquid and Vapor," Ind. and Eng. Chem 27, 1945, pp. 1010-16

61. Bromley, L.A., "Heat Transfer in Stable Film Boiling", Chem Engrg, Prog., 46, 1950, pp. 221-227.

62. Kaxokova, E.A., "Maximum Heat Transfer to Boiling Water at High Pressures", Izvestia Akademii Nauk USSR, Sept. 1950, pp. 81-87, Reviewed in Engr. Digest, Vol. 12, No. 3, 1951.

63. Cichelli, M.T., and Bonilla, C.F., "Heat Transfer to Liquids Boiling under Pressure", AIChE Trans., 41, 1945, pp. 755-787.

64. Cryder, D.S., and Gilliland, E.R., "Heat Transmission From Metal Surfaces to Boiling Liquids", Refrig, Engrg, 25, 1933, pp. 78-83.

65. Insinger, T.H., Jr., and Bliss,H., "Transmission of Heat to Boiling Liquids", AICE Trans, 36, 1940, pp. 491-513.

66. Bonilla, C.F., and Perry, C.W., "Heat Transmission to Boiling Binary Liquid Mixtures", AICE Trans, 37, 1941, pp. 685-705.

67. Henry, G., "Density Variations in Water Flowing Over a Flat Plate with Surface Boiling", M.S. Thesis, M.I.T., July, 1953.

68. Foust, A.S., et al., "Liquid Velocity and Coefficients of Heat Transfer in Natural Circulation Evaporator", Ind. and Engrg, Chem., 31, 1939, pp. 206-214.

69. Mead, R.R., Romie, F.E., and Guibert, A.G., "Liquid Superheat and Boiling Heat Transfer," Heat Transfer and Fluid Mechanics Institute, Stanford, Calif, 1951, pp. 209-216.

70. Knudsen, J.G. and Katz, D.L., "Fluid Dynamics and Heat Transfer, McGraw-Hill, New York, 1956.

71. Kline, S.J. and McClintock, F.A., "Describing Uncertainties in Single-Sample Experiments", Mechanical Engineering, Jan 1953, pp. 328.

72. Seban, R.A. and Shimazaki, T.T., "Heat Transfer to a Fluid Flowing Turbulently in a Smooth Pipe with Walls at Constant Temperature", ASME Trans, 73, 1951, pp. 803-809.

73. Clark, J.A., "Response of Temperature Measuring Elements to Thermal Transients", ASME Paper No. 55-SA-18.